Eur. Phys. J. C 41, 1–131 (2005)
Digital Object Identifier (DOI) 10.1140/epjc/s2005-02169-1

THE EUROPEAN PHYSICAL JOURNAL C

CP violation and the CKM matrix: assessing the impact of the asymmetric B factories

The CKMfitter Group

J. Charles[1,a], A. Höcker[2,b], H. Lacker[3,c], S. Laplace[4,d], F.R. Le Diberder[2,e], J. Malclès[5,f], J. Ocariz[5,g], M. Pivk[6,h], L. Roos[5,i]

[1] Centre de Physique Théorique, Campus de Luminy, Case 907, 13288 Marseille Cedex 9, France
(UMR 6207 du CNRS associée aux Universités d'Aix-Marseille I et II et Université du Sud Toulon-Var; laboratoire affilié à la FRUMAM-FR2291)
[2] Laboratoire de l'Accélérateur Linéaire, Bât. 200 BP34 91898 Orsay, France
(UMR 8607 du CNRS-IN2P3 associée à l'Université Paris XI)
[3] Technische Universität Dresden, Institut für Kern- und Teilchenphysik, 01062 Dresden, Germany
[4] Laboratoire d'Annecy-Le-Vieux de Physique des Particules, 9 Chemin de Bellevue, BP 110, 74941 Annecy-le-Vieux Cedex, France
(UMR 5814 du CNRS-IN2P3 associée à l'Université de Savoie)
[5] Laboratoire de Physique Nucléaire et de Hautes Energies, 4 place Jussieu, 75252 Paris Cedex 05, France
(UMR 7585 du CNRS-IN2P3 associée aux Universités Paris VI et VII)
[6] CERN, PH Department, 1211 Geneva 23, Switzerland

Received: 13 July 2004 /
Published online: 12 April 2005 –

Abstract. We present an up-to-date profile of the Cabibbo-Kobayashi-Maskawa matrix with emphasis on the interpretation of recent CP-violation results from the B factories. For this purpose, we review all relevant experimental and theoretical inputs from the contributing domains of electroweak interaction. We give the "standard" determination of the apex of the Unitarity Triangle, namely the Wolfenstein parameters $\overline{\rho}$ and $\overline{\eta}$, by means of a global CKM fit. The fit is dominated by the precision measurement of $\sin 2\beta$ by the B factories. A detailed numerical and graphical study of the impact of the results is presented. We propose to include $\sin 2\alpha$ from the recent measurement of the time-dependent CP-violating asymmetries in $B^0 \to \rho^+\rho^-$, using isospin relations to discriminate the penguin contribution. The constraint from ε'/ε is discussed. We study the impact from the branching fraction measurement of the rare kaon decay $K^+ \to \pi^+\nu\overline{\nu}$, and give an outlook into the reach of a future measurement of $K_L^0 \to \pi^0\nu\overline{\nu}$. The B system is investigated in detail. We display the constraint on $2\beta+\gamma$ and γ from $B^0 \to D^{(*)\pm}\pi^{\mp}$ and $B^+ \to D^{(*)0}K^+$ decays, respectively. A significant part of this paper is dedicated to the understanding of the dynamics of B decays into $\pi\pi$, $K\pi$, $\rho\pi$, $\rho\rho$ and modes related to these by flavor symmetry. Various phenomenological approaches and theoretical frameworks are discussed. We find a remarkable agreement of the $\pi\pi$ and $K\pi$ data with the other constraints in the unitarity plane when the hadronic matrix elements are calculated within QCD Factorization, where we apply a conservative treatment of the theoretical uncertainties. A global fit of QCD Factorization to all $\pi\pi$ and $K\pi$ data leads to precise predictions of the related observables. However sizable phenomenological power corrections are preferred. Using an isospin-based phenomenological parameterization, we analyze separately the $B \to K\pi$ decays, and the impact of electroweak penguins in response to recent discussions. We find that the present data are not sufficiently precise to constrain either electroweak parameters or hadronic amplitude ratios. We do not observe any unambiguous sign of New Physics, whereas there is some evidence for potentially large non-perturbative rescattering effects. Finally we use a model-independent description of a large class of New Physics effects in both $B^0\overline{B}^0$ mixing and B decays, namely in the $b \to d$ and $b \to s$ gluonic penguin amplitudes, to perform a new numerical analysis. Significant non-standard corrections cannot be excluded yet, however Standard Model solutions are favored in most cases. In the appendix to this paper we propose a frequentist method to extract a confidence level on Δm_s from the experimental information on $B_s^0\overline{B}_s^0$ oscillation. In addition we describe a novel approach to combine potentially inconsistent measurements. All results reported in this paper have been obtained with the numerical analysis package CKMfitter, featuring the frequentist statistical approach *R*fit.

Contents

[a] e-mail: charles@cpt.univ-mrs.fr
[b] e-mail: hoecker@lal.in2p3.fr
[c] e-mail: h.lacker@physik.tu-dresden.de
[d] e-mail: laplace@lapp.in2p3.fr
[e] e-mail: diberder@in2p3.fr
[f] e-mail: malcles@lpnhep.in2p3.fr
[g] e-mail: ocariz@in2p3.fr
[h] e-mail: muriel.pivk@cern.ch
[i] e-mail: lroos@lpnhep.in2p3.fr

Part I
Introduction

Within the Standard Model (SM), *CP* violation (CPV) is generated by a single non-vanishing phase in the unitary Cabibbo–Kobayashi–Maskawa (CKM) quark mixing matrix V [1,2]. A useful parameterization of V follows from the observation that its elements exhibit a hierarchy in terms of the parameter $\lambda \simeq |V_{us}|$ [3,4]. Other parameters are A, $\overline{\rho}$ and $\overline{\eta}$, where *CP* violation requires $\overline{\eta} \neq 0$. The parameters λ and A are obtained from measurements of semileptonic decay rates of K mesons, and of B meson decays involving beauty-to-charm transitions, respectively. The constraints on $\overline{\rho}$ and $\overline{\eta}$ are conveniently displayed in the complex plane where they determine the apex of the Unitarity Triangle[1] (UT), which is a graphical representation of the unitarity relation between the first and the third column of the CKM matrix. For example, semileptonic B decays yielding $|V_{ub}|$, predictions of $B^0\overline{B}^0$ oscillation and of indirect *CP* violation in the neutral kaon sector depend on $\overline{\rho}$, $\overline{\eta}$. However the understanding of this dependence is limited by theoretical uncertainties, which are mainly due to long distance QCD. In the era of the B factories, a large number of measurements has appeared that are related to the CKM phase. The most famous of them is the measurement of the *CP*-violation parameter $\sin 2\beta$ in $b \to c\bar{c}s$ transitions, which is theoretically clean. Other modes are sensitive to the angles α and γ of the UT, where in many cases one has to deal with interfering amplitudes with different *CP*-violating phases, complicating the extraction of the CKM-related parameters.

A focus of this work is the phenomenological interpretation of B-physics results. The spectacular performance of the first five years of the asymmetric-energy B factories, PEP-II and KEK B, and their experiments *BABAR* and Belle, with published results on up to $270\,\mathrm{fb}^{-1}$ integrated luminosity (combined), has produced an avalanche of publications, many of which are related to *CP* violation. In spite of the difficulties due to small branching fractions and/or hadronic uncertainties, the goal of overconstraining the UT from tree-level-dominated B decays seems achievable even if the precision may turn out insufficient to reveal a failure of the SM. Since tree decays are not expected to lead to large inconsistencies with the SM, more and more experimental and theoretical effort goes into the determination of UT angles and/or other parameters from B decays dominated by penguin-type diagrams, the most prominent of which are $b \to s\gamma^{(*)}$ and $b \to s\bar{s}s$ (e.g., $B^0 \to \phi K^0$). A number of other decay modes with net strangeness in the final state,

[1] Throughout this paper, we adopt the α, β, γ convention for the angles of the Unitarity Triangle. They are related to the ϕ_1, ϕ_2, ϕ_3 "historical" convention [5] as $\alpha = \phi_2$, $\beta = \phi_1$ and $\gamma = \phi_3$. Angles are given in units of degrees.

which are now being studied, may reveal specific signs of physics beyond the SM through unexpected *CP* violation or enhanced branching fractions.

The CKM analysis performed in this paper is threefold: the first goal of the global CKM fit is to probe the validity of the SM, that is to quantify the agreement between the SM and the experimental information; if this is confirmed, one secondly enters the metrology phase where allowed ranges for the CKM matrix elements and related quantities are determined, assuming explicitly the SM to be correct; finally, within an extended theoretical framework, one may search for signals of New Physics and constrain parameters of specific New Physics scenarios.

Analyzing data in a well defined theoretical scheme ceases to be a straightforward task when one moves away from Gaussian statistics. This is the case for the theoretically limited precision on the SM predictions of the neutral K and B mixing observables and, to a lesser extent, for the semileptonic decay rates of B decays to charmed and charmless final states. Also the interpretation of results on *CP* violation in terms of the UT angles often invokes unknown phases occurring in absorptive parts of non-leptonic transitions. The statistical approach *R*fit developed and described in detail in [6] treats these uncertainties in a frequentist framework, which allows one to determine confidence levels. The ensemble of the statistical analyses reported here is realized with the use of the program package CKMfitter[2].

This paper is the second edition [6] of our effort to collect all significant information on the CKM matrix and to combine it in a global CKM fit [8–10]. All figures given in this document as well as partially updated results can be found on the CKMfitter web site [7].

The paper is organized as follows. Part I provides a brief introduction of the CKM matrix and mainly serves to define the conventions adopted in this paper. We review in Part II the statistical approach and the analysis tools implemented in CKMfitter, the understanding of which is necessary for an adequate interpretation of the results derived in this work. Part III first defines the observables that are used as input in the so-called "standard CKM fit", which is defined as the global CKM fit that includes only those observables, which provide competitive constraints and of which the SM prediction can be considered to be quantitatively under control. We put emphasis on the discussion of the theoretical uncertainties. This introduction is followed by a compendium of numerical and graphical results of the standard CKM fit for all parameters and observables of the electroweak sector that significantly depend on the CKM matrix. Beginning with Part IV we perform rather detailed investigations of specific subsystems, related to *CP* violation in the quark sector and to the Unitarity Triangle, with emphasis on the discussion of observables not used in the standard CKM fit. We study direct *CP* violation in the kaon system and specifically derive constraints on the non-perturbative bag parameters. We discuss the impact of the measurement of rare kaon decays and give an outlook into the future where we attempt to quantify the expected uncertainties. Part V displays the constraints related to the Unitarity Triangle angle γ from the time-dependent analysis of $B^0 \to D^{(*)\pm}\pi^{\mp}$ decays and the Dalitz analysis of $B^+ \to D^0 K^+$. Part VI describes in detail the analysis of charmless B decays to $\pi\pi$, $K\pi$, $\rho\pi$ and $\rho\rho$, which, besides the global CKM fit, represents a central pillar of this work. We discuss constraints on the *CP*-violating CKM phase using various phenomenological and theoretical approaches based on flavor symmetries and factorization. In Part VII we use a model-independent parameterization of a large class of New Physics effects in both $B^0\overline{B}^0$ mixing and B decays, namely in the $b \to d$ and $b \to s$ gluonic penguin amplitudes, to perform a tentative numerical analysis. In the appendix to this work we describe the frequentist treatment of the measurement of $B_s^0\overline{B}_s^0$ oscillation incorporated in our CKM fit, and we propose a novel method to handle the problem of (apparently) inconsistent measurements.

1 The CKM matrix

Invariance under local gauge transformation prevents the bare masses of leptons and quarks to appear in the $SU(3) \times SU(2) \times U(1)$ Lagrange density of the SM. Instead, the spontaneous breakdown of electroweak symmetry dynamically generates masses for the fermions due to the Yukawa coupling of the fermion fields to the Higgs doublet. Since the latter has a non-vanishing vacuum expectation value, the Yukawa couplings g give rise to the 3×3 mass matrices

$$M_i = \frac{v g_i}{\sqrt{2}} \,, \tag{1}$$

with $i = u(d)$ for up(down)-type quarks and $i = e$ for the massive leptons. To move from the basis of the flavor (electroweak) eigenstates to the basis of the mass eigenstates, one performs the transformation

$$U_{u(d,e)} M_{u(d,e)} \tilde{U}^{\dagger}_{u(d,e)} = \mathrm{diag}\left(m_{u(d,e)}, m_{c(s,\mu)}, m_{t(b,\tau)}\right) \,, \tag{2}$$

where U_i and $\tilde{U}_i$ are unitary complex rotation matrices and the masses m_i are real. The neutral-current part of the Lagrange density in the basis of the mass-eigenstates remains unchanged (i.e., there are no flavor-changing neutral

[2] CKMfitter is a framework package that hosts several statistical approaches to a global CKM fit and the interpretation of *CP*-violation results. It is available to the public [7]. Please contact the authors for more information.

currents present at tree level), whereas the charged current part of the quark sector is modified by the product of the up-type and down-type quark mass matrices,

$$V = U_u U_d^\dagger \ , \tag{3}$$

which is the CKM mixing matrix. By convention, V operates on the $-1/3$ charged down-type quark mass eigenstates

$$V = \begin{pmatrix} V_{ud} & V_{us} & V_{ub} \\ V_{cd} & V_{cs} & V_{cb} \\ V_{td} & V_{ts} & V_{tb} \end{pmatrix} \tag{4}$$

and, being the product of unitary matrices, V itself is unitary

$$VV^\dagger = \mathrm{I} \ . \tag{5}$$

There exists a hierarchy between the elements of V both for their value (the diagonal elements dominate) and their errors (since they dominate, they are better known). The unitarity and the phase arbitrariness of fields reduce the initial nine complex elements of V to three real numbers and one phase, where the latter accounts for CP violation. It is therefore interesting to over-constrain V since deviations from unitarity would reveal the existence of new generation(s) or new couplings.

The charged current couplings among left-handed quark fields are proportional to the elements of V. For right-handed quarks, there exist no W boson interaction in the SM and the Z, photon and gluon couplings are flavor diagonal. For left-handed leptons the analysis proceeds similarly to the quarks with the notable difference that, since the neutrinos are (almost) massless, one can choose to make the same unitary transformation on the left-handed charged leptons and neutrinos so that the analog of V in the lepton sector becomes the unit matrix.

There are many ways of parameterizing the CKM matrix in terms of four parameters. The following section summarizes the most popular representations.

1.1 The Standard Parameterization

The Standard Parameterization of V was proposed by Chau and Keung [11] and is advocated by the Particle Data Group (PDG) [12]. It is obtained by the product of three (complex) rotation matrices, where the rotations are characterized by the Euler angles θ_{12}, θ_{13} and θ_{23}, which are the mixing angles between the generations, and one overall phase δ [3]

$$V = \begin{pmatrix} c_{12}c_{13} & s_{12}c_{13} & s_{13}e^{-i\delta} \\ -s_{12}c_{23} - c_{12}s_{23}s_{13}e^{i\delta} & c_{12}c_{23} - s_{12}s_{23}s_{13}e^{i\delta} & s_{23}c_{13} \\ s_{12}s_{23} - c_{12}c_{23}s_{13}e^{i\delta} & -c_{12}s_{23} - s_{12}c_{23}s_{13}e^{i\delta} & c_{23}c_{13} \end{pmatrix} \tag{6}$$

where $c_{ij} = \cos\theta_{ij}$, $s_{ij} = \sin\theta_{ij}$ for $i < j = 1, 2, 3$. This parameterization strictly satisfies the unitarity relation (5).

1.2 The Wolfenstein parameterization

Following the observation of a hierarchy between the different matrix elements, Wolfenstein [3] proposed an expansion of the CKM matrix in terms of the four parameters λ, A, ρ and η ($\lambda \simeq |V_{us}| \sim 0.22$ being the expansion parameter), which is widely used in contemporary literature, and which is the parameterization employed in this work and in CKMfitter. We use in the following as definitions to *all orders* in λ [4]

$$\begin{aligned} s_{12} &\equiv \lambda \ , \\ s_{23} &\equiv A\lambda^2 \ , \\ s_{13}e^{-i\delta} &\equiv A\lambda^3(\rho - i\eta) \ , \end{aligned} \tag{7}$$

inserted into the standard parameterization (6), so that unitarity of the CKM matrix is achieved to all orders[4].

[3] This phase δ is a CP-violating phase; it should not be confused with the CP-conserving hadronic phases that will be introduced later with the same symbol.

[4] The Taylor expansion of (7), inserted into (6), up to order $\mathcal{O}(\lambda^9)$ reads

$$V_{ud} = 1 - \frac{1}{2}\lambda^2 - \frac{1}{8}\lambda^4 - \frac{1}{16}\lambda^6\left(1 + 8A^2(\rho^2 + \eta^2)\right) - \frac{1}{128}\lambda^8\left(5 - 32A^2(\rho^2 + \eta^2)\right) \ ,$$

1.3 The Jarlskog invariant

It was shown by Jarlskog [13] that the determinant of the commutator of the up-type and down-type unitary mass matrices (1) reads

$$\det[M_u, M_d] = -2iF_uF_dJ \ , \tag{8}$$

with $F_{u(d)} = (m_{t(b)} - m_{c(s)})(m_{t(b)} - m_{u(d)})(m_{c(s)} - m_{u(d)})/m^3_{t(b)}$. The phase-convention independent measurement of CP violation, J, is given by

$$\mathrm{Im}\left[V_{ij}V_{kl}V^*_{il}V^*_{kj}\right] = J\sum_{m,n=1}^{3}\varepsilon_{ikm}\varepsilon_{jln} \ , \tag{9}$$

where V_{ij} are the CKM matrix elements and ε_{ikm} is the total antisymmetric tensor. One representation of (9) reads, for instance, $J = \mathrm{Im}[V_{ud}V_{cs}V^*_{us}V^*_{cd}]$. A non-vanishing CKM phase and hence CP violation necessarily requires $J \neq 0$. The Jarlskog parameter expressed in the Standard Parameterization (6) reads

$$J = c_{12}c_{23}c^2_{13}s_{12}s_{23}s_{13}\mathrm{sin}\delta \ , \tag{10}$$

and, using the Wolfenstein parameterization, one finds

$$J = A^2\lambda^6\eta\left(1-\lambda^2/2\right) + \mathcal{O}(\lambda^{10}) \sim 10^{-5} \ .$$

The empirical value of J is small compared to its mathematical maximum of $1/(6\sqrt{3}) \simeq 0.1$ showing that CP violation is suppressed as a consequence of the strong hierarchy exhibited by the CKM matrix elements. Remarkably, to account for CP violation (see (8)) requires not only a non-zero J but also a non-degenerated quark-mass hierarchy. Equal masses for at least two generations of up-type or down-type quarks would eliminate the CKM phase.

Phase convention invariance of the V-transformed quark wave functions is a requirement for physically meaningful quantities. Such invariants are the moduli $|V_{ij}|^2$ and the quadri-products $V_{ij}V_{kl}V^*_{il}V^*_{kj}$ (cf. the Jarlskog invariant J). Non-trivial higher order invariants can be reformulated as functions of moduli and quadri-products (see, e.g., [14]). Indeed, (9) expresses the fact that, owing to the orthogonality of any pair of different rows or columns of V, the imaginary parts of all quadri-products are equal up to their sign. We will use phase-invariant representations and formulae throughout this paper.

2 The Unitarity Triangle

The allowed region in the ρ and η space can be elegantly displayed by means of the Unitarity Triangle (UT) described by the *rescaled* unitarity relation between the first and the third column of the CKM matrix (i.e., corresponding to the B meson system)

$$\frac{V_{ud}V^*_{ub}}{V_{cd}V^*_{cb}} + \frac{V_{cd}V^*_{cb}}{V_{cd}V^*_{cb}} + \frac{V_{td}V^*_{tb}}{V_{cd}V^*_{cb}} = 0 \ . \tag{12}$$

Note that twice the area of the *non-rescaled* UT corresponds to the Jarlskog parameter J. This identity provides a geometrical interpretation of the phase convention invariance of J: a rotation of the CKM matrix rotates the UT accordingly while leaving its area, and hence J is invariant. It is the remarkable property of the UT in the B system that its three sides are governed by the same power of λ and A (so that the sides of the rescaled UT (12) are of order one), which predicts large CP-violating asymmetries in the B sector. As a comparison, the corresponding UT for the

$$\begin{aligned}
V_{us} &= \lambda - \frac{1}{2}A^2\lambda^7(\rho^2+\eta^2) \ , \\
V_{ub} &= A\lambda^3(\rho - i\eta) \ , \\
V_{cd} &= -\lambda + \frac{1}{2}A^2\lambda^5\left(1-2(\rho+i\eta)\right) + \frac{1}{2}A^2\lambda^7(\rho+i\eta) \ , \\
V_{cs} &= 1 - \frac{1}{2}\lambda^2 - \frac{1}{8}\lambda^4(1+4A^2) - \frac{1}{16}\lambda^6\left(1-4A^2+16A^2(\rho+i\eta)\right) - \frac{1}{128}\lambda^8\left(5-8A^2+16A^4\right) \ , \\
V_{cb} &= A\lambda^2 - \frac{1}{2}A^3\lambda^8\left(\rho^2+\eta^2\right) \ , \\
V_{td} &= A\lambda^3\left(1-\rho-i\eta\right) + \frac{1}{2}A\lambda^5(\rho+i\eta) + \frac{1}{8}A\lambda^7(1+4A^2)(\rho+i\eta) \ , \\
V_{ts} &= -A\lambda^2 + \frac{1}{2}A\lambda^4\left(1-2(\rho+i\eta)\right) + \frac{1}{8}A\lambda^6 + \frac{1}{16}A\lambda^8\left(1+8A^2(\rho+i\eta)\right) \ , \\
V_{tb} &= 1 - \frac{1}{2}A^2\lambda^4 - \frac{1}{2}A^2\lambda^6\left(\rho^2+\eta^2\right) - \frac{1}{8}A^4\lambda^8 \ .
\end{aligned}$$

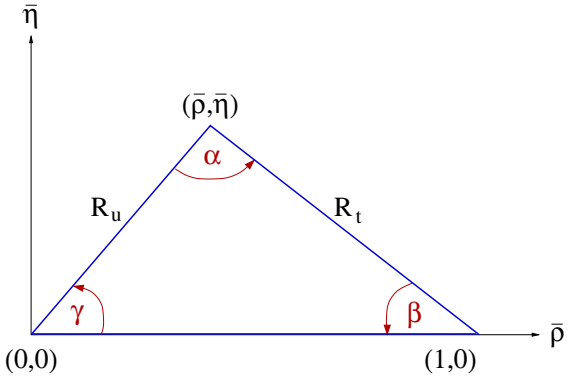

Fig. 1. The rescaled Unitarity Triangle in the Wolfenstein parameterization

kaon sector is heavily flattened

$$0 = \frac{V_{ud}V_{us}^*}{V_{cd}V_{cs}^*} + \frac{V_{cd}V_{cs}^*}{V_{cd}V_{cs}^*} + \frac{V_{td}V_{ts}^*}{V_{cd}V_{cs}^*} \sim O\left(\frac{\lambda}{\lambda}\right) + O\left(1\right) + O\left(\frac{A^2\lambda^5}{\lambda}\right) \ , \tag{13}$$

exhibiting small CP asymmetries. The UT (12) is sketched in Fig. 1 in the complex $(\overline{\rho}, \overline{\eta})$ plane, where the apex is given by the following phase-convention independent definition, to all orders in λ [4],

$$\overline{\rho} + i\overline{\eta} \ \equiv \ -\frac{V_{ud}V_{ub}^*}{V_{cd}V_{cb}^*} \ , \tag{14}$$

of which the inverse reads to all orders[5]

$$\rho + i\eta \ = \ \frac{\sqrt{1 - A^2\lambda^4}(\overline{\rho} + i\overline{\eta})}{\sqrt{1-\lambda^2}\left[1 - A^2\lambda^4(\overline{\rho} + i\overline{\eta})\right]} \ . \tag{17}$$

Equation (17) is the definition used in CKMfitter. The sides R_u and R_t of the UT (the third side being normalized to unity) read to all orders

$$R_u = \left|\frac{V_{ud}V_{ub}^*}{V_{cd}V_{cb}^*}\right| \ = \ \sqrt{\overline{\rho}^2 + \overline{\eta}^2} \ , \tag{18}$$

$$R_t = \left|\frac{V_{td}V_{tb}^*}{V_{cd}V_{cb}^*}\right| \ = \ \sqrt{(1-\overline{\rho})^2 + \overline{\eta}^2} \ . \tag{19}$$

The three angles, $\alpha,\ \beta,\ \gamma$, of the UT are defined by

$$\alpha = \arg\left[-\frac{V_{td}V_{tb}^*}{V_{ud}V_{ub}^*}\right] \ , \quad \beta = \arg\left[-\frac{V_{cd}V_{cb}^*}{V_{td}V_{tb}^*}\right] \ , \quad \gamma = \arg\left[-\frac{V_{ud}V_{ub}^*}{V_{cd}V_{cb}^*}\right] \ , \tag{20}$$

and the CKM phase in the Standard Parameterization (6) reads $\delta = \gamma + A^2\lambda^4\eta + \mathcal{O}(\lambda^6)$. The relations between the angles and the $\overline{\rho}$, $\overline{\eta}$ coordinates, again to all orders in λ, are given by

$$\cos\gamma = \overline{\rho}/R_u \ , \quad \sin\gamma = \overline{\eta}/R_u \ , \tag{21}$$

$$\cos\beta = (1-\overline{\rho})/R_t \ , \quad \sin\beta = \overline{\eta}/R_t \ , \tag{22}$$

$$\alpha = \pi - \beta - \gamma \ . \tag{23}$$

A graphical compilation of the most relevant present and future constraints (without errors) is displayed in Fig. 2. Some "standard" values for the theoretical parameters are used for this exercise in order to reproduce compatibility between the constraints.

Over-constraining the unitary CKM matrix aims at validating the three-generation SM. The interpretation of these constraints requires a robust statistical framework which protects against misleading conclusions. The following part describes the statistical approach applied for the analysis reported in this work.

[5] Expanding (14) in λ gives [4]

$$\overline{\rho} = \rho - \frac{1}{2}\rho\lambda^2 + \left(\frac{1}{2}A^2\rho - \frac{1}{8}\rho - A^2\left(\rho^2 - \eta^2\right)\right)\lambda^4 + \mathcal{O}(\lambda^6) \ , \tag{15}$$

$$\overline{\eta} = \eta - \frac{1}{2}\eta\lambda^2 + \left(\frac{1}{2}A^2\eta - \frac{1}{8}\eta - 2A^2\rho\eta\right)\lambda^4 + \mathcal{O}(\lambda^6) \ . \tag{16}$$

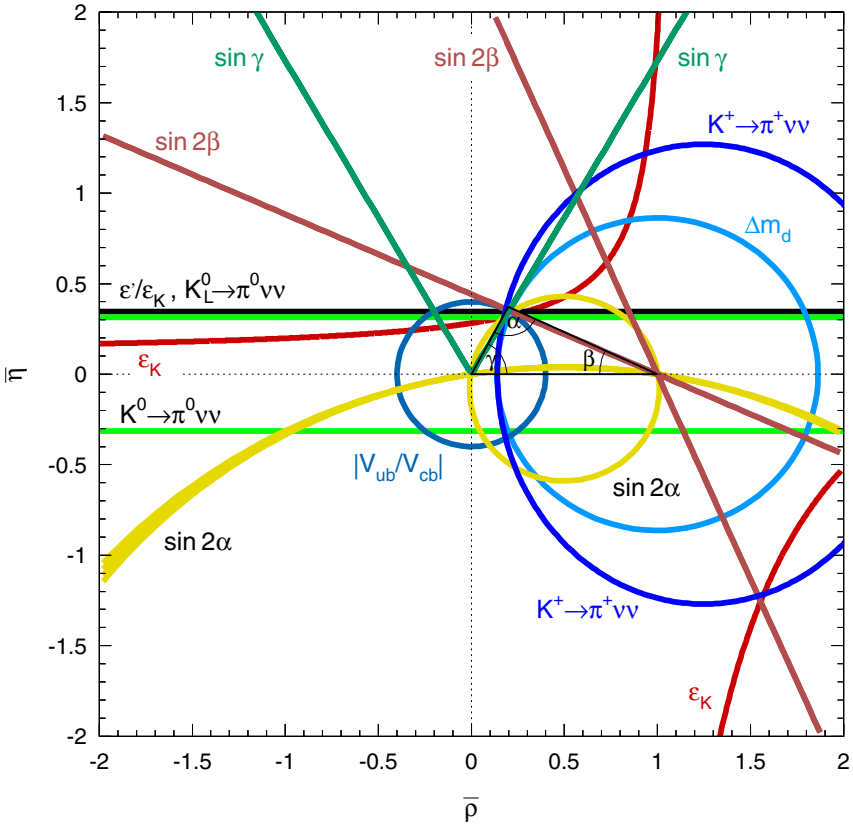

Fig. 2. Constraints in the unitarity plane for the most relevant observables. The theoretical parameters used correspond to some "standard" set chosen to reproduce compatibility between the observables

Part II
The statistical approach *R*fit

The statistical analysis performed in this paper is entirely based on the *frequentist* approach *R*fit described in detail in [6] and recalled below.

We consider an analysis involving a set of $N_{\rm exp}$ measurements collectively denoted by $x_{\rm exp} = \{x_{\rm exp}(1), \ldots, x_{\rm exp}(N_{\rm exp})\}$, described by a set of corresponding theoretical expressions $x_{\rm theo} = \{x_{\rm theo}(1), \ldots, x_{\rm theo}(N_{\rm exp})\}$. The theoretical expressions $x_{\rm theo}$ are functions of a set of $N_{\rm mod}$ parameters $y_{\rm mod} = \{y_{\rm mod}(1), \ldots, y_{\rm mod}(N_{\rm mod})\}$. Their precise definition is irrelevant for the present discussion (cf. Sect. III.2 for details) besides the fact that:

- a subset of $N_{\rm theo}$ parameters within the $y_{\rm mod}$ set are fundamental and free parameters of the theory (i.e., the four CKM unknowns in the SM, the top quark mass, etc.); these are denoted $y_{\rm theo}$, where $y_{\rm theo} = \{y_{\rm theo}(1), \ldots, y_{\rm theo}(N_{\rm theo})\}$.
- the remaining $N_{\rm QCD} = N_{\rm mod} - N_{\rm theo}$ parameters are due to our present inability to compute precisely strong interaction quantities (e.g., f_{B_d}, B_d, etc.), and are denoted $y_{\rm QCD}$, where $y_{\rm QCD} = \{y_{\rm QCD}(1), \ldots, y_{\rm QCD}(N_{\rm QCD})\}$.

There are three different goals of the global CKM analysis:

1. within the SM, to quantify the agreement between data and the theory, as a whole.
2. within the SM, to achieve the best estimate of the $y_{\rm theo}$ parameters: that is to say to perform a careful metrology of the theoretical parameters.
3. within an extended theoretical framework, e.g. Supersymmetry, to search for specific signs of New Physics by quantifying the agreement between data and the extended theory, and by pinning down additional fundamental and free parameters of the extended theory.

These goals imply three distinct statistical treatments all of which rely on a likelihood function meant to gauge the agreement between data and theory.

1 The likelihood function

We adopt a χ^2-like notation and denote

$$\chi^2(y_{\rm mod}) \equiv -2\ln(\mathcal{L}(y_{\rm mod}))\ , \tag{24}$$

where the likelihood function, $\mathcal{L}$ (defined below), is the product of two contributions:

$$\mathcal{L}(y_{\rm mod}) = \mathcal{L}_{\rm exp}(x_{\rm exp} - x_{\rm theo}(y_{\rm mod})) \cdot \mathcal{L}_{\rm theo}(y_{\rm QCD}) \ . \tag{25}$$

The first term, the experimental likelihood $\mathcal{L}_{\rm exp}$, measures the agreement between $x_{\rm exp}$ and $x_{\rm theo}$, while the second term, the theoretical likelihood $\mathcal{L}_{\rm theo}$, expresses our present knowledge of the $y_{\rm QCD}$ parameters.

It has to be recognized from the outset that the χ^2 of (24) is a quantity that can be misleading. In general, using "Prob" the well known routine from the CERN library, one *cannot* infer a confidence level (CL) from the above χ^2 value using

$$\begin{aligned} {\rm CL} &= {\rm Prob}(\chi^2(y_{\rm mod}), N_{\rm dof}) \ , & (26)\\ &= \frac{1}{\sqrt{2^{N_{\rm dof}}}\Gamma(N_{\rm dof}/2)} \int\limits_{\chi^2(y_{\rm mod})}^{\infty} e^{-t/2} t^{N_{\rm dof}/2-1}\, dt \ . & (27) \end{aligned}$$

This is because neither $\mathcal{L}_{\rm exp}$ nor $\mathcal{L}_{\rm theo}$ (they are further discussed in the sections below) are built from purely Gaussian measurements.

- In most cases $\mathcal{L}_{\rm exp}$ should handle experimental systematics, and, in some instance, it has to account for inconsistent measurements.
- In practice, $\mathcal{L}_{\rm theo}$ relies on hard to quantify educated guesswork, akin to experimental systematic errors, but in most cases even less well defined.

The first limitation is not specific to the present analysis and is not the main source of concern. The second limitation is more challenging: its impact on the analysis is particularly strong with the data presently available. The statistical treatment *R*fit is designed to cope with both of the above limitations. Notwithstanding its attractive features, the *R*fit scheme does not offer a treatment of the problem at hand free from any assumption: an ill-defined problem cannot be dealt with rigorously. However the *R*fit scheme extracts the most out of simple and clear-cut *a priori* assumptions.

1.1 The experimental likelihood

The experimental component of the likelihood is given by the product

$$\mathcal{L}_{\rm exp}(x_{\rm exp} - x_{\rm theo}(y_{\rm mod})) = \prod_{i,j=1}^{N_{\rm exp}} \mathcal{L}_{\rm exp}(i,j) \ , \tag{28}$$

where the $N_{\rm exp}$ individual likelihood components $\mathcal{L}_{\rm exp}(i,j)$ account for measurements that may be independent or not.

Ideally, the **likelihood components** $\mathcal{L}_{\rm exp}(i)$ are independent Gaussians

$$\mathcal{L}_{\rm exp}(i) = \frac{1}{\sqrt{2\pi}\sigma_{\rm exp}(i)} \exp\left[-\frac{1}{2}\left(\frac{x_{\rm exp}(i) - x_{\rm theo}(i)}{\sigma_{\rm exp}(i)}\right)^2\right] \ , \tag{29}$$

each with a standard deviation given by the experimental statistical uncertainty $\sigma_{\rm exp}(i)$ of the $i^{\rm th}$ measurement. However, in practice, one has to deal with correlated measurements and with additional experimental and theoretical systematic uncertainties.

- *Experimental systematics* are assumed to take the form of a possible biasing offset the measurement could be corrected, were it known. Their precise treatment is discussed in Sect. II.6. In practice, these systematics are usually added in quadrature to the statistical errors.
- *Theoretical systematics*, when they imply small effects, are treated as the experimental ones. However because most theoretical systematics imply large effects and affect in a non-linear way the $x_{\rm theo}$ prediction, most of them are dealt with through the theoretical likelihood component $\mathcal{L}_{\rm theo}$ (cf. Sect. II.1.2).

Identical observables and consistency: when several measurements refer to the same observable (e.g., various measurements of Δm_d) they have to be consistent, independently of the theoretical framework used for the analysis. Similarly, when several measurements refer to different observables that are linked to the same $y_{\rm theo}$ parameter, e.g., $|V_{ud}|$ and $|V_{us}|$, or determinations of $|V_{ub}|$ stemming from different observables, or measurements of $\sin 2\beta$ obtained from similar B decays, one may *decide* to overrule possible disagreement by requiring the measurements to be consistent. By doing so, one is deliberately blinding oneself to possible New Physics effects, which may have revealed themselves

otherwise. Clearly, such overruling should be applied with great caution, and it should be well advertized whenever it occurs. The method to deal with this *imposed* consistency is to account for the measurements simultaneously by merging them into a single component, and applying an "appropriate" rescaling method.

The **normalization** of each individual likelihood component is chosen such that its maximal value is equal to one. This is not important for the analysis, but it is convenient: it ensures that a measurement does not contribute numerically to the overall χ^2 value if it is in the best possible agreement with theory, and that the (so-called) χ^2 takes only positive values. In the pure Gaussian case, this simply implies dropping the normalization constant of (29): one then recovers the standard χ^2 definition.

1.2 The theoretical likelihood

The theoretical component of the likelihood is given by the product

$$\mathcal{L}_{\rm theo}(y_{\rm QCD}) = \prod_{i=1}^{N_{\rm QCD}} \mathcal{L}_{\rm theo}(i) \ , \tag{30}$$

where the individual components $\mathcal{L}_{\rm theo}(i)$ account for the imperfect knowledge of the $y_{\rm QCD}$ parameters (e.g., f_{B_d}) while more or less accurately including known correlations between them (e.g., f_{B_d}/f_{B_s}). Ideally, one should incorporate in $\mathcal{L}_{\rm exp}$ measurements from which constraints on $y_{\rm QCD}$ parameters can be derived. By doing so, one could remove altogether the theoretical component of the likelihood. However usually there is no such measurement: the *a priori* knowledge on the $y_{\rm QCD}$ stems rather from educated guesswork. As a result, the $\mathcal{L}_{\rm theo}(i)$ components are incorporated by hand in (30) and they can hardly be treated as probability distribution functions (PDF). In effect, their mere presence in the discussion is a clear sign that the problem at hand is ill-defined. It demonstrates that here, a critical piece of information is coming neither from experimental, nor from statistically limited computations, but from the minds of physicists. At present, these components play a leading role in the analysis and it is mandatory to handle them with the greatest caution.

In the default scheme, **Range Fit (*R*fit)**, we propose that the theoretical likelihoods $\mathcal{L}_{\rm theo}(i)$ do not contribute to the χ^2 of the fit while the corresponding $y_{\rm QCD}$ parameters take values within allowed ranges[6] denoted $[y_{\rm QCD}]$. The numerical derivation of these ranges is discussed in Sects. II.6 and III.2. Most of them are identified to the ranges

$$[y_{\rm QCD} - \sigma_{\rm syst} \ , y_{\rm QCD} + \sigma_{\rm syst}] \ , \tag{31}$$

where $\sigma_{\rm syst}$ is the theoretical systematics evaluated for $y_{\rm QCD}$. Hence $y_{\rm QCD}$ values are treated on an equal footing, irrespective of how close they are to the edges of the allowed range. Instances where even only one of the $y_{\rm QCD}$ parameters lies outside its nominal range are not considered.

This is the unique, simple and clear-cut assumption made in the *R*fit scheme: $y_{\rm QCD}$ parameters are bound to remain within *predefined* allowed ranges. The *R*fit scheme departs from a perfect frequentist analysis only because the allowed ranges $[y_{\rm QCD}]$ do not extend to the whole physical space where the parameters could *a priori* take their values[7].

This unique and minimal assumption, is nevertheless a strong constraint: all the results obtained should be understood as valid only if all the assumed allowed ranges contain the true values of their $y_{\rm QCD}$ parameters. However, there is no guarantee that this is the case, and this arbitrariness should be kept in mind.

2 Metrology

For metrology, one is not interested in the quality of the agreement between data and the theory as a whole. Rather, taking for granted that the theory is correct, one is only interested in the quality of the agreement between data and various realizations of the theory, specified by distinct sets of $y_{\rm mod}$ values. More precisely, as discussed in Sect. II.2.1, the realizations of the theory one considers are under-specified by various subsets of so-called relevant parameter values. In the following we denote

$$\chi^2_{{\rm min};y_{\rm mod}} \ , \tag{32}$$

the absolute minimum value of the χ^2 function of (24), obtained when letting all $N_{\rm mod}$ parameters free to vary.

[6] Note that the $y_{\rm QCD}$ parameters can also have errors with (partly) statistical components. Examples for these are parameters obtained by Lattice calculations. The treatment of this case is described in Sect. II.6.

[7] Not all $y_{\rm QCD}$ parameters need to be given an *a priori* allowed range, e.g., values taken by final state strong interaction phases appearing in B decays are not necessarily theoretically constrained.

In principle, this absolute minimum value does not correspond to a unique $y_{\rm mod}$ location. This is because the theoretical predictions used for the analysis are affected by more or less important theoretical systematics. Since these systematics are being handled by means of allowed ranges, there is always a multi-dimensional degeneracy for any value of χ^2.

For metrological purposes one should attempt to estimate as best as possible the complete $y_{\rm mod}$ set. In that case, we use the offset-corrected χ^2

$$\Delta\chi^2(y_{\rm mod}) = \chi^2(y_{\rm mod}) - \chi^2_{{\rm min};y_{\rm mod}} \ , \tag{33}$$

where $\chi^2(y_{\rm mod})$ is the χ^2 for a given set of model parameters $y_{\rm mod}$. The minimum value of $\Delta\chi^2(y_{\rm mod})$ is zero, by construction. This ensures that, to be consistent with the assumption that the SM is correct, CLs equal to unity are obtained when exploring the $y_{\rm mod}$ space.

A necessary condition is that the CL constructed from $\Delta\chi^2(y_{\rm mod})$ provides correct coverage, that is, the CL interval for a parameter under consideration covers the true parameter value with a frequency of $1-{\rm CL}$ if the measurement(s) were repeated many times. This issue will be further adressed in several subsections.

2.1 Relevant and less relevant parameters

Usually, one does not aim at a metrology of all the $y_{\rm mod}$ values, but only in a subset of them. This can be for two distinct reasons:

- the other parameters being deemed less relevant. For instance, in the SM, *CP* violation can be summarized by the value taken by the Jarlskog parameter J, or by the value of the *CP*-violating phase determined by the parameters ρ and η in the Wolfenstein parameterization: the other CKM parameters and the $y_{\rm QCD}$ parameters may thus conceivably be considered of lower interest.
- parameters that cannot be significantly constrained by the input data of the CKM fit. This is the case for most of the non-CKM parameters: $y_{\rm QCD}$ parameters, but also the quark masses, etc.

In practice, the $y_{\rm mod}$ parameters often retained as relevant for the discussion are $\overline{\rho}$ and $\overline{\eta}$. The other parameters λ, A, the quark masses (etc.) and all the $y_{\rm QCD}$ are considered as subsidiary parameters, to be taken into account in the analysis, but irrelevant for the discussion[8]. In that case, the aim of the metrological stage of the analysis is to set CLs in the $(\overline{\rho},\overline{\eta})$ plane.

We denote by a the subset of N_a parameters under discussion (e.g., $a=\{\overline{\rho},\,\overline{\eta}\}$) and μ the N_μ remaining $y_{\rm mod}$ parameters[9]. *The goal is to set CLs in the a space, irrespective of the μ values.*

The smaller the region in the a space where the CL is sizable (above ${\rm CL}_{\rm cut}=0.05$, say) the stronger the constraint is. The ultimate (and unattainable) goal is to shrink the allowed region to a point: it would then correspond to the 'true' a. This means that one seeks to exclude the largest possible region of the a space. To do so, for a fixed value of a, one has to find the μ values that maximize the agreement between data and theory, and set the CL on a at the value corresponding to this optimized μ

$${\rm CL}(a) = {\rm Max}_\mu\{{\rm CL}(a,\mu)\} \ . \tag{34}$$

Proceeding that way, one uses the most conservative estimate for a given a point: this point will be engulfed in the excluded region only if ${\rm CL}(a,\mu)<{\rm CL}_{\rm cut}$, $\forall\mu$. As long as the theoretical likelihoods contain the true value of the $y_{\rm QCD}$ parameters, the CL obtained has correct coverage and is to be understood as an upper limit of a CL.

2.2 Metrology of relevant parameters

According to the above discussion, we denote

$$\chi^2_{{\rm min};\,\mu}(a) \ , \tag{35}$$

the minimum value of the χ^2 function of (24), for a fixed value of a, when letting all μ parameters free to vary. For metrological purposes, we use the offset-corrected χ^2

$$\Delta\chi^2(a) = \chi^2_{{\rm min};\,\mu}(a) - \chi^2_{{\rm min};y_{\rm mod}} \ , \tag{36}$$

the minimum value of which is zero, by construction.

[8] This point of view does not mean that the role of the $y_{\rm QCD}$ is irrelevant. In particular, if the agreement between data and theory is not convincing one needs to set CLs in the $y_{\rm QCD}$ space.

[9] It is worth stressing that this splitting is arbitrary and that it can be changed at will: for instance one may decide to focus only on $a=\{J\}$, or to consider $a=\{\sin 2\alpha,\,\sin 2\beta\}$ or other experimental observables. In practice, constraints on observables that are functions of the $y_{\rm mod}$ parameters are obtained by means of the technique of *Lagrange multipliers*.

2.2.1 Gaussian case

In a Gaussian situation, one directly obtains the CL for a as

$$\mathrm{CL}(a) = \mathcal{P}(a) = \mathrm{Prob}(\Delta\chi^2(a), N_{\mathrm{dof}}) \ , \tag{37}$$

where $N_{\mathrm{dof}} = \min(N_{\mathrm{exp}}^{\mathrm{eff}} - N_\mu, N_a)$ and $N_{\mathrm{exp}}^{\mathrm{eff}}$ is the effective number of constraints (observables).

To illustrate the use of N_{dof}, let us first consider the standard CKM fit (see Part III). Several observables constrain the $(\overline{\rho},\overline{\eta})$ plane so that the number of degrees of freedom exceeds the dimension of the a space (N_a). The offset-corrected $\Delta\chi^2(a)$, defined in (36), reduces the number of degrees of freedom to the dimension $N_a = 2$ of the $(\overline{\rho},\overline{\eta})$ plane. However if one is to consider the constraint of only one observable, e.g., $\sin 2\beta$ in the $(\overline{\rho},\overline{\eta})$ plane, the number of degrees of freedom is one, i.e., it is smaller than the dimension of the a space. Indeed, given $\sin 2\beta$ and, e.g., $\overline{\rho}$, the value of $\overline{\eta}$ is fixed.

Other cases exist where the situation is less clear-cut: for instance, in the presence of penguins, the $C_{\pi\pi}^{+-}$ parameters in $B^0 \to \pi^+\pi^-$ decays may be non-zero and hence acquires some information on the unitarity angle α. One would thus conclude that the appropriate number of degrees of freedom should be $N_{\mathrm{dof}} = 2$. However in comparison with the $S_{\pi\pi}^{+-}$ parameter, the α constraint from $C_{\pi\pi}^{+-}$ is insignificant, so that using $N_{\mathrm{dof}} = 1$ is the better approximation. One concludes that even in a Gaussian case, ill-posed problems can occur, which must be individually studied with (toy) Monte Carlo simulation.

2.2.2 Non-Gaussian case

In a non-Gaussian situation, one has to consider $\Delta\chi^2(a)$ as a test statistic, and one must rely on a Monte Carlo simulation to obtain its expected distribution in order to compute $\mathrm{CL}(a)$. As further discussed in Sect. II.3, this does not imply taking a Bayesian approach and to make use of PDFs for the unknown theoretical parameters μ.

For the sake of simplicity, we use (37) in the present work with one exception discussed below. This implies that the experimental component $\mathcal{L}_{\mathrm{exp}}(x_{\mathrm{exp}} - x_{\mathrm{theo}}(y_{\mathrm{mod}}))$ is free from non Gaussian contributions and inconsistent measurements. However the $\Delta\chi^2(a)$ function itself does not have to be parabolic. What matters is that the $\mathcal{L}_{\mathrm{exp}}$ components are derived from Gaussian measurements, being understood that no $\mathcal{L}_{\mathrm{theo}}$ components are present. Applying (37) using $\mathcal{L}_{\mathrm{exp}}$ may lead to an under-coverage of the CL for a branching fraction measurement with a very small number of signal events. That is, the interval belonging to a given CL value constructed in this way covers the true branching fraction value with a probability lower than $1 - \mathrm{CL}$.

Under the assumption that the measurement is free from background, the probability to measure N_{obs} events for a true number of N_{true} events is given by the Poissonian probability distribution

$$f(N_{\mathrm{obs}}; N_{\mathrm{true}}) \ = \ \frac{e^{-N_{\mathrm{true}}} N_{\mathrm{true}}^{N_{\mathrm{obs}}}}{N_{\mathrm{obs}}!} \ . \tag{38}$$

One prominent example is the measurement of $N_{\mathrm{obs}} = 2$ rare $K^+ \to \pi^+\nu\bar{\nu}$ events with almost vanishing background probability by the E787 collaboration [15] (see Sect. IV.2, ignoring the recent result from E949 [16] in the discussion here). In this case, the experimental likelihood $\mathcal{L}_{\mathrm{exp}}(N_{\mathrm{true}})$ for a true number of N_{true} events given the number of N_{obs} observed events is the same equation (38). The corresponding CL is obtained by means of the following recipe.

1. In the pure Poissonian case, the exact central confidence interval $[a,b]$ at $\mathrm{CL} = 2\alpha$ with probabilities $P(n \geq N_{\mathrm{obs}}; a) = \sum_{n=N_{\mathrm{obs}}}^{\infty} f(n;a) = \alpha$ and $P(n \leq N_{\mathrm{obs}}; b) = \sum_{n=0}^{N_{\mathrm{obs}}} f(n;b) = \alpha$ is obtained by solving the following equations for a and b, respectively:

$$\alpha = \sum_{n=N_{\mathrm{obs}}}^{\infty} \frac{e^{-a}a^n}{n!} \ = \ 1 - \sum_{n=0}^{N_{\mathrm{obs}}-1} \frac{e^{-a}a^n}{n!} \ , \tag{39}$$

$$\beta = \sum_{n=0}^{N_{\mathrm{obs}}} \frac{e^{-b}b^n}{n!} \ . \tag{40}$$

Their inverse reads

$$a = \frac{1}{2} F_{\chi^2}^{-1}(\alpha; N_{\mathrm{dof}} = 2N_{\mathrm{obs}}) \ , \tag{41}$$

$$b = \frac{1}{2} F_{\chi^2}^{-1}(1-\alpha; N_{\mathrm{dof}} = 2(N_{\mathrm{obs}}+1)) \ , \tag{42}$$

where F_{χ^2} is the cumulative distribution for a χ^2 distribution for $N_{\rm dof}$ degrees of freedom. The quantities $F^{-1}_{\chi^2}$ can be calculated with the CERN library function CHISIN. Using (41) and (42) we construct the correct CL as a function of $N_{\rm true}$.
2. The experimental likelihood, $\mathcal{L}^{\rm inp}_{\rm exp}$, is obtained from the inverse $\mathrm{CL}^{-1} = \mathcal{P}^{-1}(-2\ln\mathcal{L}^{\rm inp}_{\rm exp}, 1)$. In this way, the CKM fit can again use (37) to infer a CL for the Poissonian case with very small statistics.

The situation becomes more complicated if the statistics is very small and, in addition, the amount of background is not negligible and possibly only known with limited precision. In this case, there are two possible ways to proceed. Either the experiment publishes a CL which then can be again translated into likelihood function using CL^{-1} (see above). This has been done, for example, by the BNL experiment E949 [16] (see Sect. IV.2) the successor of E747. Or, if this information is not available, the CL has to be constructed by means of a toy Monte Carlo simulation provided that the experimental information needed has been published.

2.2.3 Physical boundaries

Physical boundaries: in cases where the a value space is bounded, e.g., $\sin 2\beta \in [-1, 1]$, the confidence level $\mathcal{P}(a)$ is modified close to the boundaries, even in a Gaussian case. In general, the presence of physical boundaries improves the parameter knowledge. The easiest way to derive the appropriate CL is to use Monte Carlo techniques. The procedure is as follows:

1. choose the coordinate a_0 in the (bounded) a space at which the $\mathrm{CL}(a_0)$ shall be determined.
2. determine for the measurements at hand the offset-corrected $\Delta\chi^2(a_0)$ using (36).
3. generate Monte Carlo measurements that fluctuate according to the experimental likelihoods $\mathcal{L}_{\rm exp}$.
4. determine the global minimum $\chi^2_{{\rm min};y_{\rm mod}}$[MC] for each set of measurements by leaving all $y_{\rm mod}$ parameters free to vary.
5. determine the offset-corrected $\Delta\chi^2(a_0)$[MC] for each set of measurements using (36).
6. from the sample of Monte Carlo simulations, one builds $\mathcal{F}_{a_0}(\Delta\chi^2(a_0)[\mathrm{MC}])$, the distribution of $\Delta\chi^2(a_0)$[MC], normalized to unity.
7. the CL referring to the coordinate a_0 is then given by

$$\mathcal{P}(a_0) \;\leq \int\limits_{\Delta\chi^2 \geq \Delta\chi^2(a_0)} \mathcal{F}_{a_0}(\Delta\chi^2)\, d\Delta\chi^2 \;. \tag{43}$$

An illustration of the difference between a straight application of (37) and the accurate Monte Carlo result is given for various measurements of a hypothetical quantity $\sin(x)$ in Fig. 3. The effects can be significant close to the boundaries.

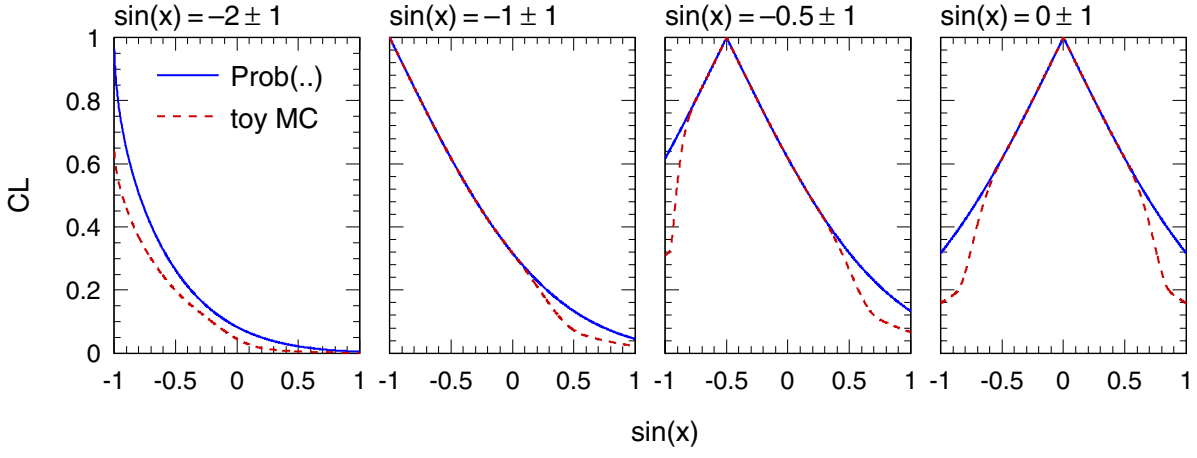

Fig. 3. Difference between (37) and a Monte Carlo evaluation of the confidence level for various measurements of a hypothetical quantity $\sin(x)$. The Monte Carlo evaluation takes into account the physical boundaries of the observable

The inclusion of the physical boundaries in a one-dimensional case is semi-analytically realized in CKMfitter as described in the digression below[10]. The results are identical to the toy Monte Carlo simulation technique introduced above.

[10] **Digression.** We consider a measurement $x_m \pm 1$ of an observable that is confined to the interval $[x_{\rm min}, x_{\rm max}]$, and derive the confidence level of a test value $x \in [x_{\rm min}, x_{\rm max}]$. The corresponding test statistic is given by

$$\Delta\chi^2 = \chi^2 - \chi^2_{\rm min} \ , \qquad \text{with} \qquad \chi^2 = (x - x_m)^2 \ , \tag{44}$$

and we aim at the solution of the convolution integral

$$\mathrm{CL}(x) = \frac{\int\limits_{\Delta\chi^2}^{\infty}\int\limits_{-\infty}^{\infty} \delta\left((x-x'_m)^2 - \Delta\chi^{2\prime}\right) \frac{1}{\sqrt{2\pi}} e^{-\frac{1}{2}(x'_m - x_m)^2} d\Delta\chi^{2\prime} dx'_m}{\int\limits_{0}^{\infty}\int\limits_{-\infty}^{\infty} \delta\left((x-x'_m)^2 - \Delta\chi^{2\prime}\right) \frac{1}{\sqrt{2\pi}} e^{-\frac{1}{2}(x'_m - x_m)^2} d\Delta\chi^{2\prime} dx'_m} \ . \tag{45}$$

The integration of (45) leads to multiple Heaviside step functions, so that several cases must be distinguished:

– **Measurement inside the allowed interval CL($x_{\rm min} \le x_m \le x_{\rm max}$):**
Using $\mathcal{P}(\chi^2) \equiv \mathrm{Prob}(\chi^2, 1) = \mathrm{erfc}(\sqrt{\chi^2/2})$ the CL obtained ignoring the possibly non-zero value of $\chi^2_{\rm min}$ (the χ^2 returned by the procedure below is offset-corrected into a $\Delta\chi^2$ for metrology reasons in CKMfitter), and denoting $P_x[x_1, x_2]$ the probability that x occurs in the range $[x_1, x_2]$ (taken to be negative if $x_1 > x_2$)

$$P_x[x_1, x_2] = \begin{cases} \frac{1}{2}\left(\mathrm{erfc}\left(|x-x_1|/\sqrt{2}\right) - \mathrm{erfc}\left(|x-x_2|/\sqrt{2}\right)\right) & \text{if } x < x_1 \ \wedge \ x < x_2 \\ \frac{1}{2}\left(\mathrm{erfc}\left(|x-x_2|/\sqrt{2}\right) - \mathrm{erfc}\left(|x-x_1|/\sqrt{2}\right)\right) & \text{if } x > x_1 \ \wedge \ x > x_2 \\ 1 - \frac{1}{2}\left(\mathrm{erfc}\left(|x-x_1|/\sqrt{2}\right) + \mathrm{erfc}\left(|x-x_2|/\sqrt{2}\right)\right) & \text{elsewhere} \end{cases} \tag{46}$$

one obtains for the different domains of x

$$\mathrm{CL} = \begin{cases} \mathcal{P}(\chi^2) & \text{if } \frac{1}{2}(x_m + x_{\rm min}) \le x \le \frac{1}{2}(x_m + x_{\rm max}) \\ \frac{1}{2}\mathcal{P}(\chi^2) & \text{if } (x = x_{\rm min} \ \vee \ x = x_{\rm max}) \ \wedge \ x \neq x_m \\ \mathcal{P}(\chi^2) - P_x\left[\frac{1}{2}\left(x + x_{\rm min} - \frac{(x-x_m)^2}{x - x_{\rm min}}\right), 2x - x_m\right] & \text{if } x < \frac{1}{2}(x_m + x_{\rm min}) \\ \mathcal{P}(\chi^2) - P_x\left[2x - x_m, \frac{1}{2}\left(x + x_{\rm max} - \frac{(x-x_m)^2}{x - x_{\rm max}}\right)\right] & \text{if } x > \frac{1}{2}(x_m + x_{\rm max}) \end{cases} \tag{47}$$

– **Measurement below the allowed interval CL($x_m < x_{\rm min}$):**

$$\mathrm{CL} = \begin{cases} 1 & \text{if } x = x_{\rm min} \\ \mathcal{P}(\chi^2) - P_x\left[2x - x_m, x + \sqrt{\Sigma}\right] & \text{if } \left\{ \begin{array}{l} x_{\rm min} < x \le \frac{1}{2}(x_{\rm min} + x_{\rm max}) \ \wedge \\ x + x_{\rm min} + \frac{(x_{\rm max} - x)^2}{x_{\rm min} - x} \le 2x_m \end{array} \right\} \\ \mathcal{P}(\chi^2) - P_x\left[\left[2x - x_m, \frac{1}{2}\left(x + x_{\rm max} + \frac{\Sigma}{x_{\rm max} - x}\right)\right]\right. & \text{if } \left\{ \begin{array}{l} x_{\rm min} < x \le \frac{1}{2}(x_{\rm min} + x_{\rm max}) \ \wedge \\ x + x_{\rm min} + \frac{(x_{\rm max} - x)^2}{x_{\rm min} - x} > 2x_m \end{array} \right\} \\ \mathcal{P}(\chi^2) - P_x\left[2x - x_m, \frac{1}{2}\left(x + x_{\rm max} + \frac{\Sigma}{x_{\rm max} - x}\right)\right] & \text{if } x > \frac{1}{2}(x_{\rm min} + x_{\rm max}) \end{cases} \tag{48}$$

where $\Sigma \equiv (x + x_{\rm min} - 2x_m)(x - x_{\rm min})$.

– **Measurement above the allowed interval CL($x_m > x_{\rm max}$):**

$$\mathrm{CL} = \begin{cases} 1 & \text{if } x = x_{\rm max} \\ \mathcal{P}(\chi^2) - P_x\left[x - \sqrt{\Xi}, 2x - x_m\right] & \text{if } \left\{ \begin{array}{l} \frac{1}{2}(x_{\rm min} + x_{\rm max}) \le x < x_{\rm max} \ \wedge \\ x + x_{\rm max} + \frac{(x_{\rm min} - x)^2}{x_{\rm max} - x} \ge 2x_m \end{array} \right\} \\ \mathcal{P}(\chi^2) - P_x\left[\frac{1}{2}\left(x + x_{\rm min} + \frac{\Xi}{x_{\rm min} - x}\right), 2x - x_m\right] & \text{if } \left\{ \begin{array}{l} \frac{1}{2}(x_{\rm min} + x_{\rm max}) \le x < x_{\rm max} \ \wedge \\ x + x_{\rm max} + \frac{(x_{\rm min} - x)^2}{x_{\rm max} - x} < 2x_m \end{array} \right\} \\ \mathcal{P}(\chi^2) - P_x\left[\frac{1}{2}\left(x + x_{\rm min} + \frac{\Xi}{x_{\rm max} - x}\right), 2x - x_m\right] & \text{if } x < \frac{1}{2}(x_{\rm min} + x_{\rm max}) \end{cases} \tag{49}$$

where $\Xi \equiv (2x_m - x - x_{\rm max})(x_{\rm max} - x)$.

3 Probing the Standard Model

By construction, the metrological phase is unable to detect if the SM fails to describe the data. This is because (36) wipes out the information contained in $\chi^2_{\mathrm{min};y_{\mathrm{mod}}}$. This value is a measure (a test statistics) of the best possible agreement between data and theory. The agreement can be quantified by the so-called p-value $\mathcal{P}(\chi^2_{\mathrm{min};y_{\mathrm{mod}}}|\mathrm{SM})$: the probability to observe a χ^2 as large as or larger than $\chi^2_{\mathrm{min};y_{\mathrm{mod}}}$ if the Standard Model is the correct theory. Ideally, in a pure Gaussian case, $\chi^2_{\mathrm{min};y_{\mathrm{mod}}}$ could be turned easily into a p-value referring to the SM as a whole in a straightforward way

$$\mathcal{P}(\chi^2_{\mathrm{min};y_{\mathrm{mod}}}|\mathrm{SM}) \leq \mathrm{Prob}(\chi^2_{\mathrm{min};y_{\mathrm{mod}}}, N_{\mathrm{dof}}) \ , \tag{50}$$

with $N_{\mathrm{dof}} = N^{\mathrm{eff}}_{\mathrm{exp}} - N_{\mathrm{mod}}$, if it were a positive value. The whole Standard Model being at stake, one should not rely on (50), but use a Monte Carlo simulation to obtain the expected distribution of $\chi^2_{\mathrm{min};y_{\mathrm{mod}}}$. The Monte Carlo simulation proceeds as follows:

1. determine for the measurements at hand the global minimum $\chi^2_{\mathrm{min};y_{\mathrm{mod}}}$ and the corresponding y_{mod} values, which are assumed to be the true ones[11]
2. generate the $x_{\mathrm{exp}}(i)$ for all measurements (i), following the individual experimental likelihood components $\mathcal{L}_{\mathrm{exp}}(i)$, having reset their central values to the values $x_{\mathrm{exp}}(i) = x_{\mathrm{theo}}(i)$ computed with the above y_{mod} solution set.
3. in contrast to the above, the $\mathcal{L}_{\mathrm{theo}}$ component of the likelihood is not modified: their central values are kept to their original settings. This is because these central values are not random numbers, but parameters contributing to the definition of $\mathcal{L}$.
4. compute the minimum of the χ^2 by allowing all y_{mod} to vary freely, as is done in the actual data analysis.
5. from this sample of Monte Carlo simulations, one builds $\mathcal{F}_{\mathrm{SM}}(\chi^2)$, the distribution of $\chi^2_{\mathrm{min};y_{\mathrm{mod}}}$, normalized to unity.
6. the p-value referring to the SM as a whole is then

$$\mathcal{P}(\chi^2_{\mathrm{min};y_{\mathrm{mod}}}|\mathrm{SM}) \ \leq \int\limits_{\chi^2 \geq \chi^2_{\mathrm{min};y_{\mathrm{mod}}}} \mathcal{F}_{\mathrm{SM}}(\chi^2)\ d\chi^2 \ . \tag{51}$$

4 Probing New Physics

If the above analysis establishes that the SM cannot accommodate the data, that is the p-value $\mathcal{P}(\chi^2_{\mathrm{min};y_{\mathrm{mod}}}|\mathrm{SM})$ is small, the next step is to probe the New Physics (NP) revealed by the observed discrepancy. The goal is akin to metrology: it is to measure new physical parameters y_{NP} (whose values, for example, are null if the SM holds) complementing the set of y_{theo} parameters of the SM. The treatment is identical to the one of Sect. II.2, using $a = \{y_{\mathrm{NP}}\}$. The outcome of the analysis is for example a 95% CL domain of allowed values for y_{NP} defined, in a first approximation, from (37)

$$\mathrm{CL}(y_{\mathrm{NP}}) = \mathrm{Prob}(\Delta\chi^2(y_{\mathrm{NP}}), N_{\mathrm{NP}}) \geq 0.05 \ . \tag{52}$$

Even if the SM cannot be said to be in significant disagreement with data, it remains worthwhile to perform this metrology of new NP for the following reasons:

- it might be able to faster detect the first signs of a discrepancy between data and the SM if the theoretical extension used in the analysis turns out to be the right one. The two approaches are complementary, the first (cf., Sect. II.3) leading to a general statement about the agreement between data and the SM independently of any assumption about the NP, the second being specific to a particular extension of the SM. In that sense, it is less satisfactory. The two approaches can nevertheless disagree: the first may conclude that the SM is in acceptable agreement with data, while the second may exclude the SM value $y_{\mathrm{NP}} = 0$, and, conversely, the first may invalidate the SM, while the second may lead to a fairly good value of $\mathrm{CL}(y_{\mathrm{NP}} = 0)$ if the extension of the SM under consideration is not on the right track.
- the most sensitive observables, and the precision to be aimed at for their determination cannot be derived by any other means than by this type of analysis. When considering new experiments, it is therefore particularly valuable to have a sensitive model of NP, to prioritize the effort and set the precision to be achieved.

[11] As discussed above, in the presence of theoretical uncertainties various y_{mod} realizations may yield identical theoretical predictions. The choice made for a particular y_{mod} solution (leading to $\chi^2_{\mathrm{min};y_{\mathrm{mod}}}$) is irrelevant.

5 Alternative statistical treatments

Several alternative statistical treatments are available and the reader is referred to [6] for a detailed discussion of the merits and drawbacks of each of the methods. In the following, we only recall the *ER*fit method as a conservative extension to *R*fit, and briefly comment on the use of Bayesian methods.

5.1 The extended conservative method (*ER*fit)

The *R*fit scheme uses $\mathcal{L}_{\rm theo}(i)$ functions that take only two values: either 1 within the allowed range, or 0 outside, thereby restricting $y_{\rm QCD}$ to the range $[y_{\rm QCD}]$. Instead, the extended *ER*fit scheme allows intermediate values between 0 and 1 for $\mathcal{L}_{\rm theo}(i)$. They are equal to 1 within $[y_{\rm QCD}]$ (there, they do not contribute at all to the full χ^2, and one recovers the *R*fit scheme) and drop smoothly to 0 outside. These functions are not treated as PDFs and hence the *ER*fit scheme is not a Bayesian scheme.

The way the *ER*fit likelihood functions decrease down to zero is arbitrary: one needs to define a standard. The proposed expressions for $\mathcal{L}_{\rm theo}(i)$ are presented in Sect. II.6. Because *ER*fit acknowledges the fact that the allowed ranges should not be taken literally, it offers two advantages over *R*fit:

- *ER*fit is more conservative than *R*fit: by construction, a *ER*fit CL is always equal or larger than the corresponding *R*fit one, and its CL surface in the a space exhibits the same plateau of equal CL = 1.
- in the case where the SM appears to be ruled out by *R*fit, the *ER*fit scheme is able to detect the $y_{\rm QCD}$ parameter(s) beyond the nominal allowed range that would restore an acceptable agreement between data and theory.

Despite the two above arguments in favor of *ER*fit, we chose *R*fit as the standard scheme used in this paper rather than *ER*fit: because it uses a simpler and unique prescription to incorporate theoretical systematics, it is less prone to be confused with a Bayesian treatment.

5.2 The Bayesian treatment

The Bayesian treatment [8] considers $\mathcal{L}$ as a PDF, from which is defined $\mathcal{F}(a)$, the PDF of a, through the convolution

$$\mathcal{F}(a) = C \int \mathcal{L}(y_{\rm mod})\ \delta(a - a(y_{\rm mod}))\ dy_{\rm mod}\ , \tag{53}$$

where the constant C is computed *a posteriori* to ensure the normalization to unity of $\mathcal{F}(a)$. In practice, the integral can be obtained conveniently by Monte Carlo techniques[12]. For each point in the a space, one sets a confidence level CL(a), for example according to:

$$\mathrm{CL}(a)\ =\ \int\limits_{\mathcal{F}(a')\leq\mathcal{F}(a)} \mathcal{F}(a')\ da'\ . \tag{54}$$

Other definitions for the domain of integration can be chosen.

New Physics is not meant to be detected by the Bayesian treatment: it is aimed at metrology mostly.

5.3 Comparison with *R*fit

Although the graphical displays appear similar, the Bayesian treatment and the *R*fit scheme are significantly different: the meaning attached to a given CL value is not the same. For the Bayesian treatment, the CL is a quantity *defined* for example by (54). The justification of this definition lies in the understanding that a CL value is meant to provide a quantitative measure of our qualitative *degree of belief*. Whereas one understands qualitatively well what is meant by *degree of belief*, because of its lack of formal definition, one cannot check that it is indeed well measured by the CL: the argument is thus circular.

The key point in the Bayesian treatment is the use of (53), even though the likelihood contains theoretical components. This implies that the $y_{\rm QCD}$ parameters, which stem from theoretical computations, are to be considered as random realizations of their true values. The PDFs of these "random" numbers are then drawn from guess-work (the $[y_{\rm QCD}]$ ranges do not fare better with respect to that.). For self-consistency, if one assumes that a large number of theorists perform the same $y_{\rm QCD}$ computation, the distribution of their results should then be interpreted as a determination of the $y_{\rm QCD}$ PDF. Once injected in (53), this PDF, the shape of which contains no information on nature,

[12] This convenience may sometimes boost the application of Bayesian techniques, since no use of sophisticated minimization techniques is necessary.

will be transformed into information pertaining to nature. This entails to a confusion between what is an experimental result and what is a thinking result. Illustrations of this are given in the appendix of [6][13].

6 Likelihoods and systematic errors

So far, we have reviewed the basic formalism of the *R*fit scheme. The treatment of experimental and theoretical systematics is the subject of this section.

Let x_0 be a quantity, which is not a random variable, but which is not perfectly known. We will consider two quantities of this type.

- A theoretical parameter which is not well determined (e.g., $x_0 = f_{B_d}$): the theoretical prediction of an observable depends on x_0 (e.g., ΔM_{B_d}).
- An experimental bias due to detector/analysis defects: the measurement should be corrected for this bias.

It is the purpose of this section to suggest a prescription of how to incorporate the limited knowledge of such quantities into the analysis. The standard treatment of this problem relies on a χ^2 analysis, which is satisfactory as long as the degree of belief we put on the knowledge of the value of x_0 is distributed like a Gaussian. However this is not necessarily what is meant when one deals with systematic errors. Rather, the theorist (resp. the experimentalist) *may* mean that the prediction (resp. the measurement) can take any value obtained by varying x_0 at will within the range $[\overline{x_0} - \zeta\sigma_o, \overline{x_0} + \zeta\sigma_o]$ (denoted *the allowed range* below, where ζ is a constant scale factor of order unity and $\overline{x_0}$ is the expected central value of x_0), but that it is unlikely that x_0 takes its true value outside the allowed range. This does *not* imply that the possible values for x_0 are equally distributed within the allowed range: they are not distributed *at all*.

If a systematic error is given such a meaning, then the statistical analysis should treat all x_0 values within the allowed range on the same footing (which again does not imply with equal *probability*): this corresponds to the *R*fit scheme (with $\zeta = 1$). On the other hand, it may be convenient to define specific tails instead of sharp cuts, thus allowing the theoretical parameters to leave their allowed ranges, if needed: this corresponds to the *ER*fit scheme.

The idea is to move from a pure χ^2 analysis to a log-likelihood one, redefining the χ^2 to be

$$\chi^2 = \left(\frac{x_{\rm exp} - x_{\rm theo}}{\sigma_{\rm exp}}\right)^2 - 2\ln\mathcal{L}_{\rm syst}(x_0) \ , \tag{55}$$

where $\mathcal{L}_{\rm syst}(x_0)$, hereafter termed the *Hat* function, is a function equal to unity for x_0 within the allowed range.

6.1 The Hat function

The Hat function $\mathcal{L}_{\rm syst}(x_0, \kappa, \zeta)$ is a continuous function defined as

$$-2\ln\mathcal{L}_{\rm syst}(x_0,\kappa,\zeta) = \begin{cases} 0 \ , & \forall x_0 \in [\overline{x_0} \pm \zeta\sigma_o] \\ \left(\dfrac{x_0 - \overline{x_0}}{\kappa\sigma_o}\right)^2 - \left(\dfrac{\zeta}{\kappa}\right)^2 \ , & \forall x_0 \notin [\overline{x_0} \pm \zeta\sigma_o] \end{cases} \tag{56}$$

where the constant κ determines the behavior of the function outside the allowed range. For the *R*fit scheme $\kappa = 0$ is used. To define a standard κ can be chosen to be a function of ζ such that the relative normalization of $\mathcal{L}_{\rm syst}(x_0, \kappa, \zeta)$

[13] Methodogical problems that may appear with the use of Bayesian statistics in metrological CKM analyses are outlined below.

- The convolution of several, arbitrary *a priori* theoretical PDFs can lead to the creation of seemingly accurate information (the convolved PDF) out of no initial knowledge. A quantification of the uncertainty related to this information is impossible.
- All $y_{\rm mod}$ parameters need *a priori* PDFs, also those that are to be determined by the fit. For instance, if the CKM parameters are the physical unknowns of the global fit, the results obtained will depend on the parameterization chosen to have a, say, uniform prior. This breaks a fundamental invariant of physics theories. For example, the CKM-related physics depends on whether the CKM matrix is parameterized with the Euler angles & phase, or with the Wolfenstein parameters.
- It frequently occurs in the phenomenological description of B decays that *a priori* unknown strong-interaction phases contribute to the $y_{\rm mod}$ parameters. While this is no problem in *R*fit (or *ER*fit), where these parameters are free to vary within their 2π periodicity, it may exhibit biases in a Bayesian approach: in particular, in the presence of multiple unknown phases, the CL obtained may depend on whether the validity range is chosen to be $[-\pi, \pi]$ or $[0, 2\pi]$ or any other 2π interval.

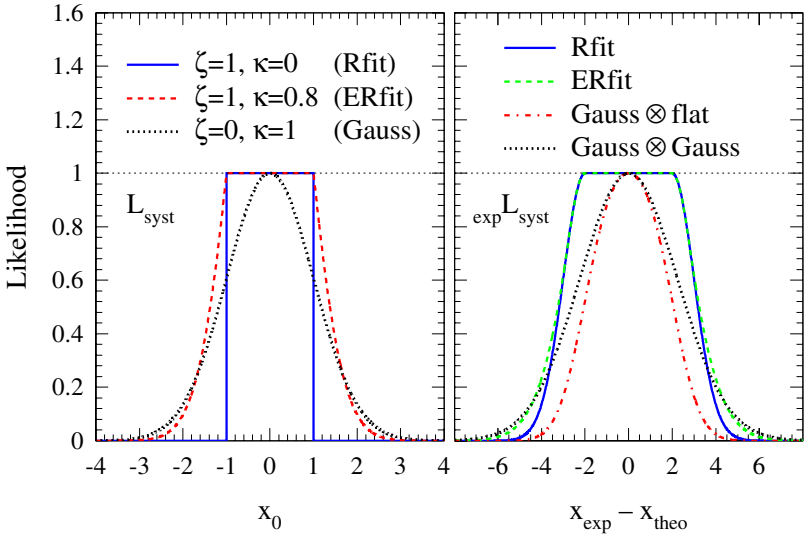

Fig. 4. *Left*: Hat functions ($\overline{x_0} = 0$ and $\sigma_o = 1$) used for the *R*fit scheme, the *ER*fit scheme, and the Gaussian treatment. *Right*: combined likelihood ${}_{\rm exp}\mathcal{L}_{\rm syst}$ (with $\overline{x_0} = 0$ and $\sigma_{\rm exp} = \sigma_o = 1$) for the *R*fit scheme, the *ER*fit scheme, a convolution of a Gaussian with a uniform distribution (hence taken as a PDF, following the Bayesian approach) and a convolution of two Gaussians

(considered here, for the purpose of defining a standard, as a PDF) be equal to the one of a Gaussian of width σ_o

$$\int_{-\infty}^{+\infty} \mathcal{L}_{\rm syst}(x_0,\kappa,\zeta)\; dx_0 \cdot \int_0^{\zeta/\sqrt{2}} e^{-t^2}\; dt = \sqrt{\pi}\,\zeta\sigma_0\ . \tag{57}$$

The parameter κ is numerically computed as a function of ζ. For the limit $\zeta \to 0$ one obtains $\kappa \to 1$, and the Hat becomes a pure Gaussian. The *ER*fit scheme is defined by $\zeta = 1$, for which one obtains $\kappa \simeq 0.8$.

Examples of Hat functions with $\overline{x_0} = 0$ and $\sigma_o = 1$ are shown on the left plot of Fig. 4. Being a likelihood and not a PDF, $\mathcal{L}_{\rm syst}(x_0)$ needs not be normalized to unity.

6.2 Combining statistical and systematic uncertainties

Having defined $\mathcal{L}_{\rm syst}(x_0)$ one proceeds with the minimization of the χ^2 of (55) by allowing x_0 to vary freely.

For theoretical systematics, the result depends on the way x_0 enters $x_{\rm theo}$, and not much more can be said in generality.

For experimental and theoretical systematics where x_0 can be assumed to be an unknown offset[14]: the quantity to be confronted to the theoretical prediction $x_{\rm theo}$ is simply $x_{\rm exp} + x_0$. Omitting the details of straightforward calculations, and assuming that $\overline{x_0} = 0$ (otherwise $x_{\rm exp}$ should be corrected for it), one obtains, after minimization of the χ^2 with respect to x_0:

- $|\, x_{\rm exp} - x_{\rm theo}\,| \leq \zeta\sigma_o$: $\quad \chi^2_{{\rm min};\,x_0} = 0$.
- $\zeta\sigma_o \leq |\, x_{\rm exp} - x_{\rm theo}\,| \leq \zeta\sigma_o(1 + (\frac{\sigma_{\rm exp}}{\kappa\sigma_o})^2)$: $\quad \chi^2_{{\rm min};\,x_0} = \left(\dfrac{|\, x_{\rm exp} - x_{\rm theo}\,| - \zeta\sigma_o}{\sigma_{\rm exp}}\right)^2$.
- $|\, x_{\rm exp} - x_{\rm theo}\,| \geq \zeta\sigma_o(1 + (\frac{\sigma_{\rm exp}}{\kappa\sigma_o})^2)$: $\quad \chi^2_{{\rm min};\,x_0} = \dfrac{(x_{\rm exp} - x_{\rm theo})^2}{\sigma^2_{\rm exp} + (\kappa\sigma_o)^2} - \left(\dfrac{\zeta}{\kappa}\right)^2$.

In the limit $\zeta \to 0$ (and hence, $\kappa \to 1$) only the third instance is met, and one recovers the usual rule of adding in quadrature the statistical and the systematic uncertainties. Otherwise, the result is non-trivial. An example of the effective likelihood ${}_{\rm exp}\mathcal{L}_{\rm syst}(x_{\rm exp} - x_{\rm theo}) \equiv -\frac{1}{2}\chi^2_{{\rm min};\,x_0}$ (with $\overline{x_0} = 0$ and $\sigma_{\rm exp} = \sigma_o = 1$) is shown in the right hand plot of Fig. 4 for the *R*fit scheme, the *ER*fit scheme, a convolution of a Gaussian with a uniform distribution (hence taken as a PDF, following the Bayesian approach) and a convolution of two Gaussians.

[14] If systematics take the form of an unknown multiplicative factor, and this is often the case for theoretical uncertainties, a treatment similar to the one discussed here applies.

Part III
The Global CKM fit

1 Introduction

With the remarkable exceptions of $\sin 2\beta$ (see Sect. 2.10) and $\sin 2\alpha$ (see Sect. 2.11), the experimental observables that are presently used to constrain $(\overline{\rho}, \overline{\eta})$ depend on hadronic matrix elements, which have to be evaluated at a much smaller energy than the weak interaction scale. Since the discovery of asymptotic freedom, Quantum Chromodynamics (QCD) is well established as *the* quantum field theory of strong interaction. It has been tested to high precision in the perturbative regime, where the coupling constant α_s is small and allows one to build a systematic expansion. Unfortunately, no general solution of QCD is known, and not even a well-controlled approximation is available (at least in an analytical form) that would be valid for an arbitrary α_s.

While it is far beyond the scope of this introduction to review the wealth of approaches to non-perturbative QCD, it is useful to recall a few general techniques to evaluate the matrix elements that are relevant for quark flavor physics. The theoretical methods can be classified, somewhat arbitrarily, into four categories: constituent quark models, QCD sum rules, lattice simulations, and effective theories of QCD.

- *Constituent quark models* comprise, to a first approximation, methods that assume a fixed number of particles and treat them in the framework of quantum mechanics. Multi-body wave functions, which satisfy bound state potential equations, are constructed, and external operators that describe flavor transitions are represented in terms of constituent quarks and then sandwiched between these wave functions.
- *QCD sum rules* rely on quark-hadron duality to identify a correlation function written in terms of quarks and gluons with its representation as a sum over hadronic bound states. The desired matrix element is then isolated from the rest of the sum and its contribution is controlled in various ways.
- *Lattice simulations* implement quantum field theory on an Euclidean space-time lattice. The path integrals that represent correlation functions are then numerically evaluated with Monte Carlo methods.
- *Effective theories of QCD* exploit additional symmetries of full QCD in specific kinematic or parametric regimes. Matrix elements are then related to others that are simpler to compute or to measure, up to corrections that are suppressed by the typical symmetry breaking scale.

2 Inputs to the standard CKM fit

This section provides a compendium of the measurements and SM predictions entering the overall constrained CKM fit, denoted *standard CKM fit* in the following. The corresponding numerical values used and the treatment of their uncertainties within *R*fit are summarized in Table 1. In cases where different independent measurements for an input quantity are available, we multiply the corresponding (*R*fit) likelihoods. Experimental and theoretical correlations, if present and known, are taken into account if not stated otherwise.

2.1 $|V_{ud}|$

The matrix element $|V_{ud}|$ has been extracted by means of three different methods: superallowed nuclear β-decays, neutron β-decay and pion β-decay.

The most precise experimental determination of $|V_{ud}|$ comes from lifetime measurements of superallowed nuclear β-decays with pure Fermi-transitions ($0^+ \to 0^+$). The ft-value is the product of the integral over the electron energy spectrum f and the electron lifetime τ: $ft = f \cdot \tau \cdot \ln 2$. Its theoretical prediction can be written as

$$ft \cdot (1 + \delta_R) \cdot (1 - \delta_C) = \frac{K}{2G_F^2 |V_{ud}|^2 (1 + \Delta_R^V)} \ , \tag{58}$$

where G_F is the Fermi constant (see Table 1), δ_R and Δ_R^V are the nucleus-dependent and nucleus-independent parts of the radiative corrections, respectively, δ_C is the charge-symmetry breaking corrections, and $K = 2\pi^3 \ln 2/m_e^5$. The charge-symmetry breaking corrections, as well as part of the nucleus-dependent radiative corrections, depend on the nuclear structure of the nucleus under consideration. Using the results for nine different superallowed nuclear β decays, the average is $|V_{ud}| = 0.9740 \pm 0.0001_{\rm exp}$ [17]. This result is however dominated by theoretical uncertainties, namely $\sigma(|V_{ud}|)[\Delta_R^V] = 0.0004$, $\sigma(|V_{ud}|)[\delta_C] = 0.0003$ and $\sigma(|V_{ud}|)[\delta_R] = 0.0001$. Adding these in quadrature results in $\sigma(|V_{ud}|) = 0.0005$, whereas adding them linearly (as in the *R*fit approach) results in $\sigma(|V_{ud}|) = 0.0008$.

A possible enhancement, $\Delta|V_{ud}| = +0.0005$, is predicted by a quark-meson coupling model due to a change of charge symmetry violation for quarks inside bound nucleons compared to unbound nucleons [18]. The theoretical error

has been enlarged by the PDG [12] by adding linearly the amount of the possible correction to the quoted error of $\sigma(|V_{ud}|) = 0.0005$, resulting in $|V_{ud}| = 0.9740 \pm 0.0010$. Since this correction may be partially contained in the charge-symmetry breaking corrections, and since the effect can be significantly smaller depending on the model used, we do not enlarge the error and use in the fit: $|V_{ud}| = 0.9740 \pm 0.0001_{\rm exp} \pm 0.0008_{\rm theo}$.

Nuclear structure effects do not play a role in neutron β decays. However, to extract $|V_{ud}|$, one needs to measure the neutron lifetime and the ratio of the axial-vector coupling constant to the vector coupling constant g_A/g_V

$$|V_{ud}|^2 = \frac{K \ln 2}{G_F^2 (1 + \Delta_R^V)(1 + 3(g_A/g_V)^2) f (1 + \delta_R) \tau_n} \ . \tag{59}$$

In contrast to nuclear β decays, these measurements are not yet dominated by theoretical uncertainties. The weighted mean for the neutron lifetime measurements is $\tau_n = (885.7 \pm 0.7)\,$s [17], where the available results are statistically consistent. Recently, the PERKEO-II experiment has measured $g_A/g_V = -1.2739 \pm 0.0019$ [19]. Using the world average for the neutron lifetime this translates into $|V_{ud}| = 0.9717 \pm 0.0013_{g_A/g_V,\tau_n} \pm 0.0004_{\rm theo}$. The experimental error on this result is a factor of two smaller than any preceding measurement with high neutron polarization [12]. When considering all data on g_A/g_V with high neutron polarization, the measurements are not consistent. A rescaling by a factor of 1.6 is therefore applied following the PDG recipe, which results in $g_A/g_V = -1.2690 \pm 0.0022$, with $|V_{ud}| = 0.9745 \pm 0.0016_{\rm stat} \pm 0.0004_{\rm theo}$ [17]. Since the PERKEO-II result was obtained using a very high neutron polarization and since $\mathcal{O}(2\%)$ corrections used to extract the final result from data are much smaller than in previous experiments, we only use this result in the fit.

The pion β decay $\pi^+ \to \pi^0 e^+ \nu_e$ is an attractive candidate to extract $|V_{ud}|$ from the branching ratio $\mathcal{B}(\pi^+ \to \pi^0 e^+ \nu_e)$ and the pion lifetime, since it is mediated by a pure vector transition and does not suffer from nuclear structure effects. However, due to the small branching ratio, $\mathcal{B}(\pi^+ \to \pi^0 e^+ \nu_e) = (1.025 \pm 0.034) \times 10^{-8}$ [12], the statistical precision is not competitive with the other methods: $|V_{ud}| = 0.967 \pm 0.016_{\mathcal{B}} \pm 0.0005_{\rm theo}$. The preliminary result from the PIBETA experiment [20], $\mathcal{B}(\pi^+ \to \pi^0 e^+ \nu_e) = (1.044 \pm 0.007_{\rm stat} \pm 0.009_{\rm sys}) \times 10^{-8}$, yields $|V_{ud}| = 0.9765 \pm 0.0055_{\mathcal{B}} \pm 0.0005_{\rm theo}$, which still has a statistical error that is a factor of four times larger than the result from neutron decay experiments. It will not be competitive even when the final expected experimental uncertainty of $\sigma(|V_{ud}|) = 0.002$ is reached.

We build a combined likelihood for the $|V_{ud}|$ determinations from superallowed β decays, from neutron β decays and from the pion β decay, taking into account the correlation due to the uncertainty on Δ_R^V. We obtain the CL $> 5\%$ interval $0.9730 < |V_{ud}| < 0.9750$.

2.2 $|V_{us}|$

The analyses of kaon and hyperon semileptonic decays provide the best determination of $|V_{us}|$. However, due to theoretical uncertainties from the breakdown of SU(3) flavor symmetry, the hyperon decay data are less reliable [21,22]. Although, as pointed out in [23], linear SU(3) breaking corrections can be avoided, we do not use results from hyperon decays since the uncertainties on the vector form factor f_1 in these decays have not been fully evaluated yet. As a consequence, we only use the value obtained from the vector transitions $K^+ \to \pi^0 \ell^+ \nu_\ell$ and $K_L^0 \to \pi^- \ell^+ \nu_\ell$. The rates for these decays depend on two form factors, $f_+(t)$ and $f_0(t)$, where $t = (p_K - p_\pi)^2$ is the four-momentum transfer-squared between the kaon and the pion. Owing to the small electron mass, only $f_+(t)$ plays a role in K_{e3} decays whose functional dependence can be extracted from data. The form factor value at zero recoil, $f_+(0)$, is calculated within the framework of chiral perturbation theory and is found to be $f_+^{K^0\pi^-}(0) = 0.961 \pm 0.008$ [24]. The error estimate for this value has been questioned in [25]. We note that a relativistic constituent quark model, successful in the description of electroweak properties of light mesons, gives the consistent result $f_+^{K^0\pi^-}(0) = 0.963 \pm 0.004$ [26].

A precise calculation of $f_+^{K^0\pi^-}(0)$ is a difficult task. Order p^6 contributions in chiral perturbation theory have been calculated only recently [27,28]. The $\mathcal{O}(p^6)$ calculation contains a "local" and a "loop" contribution leading to a strong cancellation, with the result depending on the renormalization scale. [29] quotes $f_+^{K^0\pi^-}(0)|_{p^6} = -0.001 \pm 0.010$ leading to $f_+^{K^0\pi^-}(0) = 0.981 \pm 0.010$ while emphasizing, however, that further work is needed to clarify whether the uncertainty quoted is realistic. A value of $f_+^{K^0\pi^-}(0) = 0.981 \pm 0.010$ would increase the deviation from unitarity in the first family. It is worthwhile to mention in this context that a recent quenched Lattice-QCD calculation obtains $f_+^{K^0\pi^-}(0) = 0.960 \pm 0.005_{\rm stat} \pm 0.007_{\rm sys}$ [30] in agreement with the Leutwyler-Roos value [24].

Channel-independent and channel-dependent radiative corrections [31–33] as well as charge-symmetry (K^+/K_L^0) and charge-independence (π^-/π^0) breaking corrections [24] are applied to compare the branching fraction results from both channels [12]: $f_+^{K^0\pi^-}(0)|V_{us}| = 0.2134 \pm 0.0015_{\rm exp} \pm 0.0001_{\rm rad}$ ($K^+ \to \pi^0 e^+ \nu_e$) and $f_+^{K^0\pi^-}(0)|V_{us}| = 0.2101 \pm 0.0013_{\rm exp} \pm 0.0001_{\rm rad}$ ($K_L^0 \to \pi^- e^+ \nu_e$). Their weighted average is $f_+^{K^0\pi^-}(0)|V_{us}| = 0.2114 \pm 0.0016$, where the error has been rescaled by a factor of 1.6 to account for the inconsistency between neutral and charged kaon decay data.

Using $f_+^{K^0\pi^-}(0)|V_{us}| = 0.2114 \pm 0.0016$ and the Leutwyler-Roos value $f_+^{K^0\pi^-}(0) = 0.961 \pm 0.008$ [24], one obtains $|V_{us}| = 0.2200 \pm 0.0017_{\rm exp} \pm 0.0018_{\rm theo}$. Recently, the BNL-E865 collaboration measured $\mathcal{B}(K^+_{e3}) = (5.13 \pm 0.02_{\rm stat} \pm 0.09_{\rm sys} \pm 0.04_{\rm norm})\%$ [34], which exhibits a 2.2σ deviation from the world average $\mathcal{B}(K^+_{e3}) = (4.87 \pm 0.06)\%$ [12]. The BNL-E865 result translates into $|V_{us}| = 0.2285 \pm 0.0023_{\rm exp} \pm 0.0019_{\rm theo}$ [33] when using $f_+^{K^0\pi^-}(0) = 0.961 \pm 0.008$. If this result is confirmed this would imply that the previous $\mathcal{B}(K^0_{L,e3})$ results [12] are incorrect, since it is not likely that such a discrepancy can be explained by isospin breaking effects [33]. The KLOE collaboration had presented preliminary results on K^0_{e3} and $K^0_{L\mu 3}$ decays [35] in agreement with the PDG values for K^+_{e3} decays[15]. We use a weighted average of the BNL-E865 result and the former $|V_{us}|$ average, rescale the experimental uncertainty and obtain $|V_{us}| = 0.2228 \pm 0.0039_{\rm exp} \pm 0.0018_{\rm theo}$ by using the Leutwyler-Roos value $f_+^{K^0\pi^-}(0) = 0.961 \pm 0.008$ [24]. As mentioned previously there is intense theoretical activity concerning an improved determination of this form factor value.

There are good prospects to clarify the experimental situation in the near future. The KLOE, KTeV and NA48 experiments have the potential to determine K_{l3} decays with different experimental techniques. Another promising method to measure $|V_{us}|$ from moments of the strange spectral functions in τ decays has been proposed in [38] and might be realized at the B factories where more than 10^8 τ pairs have currently been recorded.

2.3 $|V_{cd}|$ and $|V_{cs}|$

Both the $|V_{cd}|$ and $|V_{cs}|$ matrix elements can be determined from di-muon production in deep inelastic scattering (DIS) of neutrinos and anti-neutrinos on nucleons. In an analysis performed by the CDHS collaboration [39], $|V_{cd}|$ and $|V_{cs}|$ are extracted by combining the data from three experiments, CDHS [39], CCFR [40] and CHARM II [41], giving $|V_{cd}|^2 \times B_c = (4.63 \pm 0.34) \times 10^{-3}$, where $B_c = 0.0919 \pm 0.0094$ [42–44] is the weighted average of semileptonic branching ratios of charmed hadrons produced in neutrino-nucleon DIS. This results in $|V_{cd}| = 0.224 \pm 0.014$ [45]. The average DIS result from CDHS, CCFR and CHARM II is $\kappa|V_{cs}|^2 B_c = (4.53 \pm 0.37) \times 10^{-2}$, where $\kappa = 0.453 \pm 0.106^{+0.028}_{-0.096}$ is the relative contribution from strange quarks in the sea with respect to u and d quarks, leading to $|V_{cs}| = 1.04 \pm 0.16$ [12].

Similarly to $|V_{us}|$ coming from K_{e3} decays, $|V_{cs}|$ can be extracted from D_{e3} decays. However the theoretical uncertainty in the form factor calculation $f_+(0) = 0.7 \pm 0.1$ [46] limits its precision to $|V_{cs}| = 1.04 \pm 0.16$ [45] (in coincidental agreement with $|V_{cs}|$ from DIS).

Assuming unitarity and using as additional input the constraints on $|V_{ud}|$, $|V_{us}|$, $|V_{ub}|$, $|V_{cd}|$ and $|V_{cb}|$, $|V_{cs}|$ can also be extracted from the following quantities:

- $R_c^W = \Gamma(W^+ \to c\bar{q})/\Gamma(W^+ \to \text{hadrons}) = \sum_{i=d,s,b} |V_{ci}|^2 / (\sum_{i=d,s,b;\, j=u,c} |V_{ji}|^2)$. For the three-generation CKM matrix R_c^W is expected to be 1/2. The measurements [47–49] are found to be consistent with this expectation.
- $\Gamma(W \to X_c X) = R_c^{\rm W} \cdot \mathcal{B}(W \to \text{hadrons}) \cdot \Gamma_{\rm tot} \propto \sum_{i=d,s,b} |V_{ci}|^2$ [49].
- $\Gamma(W^+ \to \text{hadrons})/\Gamma(W^+ \to \text{leptons}) = \sum_{i=d,s,b;\, j=u,c} |V_{ji}|^2 \times (1 + \alpha_S(m_W)/\pi + \dots)$ [12], for which the experimental result is $\sum_{i=d,s,b;\, j=u,c} |V_{ji}|^2 = (2.039 \pm 0.025) \cdot (\mathcal{B}(W \to \ell\overline{\nu}_\ell) \pm 0.001(\alpha_S))$ [50].

For the three generation CKM matrix all these quantities have theoretical predictions that are independent of the actual values of the CKM elements involved, so that they cannot be used in a CKM fit. On the other hand, these measurements test the unitarity of a three-generation CKM matrix requiring, for example, $\sum_{i=d,s,b;\, j=u,c} |V_{ji}|^2 = 2$.

There are prospects that $|V_{cs}|$, $|V_{cd}|$ and $|V_{cs}|/|V_{cd}|$ will be determined at the CLEO-c experiment with unprecedented precision in semileptonic D-meson decays to a pseudoscalar meson $D \to P\ell^+\nu$ [51]. For a $3\,{\rm fb}^{-1}$ data sample, the relative errors on $\Gamma(D^0 \to K^-\ell^+\nu)$ and $\Gamma(D^0 \to \pi^-\ell^+\nu)$ are expected to be $\sigma(\Gamma)/\Gamma = 1.2\%$ and $\sigma(\Gamma)/\Gamma = 1.5\%$, respectively. The extraction of $|V_{cs}|$ and $|V_{cd}|$ from these decays will require a substantial improvement of the theoretical precision in the form factor calculation, which may be achieved in the forthcoming years by Lattice QCD. A relative uncertainty on the form factor of 3%, for example, would then translate into the errors $\sigma(|V_{cs}|)/|V_{cs}| = 1.6\%$ and $\sigma(|V_{cd}|)/|V_{cd}| = 1.7\%$. The ratio $|V_{cs}|/|V_{cd}|$ will be determined at CLEO-c following two different approaches that are expected to be less dependent on theoretical uncertainties. In the first approach, one compares semileptonic decays with the same initial state but with different final states as $\Gamma(D^0 \to K^-\ell^+\nu)$ and $\Gamma(D^0 \to \pi^-\ell^+\nu)$. The ratio of branching fractions depends on the product of $|V_{cs}/V_{cd}|^2$ and a form factor ratio that differs from unity only due to SU(3) breaking corrections. In the second approach, one compares reactions with different initial states but the same final state, for instance $D_s^+ \to K_S^0\ell^+\nu$ and $D^+ \to K_S^0\ell^+\nu$.

[15] In the meantime, the KLOE $K^0_{S,e3}$ result has been updated with nearly final systematic error [36]. The result for $|V_{us}|$ is now in reasonable agreement with the BNL-E865 result for K^+_{e3} and hence differs from the former determinations using K^0_{e3} decays. The understanding of final state radiation of photons plays a crucial role in these analyses and may become a key issue when comparing the results of the various experiments. Very recently, the KTeV collaboration has presented a result for semileptonic K_L branching fractions which gives $f_+^{K^0\pi^-}(0)|V_{us}| = 0.2165 \pm 0.0012$ [37] in agreement with the BNL-E865 result. However, this result has not yet been included in our average.

2.4 $|V_{cb}|$

In the Wolfenstein parameterization, $|V_{cb}|$ determines the parameter A which plays an important role for the constraints on $\overline{\rho}$, $\overline{\eta}$ from $|V_{ub}|$, $|\varepsilon_K|$ and Δm_d. Its precision also has a significant impact on the SM prediction for the rare decays $K \to \pi\nu\overline{\nu}$. It is most accurately obtained from exclusive $B \to D^{(*)}\ell\overline{\nu}_\ell$ and inclusive semileptonic b decays to charm.

Exclusive decays

In the exclusive technique, the differential spectrum $d\Gamma/dw$ for the decay $B \to D^{(*)}\ell\overline{\nu}_\ell$ is measured, where w is the scalar product of the velocity four-vectors of the B and the $D^{(*)}$ mesons. This allows one to extract the product $\mathcal{F}_{D^*}(1)|V_{cb}|$, where $\mathcal{F}_{D^*}(w=1)$ is the B-to-$D^{(*)}$ form factor at zero-recoil. In the heavy quark limit, the form factor is given by the Isgur-Wise function [52], which is equal to 1 at $w = 1$, but which receives corrections due to the finite b and c quark masses that can be calculated in the framework of Heavy Quark Effective Theory (HQET) [52,53]. At present, the most precise determination using the exclusive technique comes from the decay $B \to D^*\ell\overline{\nu}_\ell$. Due to the presence of a soft pion in the D^* decay, its reconstruction is less affected by combinatorial background than for a D-meson decay. Moreover, the phase space function for $B \to D\ell\overline{\nu}_\ell$ drops more rapidly when approaching $w = 1$, leading to a larger statistical error. Finally, the calculation of the form factor at zero-recoil is believed to have smaller theoretical uncertainties in the case of a B-to-D^* transition, since linear $1/m_Q$ corrections in the heavy quark mass m_Q vanish, a property known as Luke's theorem [54]. It has been pointed out that the form factor for B-to-D transitions may be calculable with good theoretical precision despite the presence of $1/m_Q$ corrections [55].

Previous theoretical determinations of $\mathcal{F}_{D^*}(1)$ were based either on QCD sum rules (see, e.g., [56]) or on HQET, where long-distance contributions had been estimated with the use of non-relativistic quark models [57,58]. Both methods obtained values for $\mathcal{F}_{D^*}(1)$ around 0.9 with quoted uncertainties of the order of 4%, which are however difficult to control. Recently, important progress has been achieved through the calculation of $\mathcal{F}_{D^*}(1)$ using Lattice QCD in conjunction with HQET [59,60]. Their result, $\mathcal{F}_{D^*}(1) = 0.913^{+0.030}_{-0.035}$ [61], is used in our fit. It is expected that the uncertainty can be reduced in the forthcoming years. Averaging eight different measurements, the Heavy Flavor Averaging Group (HFAG) obtains $\mathcal{F}_{D^*}(1)|V_{cb}| = (36.7 \pm 0.8) \times 10^{-3}$ [62] and $\rho^2 = 1.44 \pm 0.14$, where ρ is the slope of the form factor as a function of w. The linear correlation coefficient between the two parameters is 0.91. The goodness of the average ($\chi^2 = 30$ for 14 degrees-of-freedom, that is CL = 0.08) indicates an inconsistency among the various measurements, which is mainly driven by the somewhat large result obtained by CLEO.

It has been argued that the uncertainties in the Lattice QCD calculation of $\mathcal{F}_{D^*}(1)$ [61] can be considered as mainly statistical ones [9]. Following this reasoning and using $\mathcal{F}_{D^*}(1)|V_{cb}| = (36.7 \pm 0.8) \times 10^{-3}$ [62], we obtain $|V_{cb}| = (40.2^{+2.1}_{-1.8}) \times 10^{-3}$, which is used in the fit.

Inclusive decays

In the inclusive approach, the semileptonic width $\Gamma(B \to X\ell\nu_\ell)$ is determined experimentally from the semileptonic branching fraction $\mathcal{B}(B \to X\ell\nu_\ell) = (10.90 \pm 0.23)\%$ [62] and the B-meson lifetime, where the admixture of neutral ($\tau_{B^0} = (1.534 \pm 0.013)\,\mathrm{ps}^{-1}$ [62]) and charged ($\tau_{B^+} = (1.653 \pm 0.014)\,\mathrm{ps}^{-1}$ [62]) B mesons is understood. Relying on the concept of quark-hadron duality, the theoretical prediction for the semileptonic width is obtained by means of a Operator Product Expansion called Heavy Quark Expansion (HQE [63]), which invokes perturbative corrections and non-perturbative hadronic matrix elements that dominate the theoretical uncertainty. The theoretical expression for the semileptonic rate reads

$$\Gamma(b \to c) = \frac{G_F^2 |V_{cb}|^2 m_b^5}{192\pi^3} f\left(\frac{m_c^2}{m_b^2}\right) \left[1 + A\left(\frac{\alpha_s}{\pi}\right) + B\left(\frac{\alpha_s^2}{\pi^2}\beta_0\right) + C\left(\frac{\Lambda_{\mathrm{QCD}}^2}{m_b^2}\right) + \mathcal{O}\left(\alpha_s^2, \frac{\Lambda_{\mathrm{QCD}}^3}{m_b^3}, \frac{\alpha_s}{m_b^2}\right)\right] , \qquad (60)$$

where m_b is the b-quark mass, f corrects for the finite charm quark mass m_c, and the coefficients A, B and C are functions of hadronic matrix elements and depend on m_b and m_c. Perturbative QCD corrections are known up to order $\alpha_s^2\beta_0$. Non-perturbative corrections are suppressed by powers of $\Lambda_{\mathrm{QCD}}/m_b$. At order $(\Lambda_{\mathrm{QCD}}/m_b)^2$, the hadronic matrix elements can be expressed by the HQET parameters λ_1 and λ_2, the expectation values of the heavy-quark kinetic energy and the chromomagnetic interaction, respectively. Additional parameters occur at order $(\Lambda_{\mathrm{QCD}}/m_b)^3$. Alternatively, in the kinetic mass scheme [64], these matrix elements are given by the parameters $-\mu_\pi^2 = \lambda_1$ and $\mu_G^2/3 = \lambda_2$, up to higher-order corrections. The parameter λ_2 can be obtained from the observed hyperfine splitting in the B-meson spectrum. The semileptonic width can be written in terms of the B-meson mass m_B instead of m_b by introducing the non-perturbative parameter $\overline{\Lambda}$, that is the energy of the light-degrees-of-freedom.

Besides the total semileptonic width, HQE can be used to predict sufficiently inclusive differential distributions. Since different regions of the phase space have different sensitivity to the quark masses and the non-perturbative

parameters, spectral moments calculated from measured differential distributions can be used to constrain these parameters. However moments at too high order cannot be reliably predicted since quark-hadron duality starts to break down. In recent years, the parameters $\overline{\Lambda}$ and λ_1 have been constrained experimentally by measurements of leptonic energy and hadronic mass moments. In addition, the measured photon energy distribution in $B \to X_s\gamma$ allows one to extract $\overline{\Lambda}$ [65]. So far, the constraints on these parameters from CLEO, DELPHI and *BABAR* provide consistent results, which may be interpreted as a test of the validity of the HQE up to order $\mathcal{O}(1/m_Q^3)$. However no global fit taking into account all various measurements has been performed yet[16]. An overview of several $|V_{cb}|$ determinations using input from measured moments can be found, e.g., in [67] from which we obtain $|V_{cb}| = (42.0 \pm 0.6_{\rm stat} \pm 0.8_{\rm theo}) \times 10^{-3}$. Here, the first error arises from the experimental uncertainties on the branching fraction, the B-meson lifetime and the fit error from the determination of $\overline{\Lambda}$ and λ_1, and the second error contains the theoretical uncertainty due to higher-order ($\mathcal{O}(1/m_Q^3)$) and α_s corrections[17].

Average

In the fit, we combine the likelihoods of $|V_{cb}|$ from inclusive and exclusive measurements where we assume that they are uncorrelated.

2.5 $|V_{ub}|$

The third column element $|V_{ub}|$, with additional input from $|V_{us}|$ and $|V_{cb}|$, describes a circle in the $(\overline{\rho},\overline{\eta})$ plane. It can be extracted either from inclusive $B \to X_u\ell^-\overline{\nu}_\ell$ decays, or from exclusive decays such as $B \to \pi\ell\nu_\ell$, $B \to \rho\ell\nu_\ell$, $B \to \omega\ell\nu_\ell$ and $B \to \eta\ell\nu_\ell$.

Exclusive decays

In contrast to heavy-to-heavy transitions like $B \to D^{(*)}$, there is no heavy quark symmetry argument that allows one to constrain the form factor normalization in the heavy-to-light decays $B \to \pi, \rho, \ldots$. As a consequence, exclusive determinations – besides being experimentally challenging – suffer from large theoretical uncertainties in the form factor calculations. From a theoretical point of view, one expects that $B \to \pi\ell\nu_\ell$ will ultimately be the most promising mode for an extraction of $|V_{ub}|$ in exclusive decays, since only one form factor function is present in pseudoscalar-to-pseudoscalar transitions (while for instance three different form factor functions have to be calculated for $B \to \rho\ell\nu_\ell$ decays). On the other hand, the softer lepton spectrum in $B \to \pi\ell\nu_\ell$ with respect to $B \to \rho\ell\nu_\ell$, where the lepton momentum benefits from the polarization of the ρ, leads to an enhanced $b \to c$ background contamination in the former decay.

The *BABAR* collaboration has published a measurement of the branching fraction $\mathcal{B}(B \to \rho\ell\nu_\ell) = (3.29 \pm 0.42_{\rm stat} \pm 0.47_{\rm sys} \pm 0.60_{\rm theo}) \times 10^{-4}$ [71]. Using several form factor models they extract $|V_{ub}| = (3.64 \pm 0.22_{\rm stat} \pm 0.25_{\rm sys}{}^{+0.39}_{-0.56\,{\rm theo}}) \times 10^{-3}$. The CLEO collaboration has recently presented a combined analysis of the decays $B \to \pi\ell\nu_\ell$, $B \to \rho\ell\nu_\ell$, $B \to \omega\ell\nu_\ell$ and $B \to \eta\ell\nu_\ell$ [72]. Owing to a largely hermetic detector, CLEO also measured the rates in three different bins of q^2, the lepton-neutrino four-momentum-squared. CLEO finds the combined value $|V_{ub}| = (3.17 \pm 0.17_{\rm stat}\,{}^{+0.16}_{-0.17\,{\rm sys}}\,{}^{+0.53}_{-0.39\,{\rm theo}}) \times 10^{-3}$ for $B \to \pi\ell\nu_\ell$ and $B \to \rho\ell\nu_\ell$. Even the single CLEO number for $B \to \rho\ell\nu_\ell$ is hard to compare with the *BABAR* result [71] since different form factor calculations have been used in both experiments, and results from different q^2 regions have been taken into account. A combination of the *BABAR* and CLEO numbers is also difficult because the applied theoretical uncertainty range by itself varies. These problems in mind, we have averaged both results by symmetrizing each of the results with respect to the quoted theoretical uncertainties and assuming that they are fully correlated between both experiments. With this method, we obtain $|V_{ub}| = (3.35 \pm 0.20_{\rm exp} \pm 0.50_{\rm theo}) \times 10^{-3}$.

Inclusive decays

Starting from the inclusive semileptonic width $\Gamma(B \to X_u\ell^-\overline{\nu}_\ell)$, $|V_{ub}|$ can be predicted within the HQE framework with a theoretical uncertainty of approximately 5%. However, there is a large background from $b \to c$ transitions that is about

[16] Such a global analysis is now available in [66], which has been published after completion of this document.

[17] Very recently, the *BABAR* collaboration has been presented precisely measured electron energy and hadronic mass moments [68,69]. The value obtained $|V_{cb}| = (41.4 \pm 0.4_{\rm stat} \pm 0.4_{\rm HQE} \pm 0.6_{\rm theo}) \times 10^{-3}$ from a fit [70] in the kinetic mass scheme [64] to these moments currently provides the most precise single $|V_{cb}|$ determination. This input however has not yet been taken into account in our global fit.

50 times larger than the $b \to u$ signal. To suppress this background, experimental cuts in the three-dimensional phase space have to be applied which introduce additional theoretical uncertainties. In a first kind of analyses, $B \to X_u \ell^- \overline{\nu}_\ell$ decays are separated from $b \to c$ background by accepting leptons with center-of-mass momenta typically larger than 2.2–2.3 GeV, a region which kinematically excludes $B \to X_c \ell^- \overline{\nu}_\ell$ decays. However this requirement retains only 10–15% of the semileptonic branching fraction. In this endpoint-region, the spectrum is dominated by the so-called *shape* function, a non-perturbative object that reflects the Fermi motion of the b quark inside the B meson. Without knowledge of the shape function, the extrapolation of the measured partial branching fraction to the full semileptonic branching fraction is highly model-dependent, a drawback from which the pioneering $|V_{ub}|$ determinations by the ARGUS and CLEO collaborations suffered [73–75] (see also [76–79]). The problem can be circumvented to some extent by measuring the shape function in inclusive $B \to X_s\gamma$ decays, so far only published by the CLEO collaboration [65]. Recent lepton endpoint measurements have been presented by CLEO, *BABAR* and Belle [80–82], where all analyses are using the $B \to X_s\gamma$ measurement from CLEO [65]. There is a discussion in the literature concerning uncertainties from subleading shape functions [83–86]). From this, one deduces that an additional theoretical uncertainty on $|V_{ub}|$ of the order of a few percent may be present. One should also note that there could be sizable effects from the violation of quark-hadron duality in this small region of the phase space, which introduces theoretical uncertainties that are difficult to quantify [87].

The $b \to c$ background in inclusive decays can also be suppressed by cutting on the hadronic invariant mass m_X. Accepting only events with m_X below the D meson mass retains about 70–80% of the $B \to X_u \ell^- \overline{\nu}_\ell$ events. Due to detector resolution effects, the cut has to be lowered, which again increases the theoretical uncertainties from the shape function. The kinematic region sensitive to the shape function can be avoided by cutting in addition on q^2, which in turn increases the statistical uncertainty. A complication in the high-q^2 region is the possible significant contribution from annihilation diagrams which cannot be computed at present [88]. A possible way to quantify such annihilation contributions would be to determine the branching fraction for charged and neutral B mesons separately. Various analyses reconstructing m_X have been published in the past [89–92], some of which apply additional cuts on q^2 [91,92].

A different approach has been followed by ALEPH [93] and OPAL [94] who extract $|V_{ub}|$ from measurements of the full semileptonic branching fraction by suppressing the dominant $b \to c$ background by means of a neural network.

For an up-to-date review of $|V_{ub}|$ determinations see, e.g., [62]. Following the HFAG recipe, we have only averaged the results from experiments running on the $\Upsilon(4S)$ and obtain $|V_{ub}| = (4.45 \pm 0.09_{\rm stat,sys} \pm 0.56_{\rm theo}) \times 10^{-3}$. Similarly as in [95], we enlarge the theoretical uncertainty due to possible additional uncertainties from subleading shape function effects, annihilation contributions in the high-q^2 region and quark-hadron duality violations, resulting in $|V_{ub}| = (4.45 \pm 0.09_{\rm stat,sys} \pm 0.68_{\rm theo}) \times 10^{-3}$.

Average

In the CKM fit, we use $|V_{ub}|$ from inclusive and exclusive determinations. Usually, one would combine them by multiplying their corresponding likelihoods. However their agreement is marginal so that the two likelihoods only overlap if the theoretical uncertainties are driven to their extreme. Given the fact that several theoretical issues are not settled yet and since $|V_{ub}|$ is one of the key ingredients of the CKM fit, we adopt a more conservative treatment: the inclusive and exclusive $|V_{ub}|$ central values are averaged and as theoretical error is assigned the larger one of both determinations. This gives $|V_{ub}| = (3.90 \pm 0.08_{\rm exp} \pm 0.68_{\rm theo}) \times 10^{-3}$.

2.6 $|\varepsilon_K|$

The neutral kaon system provides constraints on the Unitarity Triangle through $K^0\overline{K}^0$ mixing, indirect[18] and direct CP violation, and the rare decays $K^+ \to \pi^+\nu\overline{\nu}$ and (yet unknown) $K_L^0 \to \pi^0\nu\overline{\nu}$. Only indirect CP violation is used in the standard CKM fit since the corresponding matrix element can be obtained by Lattice QCD with accountable systematic uncertainties. The SM prediction for neutral kaon mixing suffers from badly controlled long-distance contributions to the mixing amplitudes (see, however, [96] where Δm_K is found to be short-distance dominated). Moreover, complicated non-perturbative physics with large hadronic uncertainties prevents us from using the measurement of direct CP violation. Rare decays are much cleaner and will give precise constraints as soon as they are measured with a reasonable accuracy. We refer to Part IV for a dedicated study of direct CP violation and rare kaon decays.

The most precise measurement of the CP-violation parameter ε_K comes from the ratios of amplitudes, η_{+-} and η_{00}, of K_L^0 to K_S^0 decaying to pairs of charged and neutral pions, respectively,

$$\varepsilon_K = \frac{2}{3}\eta_{+-} + \frac{1}{3}\eta_{00} \ . \tag{61}$$

[18] The term "indirect" comprises CP violation in mixing and CP violation in the interference between decay with and without mixing. In the kaon sector, these types of CP violation are given by ${\rm Re}\varepsilon_K$ and ${\rm Im}\varepsilon_K$, respectively, which are of similar size.

We use the average $|\varepsilon_K| = (2.282 \pm 0.017) \times 10^{-3}$, obtained from the PDG values for η_{+-} and η_{00} [12] assuming no phase difference between these amplitude ratios, and taking into account the correlation induced by the measurements of ε'/ε [97]. [19] The phase of ε_K is not considered here as it does not depend on the CKM matrix elements. Other observables related to $|\varepsilon_K|$, like the charge asymmetries δ_L in semileptonic K^0_L decays, $|\eta_{+-\gamma}|$, or decay-plane asymmetries in $K^0_L \to \pi^+\pi^- e^+ e^-$ decays are not considered in this average, since their precision is not competitive.

Within the SM, CP violation is induced by $\Delta S = 2$ transitions, mediated by box diagrams. They can be related to the CKM matrix elements by means of the local hadronic matrix element

$$\langle \overline{K}^0 | (\bar{s}\gamma^\mu(1-\gamma^5)d)^2 | K^0 \rangle = \frac{8}{3} m_K^2 f_K^2 B_K \ . \tag{62}$$

The neutral kaon decay constant, $f_K = (159.8 \pm 1.5)\,\mathrm{MeV}$ [12], is extracted from the leptonic decay rate $\Gamma(K^+ \to \mu^+\nu_\mu)$, assuming negligible isospin violation. The most reliable prediction of the "bag" parameter B_K, which parameterizes the deviation with respect to the vacuum insertion approximation $B_K = 1$, is obtained from Lattice QCD. At present, calculations are performed assuming SU(3) symmetry and within the quenched approximation, *i.e.*, neglecting sea-quark contributions in closed loops, which leads to a substantial reduction in computing time. The world average is $B_K = 0.86 \pm 0.06 \pm 0.14$ [99], where the first error combines statistical and accountable systematic uncertainties and the second is an estimate of the bias from the quenched approximation and SU(3) breaking. Note that analytical approaches based on the large-N_c expansion of QCD find a significantly smaller value for B_K in the chiral limit [100]. Large chiral corrections could play an important rôle. At present, B_K is the first source of theoretical uncertainty in the SM prediction of ε_K, while the coupling $|V_{ts}| \sim |V_{cb}|$ is the second one.

Neglecting the real part of the non-diagonal element of the neutral kaon mixing matrix M_{12}, one obtains [101][20]

$$\begin{aligned} |\varepsilon_K| = \frac{G_F^2 m_W^2 m_K f_K^2}{12\sqrt{2}\pi^2 \Delta m_K} B_K \Big(& \eta_{cc} S(x_c, x_c) \mathrm{Im}\big[(V_{cs}V_{cd}^*)^2\big] + \eta_{tt} S(x_t, x_t) \mathrm{Im}\big[(V_{ts}V_{td}^*)^2\big] \\ & + 2\eta_{ct} S(x_c, x_t) \mathrm{Im}\big[V_{cs}V_{cd}^* V_{ts}V_{td}^*\big] \Big) \ , \end{aligned} \tag{63}$$

where $\Delta m_K = (3.490 \pm 0.006) \times 10^{-12}\,\mathrm{MeV}$ [12], and where $S(x_i, x_j)$ are the Inami-Lim functions [102]

$$\begin{aligned} S(x) \equiv S(x_i, x_j)_{i=j} &= x \left(\frac{1}{4} + \frac{9}{4(1-x)} - \frac{3}{2(1-x)^2} \right) - \frac{3}{2} \left(\frac{x}{1-x} \right)^3 \ln(x) \ , \\ S(x_i, x_j)_{i\neq j} &= x_i x_j \left[\left(\frac{1}{4} + \frac{3}{2(1-x_i)} - \frac{3}{4(1-x_i)^2} \right) \frac{1}{x_i - x_j} \ln(x_i) \right. \\ & \left. + (x_i \leftrightarrow x_j) - \frac{3}{4} \frac{1}{(1-x_i)(1-x_j)} \right] \ , \end{aligned} \tag{64}$$

with $x_i = m_i^2/m_W^2$ $(i = c, t)$. We use the $\overline{\mathrm{MS}}$ masses[21] $\overline{m}_t(m_t) = (167.5 \pm 4.0 \pm 0.6)\,\mathrm{GeV}$ and $\overline{m}_c(m_c) = (1.2 \pm 0.2)\,\mathrm{GeV}$, where a conservative error is assigned to the running charm quark mass. The parameters η_{ij} in (63) are next-to-leading order QCD corrections to the Inami-Lim functions. We use the values $\eta_{ct} = 0.47 \pm 0.04$ and $\eta_{tt} = 0.5765 \pm 0.0065$ [107,108], while for η_{cc}, the parameter with the largest uncertainty, we use the parameterization [107]

$$\eta_{cc} \simeq (1.46 \pm \delta_{cc}) \left[1 - 1.2 \left(\frac{\overline{m}_c(m_c)}{1.25\,\mathrm{GeV}} - 1 \right) \right] \left[1 + 52\,(\alpha_S(m_Z) - 0.118) \right] , \tag{66}$$

[19] Very recently, the KTeV collaboration has presented a new precise result on $|\eta_{+-}| = (2.228 \pm 0.010) \times 10^{-3}$ [98] to be compared to the value of $|\eta_{+-}| = (2.286 \pm 0.017)$ [12] translating in a 2.9 σ difference. This new value has not been taken into account yet as an input to our fit.

[20] Note the non-trivial CKM dependence in (63), which only reduces to a hyperbola at lowest orders in λ, and for values of $\overline{\rho}$ and $\overline{\eta}$ close to the origin.

[21] We derive the value of $\overline{m}_t(m_t)$ from the newest measurement of the pole mass $m_t = (178.0 \pm 2.7 \pm 3.3)\,\mathrm{GeV}$ by the CDF and D0 collaborations [103], where the first error given is statistical and the second systematic. We apply the pole-to-$\overline{\mathrm{MS}}$ matching at three loops [104–106] with five light quark flavors, where we neglect the mass of the light quark flavors with respect to the t-quark mass. This leads to the perturbative series

$$\frac{\overline{m}_t(m_t)}{m_t} = 1 - \frac{4}{3}\left(\frac{\alpha_S}{\pi}\right) - 9.12530\left(\frac{\alpha_S}{\pi}\right)^2 - 80.4045\left(\frac{\alpha_S}{\pi}\right)^3 \ , \tag{65}$$

where $\alpha_S \equiv \alpha_S^{(6)}(m_t) = 0.1068 \pm 0.0018$ (see Table 1) is the $\overline{\mathrm{MS}}$ strong coupling constant for six active quark flavors at the scale of the pole mass. With this we find $\overline{m}_t(m_t) = (167.5 \pm 4.0 \pm 0.6)\,\mathrm{GeV}$, where the first error is experimental and the second is due to the truncation of the perturbative series and the uncertainty on α_S.

with an uncertainty from higher-order corrections parameterized by the δ_{cc} term

$$\delta_{cc} = 0.22 \left[1 - 1.8 \left(\frac{\overline{m}_c(m_c)}{1.25\,\mathrm{GeV}} - 1 \right)\right] \left[1 + 80\,(\alpha_S(m_Z) - 0.118)\right]. \tag{67}$$

In this way, (66) agrees with the complete NLO calculation within a few percent. With $\overline{m}_c(m_c)$ given above and $\alpha_S(m_Z) = 0.118 \pm 0.003$, and treating the errors as theoretical systematics, we find for η_{cc} the range 1.0 – 2.6 at 95% CL.

2.7 Δm_d

The $B^0\overline{B}^0$ oscillation frequency is determined by the mass difference Δm_d between the two B^0 mass eigenstates, B_H and B_L. It is defined as a positive number and has been measured by many experiments to an average accuracy of almost 1% (see Table 1). In analogy to $|\varepsilon_K|$, $B^0\overline{B}^0$ oscillation in the SM is driven by effective flavor-changing neutral current (FCNC) processes through $\Delta B = 2$ box diagrams. However, in contrast to $|\varepsilon_K|$ where the large hierarchy in the Inami-Lim functions is partly compensated by the CKM matrix elements, the $\Delta B = 2$ box diagrams are dominated by top quark exchange between the virtual $W^\pm$ boson lines. This simplifies the theoretical prediction of Δm_d which is given by[22]

$$\Delta m_d = \frac{G_\mathrm{F}^2}{6\pi^2} \eta_B m_{B_d} f_{B_d}^2 B_d m_W^2 S(x_t) \left|V_{td} V_{tb}^*\right|^2 \ , \tag{68}$$

where $\eta_B = 0.551 \pm 0.007$ (for a review, see [101]) is a perturbative QCD correction to the Inami-Lim function $S(x_t)$ from perturbative QCD. The matrix element $f_{B_d}\sqrt{B_d}$ is taken from Lattice QCD. Much progress has been achieved in this domain recently, where partially unquenched calculations are now available. Nevertheless, there is an ongoing discussion in the Lattice community whether the extrapolation for the light d quark mass to the chiral-limit is well-understood (see the discussion of Δm_s below for further details). Here, we use the value and errors derived in [109] (cf. Table 1).

For leptonic B decays and the semileptonic CP asymmetry A_SL discussed in Part VII, the decay constant f_{B_d} and the bag parameter B_d are needed separately. The values and uncertainties used (cf. Table 1) are also taken from [109].

2.8 Δm_s

In the SM, the mass difference Δm_s between the heavy and the light B_s^0 mesons has only a weak relative dependence on the Wolfenstein parameters $(\overline{\rho}, \overline{\eta})$. Nevertheless, a measurement of Δm_s is useful in the CKM fit since it indirectly leads to an improvement of the constraint from the Δm_d measurement on $|V_{td}V_{tb}^*|^2$. The SM prediction

$$\Delta m_s = \frac{G_\mathrm{F}^2}{6\pi^2} \eta_B m_{B_s} f_{B_s}^2 B_s m_W^2 S(x_t) \left|V_{ts} V_{tb}^*\right|^2 \ , \tag{69}$$

can be rewritten as

$$\Delta m_s = \frac{G_\mathrm{F}^2}{6\pi^2} \eta_B m_{B_s} \xi^2 f_{B_d}^2 B_d m_W^2 S(x_t) \left|V_{ts} V_{tb}^*\right|^2 \ , \tag{70}$$

where the parameter $\xi = f_{B_s}\sqrt{B_s}/f_{B_d}\sqrt{B_d}$ quantifies SU(3)-breaking corrections to the matrix elements, which can be calculated more accurately in Lattice QCD than the matrix elements themselves. Hence a measurement of Δm_s improves the knowledge of $f_{B_d}\sqrt{B_d}$. In our previous analysis [6] we used the value $\xi = 1.16 \pm 0.05$. Recently, the uncertainty on ξ from Lattice QCD has been revisited: Lattice calculations using Wilson fermions have to work with light quark masses of $\mathcal{O}(100\,\mathrm{MeV})$, so that calculations for B^0 mesons need to be extrapolated to the "chiral limit" (this is not necessary for the B_s^0 due to the heavy strange quark). This process is controversial because of the potential presence of a curvature in the chiral extrapolation curve (see e.g. [110–115]). The recent development using "staggered" fermions allows one to perform Lattice QCD calculations with significantly smaller light quark masses. So far, these studies do not show a significant enhancement of ξ [116] but one should keep in mind that the interpretation of results obtained with the use of staggered fermions is still under discussions (cf. e.g. [109]). Based on a phenomenological

[22] The CKM factor $|V_{td}V_{tb}^*|^2$ occurring in (68) approximately describes a circle around $(1,0)$ in the $(\overline{\rho}, \overline{\eta})$ plane, to which a distortion appears at order $\mathcal{O}(\lambda^{10})$:

$$|V_{td}V_{tb}^*|^2 = \lambda^6 A^2 \left[(1-\overline{\rho})^2 + \overline{\eta}^2\right] + \lambda^{10} A^4 (2\overline{\rho} - 1) \left[(1-\overline{\rho})^2 + \overline{\eta}^2\right] + \mathcal{O}(\lambda^{12}) \ .$$

analysis, it has been shown in [115] that in the chiral limit, the double-ratio $(f_{B_s}/f_{B_d})/(f_K/f_\pi)$ does not differ much from unity resulting in $\xi = 1.21 \pm 0.04 \pm 0.05$, where the second error is due to the chiral extrapolation[23]. Interestingly, based on a quark model, the Lattice value of $\xi \approx 1.16$ was considered too low [117], even before the discussion about the chiral extrapolation had started.

Limits on Δm_s from the search for $B_s^0\overline{B}_s^0$ oscillation have been obtained by several experiments [118–122]. A convenient approach to average various results on Δm_s is the Amplitude Method [123] (see also the exhaustive study in [124]), which consists of introducing an *ad hoc* amplitude coefficient, $\mathcal{A}$, placed in front of the cosine modulation term (see Appendix A.5.2 for further details). The advantage of this indirect probe for oscillation stems from the fact that the dependence on $\mathcal{A}$ is linear and hence the measurement of $\mathcal{A}$ is Gaussian, so that merging different experimental measurements is straightforward. One can then define the experimental sensitivity for given Δm_s by $1.645 \times \sigma_{\mathcal{A}}(\Delta m_s)$ (found to be 18.7 ps^{-1} [62]), and a 95% CL lower limit for Δm_s, given by the sum of the sensitivity and the central value of the measured amplitude. It is found to be 14.4 ps^{-1} [62].

The question on how to deduce the confidence level from the available experimental information is crucial to the CKM analysis and has been scrutinized on many occasions [123–125,8,6,9]. Traditionally, $B_s^0\overline{B}_s^0$ oscillation results have been implemented into fits using $\chi^2_{|1-\mathcal{A}|} = ((1-\mathcal{A})/\sigma_{\mathcal{A}})^2$ with $\mathrm{CL}(\chi^2_{|1-\mathcal{A}|}) = \mathrm{Erfc}(|1-\mathcal{A}|/\sigma_{\mathcal{A}}/\sqrt{2}))$ [123]. However this procedure does not properly interpret the information of the amplitude spectrum. For instance, two measured amplitudes $\mathcal{A}_1$ and $\mathcal{A}_2$, where $\mathcal{A}_1 > 1$ and $\mathcal{A}_2 < 1$ but $\mathcal{A}_1 - 1 = 1 - \mathcal{A}_2$, result in the same confidence level in this approach although it would be natural to assign a larger likelihood for an oscillation to $\mathcal{A}_1$ than to $\mathcal{A}_2$. In [6], an alternative procedure, which exploits the information from the sign of $1-\mathcal{A}$ by omitting the modulus in the above definition of $\chi^2_{|1-\mathcal{A}|}$, has been proposed: $\chi^2_{1-\mathcal{A}} = 2 \cdot \left[\mathrm{Erfc}^{-1}\left(\frac{1}{2}\,\mathrm{Erfc}\left(\frac{1-\mathcal{A}}{\sqrt{2}\sigma_{\mathcal{A}}}\right)\right)\right]^2$. As pointed out in [9], this procedure is an approximation and can lead to a bias in presence of a true measurement. The information from the fit to the proper time distributions of mixed and unmixed $B_s^0\overline{B}_s^0$ decays is obtained from the ratio of the likelihood at given frequency Δm_s, $\mathcal{L}(\Delta m_s)$, to the likelihood at infinity, $\mathcal{L}(\Delta m_s = \infty)$ [123,125,8], for which the logarithm reads

$$2\Delta \ln \mathcal{L}^{\infty}(\Delta m_s) = \frac{(1-\mathcal{A})^2}{\sigma^2_{\mathcal{A}}} - \frac{\mathcal{A}^2}{\sigma^2_{\mathcal{A}}} \; . \tag{71}$$

In Appendix A we propose a frequentist method to deduce a confidence level from this information. This method is the one used in our CKM fit.

2.9 $|V_{ts}|$

Besides Δm_s, the inclusive branching fraction of the radiative decay $B \to X_s\gamma$ determines the product $|V_{ts}V_{tb}^*|$. Using the measurements from CLEO, ALEPH, *BABAR* and Belle, [126] quotes $|V_{ts}V_{tb}^*| = 0.047 \pm 0.008$. Since the precision of this constraint is not competitive it is not used in our fit.

The ratio $|V_{td}/V_{ts}|$ can be determined from the ratio of the exclusive rates for the decays $B \to \rho\gamma$ to $B \to K^*\gamma$, which eliminates the form factor dependencies up to SU(3) breaking. Based on the recent 3.5σ evidence for the decay $B \to \rho\gamma$ found by Belle [127], a phenomenological study has been performed in [128]. The constraint on $|V_{td}/V_{ts}|$ derived from the measurement is found to be in agreement with the expectation, but is not (yet) accurate enough to represent a competitive input in the global CKM fit.

2.10 $\sin 2\beta$

In $b \to c\bar{c}s$ quark-level decays, the time-dependent CP-violation parameter S measured from the interference between decays with and without mixing is equal to $\sin 2\beta$ to a very good approximation. The world average uses measurements from the decays $B^0 \to J/\psi K_S^0$, $J/\psi K_L^0$, $\psi(2S)K_S^0$, $\chi_{c1}K_S^0$, $\eta_c K_S^0$ and $J/\psi K^{*0}$ ($K^{*0} \to K_S^0\pi^0$) and gives $\sin 2\beta_{[c\bar{c}]} = 0.739 \pm 0.048$ [62]. It is dominated by the measurements from *BABAR* [129] and Belle [130]. In $b \to c\bar{c}d$ quark-level decays, such as $B^0 \to J/\psi\pi^0$ or $B^0 \to D^{(*)}D^{(*)}$, unknown contributions from (not CKM-suppressed) penguin-type diagrams carrying a different weak phase than the tree-level diagram compromises the clean extraction of $\sin 2\beta$. As a consequence, they are not taken into account in the $\sin 2\beta$ average.

Within the SM, decays mediated by the loop transitions $b \to s\bar{q}q$ ($q = u, d, s$), such as $B^0 \to \phi K^0$ or $B^0 \to K^+K^-K_S^0$, but also the recently measured $B^0 \to f_0K_S^0$, as well as $B^0 \to \eta' K_S^0$ and $B^0 \to \pi^0 K_S^0$, can be used to extract $\sin 2\beta$ in a relatively clean way (see [131–135] and [136–140,62] for the experimental results). Due to the large virtual mass scales occurring in the penguin loops, additional diagrams with heavy particles in the loops and

[23] Note that the latter error is strongly correlated with the one on $f_{B_d}\sqrt{B_d}$, because both have the same source. We neglect this correlation, which may result in an underestimation of the impact of the bound on Δm_s.

new CP-violating phases may contribute. Such a measurement of the weak phase from mixing-induced CP violation and the comparison with the SM expectation is therefore a sensitive probe for physics beyond the SM. Assuming penguin dominance and neglecting CKM-suppressed amplitudes, these decays carry approximately the same weak phase as the decay $B^0 \to J/\psi K^0_S$. As a consequence, their mixing-induced CP-violation parameters are expected to be $-\eta_f \times \sin 2\beta$ to a reasonable accuracy in the SM, where η_f is the CP eigenvalue of the final state. Recent measurements from *BABAR* and Belle give conflicting results for the mixing-induced CP parameter of ϕK^0: with the Belle result, $S_{\phi K^0_S} = -0.96 \pm 0.50^{+0.09}_{-0.11}$ [137], indicating a 3.3σ deviation from the SM, while *BABAR* finds (using both ϕK^0_S and ϕK^0_L) $-\eta_{\phi K} S_{\phi K} = 0.47 \pm 0.34^{+0.08}_{-0.06}$ [136], which is in agreement with $\sin 2\beta_{[c\bar{c}]}$. Moreover, the world averages $-S_{K^+K^-K^0_S} = 0.54 \pm 0.18^{+0.17}_{-0}$ and $S_{\eta' K^0_S} = 0.27 \pm 0.21$ [62] (*BABAR* and Belle agree for these) do not show a significant departure from the charmonium reference, though both tend to support the observation $\sin 2\beta_{\mathrm{eff},\, sq\bar{q}} < \sin 2\beta_{[c\bar{c}]}$. Finally, the recent *BABAR* measurement $-S_{f_0 K^0_S} = 1.62^{+0.51}_{-0.56} \pm 0.10$ [139] is in decent agreement with $\sin 2\beta_{[c\bar{c}]}$.

A more detailed numerical discussion of the various $\sin 2\beta$ results is given in Sect. III.3.4. At present, we do not include the results from penguin-dominated decays in the $\sin 2\beta$ average.

2.11 $\sin 2\alpha$

The measurement of the time-dependent CP-violating asymmetries in the charmless decay $B^0 \to \rho^+\rho^-$ allows us to derive a significant constraint on the angle $\sin 2\alpha$ using the Gronau–London isospin analysis [141] (extended here to include electroweak penguins), which invokes $B \to \rho\rho$ decays of all charges. While the full isospin analysis requires the measurement of (at least one of) the time-dependent CP parameters[24] in the color-suppressed decay $B^0 \to \rho^0\rho^0$, the available upper limit on its branching fraction can be used to constrain $|\alpha - \alpha_{\mathrm{eff}}|$. Albeit analytical bounds have been derived for this case [142–144], the numerical analysis performed in CKMfitter leads to equivalent results (see the detailed discussions of the isospin analysis in Sect. VI.1.2.1 and VI.5).

For the isospin-related decays we use the branching fractions $\mathcal{B}(B^0 \to \rho^+\rho^-) = (30 \pm 4 \pm 5) \times 10^{-6}$ [145] (see also the first observation and polarization measurement of this mode in [146]), $\mathcal{B}(B^+ \to \rho^+\rho^0) = (26.4^{+6.1}_{-6.4}) \times 10^{-6}$ [62,147,148], and the upper limit at 90% CL $\mathcal{B}(B^0 \to \rho^0\rho^0) < 2.1 \times 10^{-6}$ [147] (in the CKM fit we use the result $\mathcal{B}(B^0 \to \rho^0\rho^0) = (0.6^{+0.8}_{-0.6} \pm 0.1) \times 10^{-6}$, which leads to this limit). The ρ mesons in the decays $B^0 \to \rho^+\rho^-$ and $B^+ \to \rho^+\rho^0$ are found to be longitudinally polarized with the longitudinal fractions ($f_L \equiv \Gamma_L/\Gamma$): $f_L^{+-} = 0.99 \pm 0.03^{+0.04}_{-0.03}$ [145] and $f_L^{+0} = 0.962^{+0.049}_{-0.065}$ [147,148], respectively. As a consequence, the $B \to \rho\rho$ system is actually like the $B \to \pi\pi$ system. Assuming (conservatively) the relative polarization of the ρ^0 mesons in $B^0 \to \rho^0\rho^0$ to be fully longitudinal, and using the CP asymmetries $S^{+-}_{\rho\rho,L} = -0.19 \pm 0.33 \pm 0.11$ and $C^{+-}_{\rho\rho,L} = -0.23 \pm 0.24 \pm 0.14$ measured by *BABAR* [145,149] for the longitudinal fraction of the $B^0 \to \rho^+\rho^-$ event sample, together with the branching fraction and polarization measurements for the other charges, we obtain constraints on $\sin 2\alpha$ as described in Sect. VI.5.

Note that the present analysis neglects non-resonant contributions and possible other $\pi^+\pi^-$ resonances under the ρ^0, as well as effects from the radial excitations $\rho(1450)$ and $\rho(1700)$ that were found to be significant contributors to the pion form factor in e^+e^- annihilation [150] and τ decays [151]. Also neglected are isospin-violating contributions due to the finite width of the ρ [152], as well as electromagnetic and strong sources of isospin violation (see the discussion in Sect. VI.5).

3 Results of the global fit

The standard CKM fit includes those observables for which the Standard Model predictions (and hence the CKM constraints) can be considered to be quantitatively under control. We only take into account measurements that lead to significant and competitive constraints on the CKM parameters. The *standard observables* are:

$$|V_{us}|\ , \quad |V_{ud}|\ , \quad |V_{ub}|\ , \quad |V_{cb}|\ , \quad |\varepsilon_K|\ , \quad \Delta m_d\ , \quad \Delta m_s\ , \quad \sin 2\beta_{[c\bar{c}]}\ , \quad \sin 2\alpha_{[\rho\rho]}\ . \tag{72}$$

The theoretical uncertainties related to these observables are discussed in Sect. III.2.

Among the observables that are not (yet) considered are the following.

- Measurements of the remaining CKM elements as well as the constraints from the rare kaon decay $K^+ \to \pi^+\nu\overline{\nu}$ and from $B \to \rho\gamma$ are not (yet) precise enough to improve the knowledge of the CKM matrix (cf. Sect. III.2.9).
- The theoretical prediction of direct CPV in kaon decays (ε'/ε) is not yet settled (cf. Sect. III.2).

[24] Note that in contrast to $B^0 \to \pi^0\pi^0$ both, $C^{00}_{\rho\rho,L}$ and $S^{00}_{\rho\rho,L}$, are experimentally accessible in $B^0 \to \rho^0\rho^0$. Their measurement overconstrains the isospin analysis and can be used to remove some of the ambiguities on α (see Sect. VI.5).

Table 1. Inputs to the standard CKM fit. If not stated otherwise: for two errors given, the first is statistical and accountable systematic and the second stands for systematic theoretical uncertainties. The fourth and fifth columns indicate the treatment of the input parameters within *R*fit: measurements or parameters that have statistical errors (we include here experimental systematics) are marked in the "GS" column by an asterisk; measurements or parameters that have systematic theoretical errors, treated as ranges in *R*fit, are marked in the "TH" column by an asterisk. *Upper part*: experimental determinations of the CKM matrix elements. *Middle upper part*: *CP*-violation and mixing observables. *Middle lower part*: parameters used in SM predictions that are obtained from experiment. *Lower part*: parameters of the SM predictions obtained from theory

Parameter	Value ± Error(s)	Reference	Errors	
			GS	TH
$\|V_{ud}\|$ (neutrons)	$0.9717 \pm 0.0013 \pm 0.0004$	(see text)	$\star$	$\star$
$\|V_{ud}\|$ (nuclei)	$0.9740 \pm 0.0001 \pm 0.0008$	(see text)	$\star$	$\star$
$\|V_{ud}\|$ (pions)	$0.9765 \pm 0.0055 \pm 0.0005$	[20]	$\star$	$\star$
$\|V_{us}\|$	$0.2228 \pm 0.0039 \pm 0.0018$	see text	$\star$	$\star$
$\|V_{ub}\|$ (average)	$(3.90 \pm 0.08 \pm 0.68) \times 10^{-3}$	see text, [62]	$\star$	$\star$
$\|V_{cb}\|$ (incl.)	$(42.0 \pm 0.6 \pm 0.8) \times 10^{-3}$	see text	$\star$	$\star$
$\|V_{cb}\|$ (excl.)	$40.2\,^{+2.1}_{-1.8} \times 10^{-3}$	[62,61]	$\star$	-
$\|\varepsilon_K\|$	$(2.282 \pm 0.017) \times 10^{-3}$	[97]	$\star$	-
Δm_d	(0.502 ± 0.006) ps^{-1}	[62]	$\star$	-
Δm_s	Amplitude spectrum	[62]	$\star$	-
$\sin 2\beta_{[c\bar{c}]}$	0.739 ± 0.048	[62]	$\star$	-
$S^{+-}_{\rho\rho,L}$	-0.19 ± 0.35	see text	$\star$	-
$C^{+-}_{\rho\rho,L}$	-0.23 ± 0.28	see text	$\star$	-
$\mathcal{B}_{\rho\rho,L}$ all charges	see text	see text	$\star$	-
$\overline{m}_c(m_c)$	(1.2 ± 0.2) GeV	[12]	-	$\star$
$\overline{m}_t(m_t)$	$(167.5 \pm 4.0 \pm 0.6)$ GeV	[12]	$\star$	-
m_{K^+}	(493.677 ± 0.016) MeV	[12]	-	-
Δm_K	$(3.490 \pm 0.006) \times 10^{-12}$ MeV	[12]	-	-
m_{B_d}	(5.2794 ± 0.0005) GeV	[12]	-	-
m_{B_s}	(5.3696 ± 0.0024) GeV	[12]	-	-
m_W	(80.423 ± 0.039) GeV	[12]	-	-
G_F	1.16639×10^{-5} GeV^{-2}	[12]	-	-
f_K	(159.8 ± 1.5) MeV	[12]	-	-
B_K	$0.86 \pm 0.06 \pm 0.14$	[99]	$\star$	$\star$
$\alpha_S(m_Z^2)$	0.1172 ± 0.0020	[12]	-	$\star$
η_{ct}	0.47 ± 0.04	[107]	-	$\star$
η_{tt}	0.5765 ± 0.0065	[107,108]	-	-
$\eta_B(\overline{\rm MS})$	0.551 ± 0.007	[101]	-	$\star$
$f_{B_d}\sqrt{B_d}$	$(228 \pm 30 \pm 10)$ MeV	[109]	$\star$	$\star$
f_{B_d}	$(200 \pm 28 \pm 9)$ MeV	[109]	$\star$	$\star$
B_d	1.3 ± 0.12	[109]	$\star$	$\star$
ξ	$1.21 \pm 0.04 \pm 0.05$	[109]	$\star$	$\star$
$B \to \rho\rho$ amplitude params.	all floating	see text	-	$\star$

– Charmless B decays other than $B \to \rho\rho$ also lead to various interesting constraints on the angles of the Unitarity Triangle and provide sensitivity to contributions from physics beyond the SM. Detailed discussions are given in Part VI. In principle, amplitude analyses using SU(2) symmetry are theoretically safe (the isospin-breaking contributions can be controlled) so that they will be used in the standard CKM fit once they lead to significant results. SU(3)-based analyses are in general more constraining, with however the limitation that theoretical uncertainties are more difficult to control.
– Various constraints on the angle γ can be obtained from the comparison of CKM-favored and CKM-suppressed $b \to c$ decays (cf. Part V). The accumulated statistic are, however, not yet sufficient to perform fully data-driven analyses and to eliminate theoretical input with uncertain errors.

We use the observables (72) to perform constrained fits to the CKM parameters and related quantities. We place ourselves in the framework of the *R*fit scheme (cf. Part II) and hence define the theoretical likelihoods of (30) to be one within the allowed ranges and zero outside. In other words, we use $\kappa = 0$ and $\zeta = 1$ for the Hat function $\mathcal{L}_{\rm syst}(x_0)$ defined in (56). As a consequence, no hierarchy is introduced for any permitted set of theoretical parameters, i.e., the χ^2 that is minimized in the fit receives no contribution from theoretical systematics. However the theoretical parameters cannot trespass their allowed ranges. When relevant, statistical and theoretical uncertainties are combined beforehand, following the procedure outlined in Sect. II.6.1. Floating theoretical parameters are labelled by an asterisk in the "TH" column of Table 1. For parameters with insignificant theoretical uncertainties, the errors are propagated through the theoretical predictions, and added in quadrature to the experimental error of the corresponding measurements[25].

3.1 Probing the Standard Model

We have demonstrated in Part II that the metrological phase is intrinsically unable to detect a failure of the SM to describe the data. We therefore begin the CKM analysis with an interpretation of the test statistics $\chi^2_{{\rm min};y_{\rm mod}}$, which is a probe of the goodness-of-fit test for the SM hypothesis. We perform the toy Monte Carlo simulation described in Sect. II.3. The standard CKM fit returns after convergence

$$\chi^2_{{\rm min};y_{\rm mod}} = 0.6 \ , \tag{73}$$

for the full data set (including $\sin 2\beta_{[c\bar{c}]}$ and $\sin 2\alpha_{[\rho\rho]}$, where the latter has little impact only). We generate the probability density distribution $\mathcal{F}(\chi^2)$ of $\chi^2_{{\rm min};y_{\rm mod}}$ by fluctuating the measurements and $y_{\rm QCD}$ parameters according to their non-theoretical errors around the theoretical values obtained with the use of the parameter set $y^{\rm opt}_{\rm mod}$ for which $\chi^2_{{\rm min};y_{\rm mod}}$ is obtained. The resulting toy distribution is shown by the histogram in Fig. 5. Integrating the distribution according to (51) leads to the significance level (SL) represented by the smooth curve in Fig. 5. We find a p-value of

$$\mathcal{P}(\chi^2_{{\rm min};y_{\rm mod}}|{\rm SM}) \leq {\rm SL}(\chi^2_{{\rm min};y_{\rm mod}}) = 71\% \ , \tag{74}$$

for the validity of the SM. One notices that compared to previous fits [6], the "unitarity problem" in the first row, that is the incompatibility between $|V_{ud}|$ and $1 - |V_{us}|^2$, becomes insignificant with the likelihoods we use for these two quantities (see the discussion in Sect. 2.1 and subsequent paragraphs). Their average has $\chi^2_{{\rm min};|V_{ud}|,|V_{us}|} = 0.16$.

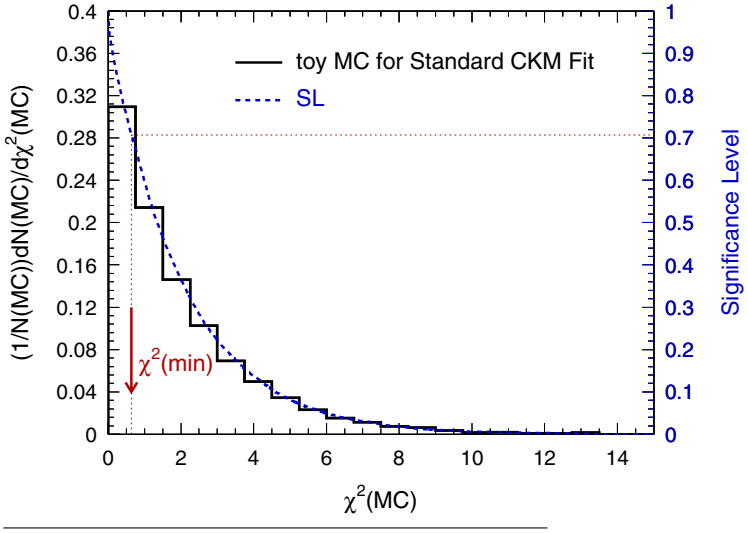

Fig. 5. Simulated $\mathcal{F}(\chi^2)$ distribution and corresponding SL curve for the standard CKM fit. The arrow indicates the corresponding minimal $\chi^2_{{\rm min};y_{\rm mod}}$ found in the analysis

[25] This procedure neglects the correlations occurring when such parameters are used in more than one theoretical prediction.

The large p-value of the electroweak sector of the SM when confronted with all CKM-related data strongly supports the KM mechanism [2] as the dominant source of CP violation at the electroweak scale. It is the necessary condition that permits us to move to the CKM metrology.

3.2 Metrology of the CKM phase

It has become customary to present the constraints on the CP-violating phase in the $(\overline{\rho},\overline{\eta})$ (unitarity) plane of the Wolfenstein parameterization. In the case of such a two-dimensional graphical display, the a parameter space (see Sect. II.2.1) is defined by the coordinates $a=\{x,y\}$ (e.g., $a=\{\overline{\rho},\,\overline{\eta}\}$) and the μ space by the other CKM parameters λ and A, as well as the $y_{\rm QCD}$ parameters. The results of the standard CKM fit are shown in the enlarged $(\overline{\rho},\overline{\eta})$ plane in Fig. 6, not including (upper plot) and including (lower plot) in the fit the world average of $\sin 2\beta$ and $\sin 2\alpha_{[\rho\rho]}$ (see Table 1). The outer contour of the combined fit corresponds to the 5% CL, and the inner contour gives the region where CL ~ 1 and hence theoretical systematics dominate (an adjustment of the μ parameters can maintain maximal agreement i.e., the $\chi^2_{\rm min;y_{mod}}$ value is reproduced therein). Also shown are the $\geq 5\%$ CL regions of the individual constraints. For $\sin 2\beta$ both the $\geq 32\%$ and $\geq 5\%$ CL regions are drawn. A zoom into the region favored by the combined fit is given in Fig. 7.

3.3 Numerical constraints on CKM parameters and related observables

Using the standard CKM fit inputs (72), we derive one-dimensional numerical constraints for the Wolfenstein parameters, the CKM matrix elements, branching ratios of rare K and B meson decays[26] as well as a selection of theoretical parameters. In the case of such one-dimensional displays, the a parameter is defined by the x coordinate, and the μ space by all the other parameters. The Wolfenstein λ has a larger error compared to the fit presented in [6] since we enlarged the uncertainty on $|V_{us}|$ as discussed in Sect. 2. Numerical and graphical results are obtained for CKM fits *including* $\sin 2\beta_{[c\bar{c}]}$ and $\sin 2\alpha_{[\rho\rho]}$. The results are quoted in Tables 2 and 3 and some representative variables are plotted in Fig. 8 for fits with and without $\sin 2\beta_{[c\bar{c}]}$ and $\sin 2\alpha_{[\rho\rho]}$. The statistical precision of the present result for $\sin 2\alpha_{[\rho\rho]}$ is not yet sufficient to give a significant improvement of the standard CKM fit (see the outlook into the future given in Sect. VI.5).

The predictions of the rare W-annihilation decays $B^+\to\ell^+\nu$ can be compared to the present (yet unpublished) upper limits $\mathcal{B}(B^+\to\tau^+\nu)<4.1\times10^{-4}$ [153] and $\mathcal{B}(B^+\to\mu^+\nu)<6.8\times10^{-6}$ [154]. While the $\mu^+\nu$ limit is still an order of magnitude larger than the expected value, the experiments approach the sensitivity required for a discovery of $B^+\to\tau^+\nu$. It may become one of the key analyses in the coming years.

3.4 Is there a $\sin 2\beta$ problem in penguin-dominated decays?

As pointed out in Sect. III.2, penguin-dominated decays like ϕK^0, $\eta' K^0_S$ and CP-even-dominated $K^+K^-K^0_S$ as well as $\pi^0 K^0_S$ ($b\to s\bar{q}q$ transitions) show on average lower experimental $\sin 2\beta$ values than $b\to c\bar{c}s$ transitions. An exception to this is the recent *BABAR* measurement using the decay $f_0K^0_S$.

The interpretation of the non-charmonium decays in terms of $\sin 2\beta$ has to be done with care, since contributions from CKM-suppressed penguins and trees may lead to deviations from the leading weak decay phase of up to $|\sin 2\beta_{s\bar{q}q}-\sin 2\beta_{c\bar{c}s}|\sim 0.2$ within the SM [135,133,134]. When averaging all penguin as well as charmonia measurements we obtain a p-value of 1.7% (2.4σ). If CKM-suppressed penguins and trees can be neglected in $b\to s\bar{q}q$ transitions this might be a hint of an anomaly. When taking into account the modifications of the CL due to the presence of the non-physical boundaries (cf. Sect. II.1.1) the overall p-value decreases to 1.1% (2.6σ).

The individual measurements[27] compared to the constraint from the standard CKM fit, not including $\sin 2\beta$, are shown in Fig. 9. The average of the $S_{\phi K}$ measurement from *BABAR* and Belle has a p-value of 4.9%, so that more data are needed to conclude. If we remove Belle's $S_{\phi K^0_S}$ from the all-mode average, we obtain for the compatibility with the charmonium results a p-value of 29%, which is 1.1σ. Hence without confirmation of Belle's $S_{\phi K^0_S}$ measurement there is no statistical justification to claim evidence for New Physics on the basis of the present data. We stress that a clear

[26] In the SM the branching ratio for the helicity-suppressed decay $B^+\to\ell^+\nu$ is given by

$$\mathcal{B}(B^+\to\ell^+\nu)=\frac{G_{\rm F}^2 m_{B_d} m_\ell^2}{8\pi}\left(1-\frac{m_\ell^2}{m_{B_d}^2}\right) f_{B_d}^2 |V_{ub}|^2 \tau_{B^+}\ .$$

[27] Note that the C coefficients, which vanish if the penguin dominance and the SM assumptions are correct, are left free to vary in the time-dependent fits performed by the experiments. All of them are found to be in reasonable agreement with zero [62].

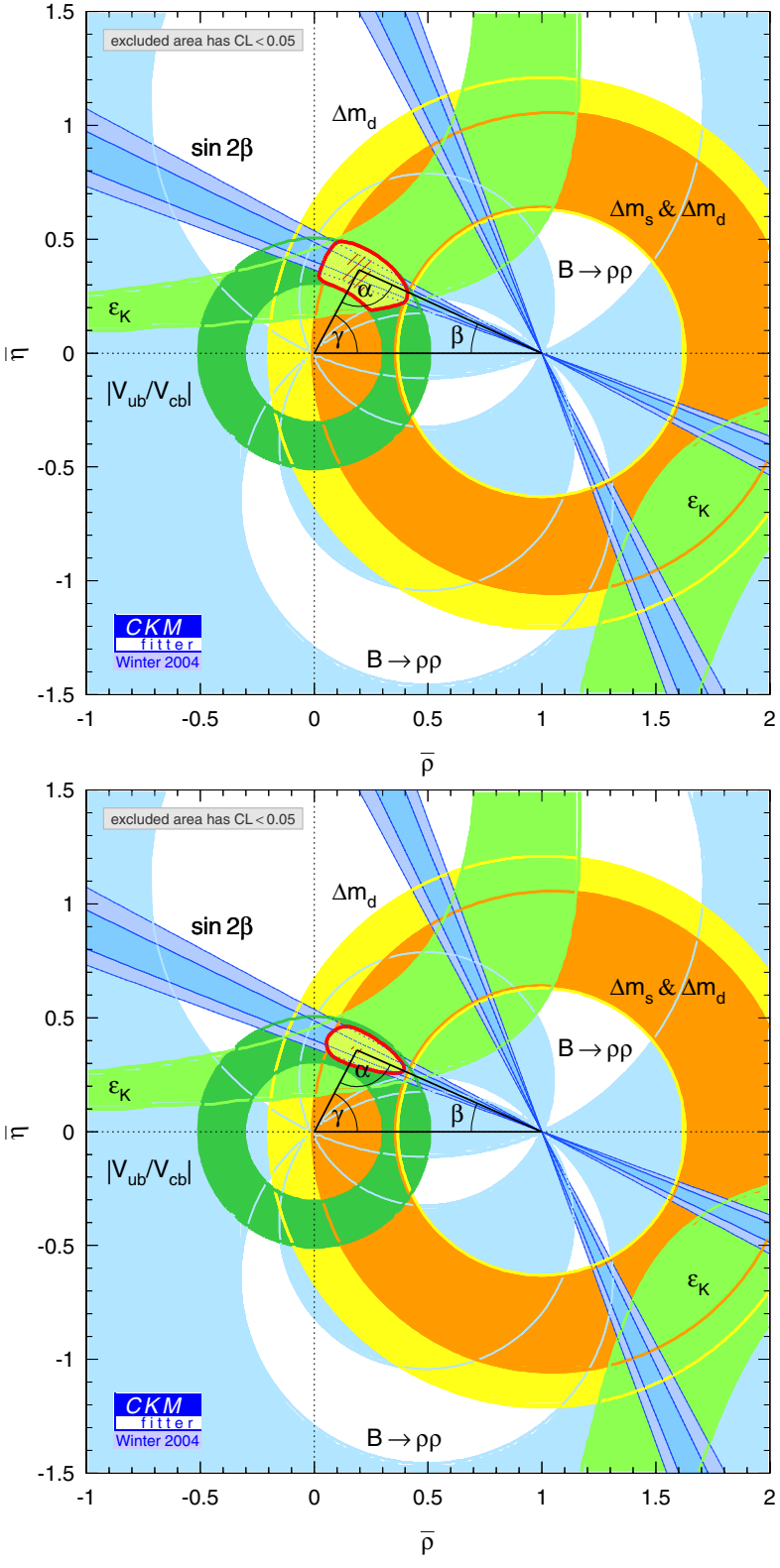

Fig. 6. Confidence levels in the enlarged $(\overline{\rho},\overline{\eta})$ plane for the global CKM fit. The shaded areas indicate the regions of $\geq 5\%$ CLs. For $\sin 2\beta$ the $\geq 32\%$ and $\geq 5\%$ CL constraints are shown. The upper (lower) plot excludes (includes) the constraints from $\sin 2\beta$ and $\sin 2\alpha$ in the combined fit. The hatched area in the center of the combined fit result indicates the region where theoretical errors dominate. The lower plot corresponds to the standard CKM fit

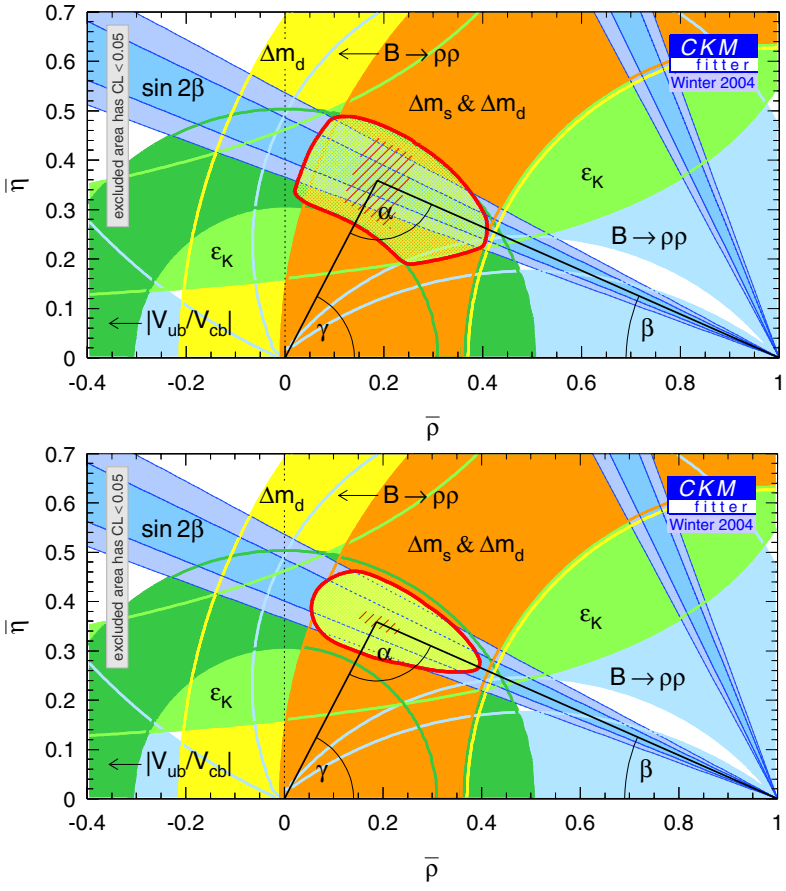

Fig. 7. Confidence levels in the $(\overline{\rho},\overline{\eta})$ plane for the global CKM fit. The shaded areas indicate the regions of $\geq 5\%$ CLs. For $\sin 2\beta$ the $\geq 32\%$ and $\geq 5\%$ CL constraints are shown. The upper (lower) plot excludes (includes) the constraints from $\sin 2\beta$ and $\sin 2\alpha$ in the combined fit. The hatched area in the center of the combined fit result indicates the region where theoretical errors dominate. The lower plot corresponds to the standard CKM fit

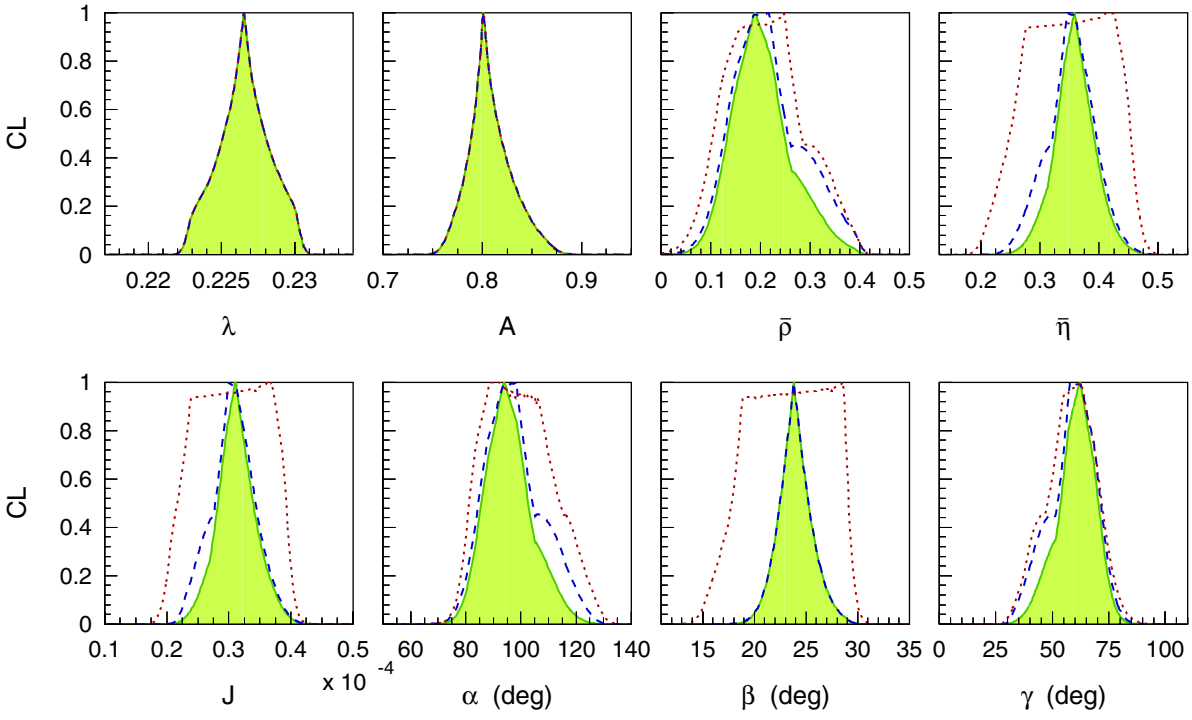

Fig. 8. Confidence levels for the Wolfenstein parameters and UT surface and angles obtained from the standard CKM fit (shaded areas). The dotted curves give the results without using $\sin 2\beta$ and $\sin 2\alpha_{[\rho\rho]}$ in the fit, while the dashed line excludes only $\sin 2\alpha_{[\rho\rho]}$

Table 2. Fit results and errors (deviations from central values at confidence levels that correspond to one-, two- and three standard deviations, respectively) using the standard input observables (72) (i.e., including the world average on $\sin 2\beta_{[c\bar{c}]}$). For results marked by "meas. not in fit", the measurement of the corresponding observable has not been included in the fit. The input parameters used for this fit are quoted in Table 1

	Central value ± error at given CL		
Quantity	CL = 0.32	CL = 0.05	CL = 0.003
λ	$0.2265^{+0.0025}_{-0.0023}$	$^{+0.0040}_{-0.0041}$	$^{+0.0045}_{-0.0046}$
A	$0.801^{+0.029}_{-0.020}$	$^{+0.066}_{-0.041}$	$^{+0.084}_{-0.054}$
$\overline{\rho}$	$0.189^{+0.088}_{-0.070}$	$^{+0.182}_{-0.114}$	$^{+0.221}_{-0.156}$
$\overline{\eta}$	$0.358^{+0.046}_{-0.042}$	$^{+0.086}_{-0.085}$	$^{+0.118}_{-0.118}$
J $[10^{-5}]$	$3.10^{+0.43}_{-0.37}$	$^{+0.82}_{-0.74}$	$^{+1.08}_{-0.96}$
$\sin 2\alpha$	$-0.14^{+0.37}_{-0.41}$	$^{+0.57}_{-0.71}$	$^{+0.74}_{-0.82}$
$\sin 2\alpha$ (meas. not in fit)	$-0.29^{+0.56}_{-0.46}$	$^{+0.77}_{-0.65}$	$^{+0.93}_{-0.70}$
$\sin 2\beta$	$0.739^{+0.048}_{-0.048}$	$^{+0.096}_{-0.095}$	$^{+0.124}_{-0.137}$
$\sin 2\beta$ (meas. not in fit)	$0.817^{+0.037}_{-0.222}$	$^{+0.053}_{-0.279}$	$^{+0.067}_{-0.334}$
α (deg)	94^{+12}_{-10}	$^{+24}_{-16}$	$^{+32}_{-22}$
α (deg) (meas. not in fit)	98^{+15}_{-16}	$^{+26}_{-22}$	$^{+31}_{-28}$
β (deg)	$23.8^{+2.1}_{-2.0}$	$^{+4.5}_{-3.8}$	$^{+6.0}_{-5.3}$
β (deg) (meas. not in fit)	$27.4^{+1.9}_{-9.2}$	$^{+2.8}_{-11.1}$	$^{+3.7}_{-13.0}$
$\gamma \simeq \delta$ (deg)	62^{+10}_{-12}	$^{+17}_{-24}$	$^{+23}_{-30}$
$\sin\theta_{12}$	$0.2266^{+0.0025}_{-0.0023}$	$^{+0.0040}_{-0.0041}$	$^{+0.0045}_{-0.0046}$
$\sin\theta_{13}$ $[10^{-3}]$	$3.87^{+0.35}_{-0.30}$	$^{+0.35}_{-0.60}$	$^{+0.35}_{-0.76}$
$\sin\theta_{23}$ $[10^{-3}]$	$41.13^{+1.37}_{-0.58}$	$^{+2.43}_{-1.16}$	$^{+3.08}_{-1.73}$
R_u	$0.405^{+0.035}_{-0.032}$	$^{+0.077}_{-0.062}$	$^{+0.093}_{-0.083}$
R_t	$0.889^{+0.073}_{-0.095}$	$^{+0.118}_{-0.196}$	$^{+0.161}_{-0.243}$
Δm_d (ps^{-1}) (meas. not in fit)	$0.54^{+0.26}_{-0.21}$	$^{+0.62}_{-0.31}$	$^{+0.94}_{-0.34}$
Δm_s (ps^{-1})	$17.8^{+6.7}_{-1.6}$	$^{+15.2}_{-2.7}$	$^{+22.1}_{-3.7}$
Δm_s (ps^{-1}) (meas. not in fit)	$16.5^{+10.5}_{-3.4}$	$^{+17.7}_{-5.7}$	$^{+23.9}_{-7.2}$
ε_K $[10^{-3}]$ (meas. not in fit)	$2.5^{+1.6}_{-1.1}$	$^{+2.4}_{-1.4}$	$^{+3.1}_{-1.6}$
$f_{B_d}\sqrt{B_d}$ (MeV) (theor. value not in fit)	215^{+28}_{-21}	$^{+79}_{-31}$	$^{+79}_{-39}$
B_K (theor. value not in fit)	$0.86^{+0.26}_{-0.30}$	$^{+0.57}_{-0.39}$	$^{+0.90}_{-0.45}$
$\overline{m}_t(m_t)$ (GeV/c^2) (meas. not in fit)	165^{+48}_{-47}	$^{+124}_{-64}$	$^{+194}_{-77}$

Table 3. Fit results and errors (deviations from central values at confidence levels that correspond to one-, two- and three standard deviations, respectively) using the standard input observables (72) (i.e., including the world average on $\sin 2\beta_{[c\bar{c}]}$). The variables in the last four lines are defined by $\lambda_i \equiv V_{id}V_{is}^*$. For results marked by "meas. not in fit", the measurement related to the corresponding observable has not been included in the fit. The input parameters used for this fit are quoted in Table 1

Quantity	Central value ± error at given CL CL = 0.32	CL = 0.05	CL = 0.003
$\mathcal{B}(K_L^0 \to \pi^0\nu\overline{\nu})$ $[10^{-11}]$	$2.89^{+0.84}_{-0.69}$	$^{+1.71}_{-1.24}$	$^{+2.41}_{-1.52}$
$\mathcal{B}(K^+ \to \pi^+\nu\overline{\nu})$ $[10^{-11}]$	$6.7^{+2.8}_{-2.7}$	$^{+3.7}_{-3.2}$	$^{+4.6}_{-3.6}$
$\mathcal{B}(B^+ \to \tau^+\nu_\mu)$ $[10^{-5}]$	$11.9^{+4.5}_{-5.7}$	$^{+10.4}_{-8.2}$	$^{+17.9}_{-10.1}$
$\mathcal{B}(B^+ \to \mu^+\nu_\mu)$ $[10^{-7}]$	$4.7^{+2.3}_{-1.7}$	$^{+4.6}_{-2.7}$	$^{+7.6}_{-3.5}$
$\lvert V_{ud}\rvert$	$0.97400^{+0.00054}_{-0.00058}$	$^{+0.00094}_{-0.00095}$	$^{+0.00106}_{-0.00106}$
$\lvert V_{us}\rvert$	$0.2265^{+0.0025}_{-0.0023}$	$^{+0.0040}_{-0.0041}$	$^{+0.0045}_{-0.0046}$
$\lvert V_{ub}\rvert$ $[10^{-3}]$	$3.87^{+0.35}_{-0.30}$	$^{+0.73}_{-0.60}$	$^{+0.73}_{-0.76}$
$\lvert V_{ub}\rvert$ $[10^{-3}]$ (meas. not in fit)	$3.87^{+0.34}_{-0.31}$	$^{+0.81}_{-0.61}$	$^{+1.27}_{-0.88}$
$\lvert V_{cd}\rvert$	$0.2264^{+0.0025}_{-0.0023}$	$^{+0.0040}_{-0.0041}$	$^{+0.0045}_{-0.0046}$
$\lvert V_{cs}\rvert$	$0.97317^{+0.00053}_{-0.00059}$	$^{+0.00094}_{-0.00097}$	$^{+0.00106}_{-0.00112}$
$\lvert V_{cb}\rvert$ $[10^{-3}]$	$41.13^{+1.36}_{-0.58}$	$^{+2.43}_{-1.16}$	$^{+3.08}_{-1.73}$
$\lvert V_{cb}\rvert$ $[10^{-3}]$ (meas. not in fit)	$41.2^{+5.1}_{-5.7}$	$^{+7.9}_{-5.8}$	$^{+9.9}_{-5.8}$
$\lvert V_{td}\rvert$ $[10^{-3}]$	$8.26^{+0.72}_{-0.86}$	$^{+1.23}_{-1.79}$	$^{+1.64}_{-2.25}$
$\lvert V_{ts}\rvert$ $[10^{-3}]$	$40.47^{+1.39}_{-0.62}$	$^{+2.42}_{-1.21}$	$^{+3.17}_{-1.78}$
$\lvert V_{tb}\rvert$	$0.999146^{+0.000024}_{-0.000058}$	$^{+0.000047}_{-0.000104}$	$^{+0.000070}_{-0.000133}$
$\lvert V_{ud}V_{ub}^*\rvert$ $[10^{-3}]$	$3.77^{+0.34}_{-0.30}$	$^{+0.71}_{-0.59}$	$^{+0.71}_{-0.75}$
$\arg\left[V_{ud}V_{ub}^*\right]$ (deg)	62^{+10}_{-12}	$^{+16}_{-24}$	$^{+22}_{-31}$
$\lvert V_{cd}V_{cb}^*\rvert$ $[10^{-3}]$	$9.31^{+0.31}_{-0.15}$	$^{+0.62}_{-0.34}$	$^{+0.80}_{-0.49}$
$\arg\left[V_{cd}V_{cb}^*\right]$ (deg)	$-179.9653^{+0.0047}_{-0.0042}$	$^{+0.0091}_{-0.0084}$	$^{+0.0122}_{-0.0107}$
$\lvert V_{td}V_{tb}^*\rvert$ $[10^{-3}]$	$8.24^{+0.73}_{-0.85}$	$^{+1.24}_{-1.78}$	$^{+1.64}_{-2.24}$
$\arg\left[V_{td}V_{tb}^*\right]$ (deg)	$-23.8^{+2.0}_{-2.1}$	$^{+3.8}_{-4.5}$	$^{+5.3}_{-6.0}$
$\lvert V_{td}/V_{ts}\rvert$	$0.204^{+0.018}_{-0.022}$	$^{+0.029}_{-0.046}$	$^{+0.039}_{-0.058}$
$\mathrm{Re}\lambda_c$	$-0.2204^{+0.0022}_{-0.0023}$	$^{+0.0038}_{-0.0037}$	$^{+0.0043}_{-0.0041}$
$\mathrm{Im}\lambda_c$ $[10^{-4}]$	$-1.41^{+0.18}_{-0.18}$	$^{+0.34}_{-0.36}$	$^{+0.44}_{-0.48}$
$\mathrm{Re}\lambda_t$ $[10^{-4}]$	$-3.04^{+0.32}_{-0.31}$	$^{+0.67}_{-0.60}$	$^{+0.86}_{-0.80}$
$\mathrm{Im}\lambda_t$ $[10^{-4}]$	$1.41^{+0.19}_{-0.17}$	$^{+0.37}_{-0.34}$	$^{+0.48}_{-0.44}$

sign of New Physics in these penguin decays would be a pattern of $\sin 2\beta_{\mathrm{eff},\, sq\bar{q}}$ values that are significantly different from $\sin 2\beta_{[c\bar{c}]}$ *and* significantly different from each other[28]. It might be that Belle's $S_{\phi K_S^0}$ measurement represents a statistical fluctuation and that very large New Physics effects are not to be expected, which of course does not imply

[28] Unless some specific symmetry or dynamical mechanism relates the New Physics to SM amplitude ratios in different channels [155].

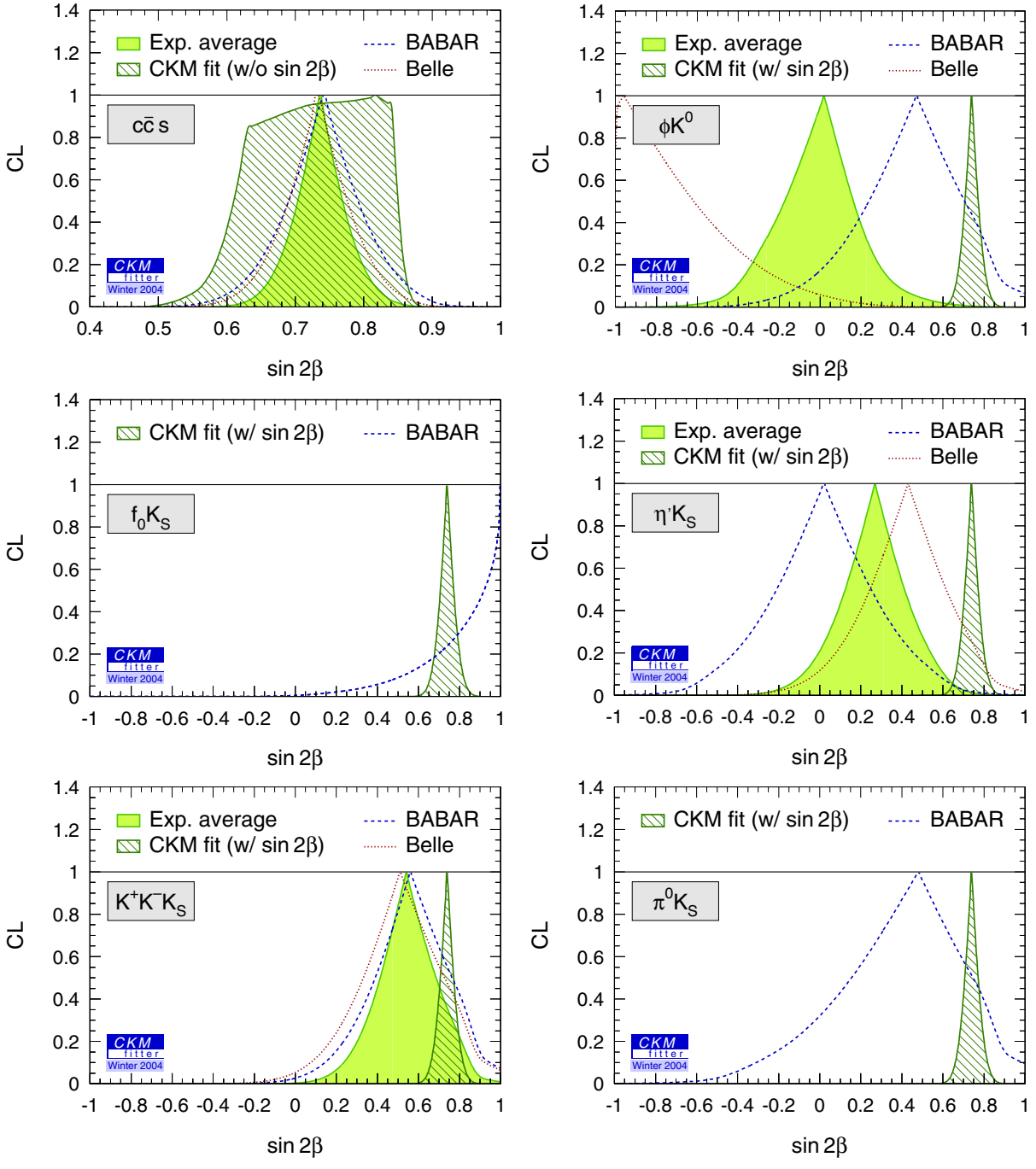

Fig. 9. Confidence levels for the various $\sin 2\beta_{[\mathrm{eff}]}$ measurements that are believed to be dominated by a single CKM phase, their averages and the result from the standard CKM fit

that more precise data will not be able to give evidence for non-standard contributions if they exist. We revisit the ϕK^0 mode in a more general New Physics framework in Sect. VII.3.

3.5 Resolving the two-fold ambiguity in 2β

In spite of the agreement with the standard CKM fit of one out of the four solutions for β from the precise $\sin 2\beta$ measurement using charmonium decays, it is still possible that, because of contributions from New Physics, the correct value of β is one of the three other solutions. The measurement of the sign of $\cos 2\beta$ would reduce the solution space

to an indistinguishable two-fold ambiguity[29]. The *BABAR* collaboration has performed a measurement of $\cos 2\beta$ in a time-dependent transversity analysis of the pseudoscalar to vector-vector decay $B^0 \to J/\psi K^{*0}(\to K^0_S\pi^0)$, where $\cos 2\beta$ enters as a factor in the interference between *CP*-even and *CP*-odd amplitudes [138]. In principle, this analysis comes along with an ambiguity on the sign of $\cos 2\beta$ due to an incomplete determination of the strong phases occurring in the three transversity amplitudes. *BABAR* resolves this ambiguity by inserting the known variation [157] of the rapidly moving P-wave phase relative to the slowly moving S-wave phase with the invariant mass of the $K\pi$ system in the vicinity of the $K^{*0}(892)$ resonance.

When fixing the $\sin 2\beta$ value to the world average, *BABAR* finds

$$\cos 2\beta \;=\; 2.72\,^{+0.50}_{-0.79} \pm 0.27 \;, \tag{75}$$

where the effect introduced by the variation of $\sin 2\beta$ within its small errors is negligible. *BABAR* quotes the probability that the true $\cos 2\beta$ is positive[30] to be 89%, where the value is obtained with the use of Monte Carlo methods. This is much less than the 3.8σ exclusion of the mirror solutions $\pi/2 - \beta$ and $3\pi/2 - \beta$, obtained from a probabilistic treatment of the result (75), using the analytical method described in Sect. II.2.2.3, and assuming that the log-likelihood function belonging to (75) has parabolic tails. Since the Monte Carlo evaluation is reliable, we conclude that a Gaussian interpretation of the errors given in (75) is flawed. Due to the lack of a more accurate experimental CL function for $\cos 2\beta$ (precisely the one obtained from Monte Carlo simulation), we do not include the present measurement in the standard CKM fit, although we will assume $\cos 2\beta > 0$ in part of our New Physics analysis (see Part VII). Proposals for alternative determinations of sign$(\cos 2\beta)$ can be found in [158–163].

4 Conclusions

The robustness of the Unitarity Triangle fit has been greatly improved since the precision measurement of $\sin 2\beta$ became available. It outperforms by far all other contributions in the combined experimental and theoretical precision. A new constraint on $\sin 2\alpha$ from the isospin analysis of $B \to \rho\rho$ decays has become available, the theoretical uncertainties of which – though not yet entirely evaluated or known – seem to be under control. Its inclusion into the standard CKM fit already leads to a modest improvement on the knowledge of α and γ. We derive a large number of quantitative results on the CKM parameters for various parameterizations and related quantities, theoretical parameters and physical observables from the standard CKM fit (see Tables 2 and 3).

The goodness-of-fit of the global CKM fit is found to be 71%. We find that penguin-dominated measurements of (to good approximation) $\sin 2\beta$ are in agreement with the reference value from B^0 decays into charmonium states. It might turn out that the large negative S value found by Belle in $B^0 \to \phi K^0_S$ represents a statistical fluctuation. A measurement of $\cos 2\beta$ in $B^0 \to J/\psi K^{*0}(\to \pi^0 K^0_S)$ decays indicates that the β solution from the $\sin 2\beta$ measurement that is favored by the standard CKM fit corresponds to the one that occurs in $B^0\overline{B}^0$ mixing.

Part IV
Constraints from kaon physics

This part presents the CKM constraints from direct *CP* violation and other *CP*-related observables in kaon decays that do not belong to the standard CKM fit. We refer to Sects. III.2.2 and III.2.6 for a discussion of the constraints from K_{e3} decays, giving $|V_{us}|$, and from indirect *CP* violation, respectively.

Section IV.1 discusses current experimental and theoretical status of constraints related to the *CP*-violating parameter ε'/ε. Conventions and input values from [164] are used. Sections IV.2 and IV.3 discuss the status of measurements of the rare kaon decays $K^+ \to \pi^+\nu\overline{\nu}$ and $K^0_L \to \pi^0\nu\overline{\nu}$, together with a study of future perspectives. For a recent detailed review of these rare kaon decays we refer to [165].

1 Direct *CP* violation in the neutral kaon system: ε'/ε

A non-zero value for the *CP*-violation parameter ε', defined as

$$\eta_{+-} = \varepsilon + \varepsilon' \;, \qquad \eta_{00} = \varepsilon - 2\varepsilon' \;, \tag{76}$$

[29] The invariance $\beta \to \pi + \beta$ remains. It cannot be lifted without theoretical input on a strong phase [156].

[30] This solution corresponds to reasonably small strong phases between transversity amplitudes, as expected in the factorization approximation [158].

Table 4. Experimental results for $\mathrm{Re}(\varepsilon'/\varepsilon)$

Experiment	Value $[10^{-4}]$	Status
NA31 [166]	23.0 ± 6.5	final
E731 [167]	7.4 ± 5.9	final
NA48 [168]	14.7 ± 2.2	final
KTeV [169]	20.7 ± 2.8	1/2 data sample
Average	16.7 ± 1.6	CL = 10%

where $\varepsilon \equiv \varepsilon_K$, establishes direct CP violation in the neutral kaon system. The corresponding experimental observable is $\mathrm{Re}(\varepsilon'/\varepsilon)$. The first evidence of direct CP violation in neutral kaons decays was found by the NA31 collaboration [166]. Statistically significant observations were obtained by the next-generation of experiments, NA48 [168] and KTeV [169]. Table 4 summarizes the available measurements that yield an average of $\mathrm{Re}(\varepsilon'/\varepsilon) = (16.7 \pm 1.6) \times 10^{-4}$, with $\chi^2 = 6.3$ for 3 degrees of freedom, that is a p-value of 10%.

The SM prediction of $\mathrm{Re}(\varepsilon'/\varepsilon)$ has large uncertainties because it relies on the precise knowledge of penguin-like hadronic matrix elements. Detailed calculations at NLO [170,171] show that two hadronic parameters $B_6^{(1/2)}$ (gluonic penguins) and $B_8^{(3/2)}$ (electroweak penguins) dominate, where the superscripts denote the dominant $\Delta I = 1/2$ and $\Delta I = 3/2$ contributions, respectively, and refer to the isospin change in the $K \to \pi\pi$ transition. It is convenient to express the SM prediction as a function of the hadronic parameters with the use of the approximate formula [164]

$$\mathrm{Re}(\varepsilon'/\varepsilon) = \mathrm{Im}(V_{td}V_{ts}^*)\,[18.7 R_6\,(1-\Omega_{\mathrm{IB}}) - 6.9 R_8 - 1.8]\,\frac{\Lambda^{(4)}_{\overline{\mathrm{MS}}}}{340\,\mathrm{MeV}}\ , \tag{77}$$

where $\Omega_{\mathrm{IB}} = 0.06 \pm 0.08$ corrects for isospin-breaking [172], $\Lambda^{(4)}_{\overline{\mathrm{MS}}} = (340 \pm 30)\,\mathrm{MeV}$ is the characteristic QCD scale for 4 active quark flavors in the $\overline{\mathrm{MS}}$ scheme, and where R_6 and R_8 are defined by

$$R_6 = B_6^{(1/2)} \left[\frac{121\,\mathrm{MeV}}{\overline{m}_s(m_c)}\right]^2\ , \qquad R_8 = B_8^{(3/2)} \left[\frac{121\,\mathrm{MeV}}{\overline{m}_s(m_c)}\right]^2\ , \tag{78}$$

with the running s-quark mass $\overline{m}_s(m_c) = (115 \pm 20)\,\mathrm{MeV}$. In the strict large-$N_c$ limit, the hadronic parameters satisfy $B_6 = B_8 = 1$. The quoted values and errors for Ω_{IB}, $\Lambda^{(4)}_{\overline{\mathrm{MS}}}$, and $\overline{m}_s(m_c)$ are taken from [164]. In the Wolfenstein parameterization one has $\mathrm{Im}(V_{td}V_{ts}^*) = A^2\lambda^5\overline{\eta} + \mathcal{O}(\lambda^7)$. Even though the experimental value of $\mathrm{Re}(\varepsilon'/\varepsilon)$ is known to 10% accuracy, reliable constraints on $\overline{\eta}$ cannot be obtained (not even on its sign) due to the present uncertainties assigned to the hadronic parameters R_6 and R_8. Various dynamical effects come into play, and while it is possible to estimate some of them thanks to appropriate theoretical methods, it is very difficult to take into account all possible contributions within a single approach.

Some consensus has been achieved on the value and error of R_8 obtained by lattice QCD. The most precise lattice calculation [173] has an accuracy of $\sim$ 10%. Taking into account other lattice results [174,175], the conservative average $R_8 = 1.00 \pm 0.20$ is quoted in [164], and the value $R_6 = 1.23 \pm 0.16$ is derived from the correlation between the experimental result for ε'/ε and R_8. The computation of R_6 on the lattice is more difficult due to the mixing with lower dimensional operators. An attempt can be found in [175]; however this study does not take into account flavor-symmetry breaking effects that come from quenching artefacts, as stressed in [176]. As for R_8, the authors of [177] argue that again significant contributions that vanish in the quenched approximation could spoil the lattice estimate. Several analyses using analytical non-perturbative techniques are also available. An approach based on dispersion relations to evaluate final state interaction finds $R_6 = 1.05 \pm 0.06$ and $R_8 = 0.84 \pm 0.05$ [172]. A chiral perturbation theory calculation gives $R_6 = 2.2 \pm 0.4$ and $R_8 = 1.1 \pm 0.3$ [178]. Another recent calculation, taking into account $\mathcal{O}(n_f/N_c)$ corrections to the large-N_c limit of QCD, finds $R_6 = 2.1 \pm 1.1$ and $R_8 = 2.20 \pm 0.40$ [177]. Noticeable disagreement in both values and errors among the different approaches is observed.

It is therefore instructive to study the constraints put upon these parameters by the experimental data. Figure 10 shows the allowed region for R_6 versus R_8, obtained from the experimental average for $\mathrm{Re}(\varepsilon'/\varepsilon)$ together with the standard CKM fit result for $\mathrm{Im}(V_{td}V_{ts}^*)$. The symbols with error bars indicate the theoretical calculations. One concludes that the various theoretical predictions provide estimates for ε'/ε that are in agreement with the experimental data, but the present size of the uncertainties and also the disagreement between the various predictions for R_6 prevents us from using ε'/ε as a constraint in the standard CKM fit. In the future, model-independent constraints on R_6 could be extracted from the measurement of CP-violation in kaon decays to three pions [179].

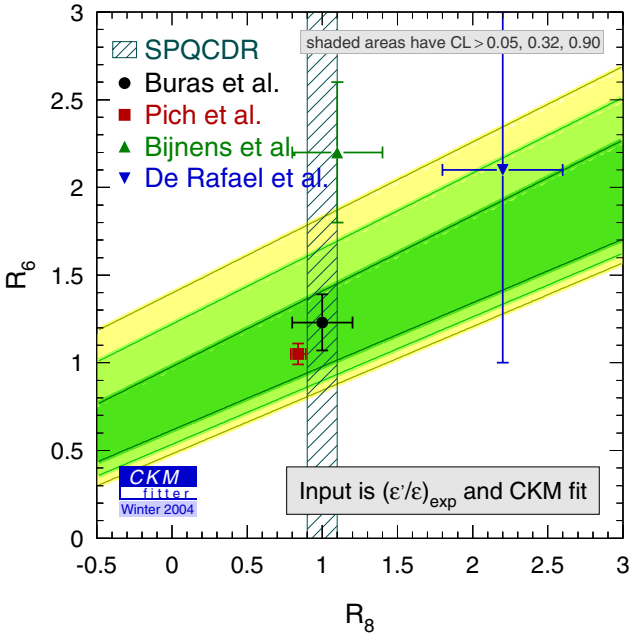

Fig. 10. Allowed values for the hadronic parameters R_6 and R_8, using the experimental average of $\mathrm{Re}(\varepsilon'/\varepsilon)$ and the result on $\mathrm{Im}(V_{td}V_{ts}^*)$ from the standard CKM fit as input. The symbols with error bars give the theoretical predictions taken from [164,172,177,178,173]

As an exercise we follow the strategy of [164] and use the average lattice QCD value for R_8, together with the experimental average of $\mathrm{Re}(\varepsilon'/\varepsilon)$ and the standard CKM fit, to constrain R_6. We find the 95% CL range

$$0.75 \;<\; R_6 \;<\; 1.80 \;.$$

2 Rare decays of charged kaons: $K^+ \to \pi^+\nu\overline{\nu}$

The BNL-E787 experiment has observed two events of the rare decay $K^+ \to \pi^+\nu\overline{\nu}$, resulting in the branching fraction $\mathcal{B}(K^+ \to \pi^+\nu\overline{\nu}) = (1.57^{+1.75}_{-0.82}) \times 10^{-10}$ [15], which due to the small expected background rate (0.15 ± 0.03 events) effectively excludes the null hypothesis. One additional event has been observed near the upper kinematic limit by the successor experiment BNL-E949 [16]. They quote the combined branching fraction $\mathcal{B}(K^+ \to \pi^+\nu\overline{\nu}) = (1.47^{+1.30}_{-0.89}) \times 10^{-10}$. The left hand plot in Fig. 11 gives the CLs for the experimental result (CL obtained from [16]) and the SM prediction (see paragraphs below), with input from the standard CKM fit.

In the SM, the branching fraction is given by [180]

$$\mathcal{B}(K^+ \to \pi^+\nu\overline{\nu}) \;=\; r_{K^+}\frac{3\alpha^2}{2\pi^2}\frac{\mathcal{B}(K^+ \to \pi^0 e^+\nu)}{|V_{us}|^2 \sin^4\theta_{\mathrm{W}}} \sum_{i=e,\mu,\tau} \left|\eta_X X_0(x_t) V_{td}V_{ts}^* + X_{\mathrm{NL}}^{(i)} V_{cd}V_{cs}^*\right|^2 \;. \tag{79}$$

Here, $r_{K^+} = 0.901$ corrects for isospin breaking [181], $X_0(x_t)$ (with $x_t = \overline{m}_t^2/m_W^2$) is the Inami-Lim function

$$X_0(x) \;=\; \frac{x}{8}\left(\frac{x+2}{x-1} + \frac{3x-6}{(x-1)^2}\ln x\right), \tag{80}$$

corrected by a phenomenological QCD factor $\eta_X = 0.994$, which is due to the top quark contribution [102] to order α_s, and the functions $X_{\mathrm{NL}}^{(\ell)}$, $\ell = e, \mu, \tau$, contain the contributions from Z^0 penguin and box diagrams with charm quarks in the loops, and have been calculated at the next-to-leading log approximation [180].

To illustrate the CKM constraint, we express (79) in the Wolfenstein parameters

$$\mathcal{B}(K^+ \to \pi^+\nu\overline{\nu}) \;=\; \kappa_+ A^4 X^2(x_t)\frac{1}{\sigma}\left[(\sigma\overline{\eta})^2 + (\rho_0 - \overline{\rho})^2\right] \;, \tag{81}$$

with

$$X(x) \;=\; \eta_X X_0(x) \;, \qquad \sigma \;=\; 1 + \lambda^2 + \mathcal{O}(\lambda^4) \;, \qquad \rho_0 \;=\; 1 + \frac{P_0}{A^2 X(x_t)} \;. \tag{82}$$

Equation (79) provides an almost elliptic constraint in the $(\overline{\rho}, \overline{\eta})$ with the center close to the $(\overline{\rho} = 1, \overline{\eta} = 0)$ apex of the Unitarity Triangle. It allows us to extract the CKM matrix element $|V_{td}|$ from the branching fraction measurement.

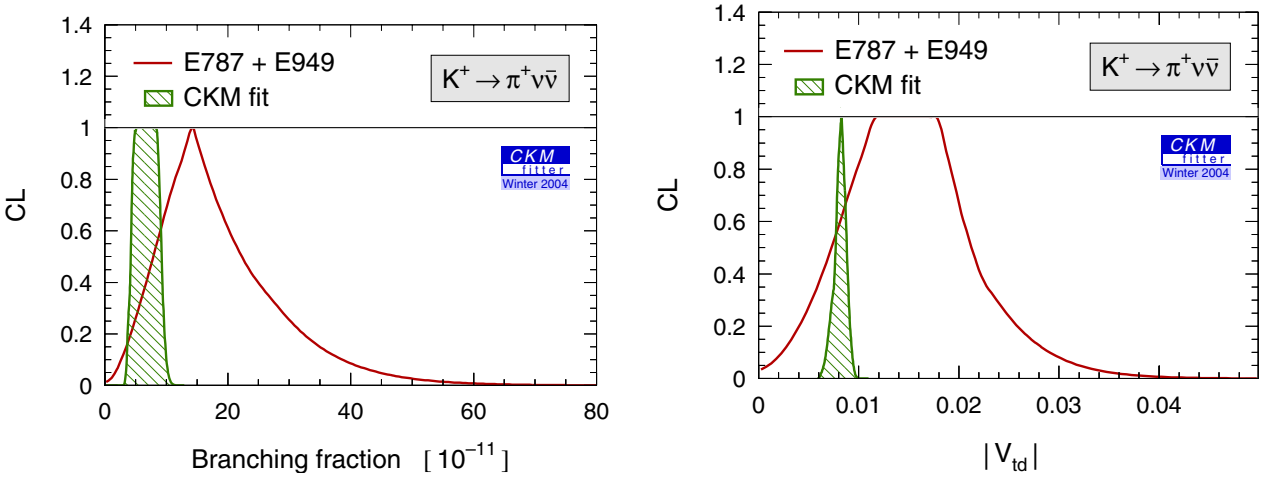

Fig. 11. Confidence level of $\mathcal{B}(K^+ \to \pi^+ \nu\overline{\nu})$ (left) and $|V_{td}|$ (right). The solid lines give to the constraints from the combined E787 and E949 measurements, and the hatched areas represent the SM predictions obtained from the standard CKM fit

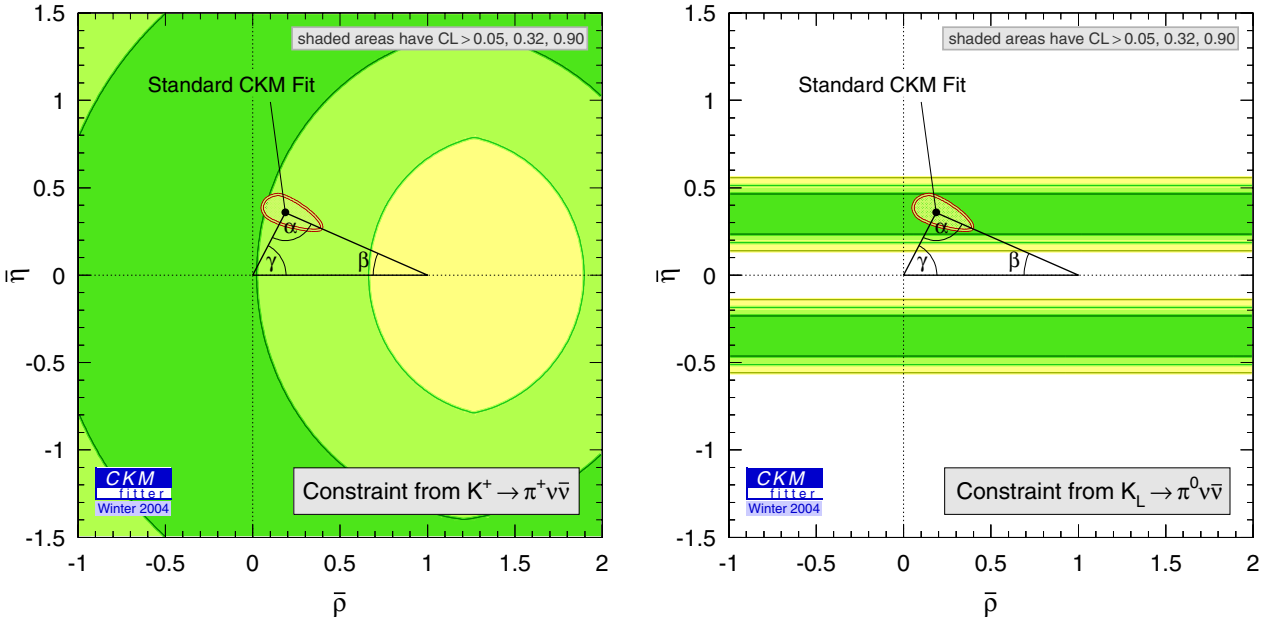

Fig. 12. Constraint in the $(\overline{\rho},\overline{\eta})$ plane from the combined E787 and E949 measurements of $\mathcal{B}(K^+ \to \pi^+ \nu\overline{\nu})$ (left), and from a hypothetical $\mathcal{B}(K_L^0 \to \pi^0 \nu\overline{\nu})$ measurement with 10% relative error (right). Dark, medium and light shaded areas have $CL > 0.90$, 0.32 and 0.05, respectively

The constant κ_+ is defined in [180]. It contains a λ^8 dependence so that $\mathcal{B}(K^+ \to \pi^+ \nu\overline{\nu})$ is a function of $\left(A\lambda^2\right)^4$, which is constrained by $|V_{cb}|$ and experimentally determined from inclusive and exclusive $b \to c\ell\nu$ transitions. Finally, the parameter P_0 quantifies the charm quark contribution and is given by

$$P_0 = \frac{1}{\lambda^4}\left[\frac{2}{3}X_{\rm NL}^e + \frac{1}{3}X_{\rm NL}^\tau\right] . \tag{83}$$

Theoretical uncertainties on P_0 arise from the charm quark mass, the renormalization scale dependence and $\Lambda_{\rm QCD}$.

The left hand plot in Fig. 12 shows the constraints in the $(\overline{\rho},\overline{\eta})$ plane obtained from the comparison of the experimental result with the SM prediction. Within the large experimental errors, the constraint is found to be compatible with the allowed region obtained from the standard CKM fit.

We concentrate in the following on the study of the constraint on $|V_{td}|$ to evaluate the potential of future $\mathcal{B}(K^+ \to \pi^+ \nu\overline{\nu})$ measurements. Relative uncertainties on the branching fraction scale approximately as $4\sigma(|V_{cb}|)/|V_{cb}|$ and $2\sigma\left(X_0\right)/X_0$, and the relative error on $|V_{td}|^2$ scales equivalently. Moreover, the charm quark contribution (83) induces an uncertainty on the center of the elliptical constraint, which translates into an uncertainty on $|V_{td}|$. The right hand

Table 5. Constraints on $|V_{td}|$ from $\mathcal{B}(K^+ \to \pi^+\nu\overline{\nu})$ for the three scenarios described in the text. The last line gives the result from the present standard CKM fit (Table 3)

Scenario	$\geq 5\%$ CL range on $\lvert V_{td}\rvert$ $[\times 10^{-3}]$	Half width
(I)	6.1–10.5	2.2
$\sigma(\overline{m}_c)$ only	6.8–9.9	1.6
$\sigma(\overline{m}_t)$ only	7.7–8.9	0.6
$\sigma(\lvert V_{cb}\rvert)$ only	7.9–8.7	0.4
(II)	7.0–9.7	1.3
(III)	7.2–9.4	1.1
standard CKM fit	6.5–9.5	1.5

plot in Fig. 11 gives the present constraints on $|V_{td}|$ for the combined E787 and E949 measurements, and the standard CKM fit, respectively. We extrapolate into the future by assuming that the branching fraction is equal to the central value obtained in the present CKM fit. Other inputs used in this study are $|V_{us}|$ (to fix the Wolfenstein parameter λ), and $|V_{ub}|$ together with $|V_{cb}|$ to intersect the elliptical constraint in a restricted area of the $(\overline{\rho},\overline{\eta})$ plane, and to hence reduce the effect of the uncertainty on the center of the ellipse. Table 5 gives a breakdown of the uncertainties contributing to the error of $|V_{td}|$ for three scenarios:

(I) using the present knowledge of the relevant input parameters and neglecting the statistical error on the $\mathcal{B}(K^+ \to \pi^+\nu\overline{\nu})$ measurement;
(II) assuming a measurement with a statistical precision of 10% and an improvement of the relevant uncertainties to a 1% error on $|V_{cb}|$, a 2 GeV error on the top quark mass, and a 50 MeV error on the charm quark mass;
(III) assuming a measurement with a statistical precision of 10%, and neglecting all theoretical uncertainties in the prediction of $\mathcal{B}(K^+ \to \pi^+\nu\overline{\nu})$.

We conclude from this exercise that, once an accurate branching fraction measurement becomes available, the quantitative knowledge of the input parameters to the SM prediction must be significantly improved so that it does not dominate the uncertainty on the $|V_{td}|$ constraint[31]. For the input values used in the Scenario (I), the charm term is the dominant source of uncertainty, mostly due to the charm quark mass and the renormalization scale dependence. Since the top quark mass is expected to be measured with increasing accuracy at current and future hadron machines, and the error used for the charm quark mass is rather conservative, an improved precision on $|V_{cb}|$ will become mandatory (see Sect. 2.4).

3 Rare decays of neutral kaons: $K_L^0 \to \pi^0\nu\overline{\nu}$

In the SM, the golden decay $K_L^0 \to \pi^0\nu\overline{\nu}$ proceeds almost entirely through a direct CP-violating amplitude dominated by the top quark contribution. The theoretical prediction of the branching fraction is given by [180]

$$\begin{aligned}\mathcal{B}(K_L^0 \to \pi^0\nu\overline{\nu}) &= \kappa_L \left(\frac{\mathrm{Im}[V_{td}V_{ts}^*]}{\lambda^5}\right)^2 X^2(x_t) \\ &= \kappa_L A^4\eta^2 X^2(x_t) + \mathcal{O}(\lambda^4)\ , \end{aligned} \tag{84}$$

where $\kappa_L = \kappa_+(r_{K_L}\tau_{K_L})/(r_{K^+}\tau_{K^+}) = (2.12 \pm 0.03) \times 10^{-10}$ [165], and where $r_{K_L} = 0.944$ accounts for isospin breaking [181]. The constant κ_+ is defined in [180]. It contains a λ^8 term so that the branching fraction is again proportional to $|V_{cb}|^4$. The constraint in the $(\overline{\rho},\overline{\eta})$ plane obtained from a future measurement of $\mathcal{B}(K_L^0 \to \pi^0\nu\overline{\nu})$ (here

[31] One could, of course, argue that instead of $|V_{td}|$ the parameter of interest is $|V_{td}V_{ts}^*|^2$. However we note that the SM prediction for $\mathcal{B}(K^+ \to \pi^+\nu\overline{\nu})$ and hence the extraction of $|V_{td}|$ is not dominated by the uncertainty on $|V_{cb}|$. Also, the interest in this mode is twofold: firstly the improvement of the knowledge of the CKM phase, and secondly the search for physics beyond the SM. In both cases $|V_{td}|$ appears to be the appropriate parameter.

Table 6. Constraints on $|\overline{\eta}|$ from $\mathcal{B}(K_L^0 \to \pi^0 \nu\overline{\nu})$, for the three scenarios described in the text. The last line gives the result from the present standard CKM fit (Table 3)

Scenario	$\geq 5\%$ CL range on $\|\overline{\eta}\|$	Half width
(I)	0.313–0.399	0.043
$\sigma(\overline{m}_t)$ only	0.333–0.379	0.023
$\sigma(\|V_{cb}\|)$ only	0.327–0.385	0.028
(II)	0.336–0.376	0.020
(III)	0.317–0.395	0.039
standard CKM fit	0.273–0.444	0.086

with 10% relative uncertainty) corresponds to two horizontal lines as illustrated on the right hand plot of Fig. 12. The relative error on $|\overline{\eta}|$ scales with $2\sigma\left(|V_{cb}|\right)/|V_{cb}|$ and $\sigma\left(X\right)/X$.

We study the CL on $|\overline{\eta}|$ obtained from a $\mathcal{B}(K_L^0 \to \pi^0 \nu\overline{\nu})$ measurement, for the same three scenarios introduced in the previous section. We assume that the branching fraction is equal to the central value from the present CKM fit. Table 6 gives a breakdown of the uncertainties contributing to the error of $|\overline{\eta}|$ for the three scenarios defined in the previous section. The dominant source of uncertainty on $|\overline{\eta}|$ in Scenario (I) is introduced by $|V_{cb}|$. Since the sensitivity to theoretical uncertainties is reduced, the constraint on $|\overline{\eta}|$ will remain statistically limited for realistic expectations on near-future measurements of the $K_L^0 \to \pi^0 \nu\overline{\nu}$ branching fraction (with $\sim$ 30–60 signal events).

4 Conclusions

Despite the success of the experimental effort that lead to a precise measurement of $\mathrm{Re}(\varepsilon'/\varepsilon)$, the present situation does not allow us to use it as a reliable constraint in the CKM fit without a substantial improvement on the theoretical side. As for the rare kaon decays, a handful of events are expected to be observed by BNL-E949 [16], while the CKM project at FNAL [182], starting around 2005, expects to collect about 100 events within a few years of data taking. Since these measurements have very small backgrounds, a $\sim 10\%$ statistical error on the $\mathcal{B}(K^+ \to \pi^+ \nu\overline{\nu})$ is expected. The prospects for a measurement of the decay $K_L^0 \to \pi^0 \nu\overline{\nu}$ are more uncertain due to the enormous experimental challenge. Long-term projects [183] are designed to collect high statistics, but even intermediate-statistics branching fraction measurements [184] may reveal potentially large deviations from the SM, and are hence of considerable interest.

Part V
Constraints on $2\beta + \gamma$ and γ from tree decays

1 CP-violating asymmetries in $B^0 \to D^{(*)\pm}\pi^{\mp}$ decays

Even though they are not CP eigenstates, partially and fully reconstructed $B^0 \to D^{(*)\pm}\pi^{\mp}$ decays are sensitive to the UT angle γ because of the interference between the CKM-favored amplitude of the decay $B^0 \to D^{(*)-}\pi^+$ with the doubly CKM-suppressed amplitude of $B^0 \to D^{(*)+}\pi^-$.[32] The relative weak phase between these two amplitudes is $-\gamma$ and, when combined with the $B^0\overline{B}^0$ mixing phase, the total phase difference is $-(2\beta+\gamma)$ to all orders in λ:

$$-(2\beta+\gamma) \;=\; \arg\left[-\frac{V_{td}V_{tb}^*}{V_{td}^*V_{tb}}\frac{V_{cd}^*V_{ub}}{V_{ud}V_{cb}^*}\right] \;. \tag{85}$$

The interpretation of the CP-violation observables in terms of the UT angles requires external input on the ratio

$$r^{(*)} \equiv \left|\frac{q}{p}\frac{A(\overline{B}^0 \to D^{(*)-}\pi^+)}{A(B^0 \to D^{(*)-}\pi^+)}\right| \;, \tag{86}$$

[32] This is similar to the situation in $B^0 \to \rho^{\pm}\pi^{\mp}$ decays (see Sect. VI.4), even if the two amplitudes there are of the same CKM order, which considerably increases their potential CP asymmetries.

which can be obtained experimentally from the corresponding flavor-tagged branching fractions, or from similar modes that are easier to measure. These can be ratios of branching fractions of the charged $B^+ \to D^{(*)+}\pi^0$ to the neutral CKM-favored decay, or ratios involving self-tagging decays with strangeness like $B^0 \to D_s^{(*)+}\pi^-$. Corrections for SU(3) breaking in the latter case generate a significant theoretical uncertainty, which is generally hard to quantify. Naively, one can estimate $r^{(*)} \sim |V_{cd}^* V_{ub}/V_{ud} V_{cb}^*| \simeq 0.02$. At present, the most precise semi-experimental determination of $r^{(*)}$ can be obtained from the SU(3)-corrected ratio

$$r^{(*)} = \frac{|V_{us}|}{|V_{ud}|}\sqrt{\frac{\mathcal{B}(B^0 \to D_s^{(*)+}\pi^-)}{\mathcal{B}(B^0 \to D^{(*)-}\pi^+)}}\,\frac{f_{D^{(*)}}}{f_{D_s^{(*)}}} \ . \tag{87}$$

Inserting the corresponding branching fractions and decay constants leads to [185]

$$r^* = 0.017\,^{+0.005}_{-0.007} \ , \qquad r = 0.014 \pm 0.004 \ . \tag{88}$$

In [185] a theoretical uncertainty of 30% of the central value is attributed in addition to the experimental errors to each of the quantities. It accounts for SU(3)-breaking corrections and the neglect of W-exchange contributions to the $B^0 \to D^{(*)+}\pi^-$ decay amplitude. However (87) already corrects for the main (factorizable) symmetry breaking; on the other hand, the exchange diagram is the only possible contribution to the $D_s^\pm K^\mp$ mode: thus one has roughly $|\text{exchange/emission}|^2 \sim \mathcal{B}(B^0 \to D_s^- K^+)/\mathcal{B}(B^0 \to D^- \pi^+) \sim 1\%$ [186]. As a consequence, taking into account the residual non factorizable SU(3) breaking and the order of magnitude of the exchange contribution, we estimate the total theoretical uncertainty to be of the order of 15% for both r and r^*, keeping in mind that a more refined estimate of this error source will be needed when the statistics increase.

BABAR [185,187] and Belle [188] use two sets of observables

$$S^{(*)\pm} = 2r^{(*)} \sin(2\beta + \gamma \pm \delta^{(*)}) \ , \tag{89}$$

where $S^{(*)\pm}$ is the coefficient of the sine term in the time evolution of the $B^0(\overline{B}^0) \to D^{(*)\pm}\pi^\mp$ system, and

$$a^{(*)} \equiv \frac{1}{2}\left(S^{(*)+} + S^{(*)-}\right) = 2r^{(*)} \sin(2\beta + \gamma)\cos(\delta^{(*)}) \ , \tag{90}$$

$$c^{(*)} \equiv \frac{1}{2}\left(S^{(*)+} - S^{(*)-}\right) = 2r^{(*)} \cos(2\beta + \gamma)\sin(\delta^{(*)}) \ , \tag{91}$$

so that $S^{(*)+} = a^{(*)} + c^{(*)}$ and $S^{(*)-} = a^{(*)} - c^{(*)}$. These definitions are valid in the limit of small $r^{(*)}$ only so that terms of order $r^{(*)\geq 2}$ can be neglected and the cosine coefficient in the time evolution is one ($C^{(*)} = (1-r^2)/(1+r^2) \to 1$). The relative strong phase $\delta^{(*)}$ is unknown and has to be determined simultaneously with $2\beta+\gamma$ from the experimental observables. Due to the disparate strength of the two interfering amplitudes, the *CP* asymmetry is expected to be small, so that the possible occurrence of *CP* violation on the tag side becomes an important obstacle. Tag side CPV is absent for semileptonic B decays (mostly lepton tags). The parameter $a^{(*)}$ is independent of tag side CPV.

The experimental results are given in Table 7. The averages quoted are taken from the HFAG [62].

For each mode the combinations $\sin(2\beta + \gamma \pm \delta_f)$ are extracted ($\delta_{D\pi} = \delta$ and $\delta_{D^*\pi} = \delta^*$). Simple trigonometry shows that, as far as the *CP* angle is concerned, this is equivalent to the determination of the quantity $|\sin(2\beta+\gamma)|$ up to a two-fold discrete ambiguity. Should the two strong phases δ and δ^* be different, the discrete ambiguity could

Table 7. Experimental results from time-dependent CP-asymmetry analyses of partially and fully reconstructed $B^0 \to D^{*\pm}\pi^\mp$ decays, respectively. The averages are taken from the HFAG [62]

	BABAR [187,185]		Belle [188]	Average
	partially reconstructed	fully reconstructed	fully reconstructed	
a^*	$-0.063 \pm 0.024 \pm 0.014$	$-0.068 \pm 0.038 \pm 0.020$	$0.063 \pm 0.041 \pm 0.016 \pm 0.013$	-0.038 ± 0.021
c^*	$-0.004 \pm 0.037 \pm 0.020$	$0.031 \pm 0.070 \pm 0.033$	$0.030 \pm 0.041 \pm 0.016 \pm 0.030$	0.012 ± 0.030
a	-	$-0.022 \pm 0.038 \pm 0.020$	$-0.058 \pm 0.038 \pm 0.013$	-0.041 ± 0.029
c	-	$0.025 \pm 0.068 \pm 0.033$	$-0.036 \pm 0.038 \pm 0.013 \pm 0.036$	-0.015 ± 0.044

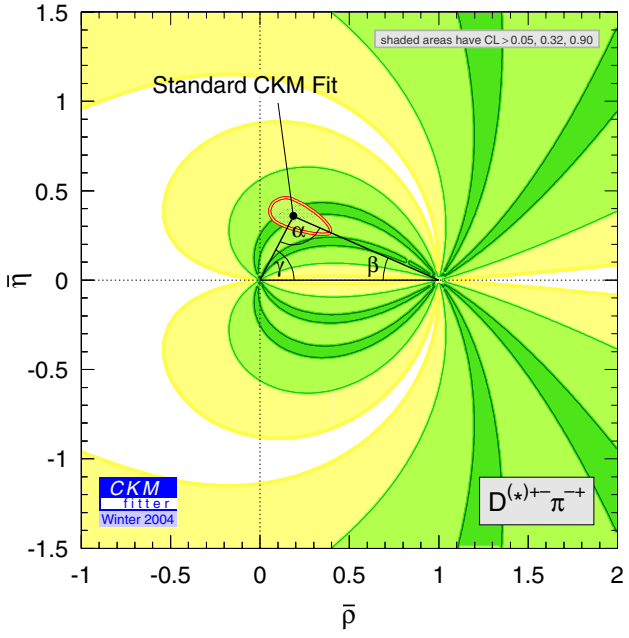

Fig. 13. Constraint in the enlarged $(\overline{\rho},\overline{\eta})$ plane from the average measurement of time-dependent CP-violating asymmetries in $B^0 \to D^{*\pm}\pi^{\mp}$ decays. The shaded areas indicate $CL > 5\%$ (light), $CL > 32\%$ (medium) and $CL > 90\%$ (dark) regions. Also shown is the $CL > 5\%$ region of the standard CKM fit

in principle be resolved, leaving a single solution for $|\sin(2\beta+\gamma)|$ (and thus four solutions for the angle $2\beta+\gamma$ itself in $[0,\pi]$).

Figure 13 shows the confidence level obtained in the $(\overline{\rho},\overline{\eta})$ plane. Also shown is the allowed region from the standard CKM fit. Good agreement is observed, although the statistical significance of the measurement is still weak. Note that we have used a Gaussian Prob$(\chi^2,1)$ here to evaluate the CL. As seen below, this tends to overestimates the CL (and hence to weaken the constraint). The left hand plot in Fig. 14 shows the confidence level for $|\sin(2\beta+\gamma)|$ obtained from the various measurements. A single peak is observed, although δ and δ^* are very close to each other (see below), because limited statistics merges the position of the two solutions. We perform a toy Monte Carlo simulation in order to evaluate the goodness of the Gaussian Prob$(\chi^2,1)$ approximation for the confidence level. Significant deviations are observed. Also shown are the prediction from the standard CKM fit as well as the result obtained when using the *BABAR* results only, which benefit from a small $|c^*|$ fluctuation in the measurement with partially reconstructed B decays. The right hand plot shows the constraint obtained on the UT angle γ when also using the world average of $\sin 2\beta_{[c\bar{c}]}$. For simplicity, we use the Prob$(\chi^2,1)$ approximation for this as well as for the upcoming plots. Also shown is the constraint from the standard CKM fit. One can use the latter prediction of $|\sin(2\beta+\gamma)|$ together with the $B^0 \to D^{(*)\pm}\pi^{\mp}$ measurements to constrain the strong phases $\delta^{(*)}$ as shown in Fig. 15.

In summary we conclude that in spite of the considerable experimental effort to achieve this first direct constraint on $2\beta+\gamma$, the present statistical accuracy is insufficient to improve the knowledge of the apex in the unitarity plane. The errors of the present world averages given in Table 7 have to be reduced by a factor of about five (approximately $5\,\mathrm{ab}^{-1}$ accumulated luminosity) to be competitive with the standard CKM fit on $|\sin(2\beta+\gamma)|$ (assuming the above 15% uncertainty on $r^{(*)}$). Such large statistics samples, which are necessary due to the smallness of the CP-violating asymmetries, are likely to increase the importance of the experimental systematic uncertainties. Similar modes like $B^0 \to D^{(*)\pm}\rho^{\mp}$ must be included in future to improve the reach of this analysis.

2 Dalitz plot analysis of $B^+ \to D^{(*)0}K^+$ decays

The golden method to measure the angle γ at the B factories has been proposed by Gronau, London and Wyler (GLW) [189,190] (see also [191,192]) and extended by Atwood, Dunietz and Soni (ADS) [193]. The GLW method consists of reconstructing the $\overline{D}^0$ (D^0) occurring in charged $B^+ \to \overline{D}^0 K^+$ ($B^+ \to D^0 K^+$) decays as a CP eigenstate (e.g., $K^0_S\pi^0$ or $K^0_S\pi^+\pi^-$) so that the CKM-favored ($b \to c$) and CKM-suppressed ($b \to u$) transition amplitudes interfere. The relative phase between these amplitudes is $\gamma+\delta$, where δ is a CP-conserving strong phase and γ the weak UT angle. The measurement of the corresponding branching fractions and CP-violating asymmetries allows one to simultaneously extract γ and the strong phase from a triangular isospin analysis, up to discrete ambiguities, even if the strong phase vanishes, but with virtually no theoretical uncertainties. The feasibility of this or related analyses crucially depends on the size of the color- and CKM-suppressed $b \to u$ transition (expected to be roughly $r_B \sim 1/8$, if color-suppression holds). Recently, the *BABAR* collaboration has determined an upper limit for the amplitude ratio

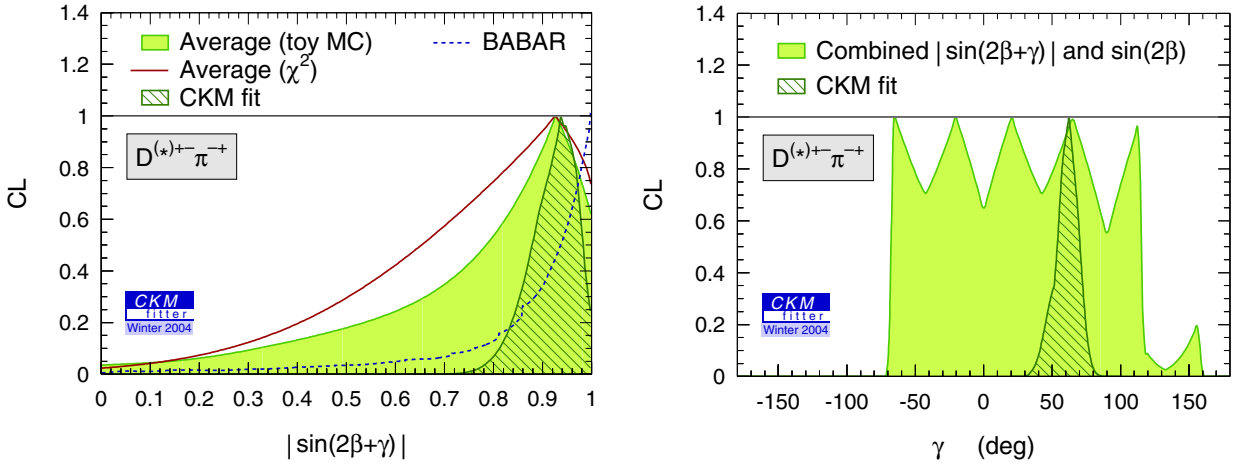

Fig. 14. *Left*: confidence level obtained for $|\sin(2\beta+\gamma)|$. The shaded area gives the average from *BABAR* and Belle obtained by means of a toy Monte Carlo simulation (see Sect. II.2.2.3). As a comparison, we show by the solid line the approximate result from the Prob$(\chi^2, 1)$ interpretation. Also shown is the result from *BABAR* only, which leads to a stronger exclusion of small $|\sin(2\beta+\gamma)|$ values due to the somewhat propitiously small value of c^* in partially reconstructed $B^0 \to D^{*\pm}\pi^{\mp}$ decays [187]. Also shown is the prediction from the standard CKM fit. *Right*: confidence level obtained for the UT angle γ when using *BABAR* and Belle's results on $|\sin(2\beta+\gamma)|$ (and $|\cos(2\beta+\gamma)|$) combined with the world average of $\sin 2\beta_{[c\bar{c}]}$. Also shown is the prediction from the standard CKM fit

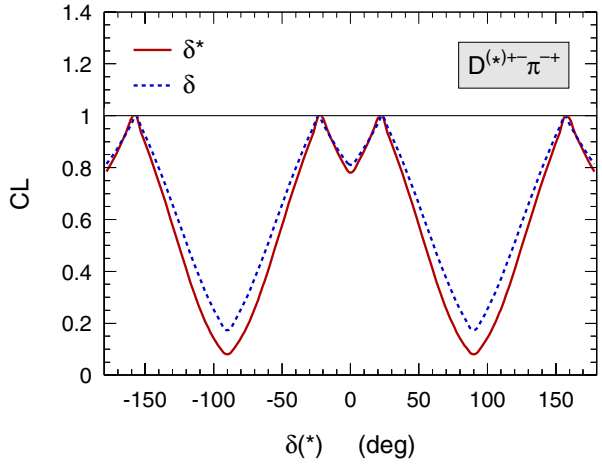

Fig. 15. Confidence levels obtained for the strong phases $\delta^{(*)}$ occurring between the CKM-favored and CKM-suppressed branches of $B^0 \to D^{*\pm}\pi^{\mp}$ decays. The standard CKM fit has been used to constrain the weak CKM phases

$r_B = |A(B^+ \to D^0K^+)/A(B^+ \to \bar{D}^0K^+)|$ of 0.22 at 90% CL [194], which dampens the hope for a performing γ analysis using the GLW or ADS techniques at the first generation B factories.

Along the line of [195], the Belle collaboration overcomes these difficulties by performing a Dalitz plot analysis of $B^+ \to D^0K^+$ (and $B^+ \to D^{*0}(\to D^0\pi^0)K^+$) decays followed by a three-body D^0 decay to $K^0_S\pi^+\pi^-$ [196][33]. The weak phase γ and the strong phase δ as well as the magnitude of the suppressed-to-favored amplitude ratio r_B are extracted from a fit to the interference pattern between D^0 and $\bar{D}^0$ in the Dalitz plot. A large number of intermediate resonances has to be considered to properly model the full $K^0_S\pi^+\pi^-$ Dalitz plot, where high-statistics samples of charm decays can be used to fit the model parameters [198]. Belle determines a probability density function (PDF) for $\phi_3 = \gamma$ by means of a Bayesian analysis with uniform priors for γ, δ and r_B. Single-sided integration of this PDF, and choosing the solution that is consistent with the standard CKM fit, results in

$$\gamma = 81^\circ \pm 19^\circ \pm 13^\circ \pm 11^\circ \ , \tag{92}$$

where the first error is statistical, the second systematic and the third is due to the amplitude model. The constraint on the second solution, which is not consistent with the standard CKM fit, is obtained by the transformation $\gamma \to \gamma + \pi$

[33] After the completion of this work, an update of the Belle analysis has been submitted [197]. By means of a frequentist analysis, Belle finds the combined result $\gamma = [77^{+17}_{-19}(\text{stat}) \pm 13(\text{syst}) \pm 11(\text{model})]^\circ$, which slightly differs from the previous value. This modification in the result does however not alter the conclusion drawn from the study of New Physics in the present work.

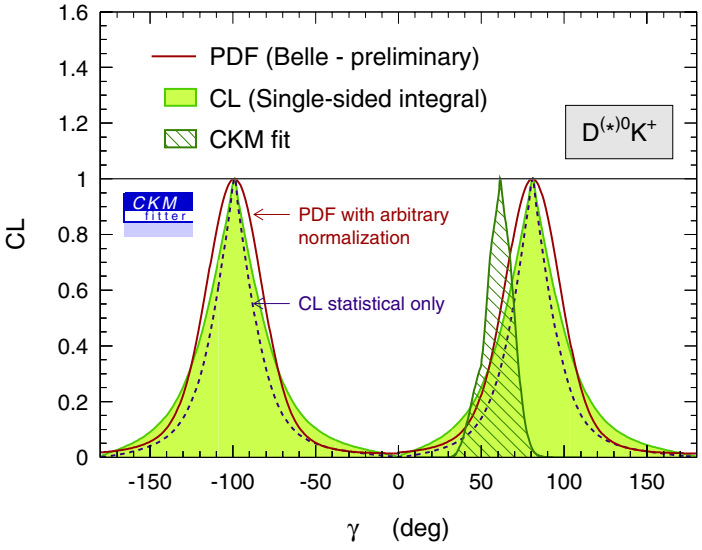

Fig. 16. Confidence level of the UT angle γ from the Dalitz plot analysis of $B^+ \to D^{(*)0}K^+$ decays [195,196]. Shown are the experimental PDF (solid line – statistical only), found by Belle, and the corresponding CL from single-sided integration (shaded area – including systematics, while the dashed line gives the CL obtained when ignoring systematic uncertainties). Also given is the constraint from the standard CKM fit

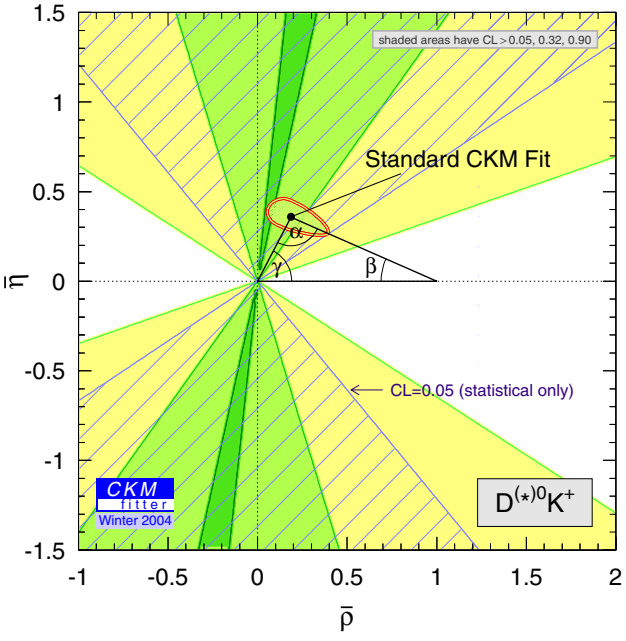

Fig. 17. Confidence level in the enlarged $(\overline{\rho},\overline{\eta})$ plane from the Dalitz plot analysis of $B^+ \to D^{(*)0}K^+$ decays [195,196]. The shaded areas indicate $CL > 5\%$ (light), $CL > 32\%$ (medium) and $CL > 90\%$ (dark) regions. The hatched area indicates the $CL > 5\%$ region when ignoring systematic uncertainties. Also shown is the $CL > 5\%$ constraint from the standard CKM fit

(the full analysis actually leads to the determination of $\tan\gamma$). We have extracted and integrated the PDF from [196] and find the confidence levels shown as a function of γ and $(\overline{\rho},\overline{\eta})$ in Figs. 16 and 17. Since systematic and model-dependent errors are not included in the PDF, we add them in quadrature to the statistical error. With these rather strong assumptions, agreement with the standard CKM fit is observed. Belle determines the magnitude of the suppressed-to-favored amplitude ratio to be $r_B = 0.28^{+0.09}_{-0.11}$, which is slightly larger than the expectation and than the 90% CL bound set by *BABAR*, though the results are still compatible within errors (23%). Since large values of r_B lead to an increased sensitivity to γ, the error given in (92) may increase if the true r_B is significantly smaller. More data are needed to clarify this.

Since the result is still preliminary, we do not introduce it in the standard CKM fit. It is however used in our analysis of New Physics presented in Part VII.

Part VI
Charmless B decays

Unlike $B^0 \to J/\psi K^0_S$ or other charmonium decays, for which amplitudes with weak phases that are different from the dominant tree phase are doubly CKM-suppressed, multiple weak phases must be considered in the analyses of charmless B decays. This complication makes the extraction of the CKM couplings from the experimental observables considerably more difficult, and at the same time richer.

The first section of this part is devoted to the extraction of α from the analysis of $B \to \pi\pi$ decays, using four different scenarios with increasing theoretical input. Section 2 presents fits of the calculation of hadronic matrix elements within the QCD Factorization approach to the $K\pi$ and $\pi\pi$ data. We give a detailed discussion of its predictive power and limitations. Section 3 describes the constraints obtained from the phenomenological analysis of $B \to K\pi$ modes only. We also study the impact from electroweak penguin amplitudes. The extraction of α from the pseudoscalar-vector final states, $\rho\pi$ and SU(2) or SU(3)-related modes, is presented in Sect. 4. Finally, we discuss the isospin analysis of $B \to \rho\rho$ decays in Sect. 5, which is similar to the $\pi\pi$ system. In most cases we attempt to evaluate the constraints obtained with higher luminosity samples.

Throughout this part, we will assume that CP violation in mixing is absent, i.e., $|q/p| = 1$, as suggested by the Standard Model ($|\Gamma_{B_H} - \Gamma_{B_L}| \ll \Gamma_{B^0}$) and confirmed by experiment ($A_{\rm SL} = -0.007 \pm 0.013$, see Sect. VII.2).

Remark on radiative corrections

We point out that the charmless analyses, published by the *BABAR* and Belle collaborations up to approximately Summer 2003, utilized Monte Carlo simulation without treatment of radiative corrections in the decays. The simulation is used by the experiments to compute selection efficiencies and to predict probability density distributions of signal events for the use in maximum-likelihood fits. A study based on [199] suggests that the branching fractions of $B^0 \to \pi^+\pi^-$ and $B^0 \to K^+\pi^-$ may be underestimated by up to 10% [200]. Since the effects strongly depend on the final state and the analysis strategy used, we do not attempt to correct the branching fraction results here. However one should be aware that this systematic may lead to increased branching fractions for modes that decay to light charged particles.

1 Analysis of $B \to \pi\pi$ and SU(3)-related decays

1.1 Basic formulae and definitions

1.1.1 Transition amplitudes

The general form of the $B^0 \to \pi^+\pi^-$ decay amplitude, accounting for the tree and penguin diagrams that correspond to the three up-type quark flavors (u, c, t) occurring in the W loop (see Fig. 18), reads

$$A^{+-} \equiv A(B^0 \to \pi^+\pi^-) = V_{ud}V^*_{ub}M_u + V_{cd}V^*_{cb}M_c + V_{td}V^*_{tb}M_t \ , \tag{93}$$

and similarly for the CP-conjugated amplitude. One can benefit from the unitarity relation (12) to eliminate one of the three amplitudes, resulting in the three conventions $\mathfrak{U}$, $\mathfrak{C}$, $\mathfrak{T}$, namely

$$A^{+-} = \begin{cases} V_{cd}V^*_{cb}(M_c - M_u) + V_{td}V^*_{tb}(M_t - M_u) & (\mathfrak{U}) \\ V_{ud}V^*_{ub}(M_u - M_c) + V_{td}V^*_{tb}(M_t - M_c) & (\mathfrak{C}) \\ V_{ud}V^*_{ub}(M_u - M_t) + V_{cd}V^*_{cb}(M_c - M_t) & (\mathfrak{T}) \end{cases} \tag{94}$$

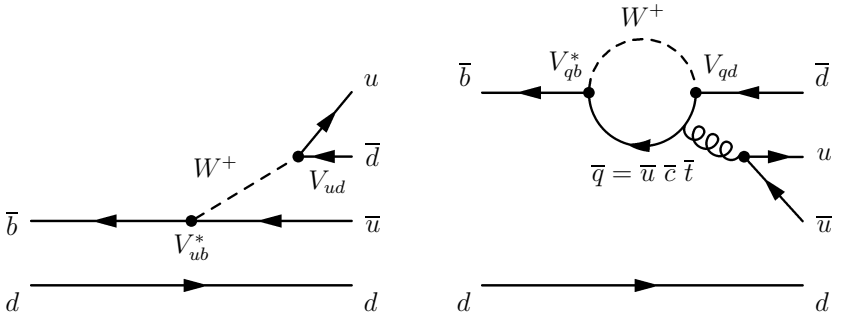

Fig. 18. Example of tree (left) and penguin (right) diagrams for the decay $B^0 \to \pi^+\pi^-$

for which the u ($\mathfrak{U}$), c ($\mathfrak{C}$) and t ($\mathfrak{T}$) amplitude coefficients have been substituted respectively. In the following, we adopt convention $\mathfrak{C}$ so that A^{+-} reads

$$A^{+-} = V_{ud}V_{ub}^* T^{+-} + V_{td}V_{tb}^* P^{+-} \ , \tag{95}$$

where T^{+-} and P^{+-} are defined by

$$T^{+-} \equiv M_u - M_c \quad \text{and} \quad P^{+-} \equiv M_t - M_c \ . \tag{96}$$

The particular choice of which amplitude to remove in the definition of a total transition amplitude is arbitrary[34] and does not have observable physical implications. However the convention does modify the contents of the phenomenological amplitudes T^{+-} and P^{+-}. We will often refer to T^{+-} and P^{+-} amplitudes as "tree" and "penguin", respectively, although it is implicitly understood that both of them receive various contributions of distinct topologies, which are mixed under hadronic rescattering.

1.1.2 *CP*-violating asymmetries

The time-dependent CP-violating asymmetry of the $B^0\overline{B}^0$ system is given by

$$\begin{aligned} a_{CP}(t) &\equiv \frac{\Gamma(\overline{B}^0(t) \to \pi^+\pi^-) - \Gamma(B^0(t) \to \pi^+\pi^-)}{\Gamma(\overline{B}^0(t) \to \pi^+\pi^-) + \Gamma(B^0(t) \to \pi^+\pi^-)} \\ &= S^{+-}_{\pi\pi}\sin(\Delta m_d t) - C^{+-}_{\pi\pi}\cos(\Delta m_d t) \ , \end{aligned} \tag{97}$$

where Δm_d is the $B^0\overline{B}^0$ oscillation frequency and t is either the decay time of the B^0 or the $\overline{B}^0$ or, at B factories running at the $\Upsilon(4S)$ mass, the time difference between the CP and the tag side decays. The coefficients of the sine and cosine terms are given by

$$S^{+-}_{\pi\pi} = \frac{2\mathrm{Im}\lambda_{\pi\pi}}{1+|\lambda_{\pi\pi}|^2} \quad \text{and} \quad C^{+-}_{\pi\pi} = \frac{1-|\lambda_{\pi\pi}|^2}{1+|\lambda_{\pi\pi}|^2} \ , \tag{98}$$

where the CP parameter $\lambda_{\pi\pi}$ is given by (we recall that it is assumed $|q/p| = 1$)

$$\lambda_{\pi\pi} = \frac{q}{p}\frac{\overline{A}^{+-}}{A^{+-}} \ , \tag{99}$$

where the phase $\arg[q/p] = 2\arg[V_{td}V_{tb}^*] \approx -2\beta$ (in our phase convention) arises due to $B^0\overline{B}^0$ mixing. We have used in the above equations that $\pi^+\pi^-$ is a CP eigenstate with eigenvalue $+1$.

In the absence of penguin contributions ($P = 0$), (99) reduces to $\lambda_{\pi\pi} = e^{2i\alpha}$ (using the triangle definition (20)) and hence

$$S^{+-}_{\pi\pi}[P^{+-} = 0] = \sin 2\alpha \quad \text{and} \quad C^{+-}_{\pi\pi}[P^{+-} = 0] = 0 \ . \tag{100}$$

In general, the phase of $\lambda_{\pi\pi}$ is modified by the interference between the penguin and the tree amplitudes. In addition, the parameter $C^{+-}_{\pi\pi}$ will be non-zero if

$$\delta^{+-} \equiv \arg[P^{+-}T^{+-*}] \neq 0 \ , \tag{101}$$

hence measuring the occurrence of direct CP violation. Defining an effective angle $\alpha_{\rm eff}$ that incorporates the phase shift

$$\lambda_{\pi\pi} \equiv |\lambda_{\pi\pi}|e^{2i\alpha_{\rm eff}} \ , \tag{102}$$

and, using $|\lambda_{\pi\pi}| = \sqrt{1-C^{+-}_{\pi\pi}}/\sqrt{1+C^{+-}_{\pi\pi}}$, one finds

$$S^{+-}_{\pi\pi} = D\sin 2\alpha_{\rm eff} \ , \tag{103}$$

where $D \equiv \sqrt{1-C^{+-\,2}_{\pi\pi}}$. Twice the effective angle $\alpha_{\rm eff}$ corresponds to the relative phase between the amplitudes $e^{-2i\beta}\overline{A}^{+-}$ and A^{+-}. It is useful for the following to define the penguin-induced phase difference

$$\Delta\alpha \equiv \frac{1}{2}(2\alpha - 2\alpha_{\rm eff}) \ , \quad (\Delta\alpha \in [0,\pi]) \ . \tag{104}$$

We note that the sign of the direct CP asymmetry is related to the $\alpha \to \pi+\alpha$ and $\delta^{+-} \to \pi+\delta^{+-}$ ambiguity through the relation

$$\mathrm{sign}(C^{+-}_{\pi\pi}) = \mathrm{sign}(\sin\alpha) \times \mathrm{sign}(\sin\delta) \ . \tag{105}$$

[34] Note that $M_{u,c,t}$ amplitudes are intrinsically divergent and only differences between them lead to finite results (see, e.g., [201]).

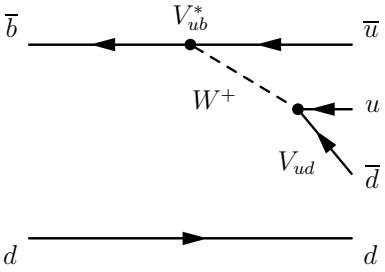

Fig. 19. Color-suppressed tree diagram for the decay $B^0 \to \pi^0\pi^0$

1.1.3 Isospin related decays

Owing to isospin invariance of strong interaction, the amplitudes of the various $B \to \pi\pi$ decays are related to each other. Gronau and London have shown [141] that the measurements of rates and CP-violating asymmetries of the charged and two neutral $\pi\pi$ final states together with the exploitation of their isospin relations provides sufficient information to extract the angle α as well as the various T and P amplitudes. Unfortunately, as far as α is concerned, the general solution is plagued by an eightfold ambiguity within $[0, \pi]$ [202].

Using convention $\mathfrak{C}$, one can write

$$\begin{aligned} \sqrt{2}A^{+0} &\equiv \sqrt{2}A(B^+ \to \pi^+\pi^0) = V_{ud}V_{ub}^* T^{+0} + V_{td}V_{tb}^* P^{\mathrm{EW}} \ , \\ \sqrt{2}A^{00} &\equiv \sqrt{2}A(B^0 \to \pi^0\pi^0) = V_{ud}V_{ub}^* T_{\mathrm{C}}^{00} + V_{td}V_{tb}^* P^{00} \ , \end{aligned} \tag{106}$$

and similarly for the CP-conjugated modes. The C subscript stands for the color-suppressed amplitude (see Fig. 19 for the color-suppressed tree diagram in the decay $B^0 \to \pi^0\pi^0$), and the EW superscript stands for the electroweak penguin amplitude contributing to $\pi^+\pi^0$. Note that the latter notation only refers to the $\Delta I = 3/2$ electroweak penguin contribution, since the $\Delta I = 1/2$ part is absorbed in the strong penguins. Indeed, gluonic quark anti-quark production has $\Delta I = 0$ so that QCD penguins can only mediate $\Delta I = 1/2$ transitions of the b quark. As a consequence, the $\Delta I = 3/2$ decay $B^+ \to \pi^+\pi^0$ has no strong penguin contribution. Applying the isospin relations [141]

$$\begin{aligned} A^{+0} &= \frac{1}{\sqrt{2}} A^{+-} + A^{00} \ , \\ \overline{A}^{+0} &= \frac{1}{\sqrt{2}} \overline{A}^{+-} + \overline{A}^{00} \ , \end{aligned} \tag{107}$$

with $\overline{A^{+0}} = A^{-0}$, one can rearrange the amplitudes (106)

$$\begin{aligned} \sqrt{2}A^{+0} &= V_{ud}V_{ub}^* \left(T^{+-} + T_{\mathrm{C}}^{00}\right) + V_{td}V_{tb}^* P^{\mathrm{EW}} \ , \\ \sqrt{2}A^{00} &= V_{ud}V_{ub}^* T_{\mathrm{C}}^{00} - V_{td}V_{tb}^* \left(P^{+-} - P^{\mathrm{EW}}\right) \ . \end{aligned} \tag{108}$$

The isospin relations between the three $\pi\pi$ amplitudes in the complex plane are drawn in Fig. 20 for the simplified case where electroweak penguins are neglected. They represent two distinct triangles for the two CP-conjugated amplitudes.

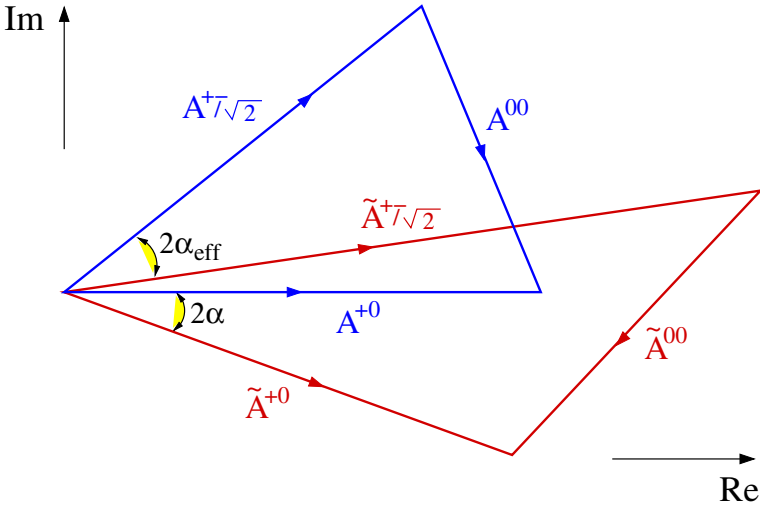

Fig. 20. The isospin relations (107) in the complex plane neglecting electroweak penguins. Note that the relative $B^0\overline{B}^0$ mixing phase is included in the $\overline{B}$ triangle ($\tilde{A^{ij}} \equiv e^{-2i\beta}\overline{A}^{ij}$)

Taking into account the phase shift due to $B^0\overline{B}^0$ mixing, the relative angle between $\tilde{A}^{+0}$ and A^{+0} adds up to 2α, as it is shown in the figure.

Equations (107) can be considered as exact to a very good approximation. Isospin-breaking corrections like, e.g., π^0–η, η' mixing [203] are expected to be below a few percent. We refer to Sect. VI.5.4 for a numerical discussion of isospin-breaking effects in the $B \to \rho\rho$ case. Nevertheless, extracting α relying on this unique theoretical assumption appears to be difficult at present, given the number of ambiguities and the experimental uncertainties. In the following, we therefore explore several scenarios which, though still relying on (107), involve additional experimental and theoretical inputs.

1.2 Theoretical frameworks

To extract α from the experimental measurements of the CP-violating asymmetries, we use four different scenarios, with rising theoretical assumptions [204]:

(I) using as input $S^{+-}_{\pi\pi}$ and $C^{+-}_{\pi\pi}$ as well the branching fractions $B \to \pi\pi$ (all charges) and strong isospin symmetry SU(2) [141];
(II) using (I) and the branching fraction $B^0 \to K^+\pi^-$ together with SU(3) flavor symmetry, and neglecting OZI-suppressed penguin annihilation topologies [202];
(III) using (II) and a phenomenological estimate of $|P^{+-}|$ by means of the decay rate of $B^+ \to K^0\pi^+$, and neglecting doubly CKM-suppressed penguin and annihilation contributions [206,202,205];
(IV) using $S^{+-}_{\pi\pi}$ and $C^{+-}_{\pi\pi}$ and the prediction of the complex penguin-to-tree ratio P^{+-}/T^{+-} in the framework of QCD Factorization [207,208].

1.2.1 Isospin analysis, isospin bounds and electroweak penguins

It was shown in [141] that using the CP-averaged branching fractions

$$\begin{aligned}
\mathcal{B}^{+-}_{\pi\pi} &\propto \frac{\tau_{B^0}}{2}\left(|A^{+-}|^2 + |\overline{A}^{+-}|^2\right) \ , \\
\mathcal{B}^{+0}_{\pi\pi} &\propto \frac{\tau_{B^+}}{2}\left(|A^{+0}|^2 + |A^{-0}|^2\right) \ , \\
\mathcal{B}^{00}_{\pi\pi} &\propto \frac{\tau_{B^0}}{2}\left(|A^{00}|^2 + |\overline{A}^{00}|^2\right) \ ,
\end{aligned} \tag{109}$$

where τ_{B^0} and τ_{B^+} are the neutral and charged B lifetimes (cf. Sect. III.2.4), and the CP-violating asymmetries

$$\begin{aligned}
C^{+-}_{\pi\pi} &= \frac{|\,A^{+-}\,|^2 - |\,\overline{A}^{+-}\,|^2}{|\,A^{+-}\,|^2 + |\,\overline{A}^{+-}\,|^2} \ , \\
S^{+-}_{\pi\pi} &= \frac{2\,\mathrm{Im}\left(\frac{q}{p}A^{+-*}\overline{A}^{+-}\right)}{|\,A^{+-}\,|^2 + |\,\overline{A}^{+-}\,|^2} \ , \\
C^{00}_{\pi\pi} &= \frac{|\,A^{00}\,|^2 - |\,\overline{A}^{00}\,|^2}{|\,A^{00}\,|^2 + |\,\overline{A}^{00}\,|^2} \ ,
\end{aligned} \tag{110}$$

one can extract the angle α, up to discrete ambiguities, provided electroweak penguin contributions are negligible ($P^{\mathrm{EW}} = 0$). The geometrical description of the isospin analysis presented in the preceding section can be conveniently complemented by the explicit solution in terms of α [209]

$$\tan\alpha = \frac{\sin(2\alpha_{\mathrm{eff}})\bar{c} + \cos(2\alpha_{\mathrm{eff}})\bar{s} + s}{\cos(2\alpha_{\mathrm{eff}})\bar{c} - \sin(2\alpha_{\mathrm{eff}})\bar{s} + c} \ , \tag{111}$$

where all quantities on the right hand side can be expressed in term of the observables as follows:

$$\begin{aligned}
\sin(2\alpha_{\mathrm{eff}}) &= \frac{S^{+-}_{\pi\pi}}{D} \ , \\
\cos(2\alpha_{\mathrm{eff}}) &= \pm\sqrt{1 - \sin^2(2\alpha_{\mathrm{eff}})} \ ,
\end{aligned}$$

$$c = \sqrt{\frac{\tau_{B^+}}{\tau_{B^0}}}\,\frac{\frac{\tau_{B^0}}{\tau_{B^+}}\mathcal{B}^{+0}_{\pi\pi} + \mathcal{B}^{+-}_{\pi\pi}(1+C^{+-}_{\pi\pi})/2 - \mathcal{B}^{00}_{\pi\pi}(1+C^{00}_{\pi\pi})}{\sqrt{2\mathcal{B}^{+-}_{\pi\pi}\,\mathcal{B}^{+0}_{\pi\pi}(1+C^{+-}_{\pi\pi})}}\ , \tag{112}$$

$$s = \pm\sqrt{1-c^2}\ ,$$

$$\overline{c} = \sqrt{\frac{\tau_{B^+}}{\tau_{B^0}}}\,\frac{\frac{\tau_{B^0}}{\tau_{B^+}}\mathcal{B}^{+0}_{\pi\pi} + \mathcal{B}^{+-}_{\pi\pi}(1-C^{+-}_{\pi\pi})/2 - \mathcal{B}^{00}_{\pi\pi}(1-C^{00}_{\pi\pi})}{\sqrt{2\mathcal{B}^{+-}_{\pi\pi}\,\mathcal{B}^{+0}_{\pi\pi}(1-C^{+-}_{\pi\pi})}}\ ,$$

$$\overline{s} = \pm\sqrt{1-\overline{c}^2}\ .$$

The eightfold ambiguity for α in the range $[0,\pi]$ is made explicit by the three arbitrary signs[35]. The quantity $S^{00}_{\pi\overline{\pi}}$ could also be considered, and would help lifting these ambiguities, but its measurement, which could make use of π^0 Dalitz decays for instance, requires very large statistics, which is not available at present.

[35] We may consider an alternative amplitude representation, which makes the occurrence of the discrete ambiguities more explicit [209]:

$$A^{+-} = \mu a\ , \qquad \overline{A}^{+-} = \mu\overline{a}\ e^{+2i\alpha_{\rm eff}}\ , \qquad A^{+0} = \mu\ e^{i(\Delta-\alpha)}\ , \qquad \overline{A}^{+0} = \mu\ e^{i(\Delta+\alpha)}\ ,$$
$$A^{00} = \mu\ e^{i(\Delta-\alpha)}\left(1-\frac{a}{\sqrt{2}}\ e^{+i(\alpha-\Delta)}\right)\ , \qquad \overline{A}^{00} = \mu\ e^{i(\Delta+\alpha)}\left(1-\frac{\overline{a}}{\sqrt{2}}\ e^{-i(\alpha+\Delta-2\alpha_{\rm eff})}\right)\ ,$$

which satisfy the triangular SU(2) relations (107), and where μ, a and $\overline{a}$ are three unknown real (and positive) parameters which drive the strength of the branching fractions, while Δ is a phase. The phase convention chosen here is such that A^{+-} is real positive, and the $\overline{A}$ amplitudes include the $B^0\overline{B}^0$ mixing phase $\arg[q/p]$. With this choice, the phase Δ is not to be viewed as arising purely from strong interaction since it absorbs the weak phase *a priori* present in A^{+-}: there is no reason to expect it to be confined to small values. In terms of the above parameterization, the observables take the form

$$\frac{1}{\tau_{B^0}}\mathcal{B}^{+-}_{\pi\pi} = \mu^2\frac{1}{2}(a^2+\overline{a}^2)\ ,$$
$$\frac{1}{\tau_{B^+}}\mathcal{B}^{+0}_{\pi\pi} = \mu^2\ ,$$
$$\frac{1}{\tau_{B^0}}\mathcal{B}^{00}_{\pi\pi} = \mu^2\frac{1}{2}\left(2+\frac{1}{2}(a^2+\overline{a}^2)-\sqrt{2}(ac+\overline{a}\overline{c})\right)\ ,$$
$$C^{+-}_{\pi\pi} = \frac{a^2-\overline{a}^2}{a^2+\overline{a}^2}\ ,$$
$$S^{+-}_{\pi\pi} = \frac{2a\overline{a}}{a^2+\overline{a}^2}\sin(2\alpha_{\rm eff})\ ,$$
$$C^{00}_{\pi\pi} = \frac{\frac{1}{2}(a^2-\overline{a}^2)-\sqrt{2}(ac-\overline{a}\overline{c})}{2+\frac{1}{2}(a^2+\overline{a}^2)-\sqrt{2}(ac+\overline{a}\overline{c})}\ ,$$
$$S^{00}_{\pi\pi} = \frac{2\sin(2\alpha)+a\overline{a}\sin(2\alpha_{\rm eff})-a\sqrt{2}\sin(\alpha+\Delta)-\overline{a}\sqrt{2}\sin(\alpha-\Delta+2\alpha_{\rm eff})}{2+\frac{1}{2}(a^2+\overline{a}^2)-\sqrt{2}(ac+\overline{a}\overline{c})}\ .$$

The eight mirror solutions (for α in $[0,\pi]$) are summarized in the table below. Solutions 5 through 8 are just $\pi/2$ minus solutions 1 through 4. The eight mirror solutions are strictly equivalent if no input is added, like $S^{00}_{\pi\pi}$ for example ($S^{00}_{\rho\rho,L}$ is experimentally accessible in the decay $B^0\to\rho^0\rho^0$, see Sect. VI.5).

Solution	α	Δ	$\alpha_{\rm eff}$
1	α	Δ	$\alpha_{\rm eff}$
2	Δ	α	$\alpha_{\rm eff}$
3	$-\alpha+2\alpha_{\rm eff}$	$-\Delta+2\alpha_{\rm eff}$	$\alpha_{\rm eff}$
4	$-\Delta+2\alpha_{\rm eff}$	$-\alpha+2\alpha_{\rm eff}$	$\alpha_{\rm eff}$
5	$\frac{\pi}{2}-\alpha$	$\frac{\pi}{2}-\Delta$	$\frac{\pi}{2}-\alpha_{\rm eff}$
6	$\frac{\pi}{2}-\Delta$	$\frac{\pi}{2}-\alpha$	$\frac{\pi}{2}-\alpha_{\rm eff}$
7	$\frac{\pi}{2}+\alpha-2\alpha_{\rm eff}$	$\frac{\pi}{2}+\Delta-2\alpha_{\rm eff}$	$\frac{\pi}{2}-\alpha_{\rm eff}$
8	$\frac{\pi}{2}+\Delta-2\alpha_{\rm eff}$	$\frac{\pi}{2}+\alpha-2\alpha_{\rm eff}$	$\frac{\pi}{2}-\alpha_{\rm eff}$

SU(2) bounds

The direct CP asymmetry $C^{00}_{\pi\pi}$ has not yet been measured so that the extraction of α itself is not possible and one has to derive upper limits on $\Delta\alpha$ instead. It was first pointed out by Grossman and Quinn [142] that a small value for the branching fraction to $\pi^0\pi^0$ would mean that the penguin contribution cannot be too large. We stress that the numerical analysis performed with CKMfitter guarantees the optimal use of the available and relevant experimental information, once the isospin relations are implemented at the amplitude level. It is nevertheless instructive to derive analytical bounds on $\Delta\alpha$. As shown by Grossman–Quinn [142], and later rediscussed by one of us [202] and Gronau–London–Sinha–Sinha (GLSS) [144], one obtains the inequality

$$\cos 2\Delta\alpha \;\geq\; \frac{1}{D}\left(1-2\frac{\tau_{B^+}}{\tau_{B^0}}\frac{\mathcal{B}^{00}_{\pi\pi}}{\mathcal{B}^{+0}_{\pi\pi}}\right)+\frac{\tau_{B^+}}{\tau_{B^0}}\frac{1}{D}\frac{\left(\mathcal{B}^{+-}_{\pi\pi}-2\frac{\tau_{B^0}}{\tau_{B^+}}\mathcal{B}^{+0}_{\pi\pi}+2\mathcal{B}^{00}_{\pi\pi}\right)^2}{4\mathcal{B}^{+-}_{\pi\pi}\,\mathcal{B}^{+0}_{\pi\pi}}\;, \tag{113}$$

or, equivalently,

$$\cos 2\Delta\alpha \;\geq\; \frac{1}{D}\left(1-4\frac{\mathcal{B}^{00}_{\pi\pi}}{\mathcal{B}^{+-}_{\pi\pi}}\right)+\frac{\tau_{B^+}}{\tau_{B^0}}\frac{1}{D}\frac{\left(\mathcal{B}^{+-}_{\pi\pi}-2\frac{\tau_{B^0}}{\tau_{B^+}}\mathcal{B}^{+0}_{\pi\pi}-2\mathcal{B}^{00}_{\pi\pi}\right)^2}{4\mathcal{B}^{+-}_{\pi\pi}\,\mathcal{B}^{+0}_{\pi\pi}}\;. \tag{114}$$

The first term on the right hand side of (113) and (114) corresponds to the limit considered in [202], while the original Grossman–Quinn bound is obtained when setting $D=1$ in the first term on the right hand side of (113).

The above bound has interesting consequences on the discrete ambiguity problem. In the limit where $\mathcal{B}^{00}_{\pi\pi}$ goes to zero, the GLSS bound (113) merges the eight mirror solutions for α (in the range $[0,\pi]$) in two distinct intervals, each of which containing one quadruplet of them.

Following the same line it is possible to derive lower and upper bounds on the branching fraction into two neutral pions [144]

$$\mathcal{B}^{00}_{\mathrm{GLSS}^-} \;\leq\; \mathcal{B}^{00}_{\pi\pi} \;\leq\; \mathcal{B}^{00}_{\mathrm{GLSS}^+}\;, \tag{115}$$

with

$$\mathcal{B}^{00}_{\mathrm{GLSS}^\pm}=\frac{\tau_{B^0}}{\tau_{B^+}}\mathcal{B}^{+0}_{\pi\pi}+\frac{1}{2}\mathcal{B}^{+-}_{\pi\pi}\pm\sqrt{\frac{\tau_{B^0}}{\tau_{B^+}}\mathcal{B}^{+0}_{\pi\pi}\mathcal{B}^{+-}_{\pi\pi}\,(1+D)}\;,$$

where the limits are weakest for $D=1$, that is vanishing direct CP violation. Equation (113) can be rewritten [209]

$$\sin^2\Delta\alpha \;\leq\; \frac{\tau_{B^+}}{\tau_{B^0}}\frac{1}{D}\frac{\left(\mathcal{B}^{00}_{\pi\pi}-\mathcal{B}^{00}_{\mathrm{GLSS}^-}\right)\left(\mathcal{B}^{00}_{\mathrm{GLSS}^+}-\mathcal{B}^{00}_{\pi\pi}\right)}{2\mathcal{B}^{+-}_{\pi\pi}\,\mathcal{B}^{+0}_{\pi\pi}}\;, \tag{116}$$

which does not provide new information but makes explicit that $\alpha=\alpha_{\mathrm{eff}}$ if $\mathcal{B}^{00}_{\pi\pi}$ *reaches either* $\mathcal{B}^{00}_{\mathrm{GLSS}^-}$ *or* $\mathcal{B}^{00}_{\mathrm{GLSS}^+}$. This is the case in the formal limit $\mathcal{B}^{00}_{\pi\pi}\to 0$, which is close to being realized in $B\to\rho\rho$ (see Sect. VI.5). However for $B\to\pi\pi$ the lower bound $\mathcal{B}^{00}_{\mathrm{GLSS}^-}$ in (115) is not so small and as soon as $\mathcal{B}^{00}_{\pi\pi}$ deviates from it, α_{eff} can be rather different from α, as described further below.

If we assume that α is known, e.g., from the standard CKM fit, we obtain the bound on $\mathcal{B}^{00}_{\pi\pi}$ [209]

$$\mathcal{B}^{00}_{\alpha:-} \;\leq\; \mathcal{B}^{00}_{\pi\pi} \;\leq\; \mathcal{B}^{00}_{\alpha:+}\;, \tag{117}$$

with

$$\mathcal{B}^{00}_{\alpha:\pm}=\frac{\tau_{B^0}}{\tau_{B^+}}\mathcal{B}^{+0}_{\pi\pi}+\frac{1}{2}\mathcal{B}^{+-}_{\pi\pi}\pm\sqrt{\frac{\tau_{B^0}}{\tau_{B^+}}\mathcal{B}^{+0}_{\pi\pi}\mathcal{B}^{+-}_{\pi\pi}\left(1+\tilde{D}_\alpha\right)}\;, \tag{118}$$

and where

$$\tilde{D}_\alpha=\sqrt{(1-\sin^2 2\alpha)(D^2-{S^{+-}_{\pi\pi}}^2)}+S^{+-}_{\pi\pi}\,\sin 2\alpha\;.$$

Since $\tilde{D}_\alpha\leq D$, this bound is tighter than (115). With known α, the CP asymmetry $C^{00}_{\pi\pi}$ is not a free parameter anymore: it can be determined using (118)

$$C^{00\,\pm}_{\pi\pi}=\frac{1}{\mathcal{B}^{00}_{\pi\pi}(1+\tilde{D}_\alpha)}\Bigg[-C^{+-}_{\pi\pi}\left(\frac{\tau_{B^0}}{\tau_{B^+}}\mathcal{B}^{+0}_{\pi\pi}-\frac{\tilde{D}_\alpha}{2}\mathcal{B}^{+-}_{\pi\pi}-\mathcal{B}^{00}_{\pi\pi}\right)$$
$$\pm\sqrt{(\mathcal{B}^{00}_{\pi\pi}-\mathcal{B}^{00}_{\alpha:-})(\mathcal{B}^{00}_{\alpha:+}-\mathcal{B}^{00}_{\pi\pi})(D^2-\tilde{D}^2_\alpha)}\Bigg]\;. \tag{119}$$

There are two solutions of $C^{00}_{\pi\pi}$ for a given $\mathcal{B}^{00}_{\pi\pi}$. An application of (119) is shown in Fig. 30.

Electroweak penguins

As pointed out by Buras and Fleischer [210] and Neubert and Rosner [211], the electroweak penguin amplitude $P^{\rm EW}$ in $B^+ \to \pi^+\pi^0$ can be related to the tree amplitude in a model-independent way using Fierz transformations of the relevant current-current operators in the effective Hamiltonian $\mathcal{H}_{\rm eff}$ for $B \to \pi\pi$ decays

$$\mathcal{H}_{\rm eff} = \frac{G_F}{\sqrt{2}} \left[\sum_{q=u,c} V_{qb}V_{qd}^*(c_1 O_1^q + c_2 O_2^q) - \sum_{i=3}^{10} V_{tb}V_{td}^* c_i O_i \right] \; + \; \text{h. c. .} \tag{120}$$

Here O_1^q and O_2^q are tree operators of the Lorentz structure $(V-A)\times(V-A)$, O_{3-6} are short-distance gluonic penguin operators, and O_{7-10} are electroweak penguin operators. The Lorentz structure of O_7 and O_8 is $(V-A)\times(V+A)$ while O_9 and O_{10} are $(V-A)\times(V-A)$. In the limit of isospin symmetry, the $\Delta I = 3/2$ part of the latter operators is Fierz-related to the operators O_1 and O_2. Since $c_{7,8}$ are small compared to $c_{9,10}$, they can be neglected so that one obtains

$$\frac{P^{\rm EW}}{T^{+0}} \simeq -\frac{3}{2}\left(\frac{c_9 + c_{10}}{c_1 + c_2}\right) = +(1.35 \pm 0.12) \times 10^{-2} \; . \tag{121}$$

The theoretical error on the numerical evaluation of this ratio has been estimated from the residual scale and scheme dependence of the Wilson coefficients [101]. It also accounts for the neglect of the contributions from O_7 and O_8 [143]. One notices that there is no strong phase difference between $P^{\rm EW}$ and T^{+0} so that electroweak penguins do not generate a charge asymmetry in $B^+ \to \pi^+\pi^0$ if this picture holds: this prediction is in agreement with the present experimental average of the corresponding asymmetry (see Table 8). Although in the SM electroweak penguins in two-pion modes appear to be small, their inclusion into the full isospin analysis is straightforward and will become necessary once high-statistics data samples are available.

1.2.2 SU(3) flavor symmetry

We extend the use of flavor symmetries to SU(3), considering the amplitude of the decay $B^0 \to K^+\pi^-$ in convention $\mathfrak{C}$

$$A_{K\pi}^{+-} \; \equiv \; A(B^0 \to K^+\pi^-) \; = \; V_{us}V_{ub}^* T_{K\pi}^{+-} + V_{ts}V_{tb}^* P_{K\pi}^{+-} \; . \tag{122}$$

With the assumption of SU(3) flavor symmetry and neglecting OZI-suppressed penguin annihilation diagrams (see right hand diagram in Fig. 21), which contribute to $B^0 \to \pi^+\pi^-$ but not to $B^0 \to K^+\pi^-$, the penguin amplitudes in $B^0 \to \pi^+\pi^-$ and $B^0 \to K^+\pi^-$ are equal

$$P^{+-} = P_{K\pi}^{+-} \; . \tag{123}$$

As in the isospin symmetry case, one can derive the following bound [202], which benefits from the CKM enhancement of the penguin contribution to the $B^0 \to K^+\pi^-$ decay

$$\cos 2\Delta\alpha \; \geq \; \frac{1}{D}\left(1 - 2\lambda^2 \frac{\mathcal{B}_{K\pi}^{+-}}{\mathcal{B}_{\pi\pi}^{+-}}\right) \; , \tag{124}$$

where λ is the Wolfenstein parameter.

Another possibility [212,213], that would eventually give stronger constraints, would be to identify T^{+-} and $T_{K\pi}^{+-}$ in addition to P^{+-} and $P_{K\pi}^{+-}$. At first sight such an approximation is similar in spirit to the neglect of OZI-suppressed

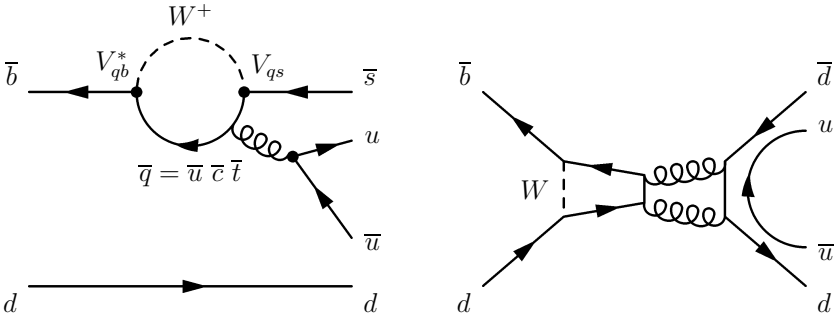

Fig. 21. *Left*: penguin diagram for the decay $B^0 \to K^+\pi^-$. *Right*: OZI-suppressed penguin annihilation diagram for the decay $B^0 \to \pi^+\pi^-$

Table 8. Compilation of experimental results on the $B \to hh'$ branching fractions (in units of 10^{-6}) and CP-violating asymmetries. Limits are quoted at 90% CL. For the averages we use the results from the HFAG [62]. $C^{00}_{K_S\pi}$ and $S^{00}_{K_S\pi}$ are defined similarly to (110) while the direct CP asymmetries A_{CP} are defined with an opposite sign: $A_{CP} = (|\overline{A}|^2 - |A|^2)/(|\overline{A}|^2 + |A|^2)$. Note that missing radiative corrections in the Monte Carlo simulations used by the experiments may lead to underestimated branching fractions for modes with light charged particles in the final state (see remark in the introduction to Part VI). The CDF collaboration has presented the preliminary result $A_{CP}(K^+\pi^-) = 0.02 \pm 0.15 \pm 0.02$ [224,231], which is however not yet included in the HFAG average

Parameter	*BABAR*	Belle	CLEO	Average
$C_{\pi\pi}^{+-}$	$-0.19 \pm 0.19 \pm 0.05$ [219]	$-0.58 \pm 0.15 \pm 0.07$ [220]	-	-0.46 ± 0.13
$S_{\pi\pi}^{+-}$	$-0.40 \pm 0.22 \pm 0.03$ [219]	$-1.00 \pm 0.21 \pm 0.07$ [220]	-	-0.73 ± 0.16
Correlation coeff.	-0.02 [219]	-0.29 [220]	-	-0.17
$C^{00}_{K_S\pi}$	$0.40\,^{+0.27}_{-0.28} \pm 0.10$ [221]	-	-	$0.40\,^{+0.27}_{-0.28} \pm 0.10$
$S^{00}_{K_S\pi}$	$0.48\,^{+0.38}_{-0.47} \pm 0.11$ [221]	-	-	$0.48\,^{+0.38}_{-0.47} \pm 0.11$
$A_{CP}(\pi^+\pi^0)$	$-0.03\,^{+0.18}_{-0.17} \pm 0.02$ [222]	$-0.14 \pm 0.24\,^{+0.05}_{-0.04}$ [223]	-	-0.07 ± 0.14
$A_{CP}(K^+\pi^-)$	$-0.107 \pm 0.041 \pm 0.013$ [224]	$-0.088 \pm 0.035 \pm 0.018$ [224]	$-0.04 \pm 0.16 \pm 0.02$ [225]	-0.095 ± 0.028
$A_{CP}(K^+\pi^0)$	$-0.09 \pm 0.09 \pm 0.01$ [222]	$+0.23 \pm 0.11$ [223]	$-0.29 \pm 0.23 \pm 0.02$ [225]	0.00 ± 0.07
$A_{CP}(K^0\pi^+)$	$-0.05 \pm 0.08 \pm 0.01$ [226]	$+0.07\,^{+0.09\,+0.01}_{-0.08\,-0.03}$ [223]	$+0.18 \pm 0.24 \pm 0.02$ [225]	$+0.02 \pm 0.06$
$\mathcal{B}(B^0 \to \pi^+\pi^-)$	$4.7 \pm 0.6 \pm 0.2$ [227]	$4.4 \pm 0.6 \pm 0.3$ [228]	$4.5\,^{+1.4\,+0.5}_{-1.2\,-0.4}$ [229]	4.55 ± 0.44
$\mathcal{B}(B^+ \to \pi^+\pi^0)$	$5.5\,^{+1.0}_{-0.9} \pm 0.6$ [222]	$5.0 \pm 1.2 \pm 0.5$ [228]	$4.6\,^{+1.8\,+0.6}_{-1.6\,-0.7}$ [229]	$5.18\,^{+0.77}_{-0.76}$
$\mathcal{B}(B^0 \to \pi^0\pi^0)$	$2.1 \pm 0.6 \pm 0.3$ [230]	$1.7 \pm 0.6 \pm 0.2$ [228]	< 4.4 [229]	1.90 ± 0.47
$\mathcal{B}(B^0 \to K^+\pi^-)$	$17.9 \pm 0.9 \pm 0.7$ [227]	$18.5 \pm 1.0 \pm 0.7$ [228]	$18.0\,^{+2.3\,+1.2}_{-2.1\,-0.9}$ [229]	18.16 ± 0.79
$\mathcal{B}(B^+ \to K^+\pi^0)$	$12.8\,^{+1.2}_{-1.1} \pm 1.0$ [222]	$12.0 \pm 1.3\,^{+1.3}_{-0.9}$ [228]	$12.9\,^{+2.4\,+1.2}_{-2.2\,-1.1}$ [229]	$12.6\,^{+1.1}_{-1.0}$
$\mathcal{B}(B^+ \to K^0\pi^+)$	$22.3 \pm 1.7 \pm 1.1$ [226]	$22.0 \pm 1.9 \pm 1.1$ [228]	$18.8\,^{+3.7\,+2.1}_{-3.3\,-1.8}$ [229]	21.8 ± 1.4
$\mathcal{B}(B^0 \to K^0\pi^0)$	$11.4 \pm 1.7 \pm 0.8$ [226]	$11.7 \pm 2.3\,^{+1.2}_{-1.3}$ [228]	$12.8\,^{+4.0\,+1.7}_{-3.3\,-1.4}$ [229]	11.7 ± 1.4
$\mathcal{B}(B^0 \to K^+K^-)$	< 0.6 [227]	< 0.7 [228]	< 0.8 [229]	
$\mathcal{B}(B^+ \to K^+\overline{K}^0)$	< 2.5 [226]	< 3.3 [228]	< 3.3 [229]	
$\mathcal{B}(B^0 \to K^0\overline{K}^0)$	< 1.8 [226]	< 1.5 [228]	< 3.3 [229]	

penguins, because it is violated by exchange diagrams only, that are expected to be power-suppressed[36]. However as shown in [202], an estimate of P^{+-} leads to the determination of the shift $\Delta\alpha$, while an estimate of T^{+-} determines the angle α itself. Hence, as far as α is concerned, the error on the estimate of P^{+-} is a second order effect, while the error on the estimate of T^{+-} is of leading order. We therefore expect the hadronic uncertainties in the relation $T^{+-} = T^{+-}_{K\pi}$ to be potentially more dangerous than in the relation $P^{+-} = P^{+-}_{K\pi}$. As a consequence, the ratio $T^{+-}_{K\pi}/T^{+-}$ is kept unconstrained in our fit.

SU(3) flavor symmetry is only approximately realized in nature and one may expect violations of the order of 30% at the amplitude level. For example, within factorization the relative size of SU(3) symmetry breaking is expected to be $(f_K - f_\pi)/f_K$, where f_K and f_π are the pion and kaon decay constants, respectively. Notwithstanding, the bound (124) can be considered conservative with respect to SU(3) breaking, since a correction would lead to a stronger bound. For example, assuming factorization the ratio of branching fractions $\mathcal{B}^{+-}_{K\pi}/\mathcal{B}^{+-}_{\pi\pi}$ would be lowered by $(f_\pi/f_K)^2 \simeq 0.67$. Since the penguin annihilation contributions, which spoil the relationship between the $B \to \pi^+\pi^-$ and $B \to K^+\pi^-$ penguin amplitudes, are power and OZI-suppressed, they are expected to be small with respect to the dominant SU(3) breaking. We will therefore study the constraints derived from (123) as if they were a consequence of strict SU(3) symmetry, although it is understood that an additional dynamical assumption is made.

[36] The term "power-suppression" refers to the quantity $\Lambda_{\rm QCD}/m_b \ll 1$.

1.2.3 Estimating $|P^{+-}|$ from $B^+ \to K^0\pi^+$

In addition to the theoretical assumptions of Scenario (II), the magnitude $|P^{+-}|$ can be estimated from the branching fraction of the penguin-dominated mode $B^+ \to K^0\pi^+$. Neglecting the doubly CKM-suppressed difference between u and c penguins, as well as the doubly CKM-suppressed tree annihilation contribution, the $B^+ \to K^0\pi^+$ transition amplitude reads

$$A^{0+}_{K\pi} \equiv A(B^+ \to K^0\pi^+) = V^*_{tb}V_{ts}P^{0+}_{K\pi} \ . \tag{125}$$

Now, if one takes the SU(3) limit and neglects the penguin annihilation and color-suppressed electroweak penguin contributions, one has [206,202,205]

$$|P^{+-}| = \frac{f_\pi}{f_K}\frac{1}{R}|P^{0+}_{K\pi}| \ . \tag{126}$$

The first factor on the right hand side corrects for factorizable SU(3) breaking, while the second factor, $R = 0.95 \pm 0.23$, is a theoretical estimate, within the QCD Factorization approach, of the residual effects that break the relation between $B \to \pi^+\pi^-$ and $B^+ \to K^0\pi^+$ penguin amplitudes[37] [208]. Our evaluation also includes the uncertainty due to the neglect of the $V_{us}V^*_{ub}$ contribution to $B^+ \to K^0\pi^+$. As in Scenario (II), the strong phase δ^{+-} remains unconstrained in Scenario (III). The size of the tree amplitude $|T^{+-}|$ is conveniently deduced from the measurement of $\mathcal{B}^{+-}_{\pi\pi}$, taking advantage of the above estimate of $|P^{+-}|$: the analytical constraint in the $(\overline{\rho}, \overline{\eta})$ plane cannot be expressed in terms of the angle α alone, but rather as a degree-four polynomial equation [202], or as a relation between α and γ. Other methods to estimate the tree amplitude are found in the literature:

- one can use the spectrum of the decay $B^0 \to \pi^+\ell^-\bar{\nu}$ near $q^2 = 0$ (that is the squared effective mass of the recoiling $\ell\nu$ system) with theoretical estimates for the form factor [205], to infer an estimate for the quantity $|V^*_{ub}| \times |T_u|$, where T_u is the semileptonic amplitude at $q^2 = 0$. The method is not used here as it provides T_u, which is not simply related to the full $|T^{+-}|$, except in the naïve factorization approximation.
- according to (108) and (109), the branching fraction of the tree-dominated decay $B^+ \to \pi^+\pi^0$ is given by (neglecting electroweak penguins)

$$2\mathcal{B}^{+0}_{\pi\pi} = |V_{ud}V^*_{ub}|^2 \left[|T^{+-}|^2 + |T^{00}_{\rm C}|^2 + 2{\rm Re}\left(T^{+-}T^{00\,*}_{\rm C}\right)\right] \ . \tag{127}$$

  Using theoretical assumptions on the ratio $|T^{00}_{\rm C}/T^{+-}|$ one may infer the size of $|T^{+-}|$ from the measured branching fraction [205].

1.2.4 Beyond naïve factorization

Considerable theoretical progress to calculate the tree and penguin amplitudes in $B \to hh'$ with the use of QCD has been achieved in the recent years. If such calculations reliably predicted the penguin and tree contributions and their relative strong phase difference, they could be used to translate a measurement of $S^{+-}_{\pi\pi}$ and $C^{+-}_{\pi\pi}$ into a constraint on the CKM couplings.

The QCD Factorization Approach (QCD FA) [207,208,135] is based on the concept of color transparency [214]. In the heavy quark limit ($m_b \gg \Lambda_{\rm QCD}$), the decay amplitudes are calculated by virtue of a new factorization theorem. To leading power in $\Lambda_{\rm QCD}/m_b$ and in lowest order in perturbation theory, the result of naïve factorization is reproduced. It is found that power-dominant non-factorizable corrections are calculable as perturbative corrections in α_s since the interaction of soft gluons with the small color-dipole of the high-energetic (W-emitted) quark-anti-quark pair is suppressed. Non-factorizable power-suppressed contributions are neglected within this framework. However, due to a chiral enhancement and although they are formally power-suppressed[38], hard-scattering spectator interactions and annihilation diagrams cannot be neglected. Since they give rise to infrared endpoint singularities when computed perturbatively, they can only be estimated in a model-dependent way. In [208] these contributions are parameterized by two complex quantities, X_H and X_A, that are logarithmically large but always appear with a relatively small factor proportional to α_s.

The QCD FA has been implemented in CKMfitter and is used in two different configurations. The first configuration defines a *leading order* (LO) calculation by neglecting the non-factorizable power-suppressed terms, i.e., the annihilation contribution and the divergent part of the hard spectator diagrams ($X_H = 0$). This configuration is not fully consistent because the power corrections that are convergent, once factorized, are kept: LO QCD FA is very close to the usual

[37] The numerical value of R and its uncertainty are obtained from (126) by estimating $|P^{+-}|$ and $|P^{0+}_{K\pi}|$ from the full QCD FA calculation, as described in Sect. VI.1.2.4.

[38] The power-suppression in annihilation diagrams and hard spectator contribution occurs by the ratio $r^\pi_\chi = 2m^2_\pi/(m_b(m_u + m_d))$, which is numerically of order one.

naïve factorization model (see, e.g., [215]), and only differs from the latter by small convergent radiative corrections. In the second configuration, the full QCD FA calculations are used and the quantities X_H and X_A are parameterized as [208]

$$X_{H,A} = \left(1 + \rho_{H,A} e^{i\phi_{H,A}}\right) \ln \frac{m_B}{\Lambda_h} \ , \tag{128}$$

where $\Lambda_h = 0.5\,\mathrm{GeV}$, $\phi_{H,A}$ are free phases ($-180^\circ < \phi_{H,A} < 180^\circ$) and $\rho_{H,A}$ are parameters varying within $[0,1]$.

In addition to X_H and X_A, other theoretical parameters used in the calculation such as quark masses, decay constants, form factors and Gegenbauer moments, are varied within the ranges given in [135]. Therefore, all scenarios defined in [135] are automatically contained in our results.

Another approach, denoted pQCD [216], differs from QCD FA mainly in the power counting in terms of $\Lambda_{\mathrm{QCD}}/m_b$. The pQCD approach has not been implemented in CKMfitter yet and is therefore not considered in the following discussion.

There is an ongoing debate among the experts concerning the reliability of these calculations. The main concerns are the computation of the chirally enhanced penguins, the endpoint singularities in hard spectator interactions and the control of non-factorizable annihilation contributions (see, e.g., [217,218]). As we will see, LO QCD FA is very predictive but fails to describe the experimental data. On the other hand, full QCD FA with parameterized power corrections is quite successful within large theoretical uncertainties, but it can no longer be viewed as a systematic expansion of QCD.

1.3 Experimental input

The experimental values for the time-dependent CP asymmetries measured by *BABAR* [219] and Belle [220] are collected in Table 8. We have reversed the sign of Belle's $A_{\pi\pi} = -C^{+-}_{\pi\pi}$ to account for the different convention adopted. Also quoted are the statistical correlation coefficients between $S^{+-}_{\pi\pi}$ and $C^{+-}_{\pi\pi}$ as reported by the experiments. Significant mixing-induced CP violation has been observed by Belle. Averaging *BABAR* and Belle, the no-CP-violation hypothesis ($S^{+-}_{\pi\pi} = 0$, $C^{+-}_{\pi\pi} = 0$) is ruled out with a p-value of 1.2×10^{-9}, and deviations of 4.7σ and 3.7σ from the $S^{+-}_{\pi\pi} = 0$ and $C^{+-}_{\pi\pi} = 0$ hypotheses are observed, respectively[39]. We note that $C^{+-}_{\pi\pi} \neq 0$ is incompatible with the naïve factorization approximation, which predicts no final state interaction phases. Since the time-dependent CP parameters measured by Belle are outside of the physical domain, we apply the procedure outlined in Sect. II.2.2.3 to obtain the corresponding CLs within ${C^{+-}_{\pi\pi}}^2 + {S^{+-}_{\pi\pi}}^2 \leq 1$. The results are given in Fig. 25 together with the theoretical predictions (discussed below).

Also given in Table 8 is the time-dependent CP asymmetry in the $B^0 \to K^0_S\pi^0$ decay measured by *BABAR*, and a compilation of the branching fractions and charge asymmetries (direct CP violation) of all the $B \to hh'$ modes ($hh' = \pi, K$). Most of the rare two-body pseudoscalar-pseudoscalar decay modes have been discovered. The unobserved $K\overline{K}$ modes are either mediated via power-suppressed W exchange/annihilation diagrams ($B^0 \to K^+K^-$, $B^+ \to K^+\overline{K}^0$, see Fig. 22) or penguin diagrams ($B^0 \to K^0\overline{K}^0$, $B^+ \to K^+\overline{K}^0$) and hence are expected to be small. The ratio of $\mathcal{B}^{+-}_{K\pi}/\mathcal{B}^{+-}_{\pi\pi} \sim 4$ is a strong indication of the presence of penguin diagrams. In effect, according to (95) and (122), if there were no penguin, it would be of the order of λ^2. Charge asymmetries are all consistent with zero so far, except for $A_{CP}(K^+\pi^-)$ which differs from zero by 3.4σ. The averages quoted in Table 8 are taken from the *Heavy Flavor Averaging Group* [62].

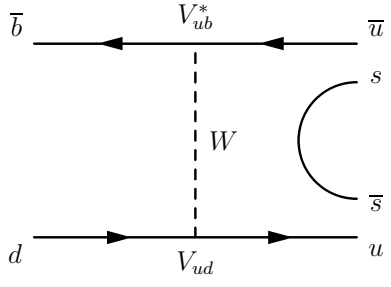

Fig. 22. W exchange diagram responsible for the decay $B^0 \to K^+K^-$

[39] These exclusion probabilities are estimates only, assuming Gaussian error propagation of the averages.

1.4 Numerical analysis of $B \to \pi\pi$ decays

We ran CKMfitter corresponding to the analysis scenarios (I) through (IV), using the inputs from Table 8[40]. If not stated otherwise, all plots are produced using the *BABAR* and Belle averages for $S^{+-}_{\pi\pi}$ and $C^{+-}_{\pi\pi}$, as well as the world averages for all other observables.

1.4.1 Constraints on α and $(\overline{\rho},\overline{\eta})$

The constraints on α and in the $(\overline{\rho},\overline{\eta})$ plane obtained for the various scenarios are plotted in Figs. 23 and 24 and discussed below[41].

- At present, we achieve essentially no useful constraint from the SU(2) analysis (Scenario (I), upper left hand plots). We find the limit $-54° < \Delta\alpha < 52°$ for CL $> 10\%$, largely dominated by the uncertainty on the contribution from gluonic penguins (see the dark shaded function in the upper left hand plot of Fig. 23). The asymmetry in the limit is due to the contribution from electroweak penguins.
- Using in addition SU(3) (Scenario (II)) one begins to rule out regions in the $(\overline{\rho},\overline{\eta})$ plane (upper right hand plots). The wide unconstrained arcs correspond to the still unfruitful bound $-29° < \Delta\alpha < 28°$ for CL $> 10\%$. These constraints cannot compete with the size of the allowed $(\overline{\rho},\overline{\eta})$ region obtained from the standard CKM fit.

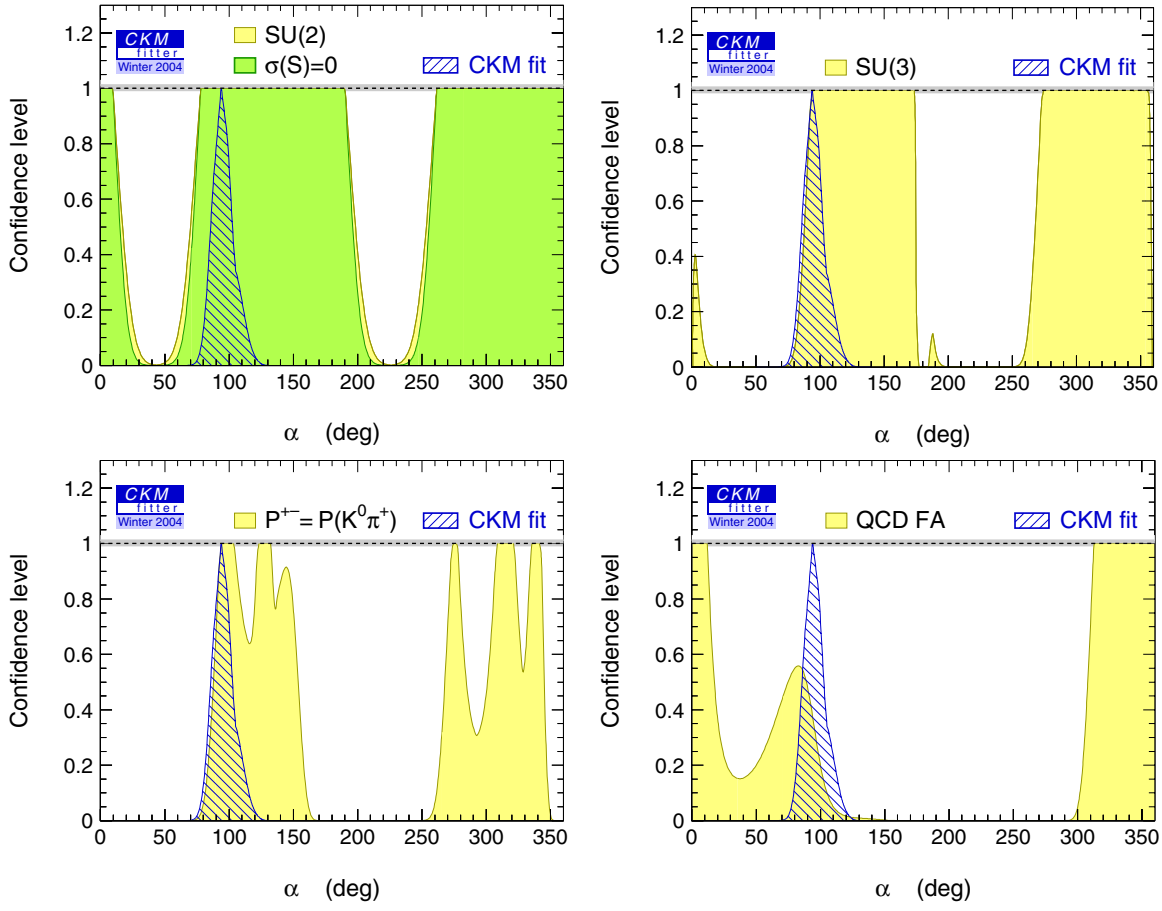

Fig. 23. Confidence levels for α for Scenarios (I) through (IV) (cf. Sect. VI.1.2) of the $B \to \pi\pi$ data. The dark shaded function on the upper left hand plot shows the constraint from SU(2) when the experimental uncertainty on $S^{+-}_{\pi\pi}$ is set to zero. It hence displays the uncertainty on $|\alpha - \alpha_{\rm eff}|$ due to the penguin contribution. Also shown on each plot is the result from the standard CKM fit

[40] Other recent analyses can be found in [232,233,218].

[41] The presence of non-zero electroweak penguins leads to a small modification in the isospin analysis which breaks the relation $\mathrm{CL}(\overline{\rho},\overline{\eta}) = \mathrm{CL}(\alpha(\overline{\rho},\overline{\eta}))$. As a consequence, the CL versus α is uniform if both $\overline{\rho}$ *and* $\overline{\eta}$ are free varying variables. As a remedy to this we also use $|V_{ub}/V_{cb}|$ (see Sect. III.2.5) in the α scans, which introduces a slight effect on the angle itself.

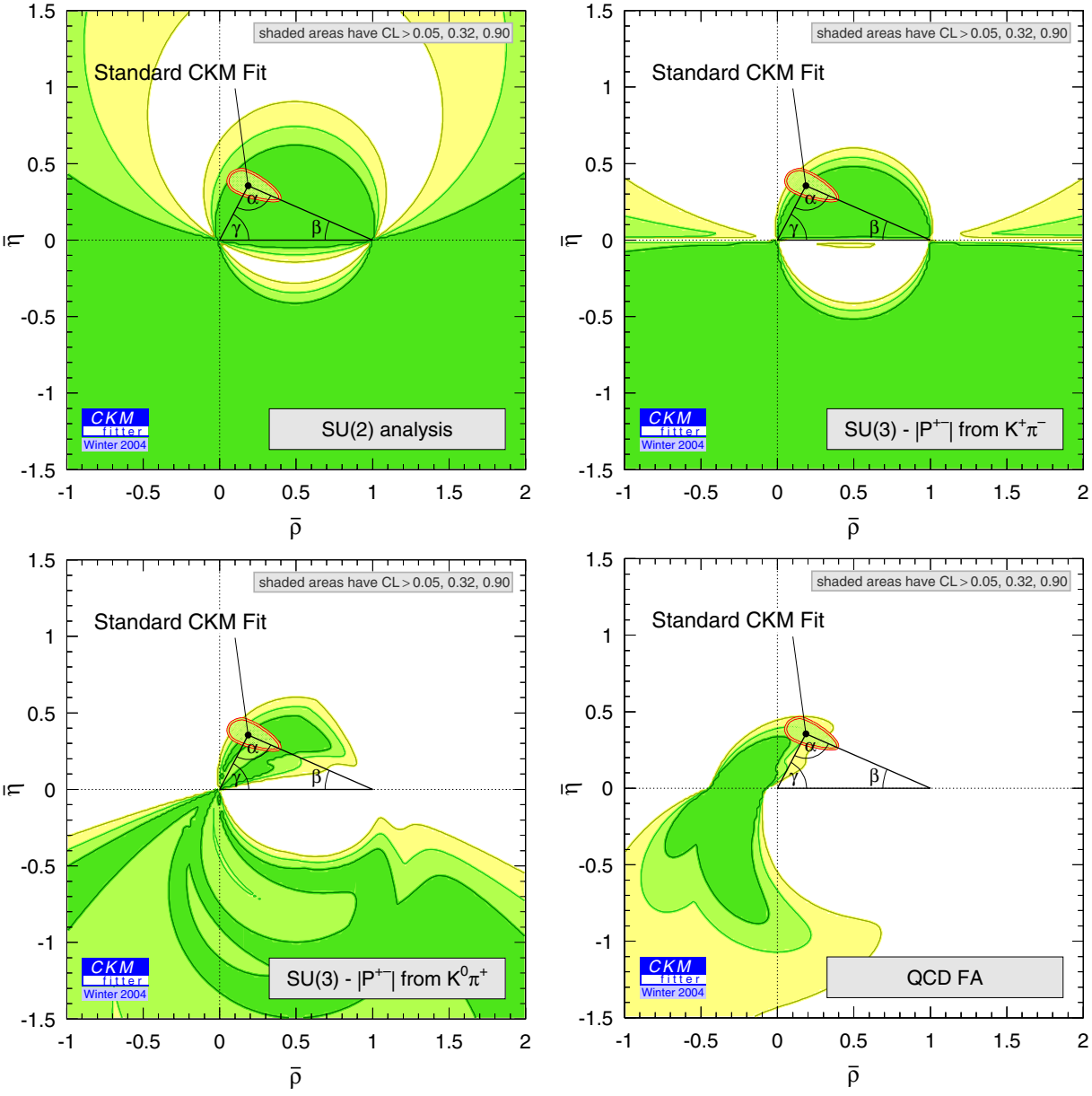

Fig. 24. Confidence levels in the $(\overline{\rho},\overline{\eta})$ plane for Scenarios (I) through (IV) of the $B \to \pi\pi$ data. Dark, medium and light shaded areas have $CL > 0.90$, 0.32 and 0.05, respectively. Also shown on each plot is the result from the standard CKM fit. Significant constraints are obtained once the penguin-to-tree ratio is determined with the use of phenomenological or theoretical input (Scenarios (III) and (IV)). Consistency with the SM is found, in spite of the sensitivity of the data to $b \to d$ transitions that could in principle receive sizable New Physics contributions

– Interesting information is obtained for Scenario (III) (lower left hand plots). The overall uncertainty is dominated by the errors on $(S^{+-}_{\pi\pi}, C^{+-}_{\pi\pi})$ on the one hand, and on the correction factor R (cf. (126)) on the other hand. For larger statistics the latter will limit the accuracy of the constraint, unless theoretical progress, together with combined fits of many SU(3)-related modes, is able to estimate R more precisely.
– The constraint is significantly improved when using QCD FA to predict the various amplitudes[42]. The preferred region is found in agreement with the standard CKM fit, despite the potential sensitivity of the observables to the suppressed $b \to d$ FCNC transitions. The main theoretical uncertainty is due to the phenomenological parameters X_A and X_H [234]. In particular, the sign of $\overline{\eta}$ cannot be constrained because the sign of δ^{+-} is not well predicted by the calculation (see Fig. 26).

[42] The full QCD FA calculation (1.2.4) is used here. See Sect. VI.2 for a discussion of the leading order (LO) approach.

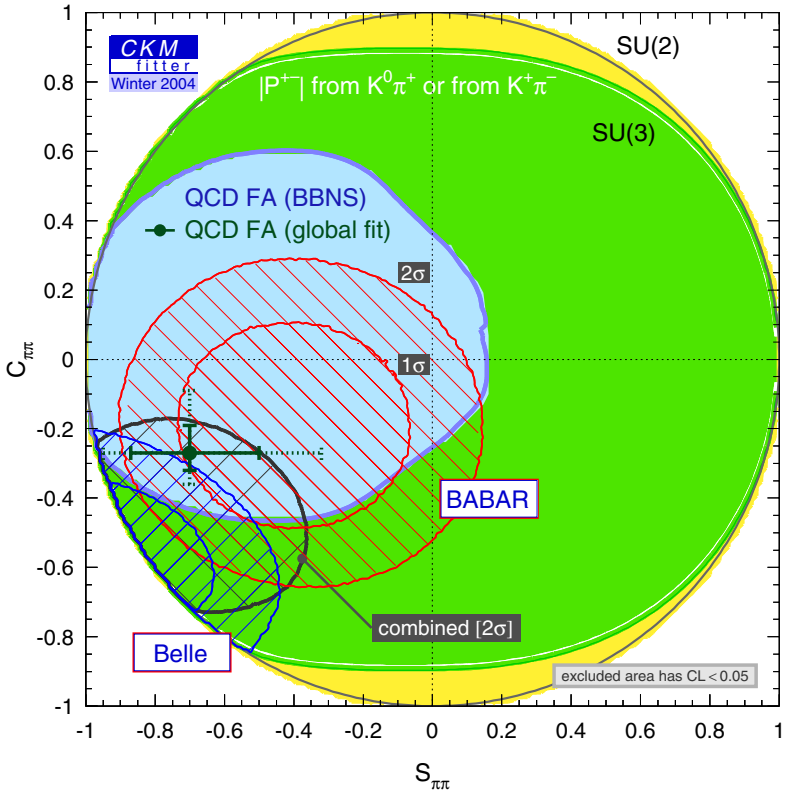

Fig. 25. Predictions for $S_{\pi\pi}^{+-}$ and $C_{\pi\pi}^{+-}$ for Scenarios (I) through (IV). Drawn are $CL = 0.05$ contours. The input values for $\overline{\rho}$ and $\overline{\eta}$ are taken from the standard CKM fit assuming the SM to hold. The dot with error bars gives the QCD FA prediction obtained from the global fit to all $B \to \pi\pi$, $K\pi$ observables (excluding $S_{\pi\pi}^{+-}$ or $C_{\pi\pi}^{+-}$ from the fit when determining $C_{\pi\pi}^{+-}$ and $S_{\pi\pi}^{+-}$, respectively) presented in Sect. II.2.3. For comparison, the CL contours corresponding to 1σ and 2σ for the experimental results from *BABAR*, Belle and their averages are overlaid. Note that we have applied the statistical method described in Sect. II.2.2.3 to account for the presence of the physical boundaries when computing the CLs

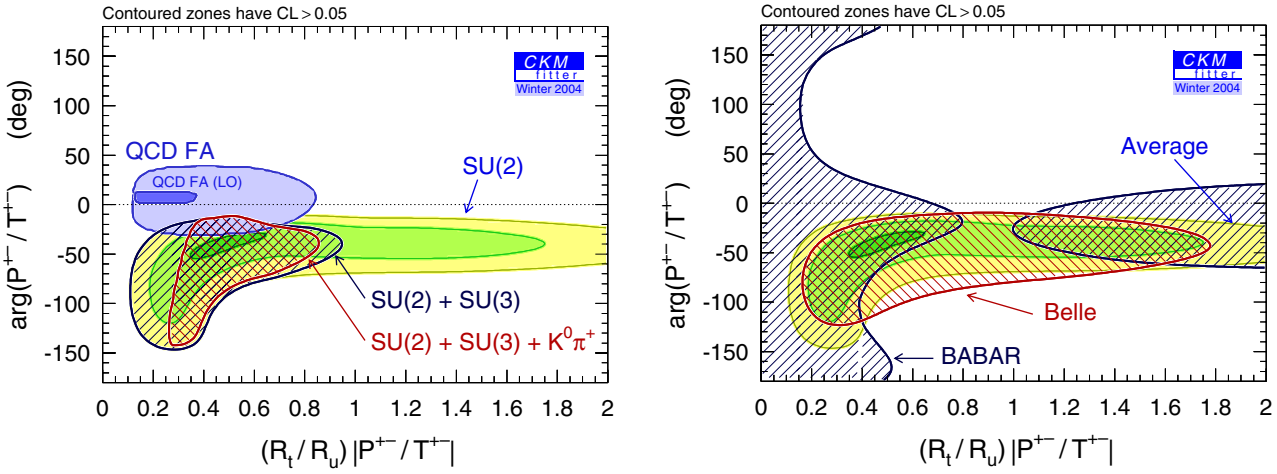

Fig. 26. Constraints on the penguin-to-tree ratio r^{+-} and the relative strong phase δ^{+-} in $B \to \pi\pi$ decays, obtained when using as additional input the CKM parameters $\overline{\rho}$ and $\overline{\eta}$ from the standard CKM fit. The gradually shaded regions give the CLs for fits of Scenario (I) (SU(2)): dark, medium and light shaded areas have $CL > 0.90$, 0.32 and 0.05, respectively. Also shown are the 5% CL contours obtained for Scenario (II) and (III). The elliptical areas are the prediction from QCD Factorization (Scenario (IV)): full calculation (light shaded) and leading order (dark shaded). On the right hand plot, constraints using Scenario (I) are given individually for *BABAR*, Belle and their averages

1.4.2 Constraints in the $(S_{\pi\pi}^{+-}, C_{\pi\pi}^{+-})$ plane

The predictions obtained for $S_{\pi\pi}^{+-}$ and $C_{\pi\pi}^{+-}$ for Scenarios (I) through (IV) are shown in Fig. 25. Input requirements to these predictions are the values of $\overline{\rho}$ and $\overline{\eta}$, as predicted by the standard CKM fit, the errors of which are properly propagated in the calculations (see Part III). In accordance with the above findings, the present experimental inputs used in the isospin analysis (I) are not sufficient to constrain $S_{\pi\pi}^{+-}$ and $C_{\pi\pi}^{+-}$. Also, little information is obtained from the SU(3) analysis (II) and Scenario (III), while the QCD FA (IV) remains the most predictive framework.

To a good approximation, the SU(2) solution in the $(S_{\pi\pi}^{+-}, C_{\pi\pi}^{+-})$ plane represents a circle of which the center is located at $(\sin 2\alpha, 0)$ and of which the radius is given by the penguin-to-tree ratio $r^{+-} \equiv (R_t/R_u) \times |P^{+-}/T^{+-}|$. The

relative strong phase δ^{+-} determines the position on the circle. Consequently, the large uncertainty on $S^{+-}_{\pi\pi}$ reflects both the relatively weak $\sin 2\alpha$ constraint of the standard CKM fit and the insufficient knowledge of r^{+-}. On the other hand, the accuracy of the $C^{+-}_{\pi\pi}$ prediction is determined by r^{+-} and, in case of Scenario (IV), by δ^{+-}. Values of $C^{+-}_{\pi\pi}$ that are far from zero, as suggested by the Belle measurement, are in marginal agreement with the QCD FA since it requires both a large relative strong phase δ^{+-} and a large r^{+-}. If such a large non-zero value for $C^{+-}_{\pi\pi}$ is confirmed, it would be a strong hint for significant rescattering effects, independently of potential New Physics contributions.

1.4.3 Constraints on amplitude ratios

One can take another point of view and constrain the unknown penguin-to-tree ratio r^{+-} and its phase δ^{+-} using the standard CKM fit as input. As in the prediction of $S^{+-}_{\pi\pi}$ and $C^{+-}_{\pi\pi}$ in the previous paragraph, this assumes that the experimental measurements are in agreement with the constraints obtained on $\overline{\rho}$ and $\overline{\eta}$ in the standard CKM fit, i.e., no New Physics comes into play. The results are shown in the left hand plot of Fig. 26. The shaded regions give the CLs obtained from a fit using Scenario (I) (SU(2)). Significant penguin contributions and strong phases are required to accommodate the fit with the data. Scenario (II) leads to an exclusion of large values for r^{+-}, while Scenario (III) increases the lower bound. We find that the preferred values for r^{+-} are in agreement with the allowed regions obtained for Scenario (IV) (QCD FA). The right hand plot of Fig. 26 shows the Scenario (I) constraints separately for *BABAR*, Belle and their average. Large non-zero r^{+-} and δ^{+-} are required by Belle's numbers.

To test color-suppression, the same procedure is applied to constrain the color-suppressed-to-color-allowed ratio $T^{00}_{\rm C}/T^{+-}$. The resulting CLs are given in Fig. 27. For the magnitude we obtain the lower limit $|T^{00}_{\rm C}/T^{+-}| > 0.41$ for CL $> 5\%$ and a central value of 0.9, which significantly exceeds the naïve 0.2 expectation from factorization. Note that a central value of order one, if confirmed, would challenge the $1/N_c \to 0$ limit of QCD independently of the validity of perturbative factorization.

1.5 Prospects for the isospin analysis

The preceding sections have shown that, at present, relevant information on α requires input from flavor symmetry other than SU(2) and/or theoretical assumptions, the accuracy of which is hard to determine. However the ultimate goal of the experimental effort should be a model-independent determination of α. This prejudice given, we shall attempt an outlook into the future to assess the performance of a full isospin analysis, where $C^{00}_{\pi\pi}$ is determined in a time-integrated measurement by the experiments.

Figure 28 (left) shows the CL of the angle α for the following set of observables (branching fractions are given in units of 10^{-6}):

$$\begin{aligned} \mathcal{B}^{+-}_{\pi\pi} &= 4.55 \pm 0.17 \pm 0.09\ , & S^{+-}_{\pi\pi} &= -0.73 \pm 0.07 \pm 0.02\ , \\ \mathcal{B}^{+0}_{\pi\pi} &= 5.18 \pm 0.28 \pm 0.16\ , & C^{+-}_{\pi\pi} &= -0.46 \pm 0.06 \pm 0.03\ , \\ \mathcal{B}^{00}_{\pi\pi} &= 1.90 \pm 0.20 \pm 0.09\ , & C^{00}_{\pi\pi} &= -0.37 \pm 0.24 \pm 0.03\ , \end{aligned}$$

where we have kept the central values of the present experimental results. For the parameter $C^{00}_{\pi\pi}$ we choose one out of the two solutions preferred by the data when inserting α from the standard CKM fit. The statistical errors

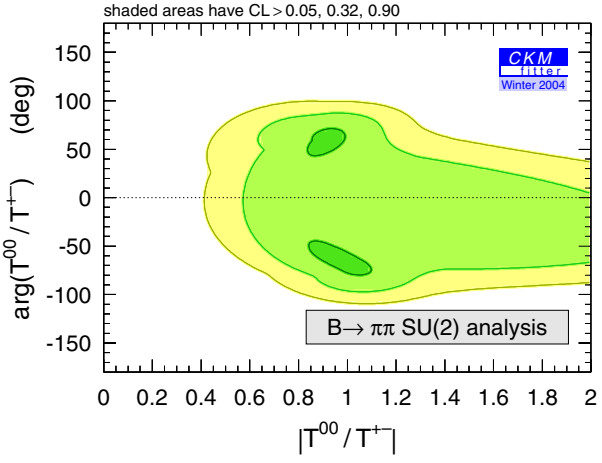

Fig. 27. Constraints from Scenario (I) (SU(2)) on magnitude and phase of the color-suppressed-to-color-allowed ratio $T^{00}_{\rm C}/T^{+-}$ in $B \to \pi\pi$ decays. The CKM parameters $\overline{\rho}$ and $\overline{\eta}$ are taken from the standard CKM fit. The gradually shaded regions indicate the CLs: dark, medium and light shaded areas have $CL > 0.90$, 0.32 and 0.05, respectively

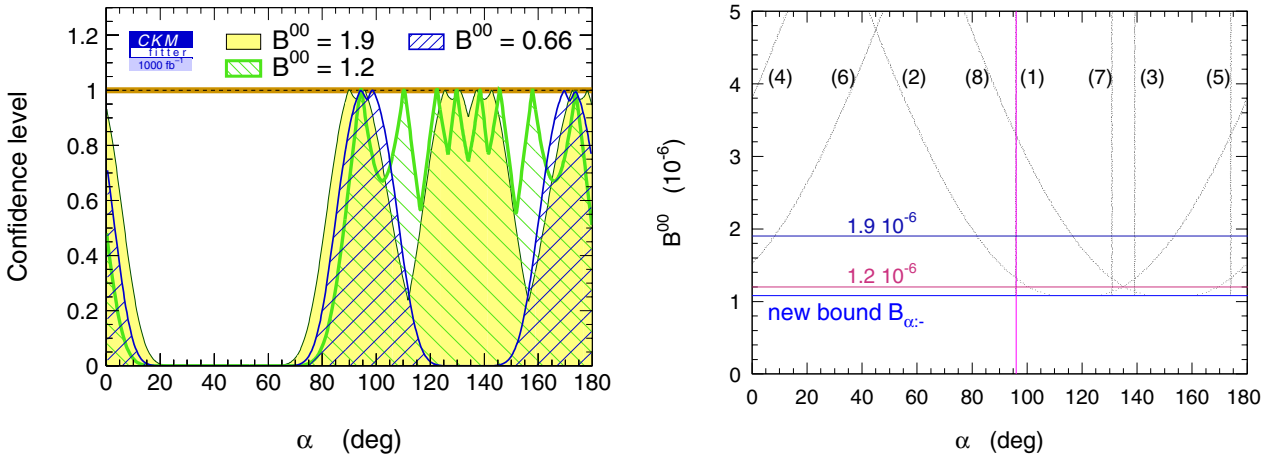

Fig. 28. *Left*: confidence level as a function of α for the full isospin analysis (including $C^{00}_{\pi\pi}$) at an integrated luminosity of $1\,\mathrm{ab}^{-1}$, and using the central values and errors given in the text (shaded area). Also shown is the CL for $\mathcal{B}^{00}_{\pi\pi} = 1.2\times10^{-6}$ (down-diagonal hatched area) for which the ambiguities move together (see right hand plot), and for $\mathcal{B}^{00}_{\pi\pi} = 0.66\times10^{-6}$ (up-diagonal hatched area), which corresponds to $\mathcal{B}^{00}_{\mathrm{GLSS}-}$, i.e., the ambiguities overlap in two quadruplets. The branching ratio values given on the figure are in units of $\times10^{-6}$. *Right*: location of the eight mirror solutions as a function of $\mathcal{B}^{00}_{\pi\pi}$. The curves refer to the present central values of branching fractions and CP-violating asymmetries. The horizontal lines indicate the bound (117), computed at the input value of α, as well as the two branching fractions used for the isospin analyses of the left hand plot. Electroweak penguins are neglected

are extrapolated to an integrated luminosity of $1\,\mathrm{ab}^{-1}$. For the systematic uncertainties we assume an optimistic development: the branching ratios are dominated by uncertainties due to the reconstruction of neutrals (2.5% per π^0), while the CP parameters are dominated by the unknown CP violation on the tag side. One observes the characteristic eightfold ambiguity within $[0,\pi]$, where the position of the peaks depends in particular on $\mathcal{B}^{00}_{\pi\pi}$ (see comments below). Although the allowed region for α largely exceeds the one obtained by the standard CKM fit, significant α domains are excluded and the peaking structure provides metrological information when combined with other α measurements. We also note that due to the significant penguin pollution in the $\pi\pi$ system, contributions from New Physics may be present in the data.

As outlined in Sect. VI.1.2.1, the central value of $\mathcal{B}^{00}_{\pi\pi}$ drives the position of the discrete ambiguities for α. The location of the eight mirror solutions as a function of $\mathcal{B}^{00}_{\pi\pi}$ are shown on the right hand plot of Fig. 28. The curves refer to the present central values of branching fractions and CP-violating asymmetries. The horizontal lines indicate the bound (117) as well as the two values used for the isospin analyses represented in the left hand plot (apart from the nominal setup given above, a second set is used with $\mathcal{B}^{00}_{\pi\pi} = 1.2\times10^{-6}$ and the corresponding value $C^{00}_{\pi\pi} = 0.13$, and with all other parameters kept unchanged). The quality of the metrological constraint on α depends on how much the different solutions overlap. The worst case occurs when several mirror solutions gather around the true value of α within a distance of about $\sigma(\alpha)$. As a consequence we note that large values of $\mathcal{B}^{00}_{\pi\pi}$ can lead to a better metrology.

In a third extrapolation we study the best-case scenario, where $\mathcal{B}^{00}_{\pi\pi}$ is chosen to be equal to one of the GLSS bounds (115). While the upper bound is excluded by experiment, the lower bound, $\mathcal{B}^{00}_{\mathrm{GLSS}-} = 0.66\times10^{-6}$, may still be reached. We choose $\mathcal{B}^{00}_{\pi\pi} = (0.66\pm0.12\pm0.03)\times10^{-6}$, as well as $S^{+-}_{\pi\pi} = -0.25\pm0.07\pm0.02$ and $C^{00}_{\pi\pi} = 0.75\pm0.39\pm0.03$, to achieve consistency between the observable set, SU(2), and the standard CKM fit. The modified $S^{+-}_{\pi\pi}$ value (with respect to the previous extrapolations) ensures that $\mathcal{B}^{00}_{\mathrm{GLSS}-} = \mathcal{B}^{00}_{\alpha:-}$, which is required for overlapping ambiguities[43]. The chosen set of observables is only marginally consistent with the present measurements. The resulting CL for α is given by the up-diagonal hatched function in the left hand plot of Fig. 28. The 1σ precision on α for this scenario is found to be 14°. This study provides an illustration of how precise the measurement of α could turn out to be in the coming years. However, one should keep in mind that if $\mathcal{B}^{00}_{\pi\pi}$ is not equal to, but only close to $\mathcal{B}^{00}_{\mathrm{GLSS}-}$, the metrology is spoilt [209].

Figure 29 shows the CLs in the $(\alpha, C^{00}_{\pi\pi})$ plane at integrated luminosities of $1\,\mathrm{ab}^{-1}$ (left) and $10\,\mathrm{ab}^{-1}$ (right), where we have used the same parameter configuration as in the above discussion, with the exception of $C^{00}_{\pi\pi}$ which is not used. It is assumed in the extrapolation that the systematic uncertainties do not decrease any further beyond $1\,\mathrm{ab}^{-1}$. As for $\mathcal{B}^{00}_{\pi\pi}$, one observes that (for given $\mathcal{B}^{00}_{\pi\pi}$ and $C^{+-}_{\pi\pi}$) the ambiguity pattern for α depends strongly on $C^{00}_{\pi\pi}$. An extraction of α with an accuracy of a few degrees should be within the reach of a next generation B factory.

[43] One notices in the up-diagonal hatched function of the left hand plot in Fig. 28 that the ambiguities do not exactly overlap. This is because electroweak penguins are neglected in the bounds (115), (117), while they are taken into account in the numerical analysis used to produce the plots.

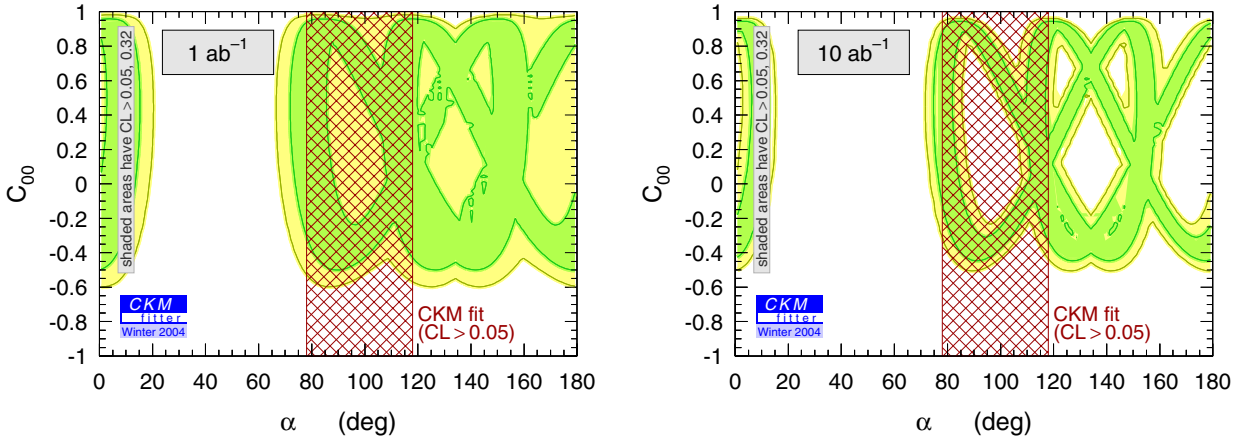

Fig. 29. Confidence level in the $(\alpha, C^{00}_{\pi\pi})$ plane at integrated luminosities of $1\,\mathrm{ab}^{-1}$ (left) and $10\,\mathrm{ab}^{-1}$ (right), respectively. The observable set and errors used are given in the text

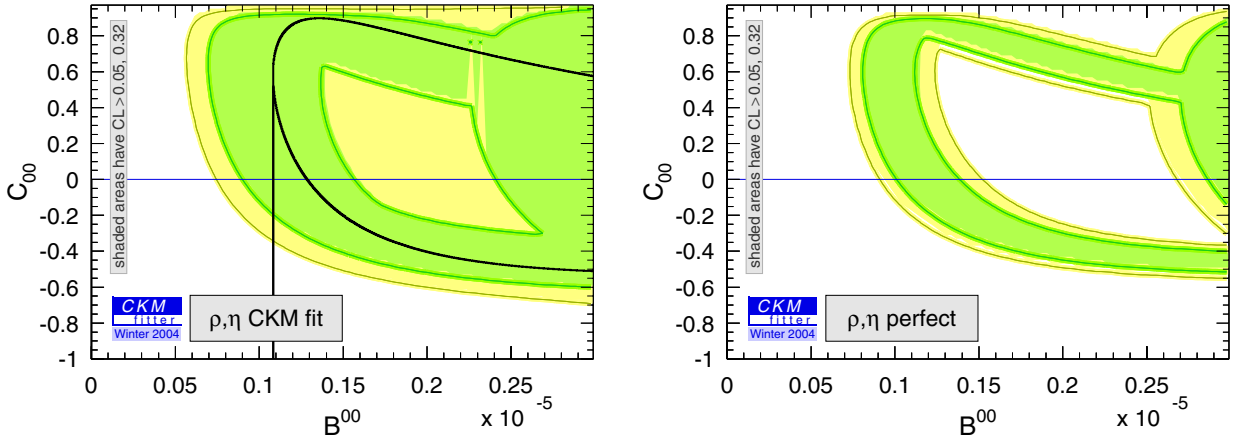

Fig. 30. Confidence level in the $(\mathcal{B}^{00}_{\pi\pi}, C^{00}_{\pi\pi})$ plane at an integrated luminosity of $1\,\mathrm{ab}^{-1}$. The left hand plot uses the standard CKM fit as input including the present uncertainties on α, while the right hand plot assumes perfect knowledge of α. Superimposed on the left hand plot is the analytical function $C^{00}_{\pi\pi}(\mathcal{B}^{00}_{\pi\pi})$ (119), where electroweak penguins are neglected which explains the difference with the CL function. The vertical line represents the bound (117)

The parameter plane $(\mathcal{B}^{00}_{\pi\pi}, C^{00}_{\pi\pi})$ is convenient to immediately display the consistency between the measurements in the $\pi\pi$ system and the standard CKM fit, because it avoids the problem of multiple solutions. The left hand plot of Fig. 30 represents the expectation for an integrated luminosity of $1\,\mathrm{ab}^{-1}$, using the standard CKM fit as input. Very large luminosities will be needed in order to significantly uncover a potential disagreement with the SM. The right hand plot of Fig. 30 is obtained assuming in addition that $\overline{\rho}$ and $\overline{\eta}$ be exactly known and fixed to their present central values (cf. Table 2).

1.6 Predicting the $B^0_s \to K^+K^-$ branching fraction and CP-violating asymmetries

It has been pointed out by Pirjol [236] and Fleischer [213] that one can use SU(3) symmetry[44] to relate the amplitudes in $B^0_s \to K^+K^-$ and $B^0 \to \pi^+\pi^-$ decays. The $B^0_s \to K^+K^-$ amplitude is given by

$$A(B^0_s \to K^+K^-) = V_{us}V^*_{ub}T^s_{KK} + V_{ts}V^*_{tb}P^s_{KK}\ , \tag{129}$$

and using SU(3) symmetry, one can identify

$$T^s_{KK} = T^{+-}\ ,$$

[44] More precisely, only the U-spin subgroup of SU(3) ($s \leftrightarrow d$ exchange) is needed. However the accuracy of this approximate symmetry is not expected to be significantly better than full SU(3). For example, the decay constants f_{π^+} and f_{K^+} have the same value in either U-spin or SU(3) limit, although experimentally $f_{K^+}/f_{\pi^+} \simeq 1.22$ [12].

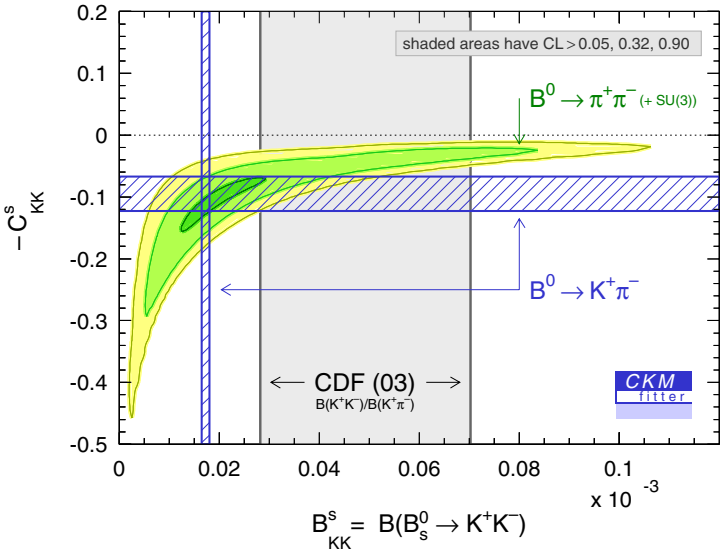

Fig. 31. Confidence level in the $(\mathcal{B}^s_{KK}, -C^s_{KK})$ plane obtained from $B \to \pi\pi$ data and the standard CKM fit, assuming SU(3) symmetry. Also shown is the preliminary result on the ratio $\mathcal{B}(B^0_s \to K^+K^-)/\mathcal{B}(B^0 \to K^+\pi^-)$ from CDF [224,231] and the branching fraction (corrected by the lifetime ratio $\tau_{B^0_s}/\tau_{B^0}$) and direct CP asymmetry in $B \to K^+\pi^-$. The bands indicate 1σ error ranges

$$P^s_{KK} = P^{+-} \ , \tag{130}$$

which leads to the relation [236,213]

$$\frac{C^s_{KK}\,\mathcal{B}^s_{KK}}{\tau_{B^0_s}} + \frac{C^{+-}_{\pi\pi}\,\mathcal{B}^{+-}_{\pi\pi}}{\tau_{B^0}} \ = \ 0 \ , \tag{131}$$

where $C^s_{KK} = C(B^0_s \to K^+K^-)$ and $\mathcal{B}^s_{KK}$ denote the direct CP-violation asymmetry and branching fraction of $B^0_s \to K^+K^-$, respectively. The ratio of the B^0_s to the B^0 lifetimes is 0.951 ± 0.038 [62]. Constraining T^{+-} and P^{+-} with the $B \to \pi\pi$ branching fractions and the $S^{+-}_{\pi\pi}$ and $C^{+-}_{\pi\pi}$ measurements, and including the standard CKM fit to predict the CKM elements, one obtains the hyperbolic shape in the $(\mathcal{B}^s_{KK}, -C^s_{KK})$ plane shown in Fig. 31. We find the CL $> 5\%$ ranges (see also [232])

$$\begin{aligned} \mathcal{B}^s_{KK} &= (5 - 91) \times 10^{-6} \ , \\ C^s_{KK} &= 0.02 - 0.32 \ . \end{aligned}$$

These predictions can be compared with the branching fraction and CP asymmetry found for $B^0 \to K^+\pi^-$ (see Table 8): assuming SU(3) and neglecting all (tree and penguin) exchange topologies they are expected to be equal. Agreement is observed as illustrated in Fig. 31. Also shown in the figure is the preliminary result from the CDF collaboration [224,231] on the ratio $\mathcal{B}(B^0_s \to K^+K^-)/\mathcal{B}(B^0 \to K^+\pi^-) = 2.71 \pm 0.73 \pm 0.35 \pm 0.08$, where the first error is statistical, the second due to the ratio of B^0 and B^0_s production in b jets, and the third is systematic. The error bands shown are at 1σ. Following the same procedure, we also predict the mixing-induced CP asymmetry in $B^0_s \to K^+K^-$ decays to be, for CL $> 5\%$,

$$S^s_{KK} \ = \ 0.12 - 0.27 \ .$$

2 Tests of QCD factorization in $B \to \pi\pi$, $K\pi$ decays

In this Section, we present several fits of the $K\pi$ and $\pi\pi$ data to the calculation of hadronic matrix elements within the QCD Factorization approach [207,208,135].

2.1 QCD factorization at leading order

All results using QCD FA presented in the previous Section were obtained with the full calculation [208] as defined in Sect. VI.1.2.4. Given the poor knowledge of the parameters X_A and X_H, one may examine whether a leading order calculation (see Sect. VI.1.2.4 for the exact definition) is sufficient to describe the data. Figure 26 shows the QCD FA predictions for r^{+-} and δ^{+-} using both approaches. The uncertainty in the full QCD FA calculation is dominated by the unknown parameters X_A and X_H. The leading order calculation predicts a small positive phase δ^{+-} and a moderate ratio r^{+-}.

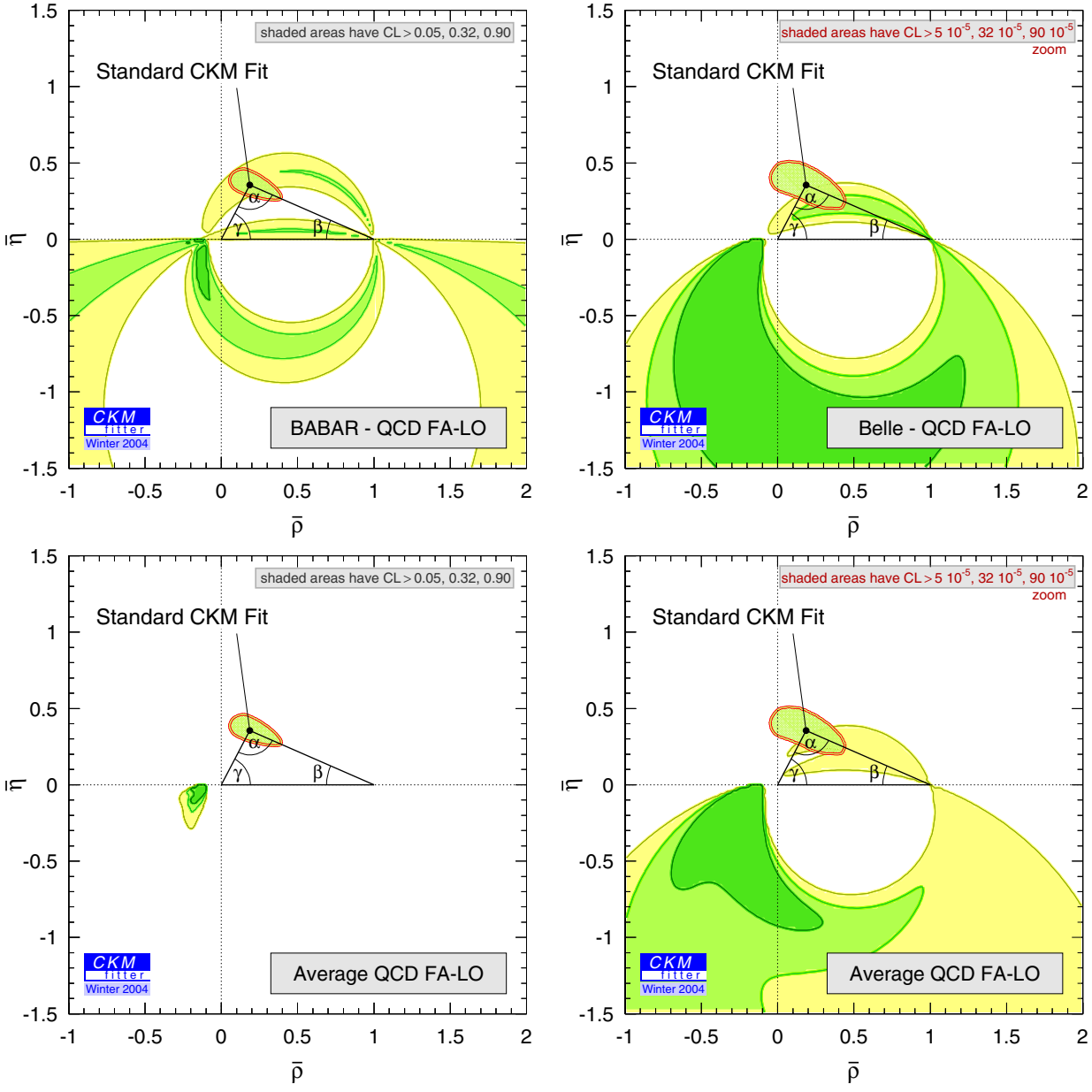

Fig. 32. Confidence levels in the $(\overline{\rho},\overline{\eta})$ plane for the QCD FA at leading order using $S^{+-}_{\pi\pi}$ and $C^{+-}_{\pi\pi}$ from *BABAR* (upper left), Belle (upper right) and their averages (bottom). *Left*: dark, medium and light shaded areas have $CL > 0.90$, 0.32 and 0.05, respectively. *Right*: the maximum CL is set to 10^{-3}: dark, medium and light shaded areas have $CL > 90\times10^{-5}$, 32×10^{-5} and 5×10^{-5}. Also shown on each plot is the result from the standard CKM fit

The constraints in the $(\overline{\rho},\overline{\eta})$ plane using the LO prediction are shown in Fig. 32 for $S^{+-}_{\pi\pi}$ and $C^{+-}_{\pi\pi}$ from *BABAR* and Belle separately as well as their averages. In all three cases, the preferred region is located in the negative $\overline{\eta}$ half-plane since δ^{+-} is predicted positive and $C^{+-}_{\pi\pi}$ is found to be negative by both experiments. Whereas the *BABAR* results are compatible with the standard CKM fit, the agreement with Belle is at the 10^{-4} level. The average of *BABAR* and Belle exhibits a compatibility with the standard CKM fit at the 5×10^{-5} level.

2.2 The full $\pi\pi$ and $K\pi$ fit

We perform a global fit of the QCD FA to all branching fractions ($\pi\pi$ and $K\pi$) and CP asymmetries given in Table 8. Since the leading order calculation cannot describe the data, we use full QCD FA here.

The upper plots of Fig. 33 show the CLs in the $(\overline{\rho},\overline{\eta})$ plane when using only the $B\to\pi\pi$ branching fractions and CP asymmetries (left), and when using only the $B\to K\pi$ data (right). The constraint from $C^{+-}_{\pi\pi}$ and $S^{+-}_{\pi\pi}$

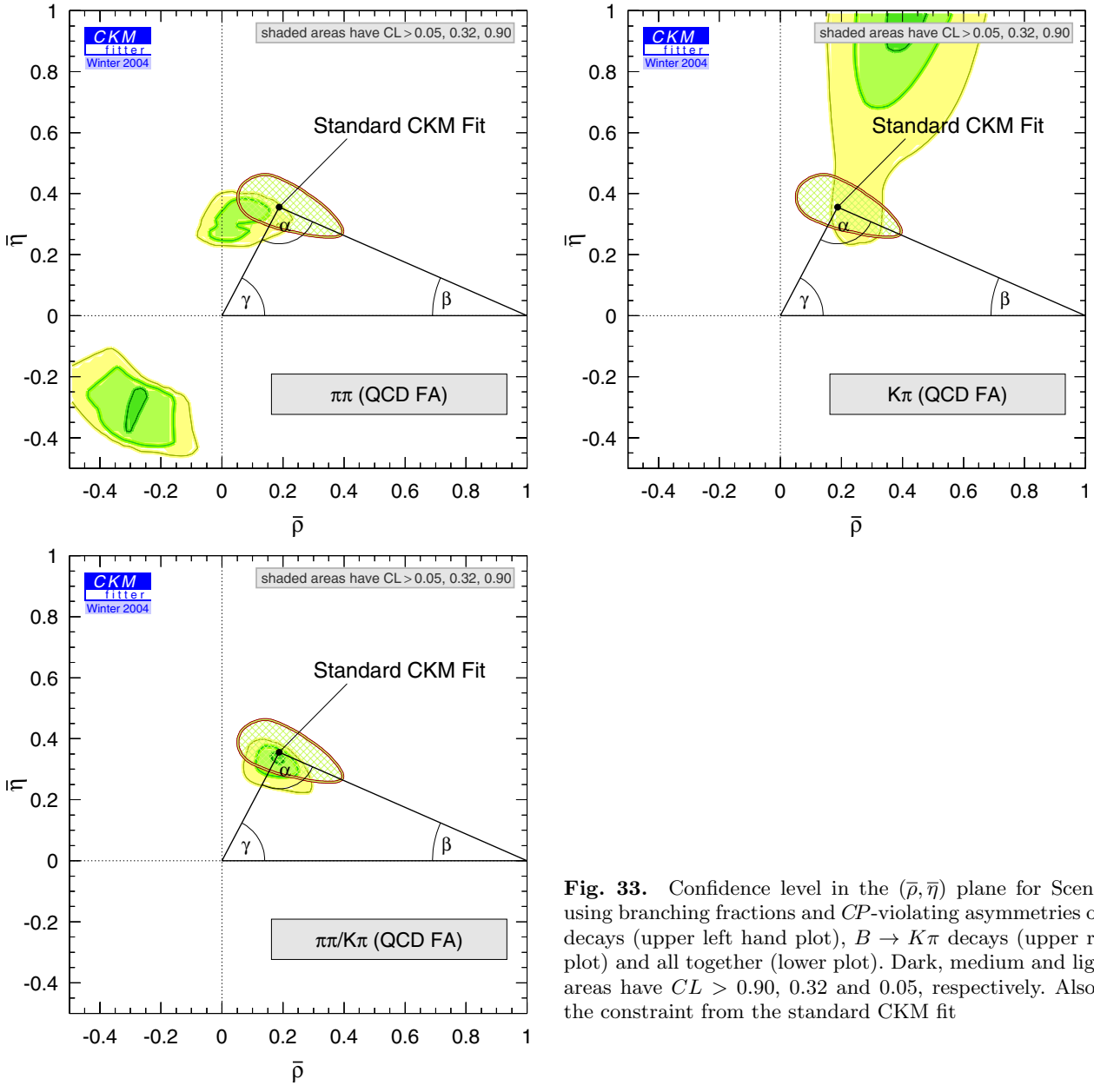

Fig. 33. Confidence level in the $(\overline{\rho},\overline{\eta})$ plane for Scenario (IV): using branching fractions and CP-violating asymmetries of $B \to \pi\pi$ decays (upper left hand plot), $B \to K\pi$ decays (upper right hand plot) and all together (lower plot). Dark, medium and light shaded areas have $CL > 0.90$, 0.32 and 0.05, respectively. Also shown is the constraint from the standard CKM fit

shown in Fig. 24 is now reduced to two distinct zones in the first and the third quadrant of the $(\overline{\rho},\overline{\eta})$ plane. The $K\pi$ measurements prefer large positive values of $\overline{\eta}$. Given the present experimental accuracy, the compatibility of the $K\pi$ data (using QCD FA) with the standard CKM fit is at the 20% level.

The combined fit to all $B \to \pi\pi$, $K\pi$ observables in the $(\overline{\rho},\overline{\eta})$ plane is shown in the lower plot of Fig. 33. The preferred area is found in excellent agreement (p-value for the $\chi^2_{\rm min}$ of 21%) with the standard CKM fit and has competitive precision. We find

$$\overline{\rho} = 0.182\,^{+0.045}_{-0.047}\,\left[^{+0.089}_{-0.092}\right] \ , \tag{133}$$

$$\overline{\eta} = 0.332\,^{+0.032}_{-0.036}\,\left[^{+0.056}_{-0.081}\right] \ , \tag{134}$$

where the errors outside (inside) brackets are at 1σ (2σ). For the UT angle γ, we find

$$\gamma = \left(62\,^{+6}_{-9}\,\left[^{+12}_{-18}\right]\right)^\circ \ . \tag{135}$$

Since to leading order in the Cabibbo angle λ the $K\pi$ system is independent of the CKM phase, the constraint on $(\overline{\rho},\overline{\eta})$ from the combined $\pi\pi$, $K\pi$ fit is dominated by the $\pi^+\pi^-$ observables. The $\chi^2_{\rm min}$ amounts to 13.4 and is dominated

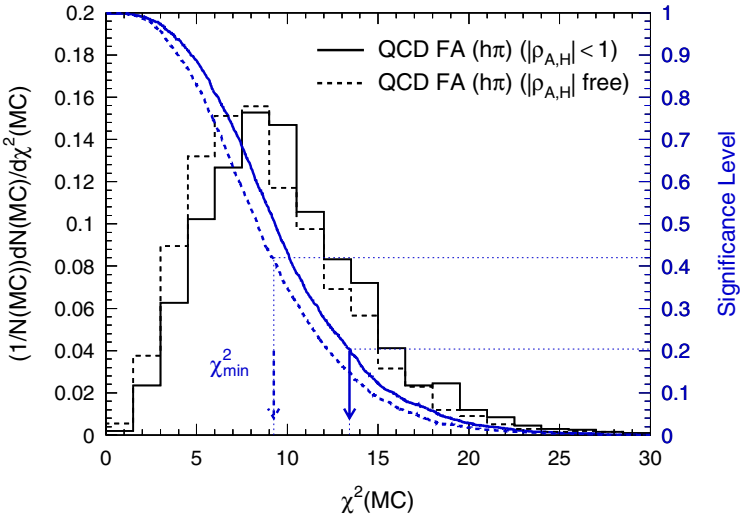

Fig. 34. Distributions of $\chi^2_{\rm min}$ from toy Monte Carlo experiments and corresponding significance level curves for full QCD FA fits to combined $B \to \pi\pi$ and $B \to K\pi$ results (solid line). *BABAR* and Belle averages are used for $S^{+-}_{\pi\pi}$ and $C^{+-}_{\pi\pi}$. The dashed lines give the results for unbound parameters ρ_A and ρ_H (see text for details)

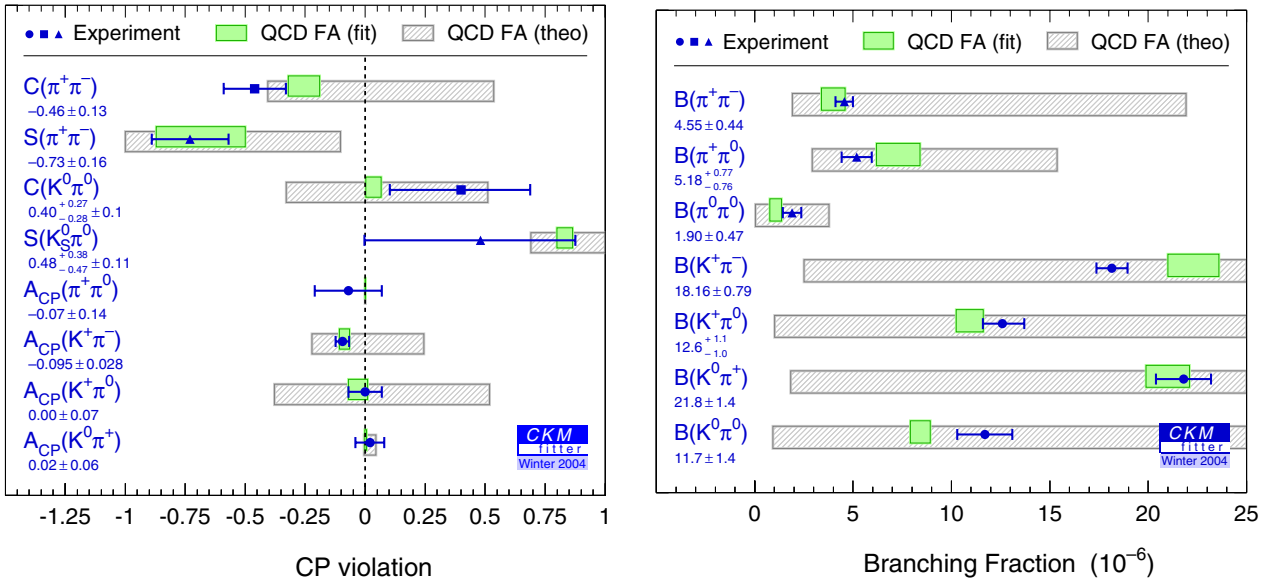

Fig. 35. Comparison of the results from the global QCD FA fit to $B \to \pi\pi$, $K\pi$ data (shaded boxes) and the unconstrained QCD FA predictions with experiment for the CP-violating asymmetries (left) and the branching fractions (right) in $B \to hh'$ $(h, h' = \pi, K)$ decays. The predictions are obtained ignoring the measurement associated with the observable in the fit. The experimental results are the world averages quoted in Table 8 and the theory values are those from Table 9. All theory predictions use the standard CKM fit result as input. The error ranges shown correspond to 1σ

by contribution from the $K\pi$ data. The corresponding $\chi^2_{\rm min}$ distribution is given in Fig. 34 (solid line histogram). The dashed histogram is obtained with unbound parameters $\rho_{H,A}$ (we recall that in full QCD FA they are constrained within $[0, 1]$). The χ^2 probability (p-value) rises to 42% at $\rho_A = 1.4$ and $\rho_H = 9.2$, where such large values cannot be considered as corrections anymore. In other words, two additional free parameters parametrizing power corrections suffice to reconcile the QCD factorization approach with the data. The measured branching fractions for $B^0 \to K^+\pi^-$ and $B^0 \to K^0\pi^0$ are in marginal agreement with QCD FA (cf. Table 9). Removing each of these branching fractions from the nominal ($\rho_{H,A} < 1$) combined $\pi\pi$, $K\pi$ fit decreases the $\chi^2_{\rm min}$ from 13.4 to 7.3 and from 13.4 to 8.5, respectively.

2.3 Data driven predictions for the $\pi\pi$ and $K\pi$ system

In the spirit of likelihood projections, we study the predictions of the combined $\pi\pi$, $K\pi$ QCD FA fit on each observable, ignoring the measurement associated with the observable in the fit. The results are hence unbiased by the actual measurement. In addition to the charmless data we include the standard CKM fit here. The predictions obtained are summarized in Table 9 and plotted in comparison with the experimental values in Fig. 35. Also given are the results

Table 9. QCD FA fit results and predictions of $\pi\pi$ and $K\pi$ branching fractions and CP-violating asymmetries. Left hand part: for each quantity, a full QCD FA fit is performed to all $\pi\pi$ and $K\pi$ data but the one that is predicted. Central values and $CL = 0.32$ and $CL = 0.05$ uncertainties are quoted in the two first columns; the third column gives the contribution of the quantity (when included in the fit) to the overall χ^2. Right hand part: raw predictions from QCD FA without constraints from data. In both configurations, the CKM parameters obtained from the standard CKM fit are also included. Branching fractions are given in units of 10^{-6}

	Fit result			Full prediction
Quantity	Central value $\pm$CL $= 0.32$	$\pm$CL $= 0.05$	$\Delta\chi^2_{\min}$	CL $> 5\%$ range
$C^{+-}_{\pi\pi}$	$-0.27\,^{+0.08}_{-0.05}$	$^{+0.18}_{-0.09}$	1.0	-0.45–0.59
$S^{+-}_{\pi\pi}$	$-0.70\,^{+0.20}_{-0.17}$	$^{+0.38}_{-0.25}$	0.0	-1.00–0.11
$C^{00}_{K_S\pi}$	$0.039\,^{+0.028}_{-0.036}$	$^{+0.045}_{-0.085}$	1.4	-0.36–0.56
$S^{00}_{K_S\pi}$	$0.827\,^{+0.037}_{-0.028}$	$^{+0.071}_{-0.056}$	0.7	0.63–1.00
$A_{CP}(\pi^+\pi^0)$ $[10^{-4}]$	$-5.2\,^{+1.6}_{-0.4}$	$^{+3.6}_{-0.9}$	0.2	-6–15
$A_{CP}(K^+\pi^-)$	$-0.100\,^{+0.035}_{-0.007}$	$^{+0.063}_{-0.013}$	0.0	-0.23–0.26
$A_{CP}(K^+\pi^0)$	$-0.035\,^{+0.042}_{-0.038}$	$^{+0.072}_{-0.131}$	0.2	-0.40–0.55
$A_{CP}(K^0\pi^+)$	$0.0018\,^{+0.0036}_{-0.0041}$	$^{+0.0059}_{-0.0044}$	0.1	-0.005–0.048
$\mathcal{B}(B^0 \to \pi^+\pi^-)$	$3.80\,^{+0.79}_{-0.40}$	$^{+1.92}_{-0.90}$	0.7	1.7–24.8
$\mathcal{B}(B^+ \to \pi^+\pi^0)$	$7.4\,^{+0.9}_{-1.2}$	$^{+2.0}_{-2.2}$	2.5	2.6–17.0
$\mathcal{B}(B^0 \to \pi^0\pi^0)$	$1.05\,^{+0.31}_{-0.29}$	$^{+0.68}_{-0.50}$	2.3	0.2–4.4
$\mathcal{B}(B^0 \to K^+\pi^-)$	$22.4\,^{+1.2}_{-1.4}$	$^{+2.3}_{-3.0}$	6.1	2.1–74.3
$\mathcal{B}(B^+ \to K^+\pi^0)$	$10.87\,^{+0.74}_{-0.62}$	$^{+1.69}_{-1.22}$	2.0	0.6–45.5
$\mathcal{B}(B^+ \to K^0\pi^+)$	$21.1\,^{+1.0}_{-1.2}$	$^{+1.9}_{-3.2}$	0.1	1.5–86.0
$\mathcal{B}(B^0 \to K^0\pi^0)$	$8.36\,^{+0.56}_{-0.44}$	$^{+1.36}_{-0.86}$	4.9	0.7–37.0

obtained from QCD FA and the standard CKM fit alone, for which in most cases the uncertainty largely exceeds the experimental precision[45]. Instead when the fit is constrained by the experimental data, the combined constraints determine rather precisely the parameters that are only loosely bounded by the theory. The

predictions of the full QCD FA fit are accurate and found to be in good agreement with the measurements, with the exception of the above mentioned $\mathcal{B}(B^0 \to K^+\pi^-)$ and $\mathcal{B}(B^0 \to K^0\pi^0)$, for which however the discrepancy does not exceed 2.5σ at present. Due to the common uncertainties on the theoretical parameters, the results for the branching fractions exhibit significant correlations, which have to be taken into account when interpreting the results. For completeness, we give the linear correlation coefficients evaluated with toy Monte Carlo simulation[46] in Table 10. As an example, the CLs of $\mathcal{B}(B^0 \to K^+\pi^-)$ versus $\mathcal{B}(B^0 \to K^0\pi^0)$ are plotted in Fig. 36 (the correlation coefficient is $+0.57$) and compared with the measurements. A potential increase in the experimental value for $\mathcal{B}(B^0 \to K^+\pi^-)$ (due to radiative corrections that were previously neglected, see the remark in the introduction to Part VI) could help to reconcile theory and experiment. One observes a significant positive correlation between the direct CP-violation parameters in $\pi^+\pi^-$ and $K^+\pi^-$ decays, which is expected from SU(3) symmetry. We note in addition that

[45] The predictions of [135] from the same inputs appear to be much more precise, due to the treatment of the uncertainties on the theoretical parameters, which the authors vary independently and finally add in quadrature. On the contrary, our approach *R*fit amounts to scan democratically the whole parameter space. While the (commonly found) approach of [135] likely underestimates the overall uncertainty, *R*fit may overestimate it, by ignoring possible fine-tuning configurations where many theoretical parameters take extreme values in the allowed ranges.

[46] The procedure is as follows: for each toy experiment, the experimental observables are fluctuated within their Gaussian experimental errors; the full QCD FA fit is performed, and the variance between the fit results for the observables is computed. The coefficients quoted in Table 10 correspond to 500 toy experiments.

Table 10. Linear correlation coefficients for the QCD FA fit results given in Table 9. The $\mathcal{A}^{ij}_{pq}$ stand for the direct CP-asymmetry parameters $A_{CP}(p^i q^j)$, and the $\mathcal{B}^{ij}_{pq}$ denote the corresponding branching fractions. Note that these correlations are not of experimental origin, but due to the uncertainties in the theoretical parameters

	$C^{+-}_{\pi\pi}$	$\mathcal{A}^{+0}_{\pi\pi}$	$\mathcal{A}^{+-}_{K\pi}$	$\mathcal{A}^{0+}_{K\pi}$	$\mathcal{A}^{+0}_{K\pi}$	$C^{00}_{K_S\pi}$	$S^{00}_{K_S\pi}$	$\mathcal{B}^{+-}_{\pi\pi}$	$\mathcal{B}^{+0}_{\pi\pi}$	$\mathcal{B}^{00}_{\pi\pi}$	$\mathcal{B}^{+-}_{K\pi}$	$\mathcal{B}^{0+}_{K\pi}$	$\mathcal{B}^{+0}_{K\pi}$	$\mathcal{B}^{00}_{K\pi}$
$S^{+-}_{\pi\pi}$	−0.44	−0.45	−0.39	+0.10	−0.07	−0.15	+0.39	+0.04	−0.06	+0.08	+0.07	−0.28	+0.34	−0.43
$C^{+-}_{\pi\pi}$	+1.00	+0.47	+0.79	−0.49	+0.55	−0.35	−0.21	+0.48	+0.01	−0.29	−0.22	+0.22	−0.09	+0.05
$\mathcal{A}^{+0}_{\pi\pi}$	-	+1.00	+0.23	+0.02	−0.24	+0.43	+0.13	+0.20	+0.36	+0.11	−0.10	+0.08	−0.28	+0.26
$\mathcal{A}^{+-}_{K\pi}$	-	-	+1.00	−0.66	+0.72	−0.47	−0.21	−0.02	+0.01	+0.02	−0.00	+0.19	+0.05	+0.05
$\mathcal{A}^{0+}_{K\pi}$	-	-	-	+1.00	−0.74	+0.71	+0.13	−0.04	−0.07	−0.03	+0.16	−0.10	−0.08	+0.13
$\mathcal{A}^{+0}_{K\pi}$	-	-	-	-	+1.00	−0.93	−0.14	+0.03	+0.05	+0.04	−0.12	+0.13	+0.31	−0.29
$C^{00}_{K_S\pi}$	-	-	-	-	-	+1.00	−0.11	+0.07	+0.02	+0.00	−0.15	+0.10	+0.35	−0.37
$S^{00}_{K_S\pi}$	-	-	-	-	-	-	+1.00	+0.13	+0.75	+0.66	+0.09	−0.24	−0.09	+0.06
$\mathcal{B}^{+-}_{\pi\pi}$	-	-	-	-	-	-	-	+1.00	−0.01	−0.51	−0.00	+0.26	+0.05	+0.09
$\mathcal{B}^{+0}_{\pi\pi}$	-	-	-	-	-	-	-	-	+1.00	+0.83	+0.04	+0.03	−0.21	+0.29
$\mathcal{B}^{00}_{\pi\pi}$	-	-	-	-	-	-	-	-	-	+1.00	+0.14	−0.12	−0.10	+0.17
$\mathcal{B}^{+-}_{K\pi}$	-	-	-	-	-	-	-	-	-	-	+1.00	+0.74	+0.57	+0.57
$\mathcal{B}^{0+}_{K\pi}$	-	-	-	-	-	-	-	-	-	-	-	+1.00	+0.46	+0.63
$\mathcal{B}^{+0}_{K\pi}$	-	-	-	-	-	-	-	-	-	-	-	-	+1.00	−0.27

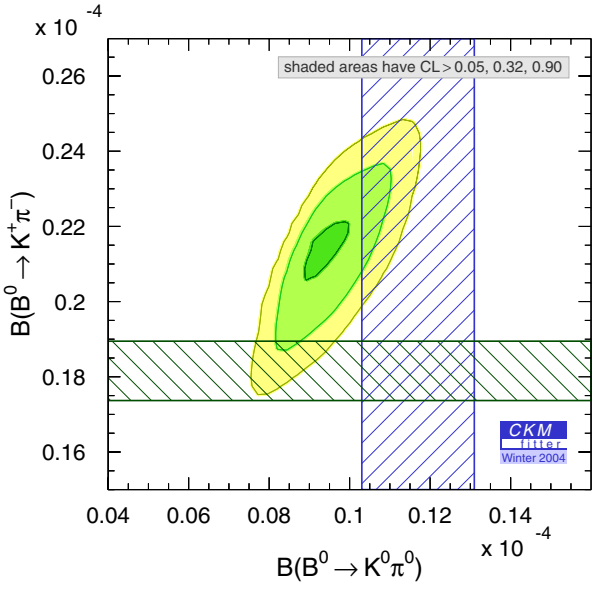

Fig. 36. Confidence level in the $(\mathcal{B}(K^0\pi^0), \mathcal{B}(K^+\pi^-))$ plane obtained from the global QCD FA fit to $B \to \pi\pi$, $K\pi$ data ignoring the measurements associated with the observables shown. Dark, medium and light shaded areas have $CL > 0.90$, 0.32 and 0.05, respectively. The hatched areas indicate the 1σ error bands of the experimental results

– the prediction for the not yet measured direct asymmetry in the $B^0 \to \pi^0\pi^0$ decay is

$$C^{00}_{\pi\pi} = 0.06\,^{+0.10}_{-0.12}\,\left[^{+0.37}_{-0.24}\right] \ , \tag{136}$$

where the errors outside (inside) brackets are at 1σ (2σ);
– a large negative value for $S^{+-}_{\pi\pi}$ is predicted, in contrast to the small value $\sin 2\alpha$ (see Table 2) that would be obtained from the standard CKM fit in the no-penguin case;
– the deviation between $\sin 2\beta_{\rm eff} \equiv S^{00}_{K_S\pi}$ measured in $B^0 \to K^0_S\pi^0$ and the charmonium reference is $\sin 2\beta_{\rm eff} - \sin 2\beta = 0.09 \pm 0.04$;
– the experimental evidence for negative direct CP violation in $K^+\pi^-$ is consistent with the (precise) expectation;
– the qualitative picture (hierarchy) of the branching fractions is understood in the SM.

Despite this success and given that both experimental and theoretical uncertainties are still large, particular care is mandatory when analyzing possible anomalies in $B \to K\pi$ decays. In Sect. VI.3 we revisit the $K\pi$ system with the use of a more phenomenological approach.

3 Phenomenological analysis of $B \to K\pi$ decays

The decays $B \to K\pi$ have received considerable attention in the recent literature [238,239,232,240] since a fit to the data leads to an apparent violation of the approximate sum rule derived in [237]. Although the errors remain large, it has been argued by the authors of [239,232,240] that a better phenomenological description could be achieved by including non-standard contributions in electroweak penguins, that is, $\Delta I = 1$ $b \to s$ transitions.

In this section we discuss the implications of the experimental results on strong isospin symmetry in $B \to K\pi$ decays, by performing fits to the data under various dynamical hypotheses. We interpret the numerical results by comparing them to those of the $\pi\pi$ modes, and give our understanding of the present situation.

3.1 Experimental input

We use the branching fractions and charge asymmetries for the $B \to K\pi$ modes given in Table 8 as inputs to our fits. The CP-averaged branching fractions are defined by

$$\mathcal{B}^{ij} \propto \frac{\tau_{B^{i+j}}}{2}\left(|A^{ij}|^2 + |\overline{A}^{ij}|^2\right) \ , \tag{137}$$

and the four CP-violating asymmetries by

$$\mathcal{A}^{ij} = \frac{|\overline{A}^{ij}|^2 - |A^{ij}|^2}{|\overline{A}^{ij}|^2 + |A^{ij}|^2} \ , \tag{138}$$

where $(i,j) = (+,-)\ ,(0,+)\ ,(+,0)\ ,(0,0)$ and $i+j$ is the charge of the B meson. Note that $\mathcal{A}^{0+}$ is zero by definition in some of the approximations considered below. The CP asymmetries $C^{00}_{K_S\pi} = -\mathcal{A}^{00}$ and $S^{00}_{K_S\pi}$ are defined by

$$C^{00}_{K_S\pi} = \frac{1 - |\lambda_{K^0_S\pi^0}|^2}{1 + |\lambda_{K^0_S\pi^0}|^2} \ , \tag{139}$$

$$S^{00}_{K_S\pi} = \frac{2\mathrm{Im}\lambda_{K^0_S\pi^0}}{1 + |\lambda_{K^0_S\pi^0}|^2} \ , \tag{140}$$

where $\lambda_{K^0_S\pi^0} = -\exp\left\{i\arg[(V_{td}V^*_{tb})^2]\right\}\overline{A}^{00}/A^{00}$ in our phase convention.

3.2 Transition amplitudes

Using the unitarity relation (5) and adopting convention $\mathfrak{C}$ (cf. Sect. VI.1.1.1), each $B \to K^i\pi^j$ decay amplitude can be parameterized by $V_{us}V^*_{ub}$, $V_{ts}V^*_{tb}$ and two complex quantities denoted T^{ij} and P^{ij}. For example, for $B^0 \to K^+\pi^-$ one has

$$A^{+-} \equiv A(B^0 \to K^+\pi^-) = V_{us}V^*_{ub}T^{+-} + V_{ts}V^*_{tb}P^{+-} \ , \tag{141}$$

and similarly for the other modes. The amplitudes T^{ij} and P^{ij} implicitly include strong phases while the weak phases are explicitly contained in the CKM factors. An important difference with respect to the $\pi\pi$ modes is that the CKM ratio $|V_{ts}V^*_{tb}/(V_{us}V^*_{ub})| \sim 50$ enhances considerably the contribution of loops with respect to tree topologies: this implies a potentially better sensitivity to unknown virtual particles, and thus to New Physics, but at the same time this involves more complicated hadronic dynamics.

Without loss of generality, the complete $B \to K\pi$ system can be parameterized by eight amplitudes and the CKM couplings $V_{us}V^*_{ub}$ and $V_{ts}V^*_{tb}$. In the following, we will assume isospin symmetry, so that there is a quadrilateral relation between these amplitudes.

3.3 Isospin relations and dynamical scenarios

Using strong isospin invariance, the $B \to K\pi$ amplitudes satisfy the relations [241]

$$A^{0+} + \sqrt{2}A^{+0} = \sqrt{2}A^{00} + A^{+-} \ , \tag{142}$$

$$\overline{A}^{0+} + \sqrt{2}\overline{A}^{+0} = \sqrt{2}\overline{A}^{00} + \overline{A}^{+-} \ . \tag{143}$$

Note that for the CP-conjugate amplitudes one reads for instance $\overline{A}^{0+} \equiv A(B^- \to \overline{K}^0\pi^-)$ and accordingly for the other charges.

3.3.1 Neglecting electroweak penguin but not annihilation diagrams

In the absence of electroweak penguin diagrams the isospin analysis leads to two additional constraints since the two quadrilaterals share the $I = 3/2$ amplitude as common diagonal, with a length determined from the branching fractions, while the second diagonals bisect each other [241]:

$$A^{+-} + \sqrt{2}A^{00} = \tilde{A}^{+-} + \sqrt{2}\tilde{A}^{00} \ , \tag{144}$$

$$\sqrt{2}A^{00} + \sqrt{2}A^{+0} = \sqrt{2}\tilde{A}^{00} + \sqrt{2}\tilde{A}^{+0} \ , \tag{145}$$

where $\tilde{A} = \exp\left[2i\arg(V_{us}V_{ub}^*)\right]\,\bar{A}$. The argument goes as follows: since gluonic penguins are $\Delta I = 0$ transitions, in the absence of electroweak penguins the amplitude $A_{\Delta I=1,I_f=3/2}$ of the transition from $I_i = 1/2$ to $I_f = 3/2$ is proportional to $V_{us}V_{ub}^*$ and hence

$$A_{1,3/2} \ = \ \tilde{A}_{1,3/2} \ . \tag{146}$$

Note that (144) and (145) separately hold for the T^{ij} and P^{ij}. Under these assumptions it is possible to describe the full $B \to K\pi$ system with four out of the seven complex quantities T^{ij} and P^{ij}. In the following parameterization, we use P^{+-} and the three tree amplitudes T^{+-}, $N^{0+} = T^{0+}$ and $T_{\rm C}^{00} = T^{00}$. The notation N^{0+} refers to the fact that the tree contribution to the $K^0\pi^+$ mode has an annihilation topology (it also receives contributions from long-distance u and c penguins). Since $B^0 \to K^0\pi^0$ is color-suppressed, its tree amplitude is denoted $T_{\rm C}^{00}$.

$$\begin{aligned}
A^{+-} &= V_{us}V_{ub}^*\,T^{+-} + V_{ts}V_{tb}^*\,P^{+-} \ , \\
A^{0+} &= V_{us}V_{ub}^*\,N^{0+} - V_{ts}V_{tb}^*\,P^{+-} \ , \\
\sqrt{2}A^{+0} &= V_{us}V_{ub}^*\,(T^{+-} + T_{\rm C}^{00} - N^{0+}) + V_{ts}V_{tb}^*\,P^{+-} \ , \\
\sqrt{2}A^{00} &= V_{us}V_{ub}^*\,T_{\rm C}^{00} - V_{ts}V_{tb}^*\,P^{+-} \ .
\end{aligned} \tag{147}$$

In the absence of electroweak penguins, it is possible to invert the expressions for the amplitudes and to extract the eight unknown quantities: $|V_{us}V_{ub}^*\,T^{+-}|$, $|V_{us}V_{ub}^*\,N^{0+}|$, $|V_{us}V_{ub}^*\,T_{\rm C}^{00}|$, $|V_{ts}V_{tb}^*\,P^{+-}|$, three relative strong phases and the weak phase α from the experimental observables[47] (the so-called Nir–Quinn method [241]). However, as was stressed in [242], the discrete ambiguity problem is even more delicate than in the $\pi\pi$ case, because the relative angles between the amplitudes are not well constrained by the quadrilateral construction.

The constraint obtained on the angle α is shown in Fig. 37. Although it peaks near the value from the standard CKM fit, the constraint is weak. Very large statistics would be required for a meaningful determination of α by this method. More interesting, perhaps, is the constraint on the annihilation-to-emission ratio, represented by the quantity $|N^{0+}/T^{+-}|$ given on the right hand plot of Fig. 37: although this ratio is expected to be suppressed from the point of view of QCD factorization (see the next Section), large values (of order one) cannot be excluded. Note that large contributions from annihilation topologies, if extrapolated to $B^+ \to K^+\overline{K}^0$ in the SU(3) limit, would eventually enter in conflict with the experimental bounds [135].

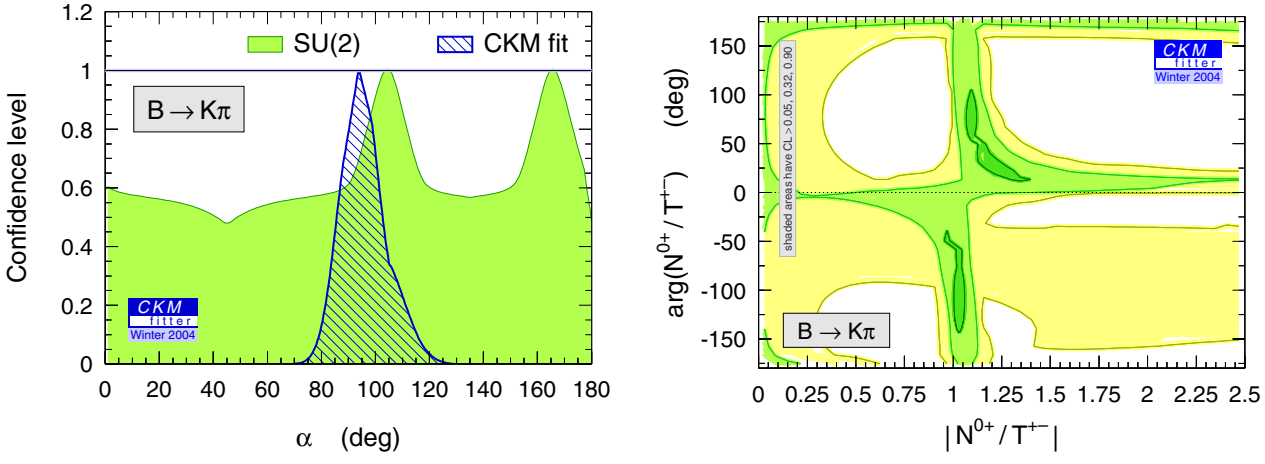

Fig. 37. *Left*: confidence level as a function of the CKM angle α, in the Nir–Quinn approximation (no electroweak penguins). The hatched region represents the constraint from the standard CKM fit. *Right*: constraint on the annihilation-to-tree amplitude ratio $|N^{0+}/T^{+-}|$, as defined in (147). Electroweak penguins are neglected

[47] The dependence with respect to α comes from the interference between $V_{us}V_{ub}^*$ in the $\Delta I = 1$ amplitude with $V_{td}V_{tb}^*$ in the $B^0\overline{B}^0$ mixing.

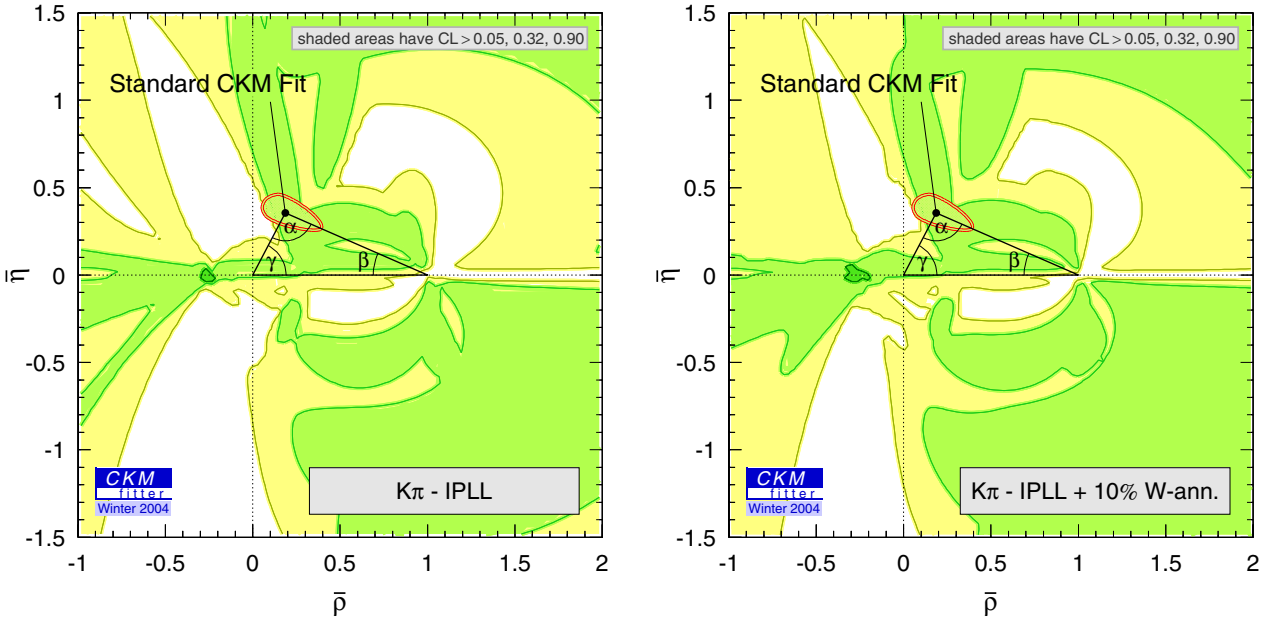

Fig. 38. Confidence level in the $(\overline{\rho},\overline{\eta})$ plane for the isospin analysis of $B \to K\pi$ decays within the framework of [243] (see text). In the left hand plot N^{0+} is set to zero, while in the right hand plot it is allowed to vary freely within 10% of the T^{+-} dominant amplitude. Dark, medium and light shaded areas have $CL > 0.90$, 0.32 and 0.05, respectively. Also shown on each plot is the prediction from the standard CKM fit

3.3.2 Standard Model electroweak penguins and vanishing annihilation topologies

Since the pioneering work of Nir and Quinn it has been realized that gluonic penguins are likely to dominate in $B \to K\pi$, and that CKM-enhanced electroweak penguins would even compete with CKM-suppressed T-type amplitudes [244]. Thus one can add two $\Delta I = 1$ amplitudes $P^{\rm EW}$ and $P_{\rm C}^{\rm EW}$ that come with the CKM factor[48] $V_{ts}V_{tb}^*$:

$$\begin{aligned} A^{+-} &= V_{us}V_{ub}^*\, T^{+-} + V_{ts}V_{tb}^*\, P^{+-} \ , \\ A^{0+} &= V_{us}V_{ub}^*\, N^{0+} + V_{ts}V_{tb}^*\, (-P^{+-} + P_{\rm C}^{\rm EW}) \ , \\ \sqrt{2}A^{+0} &= V_{us}V_{ub}^*\, (T^{+-} + T_{\rm C}^{00} - N^{0+}) + V_{ts}V_{tb}^*\, (P^{+-} + P^{\rm EW} - P_{\rm C}^{\rm EW}) \ , \\ \sqrt{2}A^{00} &= V_{us}V_{ub}^*\, T_{\rm C}^{00} + V_{ts}V_{tb}^*\, (-P^{+-} + P^{\rm EW}) \ , \end{aligned} \tag{148}$$

where $P_{\rm C}^{\rm EW}$ is expected to be color-suppressed with respect to $P^{\rm EW}$.

The general parameterization (148) involves 11 hadronic parameters and the CKM couplings, which cannot be extracted from the nine independent $K\pi$ observables. In the SU(3) symmetry limit, the $P^{\rm EW}$ amplitude can be expressed model-independently in terms of the sum $T^{+-} + T_{\rm C}^{00}$, just the same way as for $\pi\pi$ [211]: this removes two hadronic parameters, which is however not yet enough to close the system. Hence *without an additional dynamical assumption one cannot extract a correlation in the* $(\overline{\rho},\overline{\eta})$ *plane from the* $K\pi$ *observables alone.*

Faced with this problem the authors of [243] proposed to neglect all exchange and annihilation topologies and showed that in principle the apex of the Unitarity Triangle can be determined, up to discrete ambiguities (see also [245] for a short review of other approaches analyzing the $K\pi$ system). The additional hypotheses are

– negligible annihilation and long-distance penguin contributions to $B^+ \to \overline{K}^0\pi^+$:

$$N^{0+} = 0 \ . \tag{149}$$

– SU(3) limit for the color-allowed electroweak penguin amplitude:

$$P^{\rm EW} = R^+ \left(T^{+-} + T_{\rm C}^{00}\right) \ . \tag{150}$$

– SU(3) limit and negligible exchange contributions for the color-suppressed electroweak penguin amplitude:

$$P_{\rm C}^{\rm EW} = \frac{R^+}{2}\left(T^{+-} + T_{\rm C}^{00}\right) - \frac{R^-}{2}\left(T^{+-} - T_{\rm C}^{00}\right) \ . \tag{151}$$

[48] The $\Delta I = 0$ contribution from electroweak penguins can be absorbed in the P^{+-} amplitude.

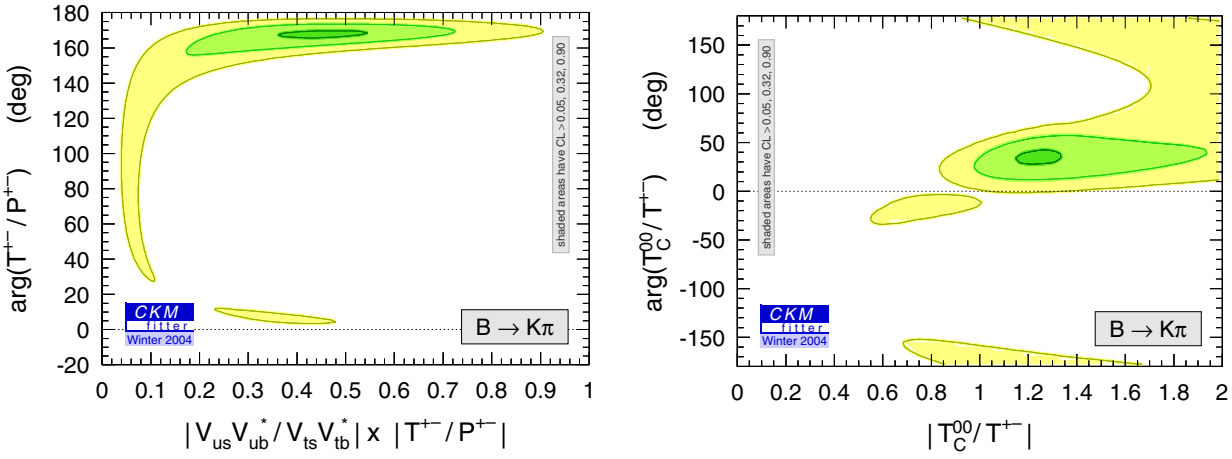

Fig. 39. Constraints on the complex tree-to-penguin amplitude ratio in $B^0 \to K^+\pi^-$ decays (left), and the complex color-suppressed-to-color-allowed amplitude ratio (right), obtained when using as additional input the CKM parameters $\overline{\rho}$ and $\overline{\eta}$ from the standard CKM fit. The gradually shaded regions give the CLs within the framework of [243]: dark, medium and light shaded areas have $CL > 0.90$, 0.32 and 0.05, respectively

In the above equations R^+ and R^- are constants given by[49]

$$R^+ = -\frac{3}{2}\frac{c_9 + c_{10}}{c_1 + c_2} = +(1.35 \pm 0.12)\ 10^{-2}\ ,$$
$$R^- = -\frac{3}{2}\frac{c_9 - c_{10}}{c_1 - c_2} = +(1.35 \pm 0.13)\ 10^{-2}\ . \qquad (152)$$

The phenomenological fit is thus expressed in terms of T^{+-}, P^{+-}, T_C^{00} and $(\overline{\rho}, \overline{\eta})$, that is five hadronic parameters and two CKM parameters. Figure 38 (left) shows the constraints on the unitarity plane obtained within this approach. The intricate shape of the CLs is mainly due to the convolution of the Nir–Quinn constraints on the CKM angle α and the explicit CKM dependence of the electroweak penguins in (150)–(151).

Using the same framework and the standard CKM fit as an additional input, we have performed a constrained fit of the tree-to-penguin and color-suppressed-to-leading-tree amplitude ratios (Fig. 39 left and right, respectively). Because of the 3.3σ evidence of negative direct CP asymmetry in $B^0 \to K^+\pi^-$, the relative tree-to-penguin phase (left hand plot) is positive. It is surprising that the measurements seem to indicate that the expected double CKM suppression of the tree-to-penguin ratio is well compensated by a large ratio of the hadronic matrix elements (Fig. 39, left), which tends to contradict the trend observed in the $\pi\pi$ system. We further discuss this point in Sect. VI.6. Another striking feature of the fit results, which has been already observed in $\pi^0\pi^0$ versus $\pi^+\pi^-$, is the value of the color-suppressed amplitude as compared to the leading-tree one (Fig. 39, right): order one is preferred, and a zero value for this amplitude is excluded.

3.3.3 Including a correction to the no-rescattering assumption

To correct the assumption of a negligible $V_{us}V_{ub^*}$ term in $B^+ \to K^0\pi^+$, we attempt to include an estimate for it into the amplitude parameterization. Model-dependent contributions to this term have been evaluated in the QCD FA formalism [208,135] and are found to be around 10% in magnitude with respect to the leading T^{+-} amplitude. Since this estimate is fairly uncertain[50], we assign a 100% theoretical error to $|N^{0+}|$ and let its phase δ^{0+} vary in the fit:

$$N^{0+} = (0.1 \pm 0.1)\ |T^{+-}|\ e^{i\delta^{0+}}\ . \qquad (153)$$

The transition amplitudes then read as in (148). Note that in this model, the expressions for the electroweak penguin remain unchanged with respect to (150), (151). While this is true for $P^{\rm EW}$ (up to a small correction coming from $Q_{7,8}$ operators), it is incorrect for $P_C^{\rm EW}$, which receives a contribution from exchange topologies that cannot be expressed in terms of the $K\pi$ amplitudes alone [246]. We assume that the effect of this approximation is negligible.

[49] The numerics for R^+ and R^- has been worked out as in the $\pi\pi$ case (121), while the correlation between them is neglected. Equation (151) has been first derived in [246].

[50] Annihilation topologies are expected to be suppressed by $\Lambda_{\rm QCD}/m_b$. The authors of [208] estimate them from a hard-scattering point of view, which results in a stronger, model-dependent suppression proportional to $\alpha_S\Lambda_{\rm QCD}/m_b$.

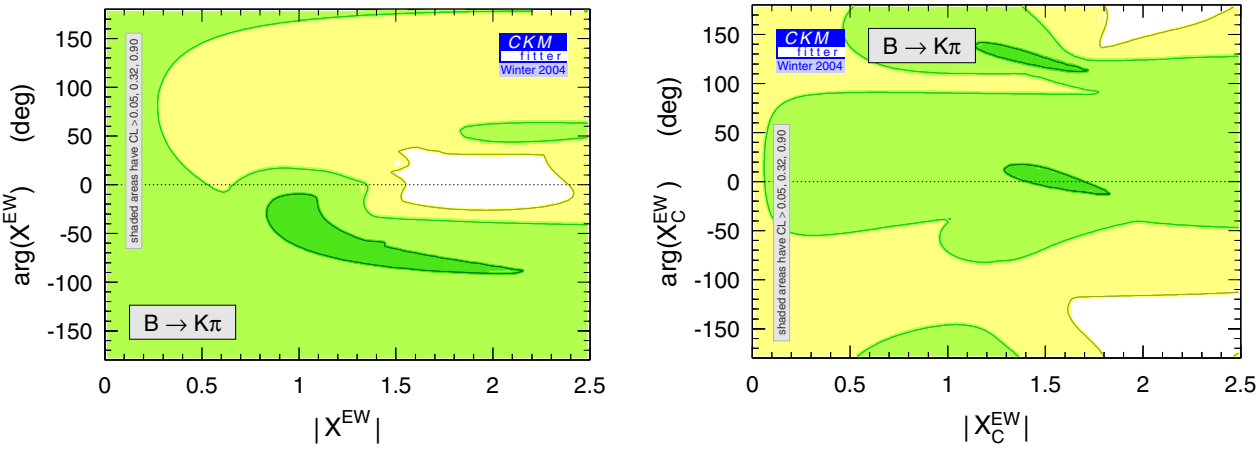

Fig. 40. Constraints on the complex quantities $X^{\rm EW}$ (left, where $X_{\rm C}^{\rm EW}$ is fixed to 1) and $X_{\rm C}^{\rm EW}$ (right, where $X^{\rm EW}$ is fixed to 1) defined in (154) and (155), respectively. Dark, medium and light shaded areas have $CL > 0.90$, 0.32 and 0.05, respectively. The standard CKM fit is used as input to obtain these plots

The constraints obtained in the unitarity plane are shown on the right hand plot of Fig. 38. The relaxed framework does not lead to major differences with respect to the $N^{0+} = 0$ hypothesis (left hand plot of Fig. 38). We stress that no significant constraint is obtained on the phase δ^{0+}, and that the fit converges systematically towards the maximal allowed value for $\left|N^{0+}\right|$ in (153). With much improved experimental accuracy, the $N^{0+} = 0$ assumption will become crucial to obtain meaningful constraints on $\overline{\rho}$ and $\overline{\eta}$.

3.3.4 Constraining the electroweak penguins

To investigate whether the data together with the standard CKM fit can reveal indirect evidence of electroweak penguin contributions, we correct (150), (151) by introducing two new complex parameters $X^{\rm EW}$ and $X_{\rm C}^{\rm EW}$

$$P^{\rm EW} = X^{\rm EW}\left[R\left(T^{+-} + T_{\rm C}^{00}\right)\right] \ , \tag{154}$$

$$P_{\rm C}^{\rm EW} = X_{\rm C}^{\rm EW}\left[RT_{\rm C}^{00}\right] \ , \tag{155}$$

where we have imposed $R^+ = R^- \equiv R$. Within the SM and under the assumptions already explicitly stated, we expect $X^{\rm EW} \approx X_{\rm C}^{\rm EW} \approx 1$. We introduce two new fit scenarios: a first where $X^{\rm EW} \equiv 1$ and $X_{\rm C}^{\rm EW}$ is free to vary in the fit (magnitude *and* phase), and a second where conversely $X_{\rm C}^{\rm EW} \equiv 1$ and $X^{\rm EW}$ is let free.

The CLs (using the standard CKM fit as input) found for $X^{\rm EW}$ (left) and $X_{\rm C}^{\rm EW}$ (right) are given in Fig. 40. The constraints on both electroweak penguin contributions are marginal and essentially any value of the relevant parameters can accommodate the data. This said, one notices that the standard values $X^{\rm EW} = X_{\rm C}^{\rm EW} = 1$ correspond to large CL regions. We also point out that current data do not particularly favor a zero value for the strength of the color-suppressed electroweak penguin $X_{\rm C}^{\rm EW}$. Hence, from our point of view, it is not justified in (148) to neglect $P_{\rm C}^{\rm EW}$ while keeping $P^{\rm EW}$, as is done by the authors of [239,232]: both electroweak penguin amplitudes may be comparable in magnitude.

3.4 $K\pi$ observables from $\pi\pi$ hadronic parameters

In Sect. VI.3.3.2 we have found that the present data point towards noticeably different values for the hadronic parameters T^{+-}, P^{+-} and $T_{\rm C}^{00}$ in the $K\pi$ system, compared to the $\pi\pi$ one, whereas they are expected to be equal in the SU(3) limit, if annihilation and exchange topologies are negligible. Another manifestation of the same trend has been explored in [239,232], where the authors compute the $K\pi$ observables with the use of the hadronic parameters found in fits to $\pi\pi$ decays. The pattern obtained that way differs from the one observed in the $K\pi$ data. We repeat this exercice with CKMfitter, using the following ratios of CP-averaged branching fractions[51]

$$R_{nc} = \frac{\tau_{B^+}}{\tau_{B^0}} \frac{\mathcal{B}(B^0 \to K^+\pi^-) + \mathcal{B}(\overline{B}^0 \to K^-\pi^+)}{\mathcal{B}(B^+ \to K^0\pi^+) + \mathcal{B}(B^- \to \overline{K}^0\pi^-)} = 0.91^{+0.08}_{-0.07} \ \ [1.2\sigma] \ ,$$

[51] The ratio R_{nc} is denoted R in [239,232].

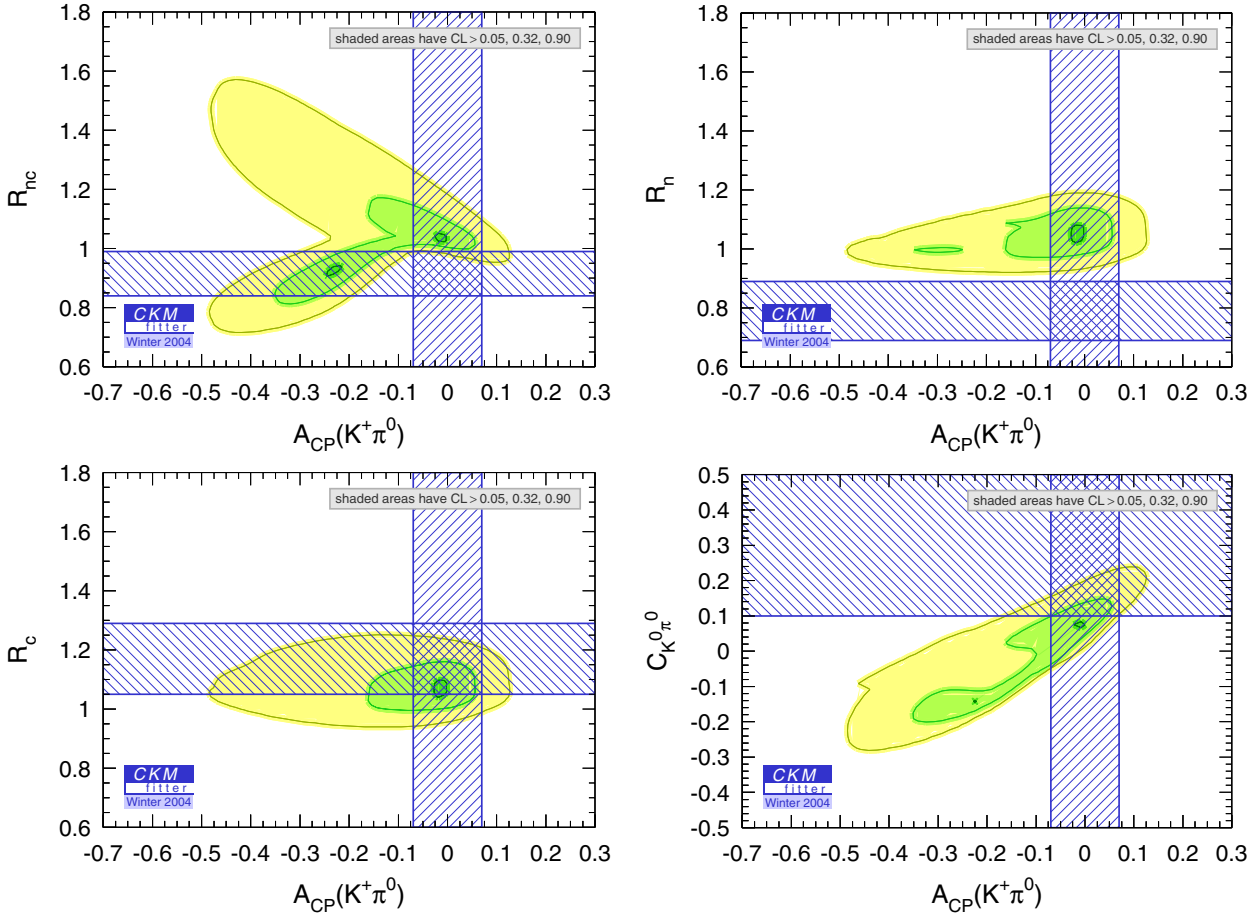

Fig. 41. Ratios of branching fractions (156) versus the direct CP asymmetry parameter in $B^+ \to K^+\pi^0$ decays as predicted from $B \to \pi\pi$ and the standard CKM fit, assuming SU(3) flavor symmetry and neglecting all annihilation and exchange diagrams. Dark, medium and light shaded areas have $CL > 0.90$, 0.32 and 0.05, respectively. The hatched bands indicate the 1σ regions of the corresponding measurements. (See also Fig. 31)

$$R_n = \frac{1}{2}\frac{\mathcal{B}(B^0 \to K^+\pi^-) + \mathcal{B}(\overline{B}^0 \to K^-\pi^+)}{\mathcal{B}(B^0 \to K^0\pi^0) + \mathcal{B}(\overline{B}^0 \to \overline{K}^0\pi^0)} = 0.78^{+0.11}_{-0.09}\ \ [1.8\sigma]\ , \tag{156}$$

$$R_c = 2\frac{\mathcal{B}(B^+ \to K^+\pi^0) + \mathcal{B}(B^- \to K^-\pi^0)}{\mathcal{B}(B^+ \to K^0\pi^+) + \mathcal{B}(B^- \to \overline{K}^0\pi^-)} = 1.16^{+0.13}_{-0.11}\ \ [1.4\sigma]\ ,$$

where the numbers in brackets indicate the departure (in standard deviations) from one, the value predicted by gluonic penguin dominance. Note in this context that the ratio of two Gaussian quantities (like branching fractions) does *not* have a Gaussian probability density (see, e.g., the discussion in Appendix C of [6]).

We assume in the following the same (strong) hypotheses as in [212,239,232], namely exact SU(3) symmetry and neglect of all annihilation and exchange topologies. This allows us to identify

$$T^{+-}_{K\pi} = T^{+-}_{\pi\pi}\ , \quad P^{+-}_{K\pi} = P^{+-}_{\pi\pi}\ , \quad T^{00}_{K\pi} = T^{00}_{\pi\pi}\ , \tag{157}$$

while electroweak penguins remain estimated according to (150), (151). The $\pi\pi$ tree and penguin amplitudes are extracted from the corresponding data using the standard CKM fit, along the line described in Sect. VI.1.4.3. The $K\pi$ observables evaluated that way are shown on Fig. 41, where the R_{nc}, R_n and R_c ratios, as well as the CP asymmetry $C_{K^0\pi^0}$, are represented as functions of the CP asymmetry $A_{CP}(K^+\pi^0)$. The overall normalization of the branching fractions as given by, e.g., $\mathcal{B}(K^+\pi^-)$, and the CP asymmetry $A_{CP}(K^+\pi^-)$ can be read off Fig. 31[52]. The experimental values are indicated by the hatched 1σ error bands.

The two-fold discrete ambiguity (Fig. 41) corresponds to the two possible solutions for the phase of T^{00}_C/T^{+-} in the $\pi\pi$ system (see Fig. 27). The negative one for the latter is preferred by the measurement of $A_{CP}(K^+\pi^0)$,

[52] As already pointed out, in the absence of annihilation and exchange topologies, the amplitudes for $B^0 \to K^+\pi^-$ and $B^0_s \to K^+K^-$ are equal: hence one may read $B^0 \to K^+\pi^-$ instead of $B^0_s \to K^+K^-$ on Fig. 31.

which is consistent with zero. While there is agreement between the predicted values of R_c and $C_{K^0\pi^0}$ and the corresponding measurements, a larger R_n is found, which emphasizes the somewhat large branching fraction of $B^0 \to K^0\pi^0$ (and confirms the findings of [237,135,238,239,232]). As a consequence, we find that the predicted R_{nc} exceeds the measurement, which is due to the contribution of $P_{\rm C}^{\rm EW}$. Putting the latter amplitude to zero like [239,232] would decrease the central value of R_{nc} to ~ 0.94 (while not changing the two other ratios), in better agreement with the experimental value.

Despite the intriguing aspect of the plots in Fig. 41, we stress that the present experimental accuracy does not allow us to draw definite conclusions. To assess the overall compatibility, we have performed a global $\pi\pi$ and $K\pi$ fit with the assumptions (157) and with the input of the standard CKM fit, resulting in a decent p-value of 25%: this is significantly better than the 1.6% compatibility (2.4σ) that is found from the evaluation of an approximate sum rule [238]. This is however consistent with the findings of [235]. *To date we cannot exclude the hypotheses (157) within the SM.*

Nevertheless, if more precise data confirm the present pattern of the $K\pi$ modes with respect to the $\pi\pi$ ones, a challenge would be given to the theory. Various effects could come into play.

- Significant annihilation and exchange topologies and/or SU(3) breaking (in other words, non-trivial rescattering effects): while large contributions of this type are unlikely, one has learned from D meson decays, from $B^0 \to D_s^- K^+$, and from unexpectedly large color-suppressed transitions from beauty to charm, that the calculation of the heavy meson non-leptonic decays is very difficult. As for charmless final states, fits using QCD FA (Sect. VI.2) require non-vanishing power corrections, even if they finally turn out to be moderate. Hopefully, with the decrease of the experimental bounds on the suppressed $B \to K\overline{K}$ modes, multichannel studies will provide more information.
- Experimental effects: absolute measurements of rates represent difficult analyses. For example, radiative corrections to the decays with charged particles in the final states have not been taken into account so far by the experiments. Their inclusion is expected to lead to increased branching fractions of modes with (light) charged particles in the final state (cf. the introduction to Part VI). As a consequence, the ratios R_{nc} and R_n should increase, which could improve the agreement with the indirect constraints from the $\pi\pi$ system (see Fig. 41).
- New Physics in loop-dominated amplitudes: according to the quantum numbers of the new field, one may have anomalies in $b \to d$, $\Delta I = 1/2$ (gluonic) and/or $\Delta I = 3/2$ (electroweak) penguin amplitudes, and/or in $b \to s$, $\Delta I = 0$ (gluonic) and/or $\Delta I = 1$ (electroweak) penguin amplitudes. This would require the introduction of new parameters, which would need sufficiently accurate data to be fitted.

The authors of [239,232] have studied the latter possibility within a specific class of New Physics models, where the hierarchy between $b \to d$ and $b \to s$ transitions is the same as in the SM ($\sim \lambda$), and where New Physics only enters as an enhanced $\Delta S = \Delta I = 1$ electroweak penguin amplitude $P^{\rm EW}$ with a single (unknown) weak phase. This scenario is minimal in the sense that only one magnitude and one phase has to be adjusted in order to describe the data. As a by-product of its simplicity, its "naturalness" can be questioned: there is no obvious reason to exclude the possibility that the failure of color-suppression in the $\pi\pi$ modes is a consequence of significant non-standard corrections; moreover, the complete NP effect may not be proportional to a single CP-violating phase[53], and finally, the assumption that $P^{\rm EW}$ is real with respect to the sum $T^{+-} + T_C^{00}$, as it is in the SM[54], may be significantly violated.

4 Analysis of $B \to \rho\pi$ decays

In this section we discuss the phenomenological implications of the experimental results from the *BABAR* collaboration [247] on time-dependent CP-violating asymmetries in $B^0 \to \rho^\pm\pi^\mp$ decays. We use amplitude relations based on flavor symmetries as explicit theoretical input to dynamical constraints[55]. The analysis is restricted to the quasi-two-body representations of $B^0 \to (\pi^\pm\pi^0)\pi^\mp$ decays, corresponding to distinct bands in the three-pion Dalitz plot. Wrong charge assignments due to the finite width of the ρ resonance and interference effects between different two-body states are neglected. It has been pointed out in [252] that this neglect induces biases on the observed CP and dilution parameters that can amount to up to 8% depending on the size of the $B^0 \to \rho^0\pi^0$ amplitude[56]. In the future full Dalitz plot CP analyses [253,201], these model-dependent uncertainties will be significantly reduced.

[53] The most general parameterization would imply to introduce two new CP-violating phases, because the arbitrary sum $\sum_i M_i^{\rm NP} e^{\pm i\phi_i}$ can be rewritten as $\tilde{M}_1^{\rm NP} e^{i\pm\tilde{\phi}_1} + \tilde{M}_2^{\rm NP} e^{i\pm\tilde{\phi}_2}$, where the M_i are CP-conserving complex numbers and the ϕ_i are CP-odd.

[54] For this to be true, one would have to show that NP does not enhance the coefficients $c_{7,8}$, see (150).

[55] The present analysis does not include a discussion of results on pseudoscalar-vector modes from QCD Factorization [135,248–250] or SU(3) symmetry including all SU(3) multiplets [251], since this goes beyond the scope of this paper. A dedicated work on this will be forthcoming.

[56] Whereas the main part of the interference region between the ρ^+ and ρ^- has been removed from the analysis, the ones between charged and neutral ρ's are kept [247].

As in all charmless analyses related to the UT angle α, the phenomenological effort focuses on the determination of the penguin contribution to the transition amplitudes. We approach the problem following a similar hierarchical structure as in Sect. VI.1.

(I) Using as input the present (yet incomplete) measurements or bounds on branching fractions of the modes involved with the SU(2) analysis. Contributions from electroweak penguins are neglected[57]. We also extrapolate the isospin analysis to future integrated luminosities of $1\,\mathrm{ab}^{-1}$ and $10\,\mathrm{ab}^{-1}$, using educated guesses for measurements and experimental errors.

(II) Using (I) and the rates of $B^0 \to K^{*+}\pi^-$ and $B^0 \to \rho^- K^+$ decays together with $SU(3)$ flavor symmetry and neglecting OZI-suppressed penguin annihilation topologies.

(III) Using (II) and phenomenological estimates of $|P^{+-}|$ and $|P^{-+}|$ from the rates of $B^+ \to K^{*0}\pi^+$ (measured) and $B^+ \to \rho^+ K^0$ (upper limit) decays, respectively, together with $SU(3)$ flavor symmetry and neglecting annihilation and long-distance penguin topologies.

4.1 Basic formulae and definitions

We follow the conventions adopted in Sect. VI.1 and use the unitarity of the weak Hamiltonian to eliminate the charm quark loop out of the penguin diagrams ($\mathfrak{C}$ convention) in the transition amplitudes. The complex Standard Model amplitudes of the relevant processes represent the sum of complex tree (T) and penguin (P) amplitudes with different weak and strong phases. The corresponding diagrams for the decay $B^0 \to \rho^\pm\pi^\mp$ are the same as for $B^0 \to \pi^+\pi^-$ (see examples in Fig. 18). The transition amplitudes read

$$\begin{aligned}
A^{+-} &\equiv A(B^0 \to \rho^+\pi^-) = V_{ud}V_{ub}^* T^{+-} + V_{td}V_{tb}^* P^{+-} \;, \\
A^{-+} &\equiv A(B^0 \to \rho^-\pi^+) = V_{ud}V_{ub}^* T^{-+} + V_{td}V_{tb}^* P^{-+} \;, \\
\overline{A}^{+-} &\equiv A(\overline{B}^0 \to \rho^+\pi^-) = V_{ud}^* V_{ub} T^{-+} + V_{td}^* V_{tb} P^{-+} \;, \\
\overline{A}^{-+} &\equiv A(\overline{B}^0 \to \rho^-\pi^+) = V_{ud}^* V_{ub} T^{+-} + V_{td}^* V_{tb} P^{+-} \;,
\end{aligned} \tag{158}$$

where the ρ meson is emitted by the W boson in the case of A^{+-} and $\overline{A}^{-+}$, while it contains the spectator quark in the case of A^{-+} and $\overline{A}^{+-}$.

The time-dependent CP asymmetries is given by

$$\begin{aligned}
a_{CP}^{\pm}(t) &\equiv \frac{\Gamma(\overline{B}^0(t) \to \rho^\pm\pi^\mp) - \Gamma(B^0(t) \to \rho^\pm\pi^\mp)}{\Gamma(\overline{B}^0(t) \to \rho^\pm\pi^\mp) + \Gamma(B^0(t) \to \rho^\pm\pi^\mp)} \\
&= (S_{\rho\pi} \pm \Delta S_{\rho\pi}) \sin(\Delta m_d t) - (C_{\rho\pi} \pm \Delta C_{\rho\pi}) \cos(\Delta m_d t) \;,
\end{aligned} \tag{159}$$

where the quantities $S_{\rho\pi}$ and $C_{\rho\pi}$ parameterize mixing-induced CP violation and flavor-dependent direct CP violation, respectively. The parameters $\Delta S_{\rho\pi}$ and $\Delta C_{\rho\pi}$ are CP-conserving: $\Delta S_{\rho\pi}$ is related to the strong phase difference between the amplitudes contributing to $B^0 \to \rho^\pm\pi^\mp$ decays, while $\Delta C_{\rho\pi}$ describes the asymmetry (dilution) between the rates $\Gamma(B^0 \to \rho^+\pi^-) + \Gamma(\overline{B}^0 \to \rho^-\pi^+)$ and $\Gamma(B^0 \to \rho^-\pi^+) + \Gamma(\overline{B}^0 \to \rho^+\pi^-)$. Owing to the fact that $B^0 \to \rho^\pm\pi^\mp$ is not a CP eigenstate, one must also consider the time- and flavor-integrated charge asymmetry

$$\mathcal{A}_{\rho\pi} \equiv \frac{|A^{+-}|^2 + |\overline{A}^{+-}|^2 - |A^{-+}|^2 - |\overline{A}^{-+}|^2}{|A^{+-}|^2 + |\overline{A}^{+-}|^2 + |A^{-+}|^2 + |\overline{A}^{-+}|^2} \;, \tag{160}$$

as another source of possible direct CP violation.

We reorganize the experimentally convenient, namely uncorrelated, direct CP-violation parameters $C_{\rho\pi}$ and $\mathcal{A}_{\rho\pi}$ into the physically more intuitive quantities $\mathcal{A}_{\rho\pi}^{+-}$, $\mathcal{A}_{\rho\pi}^{-+}$, defined by

$$\begin{aligned}
\mathcal{A}_{\rho\pi}^{+-} &\equiv \frac{|\kappa^{+-}|^2 - 1}{|\kappa^{+-}|^2 + 1} = -\frac{\mathcal{A}_{\rho\pi} + C_{\rho\pi} + \mathcal{A}_{\rho\pi}\Delta C_{\rho\pi}}{1 + \Delta C_{\rho\pi} + \mathcal{A}_{\rho\pi} C_{\rho\pi}} \;, \\
\mathcal{A}_{\rho\pi}^{-+} &\equiv \frac{|\kappa^{-+}|^2 - 1}{|\kappa^{-+}|^2 + 1} = \frac{\mathcal{A}_{\rho\pi} - C_{\rho\pi} - \mathcal{A}_{\rho\pi}\Delta C_{\rho\pi}}{1 - \Delta C_{\rho\pi} - \mathcal{A}_{\rho\pi} C_{\rho\pi}} \;,
\end{aligned} \tag{161}$$

[57] The treatment advertised in (120) cannot be directly translated to the $\rho\pi$ system, if considered as a two-body decay. Only in the case of a full Dalitz plot analysis, that allows one to extract the $\Delta I = 3/2$ tree amplitude, is it possible to take into account EW penguin contributions in a model-independent way [143]. Since we learned from the $\pi\pi$ system that these effects are small, we can choose to neglect them for the numerical discussion of present $\rho\pi$ CP results.

where

$$\kappa^{+-} \equiv \frac{q}{p}\frac{\overline{A}^{-+}}{A^{+-}} \ , \qquad \kappa^{-+} \equiv \frac{q}{p}\frac{\overline{A}^{+-}}{A^{-+}} \ , \tag{162}$$

so that $\mathcal{A}^{+-}_{\rho\pi}$ ($\mathcal{A}^{-+}_{\rho\pi}$) involves only diagrams where the ρ meson is emitted by the W boson (contains the spectator quark).

In analogy to the $\pi\pi$ system, we introduce the effective weak angles that reduce to 2α in the absence of penguins

$$2\alpha^{+-}_{\rm eff} \equiv \arg\kappa^{+-} \ , 2\alpha^{-+}_{\rm eff} \equiv \arg\kappa^{-+} \ , \tag{163}$$

so that $S_{\rho\pi}$ and $\Delta S_{\rho\pi}$, which are given by

$$\begin{aligned} S + \Delta S_{\rho\pi} &= \frac{2{\rm Im}\lambda^{+-}}{1+|\lambda^{+-}|^2} \ , \\ S - \Delta S_{\rho\pi} &= \frac{2{\rm Im}\lambda^{-+}}{1+|\lambda^{-+}|^2} \ , \end{aligned} \tag{164}$$

where[58]

$$\lambda^{+-} \equiv \frac{q}{p}\frac{\overline{A}^{+-}}{A^{+-}} \ , \qquad \lambda^{-+} \equiv \frac{q}{p}\frac{\overline{A}^{-+}}{A^{-+}} \ , \tag{165}$$

can be rewritten as

$$\begin{aligned} S + \Delta S_{\rho\pi} &= \sqrt{1-(C+\Delta C_{\rho\pi})^2}\,\sin(2\alpha^{+-}_{\rm eff} + \hat{\delta}) \ , \\ S - \Delta S_{\rho\pi} &= \sqrt{1-(C-\Delta C_{\rho\pi})^2}\,\sin(2\alpha^{-+}_{\rm eff} - \hat{\delta}) \ , \end{aligned} \tag{166}$$

[58] The $\lambda^{+-(-+)}$ involve only one $\rho\pi$ charge combination, but both amplitude types $T(P)^{+-}$ and $T(P)^{-+}$. They are insensitive to direct CPV but their imaginary part is directly related to the weak phase α (though complicated by strong phase shifts and penguins). The quantities $\kappa^{+-(-+)}$ involve both $\rho\pi$ charges, but only one amplitude type, corresponding to whether ([−+]) or not ([+−]) the ρ has been produced involving the spectator quark. Their moduli are linked to direct CPV while their phases measure effective weak angles $\alpha^{-+(+-)}_{\rm eff}$ defined further below.
Compared to CP eigenstates, the λ^{+-} and λ^{-+} do not have the desired properties under CP transformation, i.e., $\lambda^{+-} \neq 1$ or $\lambda^{-+} \neq 1$ does not automatically entail CP violation. These inequalities are a necessary but not a sufficient condition. Appropriate λ's can be easily constructed. They should reflect the CP and the flavor specific character of $B^0 \to \rho^{\pm}\pi^{\mp}$ decays. A possible definition is

$$\tilde{\lambda_{CP}} \equiv \lambda^{+-}\cdot\lambda^{-+} \ , \qquad \tilde{\lambda_{\rm tag}} \equiv \lambda^{+-}/\lambda^{-+} \ ,$$

where $\tilde{\lambda_{CP}} \neq 1$ in case of direct or mixing induced CP violation, and for example $\tilde{\lambda_{\rm tag}} = 0$ for the case that $B^0 \to \rho^+\pi^-$ is a flavor eigenstate. A more practical definition is given by:

$$|\lambda_{CP}|^2 \equiv \frac{|\lambda^{+-}|^2 + |\lambda^{-+}|^2 + 2|\lambda^{+-}|^2|\lambda^{-+}|^2}{2+|\lambda^{+-}|^2+|\lambda^{-+}|^2} \ ,$$

$$|\lambda_{\rm tag}|^2 \equiv \frac{1+2|\lambda^{+-}|^2+|\lambda^{+-}|^2|\lambda^{-+}|^2}{1+2|\lambda^{-+}|^2+|\lambda^{-+}|^2|\lambda^{+-}|^2} \ ,$$

$${\rm Im}\lambda_{CP} \equiv \frac{{\rm Im}\lambda^{+-}(1+|\lambda^{-+}|^2)+{\rm Im}\lambda^{-+}(1+|\lambda^{+-}|^2)}{2+|\lambda^{+-}|^2+|\lambda^{-+}|^2} \ ,$$

$${\rm Im}\lambda_{\rm tag} \equiv \frac{{\rm Im}\lambda^{+-}(1+|\lambda^{-+}|^2)-{\rm Im}\lambda^{-+}(1+|\lambda^{+-}|^2)}{1+2|\lambda^{-+}|^2+|\lambda^{-+}|^2|\lambda^{+-}|^2} \ ,$$

which has the desired properties, since if:

- $B^0 \to \rho^+\pi^-$ is flavor eigenstate, e.g., $A^{-+} = \overline{A}^{+-} = 0$ so that $\lambda^{+-} = 0$ and $\lambda^{-+} = \infty$, one has $\lambda_{\rm tag} = 0$ with maximal dilution. The mode is self-tagging as is, e.g., $B^0 \to \rho^- K^+$, and no mixing-induced CPV can occur.
- $B^0 \to \rho^{\pm}\pi^{\mp}$ behaves like a CP eigenstate, i.e., $|A^{+-}| = |A^{-+}|$ and $|\overline{A}^{+-}| = |\overline{A}^{-+}|$ so that $|\lambda^{+-}| = |\lambda^{-+}| = |\lambda|$, one has $|\lambda_{\rm tag}| = 1$ with minimal dilution, and $\lambda_{CP} = \lambda$. One could hence disregard the charge of the ρ in the analysis and just look at the time-dependent asymmetry between $B^0 \to (\rho\pi)^0$ and $\overline{B}^0 \to (\rho\pi)^0$.

Note that in the presence of penguins, the value of $\lambda_{\rm tag}$ does depend on the weak phase α.

with[59] $\hat{\delta} = \arg[\lambda^{+-}\kappa^{-+*}] = \arg[\lambda^{-+*}\kappa^{+-}] = \arg[A^{-+}A^{+-*}]$.

In the absence of penguin contributions ($P^{+-} = P^{-+} = 0$), one has $|\kappa^{+-}| = |\kappa^{-+}| = |\lambda^{+-}\lambda^{-+}| = 1$, that is $\alpha_{\rm eff}^{+-} = \alpha_{\rm eff}^{-+} = \alpha$, so that the observables reduce to simple functions of α, $\hat{\delta}$ and $\hat{r}$:

$$\begin{aligned} S_{\rho\pi} &= \frac{2\hat{r}}{1+\hat{r}^2}\,\sin 2\alpha\,\cos\hat{\delta}\ , \\ \Delta S_{\rho\pi} &= \frac{2\hat{r}}{1+\hat{r}^2}\,\cos 2\alpha\,\sin\hat{\delta}\ , \\ C_{\rho\pi} &= 0\ , \\ \Delta C_{\rho\pi} &= \frac{1-\hat{r}^2}{1+\hat{r}^2}\ , \\ \mathcal{A}_{\rho\pi} &= 0\ , \\ \mathcal{A}_{\rho\pi}^{+-} &= \mathcal{A}_{\rho\pi}^{-+} = 0\ , \end{aligned} \tag{167}$$

with $\hat{r} = |T^{-+}/T^{+-}|$. Hence α can be determined up to an eightfold ambiguity within $[0,\pi]$[60]. If furthermore $B^0 \to \rho^\pm\pi^\mp$ represents an effective CP eigenstate ($T^{+-} = T^{-+}$), the parameters simplify to $S_{\rho\pi} = \sin 2\alpha$ and $\Delta S_{\rho\pi} = C_{\rho\pi} = \Delta C_{\rho\pi} = \mathcal{A}_{\rho\pi} = 0$, hence reproducing the zero-penguin case in $B^0 \to \pi^+\pi^-$ decays. If the relative strong phase vanishes, but there exists a non-zero dilution $r_{T^{+-}} \neq 0$ (i.e., $\Delta C_{\rho\pi} \neq 0$), one has $S_{\rho\pi} = \sqrt{1-\Delta C_{\rho\pi}^2}\sin 2\alpha$.

Branching fractions are in general given by the sum of the contributing squared amplitudes, where final states ($\rho\pi$ charges) are summed and initial states (B flavors) are averaged. The $B^0 \to \rho^\pm\pi^\mp$ branching fraction reads

$$\mathcal{B}_{\rho\pi}^{\pm\mp} \ \propto\ \frac{\tau_{B^0}}{2}\left(|A^{+-}|^2 + |\overline{A}^{-+}|^2 + |A^{-+}|^2 + |\overline{A}^{+-}|^2\right)\ . \tag{168}$$

Observables from other modes

The various analyses discussed here involve SU(2) and SU(3) flavor partners of the signal mode $B^0 \to \rho^\pm\pi^\mp$. We use branching fractions ($\mathcal{B}$) as well as charge asymmetries ($\mathcal{A}$) for the charged B and self-tagging channels. They are defined by

$$\mathcal{B}_{hh'} \equiv \mathcal{B}(B \to hh') \ \propto\ \frac{\tau_B}{2}\left(|A_{hh'}|^2 + |\overline{A}_{hh'}|^2\right)\ , \tag{169}$$

$$\mathcal{A}_{hh'} \equiv \frac{|\overline{A}_{hh'}|^2 - |A_{hh'}|^2}{|\overline{A}_{hh'}|^2 + |A_{hh'}|^2}\ , \tag{170}$$

where τ_B denotes the lifetime of the decaying B meson (neutral or charged). More details are given in the following.

4.2 Experimental input

The present (Winter 2004) results (including world averages taken from the HFAG [62]) for the branching fractions and CP-violating asymmetries of all $B \to \rho\pi$ decays are given in Table 11. Also given are the results for the modes

[59] The alternative parameterization introduced in [209] (see Footnote 35 in Sect. VI.1.2.1) can be extended to the $B \to \rho\pi$ system. Restricted to the $B^0 \to \rho^\pm\pi^\mp$ amplitudes, one has

$$\begin{aligned} A_{\prime}^{+-} &= \mu a^{+-} e^{-i\hat{\delta}/2}\ , \\ A_{\prime}^{-+} &= \mu a^{-+} e^{+i\hat{\delta}/2}\ , \\ (q/p)\overline{A}_{\prime}^{+-} &= \mu \overline{a}^{+-} e^{+i(2\alpha_{\rm eff}^{+-}+\hat{\delta}/2)}\ , \\ (q/p)\overline{A}_{\prime}^{-+} &= \mu \overline{a}^{-+} e^{+i(2\alpha_{\rm eff}^{-+}-\hat{\delta}/2)}\ , \end{aligned}$$

where μ (overall scale) and the $a^{+-}, \ldots$, are real numbers and where we have rotated the amplitudes by the (arbitrary) global phase $A_{\prime}^{ij} = A^{ij}e^{i(\arg[A^{+-*}]-\hat{\delta}/2)}$.

[60] In the absence of penguin contributions, the eight solutions for α and $\hat{\delta}$ satisfying (166) and (167) read [254]

$\alpha \to$	$\pi/4 - \hat{\delta}/2$,	$\pi/2 + \alpha$,	$3\pi/4 - \hat{\delta}/2$,	$\pi/4 + \hat{\delta}/2$,	$\pi/2 - \alpha$,	$3\pi/4 + \hat{\delta}/2$,	$\pi - \alpha$
$\hat{\delta} \to$	$\pi/2 - 2\alpha$,	$\pi + \hat{\delta}$,	$3\pi/2 - 2\alpha$,	$-\pi/2 + 2\alpha$,	$-\hat{\delta}$,	$-3\pi/2 + 2\alpha$,	$\pi - \hat{\delta}$

Table 11. Compilation of results (from data up to Winter 2004) on $B \to \rho\pi$ branching fractions (in units of 10^{-6}) and CP asymmetries as well as dilution parameters. Limits are quoted at 90% confidence level (CL). Also given are the branching fractions and direct CP asymmetries for the modes $B^0 \to K^{*+}\pi^-$, $B^0 \to \rho^- K^+$, $B^+ \to K^{*0}\pi^+$ and $B^+ \to \rho^+ K^0$ related to $\rho\pi$ via SU(3) flavor symmetry

Obs.	*BABAR*	Belle	CLEO	Average
$\mathcal{B}^{\pm\mp}_{\rho\pi}$	$22.6 \pm 1.8 \pm 2.2$ [247]	$29.1\,^{+5.0}_{-4.9} \pm 4.0$ [255]	$27.6\,^{+8.4}_{-7.4} \pm 4.2$ [256]	24.0 ± 2.5
$\mathcal{A}_{\rho\pi}$	$-0.114 \pm 0.062 \pm 0.027$ [247]	–	–	-0.114 ± 0.067
$S_{\rho\pi}$	$-0.13 \pm 0.18 \pm 0.04$ [247]	–	–	-0.13 ± 0.18
$\Delta S_{\rho\pi}$	$0.33 \pm 0.18 \pm 0.03$ [247]	–	–	0.33 ± 0.18
$C_{\rho\pi}$	$0.35 \pm 0.13 \pm 0.05$ [247]	–	–	0.35 ± 0.14
$\Delta C_{\rho\pi}$	$0.20 \pm 0.13 \pm 0.05$ [247]	–	–	0.20 ± 0.14
$\mathcal{A}^{+-}_{\rho\pi}$	$-0.18 \pm 0.13 \pm 0.05$	–	–	-0.18 ± 0.14
$\mathcal{A}^{-+}_{\rho\pi}$	$-0.52\,^{+0.17}_{-0.19} \pm 0.07$	–	–	$-0.52\,^{+0.18}_{-0.20}$
$\mathcal{B}^{+0}_{\rho\pi}$	$11.0 \pm 1.9 \pm 1.9$ [257,258]	$13.2 \pm 2.3\,^{+1.4}_{-1.9}$ [259]	<43 [256]	12.0 ± 2.0
$\mathcal{A}^{+0}_{\rho\pi}$	$0.23 \pm 0.16 \pm 0.06$ [257,258]	$0.06 \pm 0.19 \pm\,^{+0.04}_{-0.06}$ [259]	–	0.16 ± 0.13
$\mathcal{B}^{0+}_{\rho\pi}$	$9.3 \pm 1.0 \pm 0.8$ [257,258]	$8.0\,^{+2.3}_{-2.0} \pm 0.7$ [255]	$10.4\,^{+3.3}_{-3.4} \pm 2.1$ [256]	9.1 ± 1.1
$\mathcal{A}^{0+}_{\rho\pi}$	$-0.17 \pm 0.11 \pm 0.02$ [257,258]	–	–	-0.17 ± 0.11
$\mathcal{B}^{00}_{\rho\pi}$	$0.9 \pm 0.7 \pm 0.5 (< 2.9)$ [257,258]	$5.1 \pm 1.6 \pm 0.9$ [260]	<5.5 [256]	1.7 ± 0.8
$C^{00}_{\rho\pi}$	–	–	–	–
$S^{00}_{\rho\pi}$	–	–	–	–
$\mathcal{B}^{-+}_{\rho K}$	$7.3\,^{+1.3}_{-1.2} \pm 1.3$ [247]	$15.1\,^{+3.4}_{-3.3}\,^{+2.4}_{-2.6}$ [261]	$16.0\,^{+7.6}_{-6.4} \pm 2.8$ [256]	9.0 ± 1.6
$\mathcal{A}^{-+}_{\rho K}$	$0.18 \pm 0.12 \pm 0.08$ [247]	$0.22\,^{+0.22}_{-0.23} \pm 0.02$ [261]	–	0.19 ± 0.12
$\mathcal{B}^{+-}_{K^*\pi}$	–	$14.8\,^{+4.6}_{-4.4}\,^{+2.8}_{-1.3}$ [261]	$16\,^{+6}_{-5} \pm 2$ [262]	$15.3\,^{+4.1}_{-3.5}$
$\mathcal{A}^{+-}_{K^*\pi}$	–	–	$0.26\,^{+0.33}_{-0.34}\,^{+0.10}_{-0.08}$ [262]	0.26 ± 0.34
$\mathcal{B}^{+0}_{\rho K}$	–	–	<48 [263]	<48
$\mathcal{B}^{0+}_{K^*\pi}$	$15.5\,^{+1.8}_{-1.5} \pm 4.0$ [264]	$8.5\,^{+0.9}_{-1.1} \pm 0.9$ [265]	$7.6\,^{+3.5}_{-3.0} \pm 1.6$ [256]	$9.0\,^{+1.3}_{-1.2}$

$B^0 \to K^{*+}\pi^-$ and $B^0 \to \rho^- K^+$, which are the SU(3) partners of the decays $B^0 \to \rho^+\pi^-$ and $B^0 \to \rho^-\pi^+$, respectively. There is some disagreement on possible evidence for the decay $B^0 \to \rho^0\pi^0$, which has not been seen by *BABAR* whereas Belle finds a large central value for the branching fraction that may indicate a large color-suppressed tree amplitude or significant penguin contributions.

4.2.1 Direct CP violation

The direct CP asymmetries $\mathcal{A}^{+-}_{\rho\pi}$ and $\mathcal{A}^{-+}_{\rho\pi}$ (see Table 11) have been computed from (161) and (162), using the linear correlation coefficients given in Table 12. We find a linear correlation coefficient between $\mathcal{A}^{+-}_{\rho\pi}$ and $\mathcal{A}^{-+}_{\rho\pi}$ of 0.51. Confidence levels in the $(\mathcal{A}^{+-}_{\rho\pi}, \mathcal{A}^{-+}_{\rho\pi})$ plane are shown in the left hand plot of Fig. 42. The *BABAR* experiment finds some indication for direct CP violation (approximately 2.5 standard deviations including systematics) mainly in the modes involving the A^{-+} and $\overline{A}^{+-}$ decay amplitudes. This result is rather unexpected since, if confirmed, it would require sizable penguin contributions to these amplitudes, with a hierarchy opposite to the naïve factorization

Table 12. Correlation coefficients (in %) between the parameters in the time-dependent fit to $B^0 \to \rho^\pm\pi^\mp$ decays as measured by *BABAR* [247]. Note that the correlations between events yields and the CP parameters are taken from the branching fraction analysis [247]

	$\mathcal{A}_{\rho\pi}$	$C_{\rho\pi}$	$\Delta C_{\rho\pi}$	$S_{\rho\pi}$	$\Delta S_{\rho\pi}$	$N_{\rho\pi}$
$\mathcal{A}_{\rho\pi}$	100	−7.6	−6.7	−3.1	1.5	3.9
$C_{\rho\pi}$		100	13.9	−7.7	−10.0	−7.4
$\Delta C_{\rho\pi}$		-	100	−9.5	−7.7	−6.8
$S_{\rho\pi}$		-	-	100	22.9	1.2
$\Delta S_{\rho\pi}$		-	-	-	100	−3.0

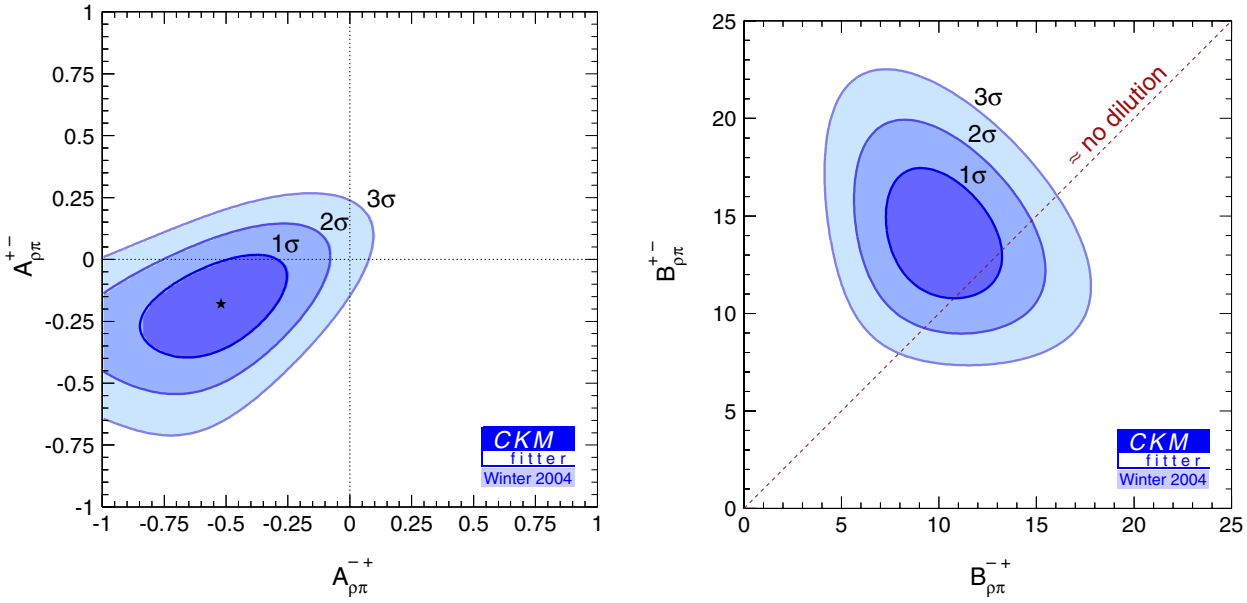

Fig. 42. Confidence level in the $\mathcal{A}^{+-}_{\rho\pi}$ versus $\mathcal{A}^{-+}_{\rho\pi}$ (left plot) and $\mathcal{B}^{+-}_{\rho\pi}$ versus $\mathcal{B}^{-+}_{\rho\pi}$ (right plot) planes. Shown are the 1σ (dark shaded), 2σ (medium shaded) and the 3σ (light shaded) regions. The dashed line in the right hand plot approximately indicates vanishing dilution ($\Delta C_{\rho\pi} = 0$, neglecting $\mathcal{A}_{\rho\pi} C_{\rho\pi} \neq 0$)

expectation [266]

$$P^{-+} \ll P^{+-} \lesssim P^{+-}_{\pi\pi} \ . \tag{171}$$

QCD factorization predicts potentially large corrections to the above hierarchy [135]; on the other hand, because the strong phases are suppressed, direct CP violation in $B^0 \to \rho^\pm\pi^\mp$ is expected to remain below 10%.

4.2.2 Charge-flavor specific branching fractions

The yields and CP-violation results are expressed in the basis defined in (159), (160) and (168). Since it is complete, we can transform it to any other complete basis, e.g., the branching fractions of the four individual tag-charge contributions. The individual (i.e., not B-flavor-averaged) branching fractions

$$\begin{aligned} \mathcal{B}_{\rho^+\pi^-} &= \mathcal{B}(B^0 \to \rho^+\pi^-) \ , & \mathcal{B}_{\rho^-\pi^+} &= \mathcal{B}(B^0 \to \rho^-\pi^+) \ , \\ \bar{\mathcal{B}}_{\rho^+\pi^-} &= \mathcal{B}(\overline{B}^0 \to \rho^+\pi^-) \ , & \bar{\mathcal{B}}_{\rho^-\pi^+} &= \mathcal{B}(\overline{B}^0 \to \rho^-\pi^+) \ , \end{aligned} \tag{172}$$

are obtained via

$$\mathcal{B}_{\rho^Q\pi^{-Q}}(f, Q) = \frac{1}{2}\left(1 + Q\mathcal{A}_{\rho\pi}\right)\left(1 + f \cdot \left(C_{\rho\pi} + Q\Delta C_{\rho\pi}\right)\right)\mathcal{B}^{\pm\mp}_{\rho\pi} \ , \tag{173}$$

with the B^0 flavors $f(B^0) = 1$, $f(\overline{B}^0) = -1$, and the ρ charges $Q(\rho^\pm) = \pm 1$. Adding statistical and systematic errors in quadrature, we find (in units of 10^{-6}):

$$\begin{aligned} \mathcal{B}_{\rho^+\pi^-} &= 16.5\,^{+3.1}_{-2.8}\,, & \mathcal{B}_{\rho^-\pi^+} &= 15.4\,^{+3.2}_{-2.9}\,, \\ \overline{\mathcal{B}}_{\rho^+\pi^-} &= 4.8\,^{+2.6}_{-2.3}\,, & \overline{\mathcal{B}}_{\rho^-\pi^+} &= 11.4\,^{+2.8}_{-2.6}\,, \end{aligned} \tag{174}$$

and the correlation coefficients

$$\begin{array}{c|ccc} & \mathcal{B}_{\rho^-\pi^+} & \overline{\mathcal{B}}_{\rho^+\pi^-} & \overline{\mathcal{B}}_{\rho^-\pi^+} \\ \hline \mathcal{B}_{\rho^+\pi^-} & -0.17 & -0.47 & -0.14 \\ \mathcal{B}_{\rho^-\pi^+} & 1 & -0.08 & -0.40 \\ \overline{\mathcal{B}}_{\rho^+\pi^-} & - & 1 & -0.06 \end{array} \tag{175}$$

One notices a significant lack of $\overline{B}^0 \to \rho^+\pi^-$ decays in the results (174). We can infer from these numbers the B-flavor-averaged branching fractions (in units of 10^{-6})

$$\begin{aligned} \mathcal{B}^{+-}_{\rho\pi} &\equiv \frac{1}{2}\left(\mathcal{B}_{\rho^+\pi^-} + \overline{\mathcal{B}}_{\rho^-\pi^+}\right) = \frac{1}{2}\left(1 + \Delta C_{\rho\pi} + \mathcal{A}_{\rho\pi} C_{\rho\pi}\right) \mathcal{B}^{\pm\mp}_{\rho\pi} = 13.9\,^{+2.2}_{-2.1}\,, \\ \mathcal{B}^{-+}_{\rho\pi} &\equiv \frac{1}{2}\left(\mathcal{B}_{\rho^-\pi^+} + \overline{\mathcal{B}}_{\rho^+\pi^-}\right) = \frac{1}{2}\left(1 - \Delta C_{\rho\pi} - \mathcal{A}_{\rho\pi} C_{\rho\pi}\right) \mathcal{B}^{\pm\mp}_{\rho\pi} = 10.1\,^{+2.1}_{-1.9}\,, \end{aligned} \tag{176}$$

with a linear correlation coefficient of -0.28 between $\mathcal{B}^{+-}_{\rho\pi}$ and $\mathcal{B}^{-+}_{\rho\pi}$. The CLs of the rates (176) are depicted in the right hand plot of Fig. 42. The branching fractions $\mathcal{B}^{+-}_{\rho\pi}$ and $\mathcal{B}^{-+}_{\rho\pi}$ correspond to transitions where the ρ meson is emitted by the W boson or originates from the spectator interaction, respectively. Simple form factor arguments predict that $\mathcal{B}^{+-}_{\rho\pi}$ should be larger than $\mathcal{B}^{-+}_{\rho\pi}$, which is reproduced by experiment.

Also given in Table 11 are the $\rho\pi$ flavor partners. Since $\rho^0\pi^0$ is a CP eigenstate (in the two-body decay approximation), its sine and cosine coefficients, $S^{00}_{\rho\pi}$, $C^{00}_{\rho\pi}$, can be measured in a time-dependent analysis, provided that the experimental sensitivity is sufficient. The other $\rho\pi$ modes are charged so that they provide two observables, one of which describes CP violation. The decays $B^0 \to K^{+(*)}h^-$ are self-tagging so that they also provide two observables.

4.3 Penguins

The experimental results on $K^*\pi$ and $K\rho$ modes summarized in Table 11 indicate that large penguin contributions may be present in the SU(3)-related $B^0 \to \rho^\pm\pi^\mp$ decay amplitudes. On the other hand, within QCD Factorization, the penguin-to-tree ratio for both charge combinations is predicted to be significantly smaller (a factor of three) than for $B^0 \to \pi^+\pi^-$ decays [135].

4.3.1 Zero-penguin case

As an exercise, we assume here that the penguin amplitudes P^{+-} and P^{-+} are zero so that $\alpha^{+-}_{\rm eff} = \alpha^{-+}_{\rm eff} = \alpha$ (cf. (166) and 167). The compatibility of a theory without penguins with the $B^0 \to \rho^\pm\pi^\mp$ data is marginal. We find $\chi^2 = 8.6$ for two degrees of freedom which corresponds to a CL of 0.014 (2.5σ - which is equal to the significance of direct CP violation).

Figure 43 shows the constraint on α obtained in this simplified setup. The eightfold ambiguity within $[0, \pi]$ arises due to the unknown strong phase $\hat{\delta}$. Although vanishing penguin amplitudes are not a likely scenario, it allows us to assess the statistical power of the present data: if all strong phases were known, α could be determined with an accuracy of 5.4° per solution. Further setting $\hat{\delta} = 0$ leads to a twofold ambiguity, one of which is in agreement with the standard CKM fit.

4.3.2 Constraining the penguins

In analogy to the $B^0 \to \pi^+\pi^-$ case, we can constrain the penguin contributions by inserting the value of α from the standard CKM fit. Whereas the information from the other charges (via isospin) is used there, we restrict the analysis to $B^0 \to \rho^\pm\pi^\mp$ here. Figure 44 gives the CLs obtained in the P^{+-}/T^{+-} complex plane (left hand plot) as well as the

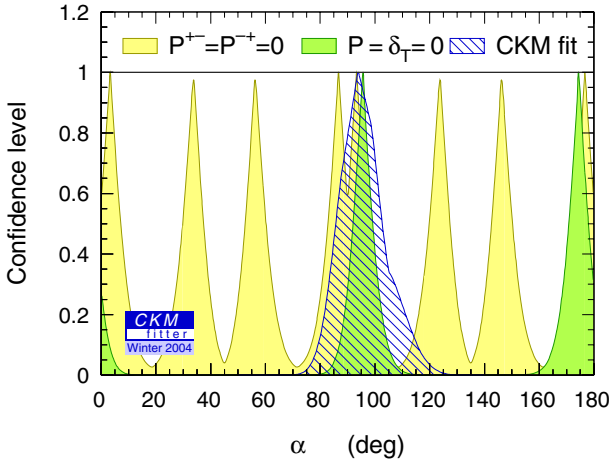

Fig. 43. Constraint on the UT angle α using the CP and branching fraction results for $B^0 \to \rho^{\pm}\pi^{\mp}$ decays and assuming vanishing penguin contributions. Indicated by the dark-shaded areas are the solutions when further fixing the relative strong phase $\hat{\delta}$ to zero. Also shown is the constraint from the standard CKM fit

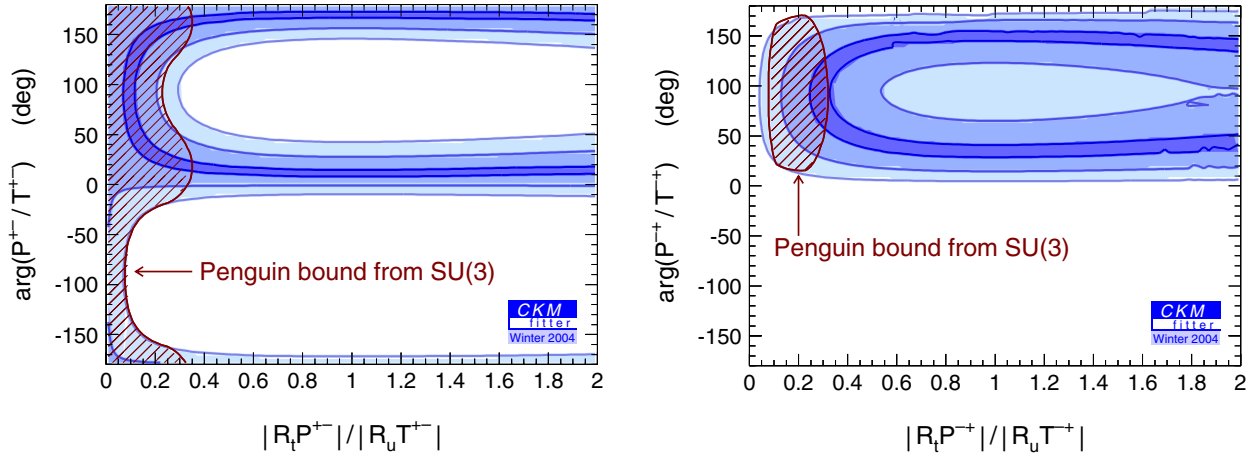

Fig. 44. Confidence levels in the complex planes $|R_t/R_u|(P^{+-}/T^{+-})$ (left) and $|R_t/R_u|(P^{-+}/T^{-+})$ (right), using α from the standard CKM fit as input. Dark, medium and light shaded areas have $CL > 0.90$, 0.32 and 0.05, respectively. Shown by the hatched areas are the corresponding $CL > 0.05$ regions obtained when using in addition SU(3) flavor symmetry (Scenario (II), see Sect. 4.5)

P^{-+}/T^{-+} complex plane (right hand plot). Due to the negative values of the direct CP-violating asymmetries (161) (cf. Table 11), positive strong phases are preferred for both ratios. Since the decays governed by the A^{-+} and $\overline{A}^{+-}$ amplitudes (for which the ρ meson contains the spectator quark) exhibit larger direct CPV, more sizable penguin-to-tree ratios are required here. The characteristic hyperbolic shapes of the constraints is due to the fact that direct CP violation is the product of penguin-to-tree ratio and strong phase difference. Also shown in Fig. 44 are the CL > 0.05 regions obtained when using SU(3) flavor symmetry and neglecting OZI-suppressed annihilation terms, which due to the CKM-favored penguin amplitudes provides improved bounds (see the discussion in Sect. 4.5).

4.4 SU(2) symmetry

Similarly to the Gronau-London analysis in $B \to \pi\pi$ and longitudinally polarized $B \to \rho\rho$ decays [141], the full isospin analysis of $B \to \rho\pi$ decays allows one to constrain the angle α up to discrete ambiguities [267]. However, instead of a triangular isospin relation, a pentagon has to be determined in the complex plane, which reduces the sensitivity to α.

4.4.1 Isospin analysis

The SU(2) flavor decomposition of the neutral and charged $B \to \rho\pi$ amplitudes is given, e.g., in [267,201]. Here we recall only the relevant relations, which complete (158)

$$2A^{00} \equiv 2A(B^0 \to \rho^0\pi^0) = V_{ud}V_{ub}^* T_{\rm C}^{00} - V_{td}V_{tb}^* \left(P^{+-} + P^{-+}\right) ,$$

$$\sqrt{2}A^{0+} \equiv \sqrt{2}A(B^+ \to \rho^0\pi^+) = V_{ud}V_{ub}^* T^{0+} - V_{td}V_{tb}^* \left(P^{+-} - P^{-+}\right) \ , \tag{177}$$
$$\sqrt{2}A^{+0} \equiv \sqrt{2}A(B^+ \to \rho^+\pi^0) = V_{ud}V_{ub}^* \left(T^{+-} + T^{-+} + T_{\rm C}^{00} - T^{0+}\right) + V_{td}V_{tb}^* \left(P^{+-} - P^{-+}\right) \ ,$$

and equivalently for the CP-conjugated amplitudes. The amplitudes satisfy the pentagonal relations

$$\sqrt{2}\left(A^{+0} + A^{0+}\right) = 2A^{00} + A^{+-} + A^{-+} \ ,$$
$$\sqrt{2}\left(\overline{A}^{+0} + \overline{A}^{0+}\right) = 2\overline{A}^{00} + \overline{A}^{+-} + \overline{A}^{-+} \ . \tag{178}$$

As in the case of $B \to \pi\pi$, the color-suppressed mode $B^0 \to \rho^0\pi^0$ constrains the (sum of the) penguin contributions to $B^0 \to \rho^\pm\pi^\mp$. The above isospin relations take advantage of the fact that QCD penguins can only mediate $\Delta I = 1/2$ transitions in the SU(2) limit. Electroweak penguins, that we neglect here (see Footnote 57 in Sect. VI.4), can have $\Delta I = 3/2$ and would thus lead to additional terms proportional to $V_{td}V_{tb}^*$.

Information counting results in 12 unknowns (6 complex amplitudes and the weak phase $\alpha = \pi - \beta - \gamma$ minus one arbitrary global phase), and 13 observables for the complete SU(2) analysis. The isospin analysis constrains the weak phase α up to discrete ambiguities, which however are not necessarily degenerate thanks to the fact that the system is over-determined (all observables are experimentally accessible). This is similar to the $B \to \rho\rho$ system (cf. Sect. VI.5).

4.4.2 SU(2) bounds

Using the SU(2) relations and the CP-averaged branching fractions, one can derive simple bounds on the deviation from α induced by the penguin contributions [143,268]

$$|\alpha - \alpha_{\rm eff}^\pm| \ \leq \ \frac{1}{2}\arccos\left[\frac{1}{\sqrt{1 - {\mathcal{A}_{\rho\pi}^\pm}^2}}\left(1 - 4\frac{\mathcal{B}_{\rho\pi}^{00}}{\mathcal{B}_{\rho\pi}^\pm}\right)\right] \ , \tag{179}$$

where we use the CP-averaged quantities

$$2\alpha_{\rm eff}^\pm \equiv \arg\left[\frac{q}{p}\frac{\overline{A}^{+-} + \overline{A}^{-+}}{A^{+-} + A^{-+}}\right] \ , \tag{180}$$

$$\mathcal{A}_{\rho\pi}^\pm \equiv \frac{|\overline{A}^{+-} + \overline{A}^{-+}|^2 - |A^{-+} + A^{+-}|^2}{|\overline{A}^{+-} + \overline{A}^{-+}|^2 + |A^{-+} + A^{+-}|^2} \ , \tag{181}$$

$$\mathcal{B}_{\rho\pi}^\pm \propto \frac{\tau_{B^0}}{4}\left(|A^{+-} + A^{-+}|^2 + |\overline{A}^{-+} + \overline{A}^{+-}|^2\right) \ . \tag{182}$$

The latter two cannot be experimentally determined in a quasi-two-body analysis since they involve the relative phases $\arg[\kappa^{-+}\lambda^{+-*}]$ and $\arg[\kappa^{+-}\lambda^{+-*}]$, which depend on the interference between the two charge states $\rho^+\pi^-$ and $\rho^-\pi^+$ in the Dalitz plot. Indirect isospin constraints on $\mathcal{B}_{\rho\pi}^\pm$ and $\mathcal{A}_{\rho\pi}^\pm$ using the current results (Table 11) are insignificant [252]. As a consequence, no useful constraint on $|\alpha - \alpha_{\rm eff}^\pm|$ is obtained from the bound (179).

The presently available experimental information is insufficient to obtain a meaningful constraint on α. We thus attempt to give an outlook to future integrated luminosities accumulated at the B factories.

4.4.3 Prospects for the full isospin analysis

To perform an educated study of the full isospin analysis, we assume $\alpha = 94^\circ$ and a set of generating decay amplitudes chosen (arbitrarily) to approximately reproduce the experimental results given in Table 11. We obtain from these amplitudes the inputs

$$\begin{aligned}
\mathcal{B}_{\rho\pi}^{\pm\mp} &= 22.8 \pm 0.82\ [0.26]\ , & \mathcal{A}_{\rho\pi} &= -0.12 \pm 0.025\ [0.13]\ , & C_{\rho\pi}^{00} &= \ \ 0.66 \pm 0.162\ [0.056]\ ,\\
\mathcal{B}_{\rho\pi}^{00} &= \ \ 1.2 \pm 0.19\ [0.06]\ , & C_{\rho\pi} &= \ \ 0.41 \pm 0.052\ [0.029]\ , & S_{\rho\pi}^{00} &= -0.69 \pm 0.222\ [0.072]\ ,\\
\mathcal{B}_{\rho\pi}^{+0} &= \ \ 8.6 \pm 0.76\ [0.24]\ , & \Delta C_{\rho\pi} &= \ \ 0.20 \pm 0.052\ [0.029]\ , & \mathcal{A}_{\rho\pi}^{+0} &= -0.29 \pm 0.051\ [0.028]\ ,\\
\mathcal{B}_{\rho\pi}^{0+} &= 16.5 \pm 0.40\ [0.13]\ , & S_{\rho\pi} &= -0.12 \pm 0.065\ [0.026]\ , & \mathcal{A}_{\rho\pi}^{0+} &= -0.16 \pm 0.032\ [0.013]\ ,\\
& & \Delta S_{\rho\pi} &= \ \ 0.30 \pm 0.065\ [0.016]\ , & &
\end{aligned}$$

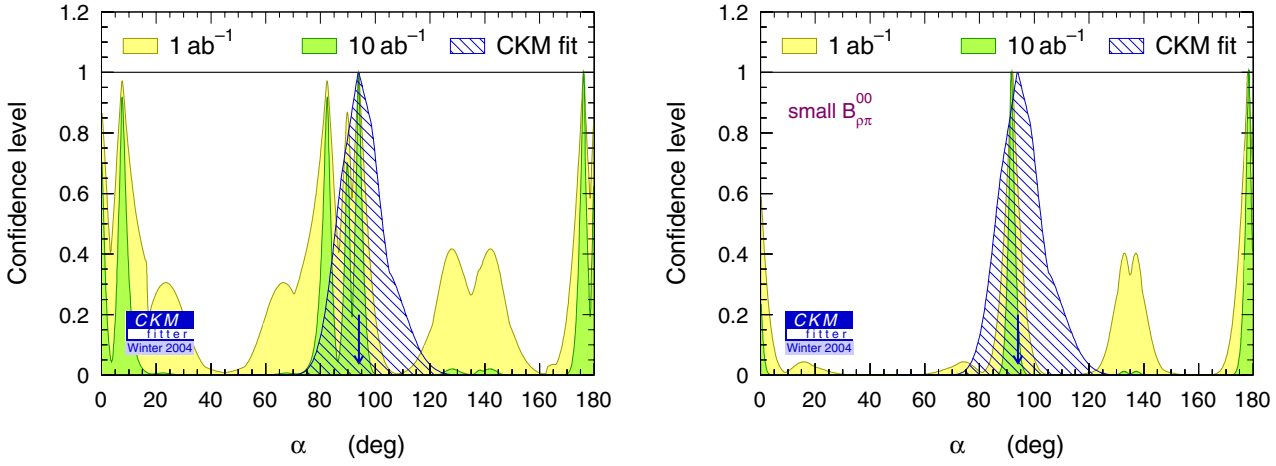

Fig. 45. *Left*: constraint on α using the full $B \to \rho\pi$ isospin analysis and assuming projections into future integrated luminosities of $1\,\mathrm{ab}^{-1}$ and $10\,\mathrm{ab}^{-1}$. The assumptions made on the generating amplitudes are given in the text. The arrow indicates the true value of α used for the generation of the toy observables. The hatched area shows the constraint obtained from the present standard CKM fit. *Right*: same as left hand plot but with a ten times smaller $\mathcal{B}^{00}_{\rho\pi}$

where the errors are extrapolated to integrated luminosities of $1\,\mathrm{ab}^{-1}$ [$10\,\mathrm{ab}^{-1}$]. The statistical errors are assumed to scale with the inverse of the square-root of the integrated luminosity. The systematic uncertainties are dominated by the limited knowledge of the backgrounds arising from other B decays. Because this knowledge, however, improves when more data become available, the related uncertainty is assumed to decrease like the statistical errors. We neglect possible irreducible systematics from tracking and neutral reconstruction efficiencies or other effects. For the CP parameters, we assume the systematics decrease with the square root of the luminosity up to $1\,\mathrm{ab}^{-1}$ due to an improved knowledge of the CP content of the primary B-background modes, but then do not decrease any further since unknown effects, like CP violation on the tag side, become dominant.

We derive the constraints on α shown in the left hand plot of Fig. 45. A wide range of solutions exists besides the true value α, indicated by the arrow. The right hand plot of Fig. 45 shows the CLs obtained for α when the branching fraction of $B^0 \to \rho^0\pi^0$ is below the experimental sensitivity ($\mathcal{B}^{00}_{\rho\pi} = 0.1 \times 10^{-6}$). The constraint improves compared to the previous case.

The conclusions drawn from this exercise are similar to what has been observed in $B^0 \to \pi^+\pi^-$ decays: unless the branching fraction $\mathcal{B}^{00}_{\rho\pi}$ is very small (even smaller than expected from the color-suppression mechanism), very large statistics is needed to significantly constrain α from $\rho\pi$ data alone using the quasi-two-body isospin analysis. It is effectively beyond the reach of the first generation B factories.

4.5 SU(3) flavor symmetry

Similarly to the studies in $B^0 \to hh'$ decays, one can use SU(3) flavor symmetry and dynamical hypotheses to obtain additional information on the penguin amplitudes contributing to $B^0 \to \rho^\pm\pi^\mp$.

4.5.1 Estimating $|P^{+-}|$ and $|P^{-+}|$ from $B^0 \to \rho^- K^+$ and $B^0 \to K^{*+}\pi^-$

As proposed in [143], the penguin amplitudes in $B^0 \to \rho^\pm\pi^\mp$ can be more effectively constrained with the use of the corresponding charge states in $b \to u\bar{u}s$ transitions, namely the decays $B^0 \to K^{*+}\pi^-$ and $B^0 \to \rho^- K^+$ (Scenario (II)) for which the amplitudes read

$$\begin{aligned} A^{+-}_{K^*\pi} &\equiv A(B^0 \to K^{*+}\pi^-) = V_{us}V^*_{ub}T^{+-}_{K^*\pi} + V_{ts}V^*_{tb}P^{+-}_{K^*\pi}\,, \\ A^{-+}_{\rho K} &\equiv A(B^0 \to \rho^- K^+) = V_{us}V^*_{ub}T^{-+}_{\rho K} + V_{ts}V^*_{tb}P^{-+}_{\rho K}\,. \end{aligned} \tag{183}$$

Under the assumption of SU(3) flavor symmetry, and neglecting OZI-suppressed penguin annihilation diagrams (see right hand diagram in Fig. 21), which contribute to $B \to \rho\pi$ but not to $B \to \rho K, K^*\pi$, the penguin amplitudes in (183) and those entering A^{+-} (A^{-+}) are equal (Scenario (II)):

$$P^{+-} = P^{+-}_{K^*\pi}\,, \qquad P^{-+} = P^{-+}_{\rho K}\,. \tag{184}$$

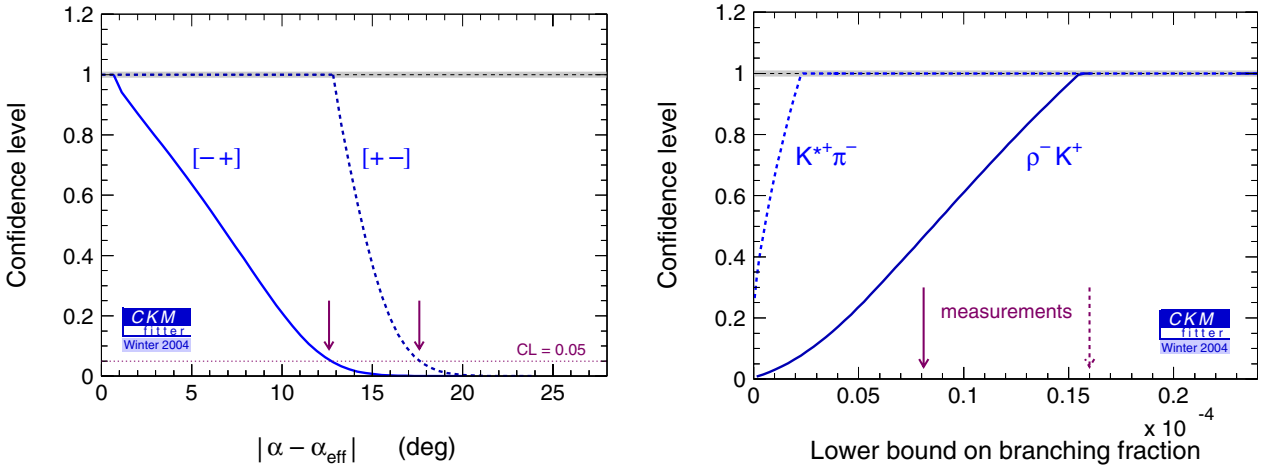

Fig. 46. *Left*: Confidence levels for the SU(3) bounds (185) (dashed line) and (186) (solid line). The arrows indicate the $CL = 0.05$ crossing values given in (187). *Right*: Lower bounds on the branching fractions $\mathcal{B}^{+-}_{K^{*}\pi}$ (dashed line) and $\mathcal{B}^{-+}_{\rho K}$ (solid line) obtained with the use of SU(3) symmetry and inserting α from the standard CKM fit. The arrows indicate the corresponding experimental values (same line types)

This leads to the bounds [143]

$$|\alpha - \alpha^{+-}_{\rm eff}| \leq \frac{1}{2}\arccos\left[\frac{1}{\sqrt{1-\mathcal{A}^{+-\,2}_{\rho\pi}}}\left(1-2\lambda^2\frac{\mathcal{B}^{+-}_{K^{*}\pi}}{\mathcal{B}^{+-}_{\rho\pi}}\right)\right] , \tag{185}$$

$$|\alpha - \alpha^{-+}_{\rm eff}| \leq \frac{1}{2}\arccos\left[\frac{1}{\sqrt{1-\mathcal{A}^{-+\,2}_{\rho\pi}}}\left(1-2\lambda^2\frac{\mathcal{B}^{-+}_{\rho K}}{\mathcal{B}^{-+}_{\rho\pi}}\right)\right] , \tag{186}$$

where λ is the Wolfenstein parameter. Compared to the bound (179), the above SU(3) bounds benefit from the relative CKM enhancement (suppression) of the penguin (tree) amplitudes in the strange modes with respect to the $b \to u$ transitions. The left-hand plot of Fig. 46 shows the CLs for $|\alpha - \alpha^{+-}_{\rm eff}|$ and $|\alpha - \alpha^{-+}_{\rm eff}|$ obtained with the use of the results for the branching fractions given in Table 11. At 95% CL, we find[61]

$$|\alpha - \alpha^{+-}_{\rm eff}| < 17.6^\circ , \qquad |\alpha - \alpha^{-+}_{\rm eff}| < 12.6^\circ , \tag{187}$$

which are more restrictive than the corresponding bounds obtained in the $\pi\pi$ system (see Sect. VI.1.4)

Owing to the fact that non-zero direct CPV requires sizable penguin contributions, we can reverse the procedure and infer lower limits on $\mathcal{B}^{+-}_{K^{*}\pi}$ and $\mathcal{B}^{-+}_{\rho K}$, using SU(3) and inserting α from the standard CKM fit. The CLs obtained for both branching fractions are shown in the right hand plot of Fig. 46. The arrows indicate the corresponding measurements. As expected, the relatively large CP asymmetry $\mathcal{A}^{-+}_{\rho\pi}$ requires an increased $\mathcal{B}^{-+}_{\rho K}$, while no useful lower bound is obtained for $\mathcal{B}^{+-}_{K^{*}\pi}$. Although compatible within the rather large experimental errors (CL = 0.46), one can conclude from this observation that if the SU(3) picture holds within the SM, improved statistics is expected to give a lower value of $|\mathcal{A}^{-+}_{\rho\pi}|$ than the current one, since $\mathcal{B}^{-+}_{\rho K}$ is already known to good precision. Following the same line, we have attempted to obtain a lower bound on the branching fraction $\mathcal{B}^{00}_{\rho\pi}$, which is however insignificant at present [252]. In turn, we have attempted in Fig. 47 to use the CP-conserving branching fractions $\mathcal{B}^{+-}_{\rho\pi}$ and $\mathcal{B}^{-+}_{\rho\pi}$ as the only experimental input (or equivalently $\mathcal{B}^{\pm\mp}_{\rho\pi}$, $\Delta C_{\rho\pi}$ and the CP-conserving product $C_{\rho\pi}\cdot\mathcal{A}_{\rho\pi}$) as well as their SU(3) partners $\mathcal{B}^{+-}_{K^{*}\pi}$ and $\mathcal{B}^{-+}_{\rho K}$, to infer bounds[62] on $\mathcal{A}^{+-}_{\rho\pi}$ and $\mathcal{A}^{-+}_{\rho\pi}$. Since branching fractions are not sensitive to the sign of direct CPV, the figure is symmetric around the zero axes. We determine the allowed domains (CL > 0.05)

[61] Note that the numerical analysis performed with CKMfitter does not explicitly involve (185) and (186), since the full amplitude parameterizations are implemented. Fitting all experimental results to these amplitudes, and using the SU(3) constraints (184), automatically reproduces the analytical bounds.

[62] The analytical SU(3) bounds on the direct CP asymmetries read

$$\mathcal{A}^{+-}_{\rho\pi} < \sqrt{1-\left(1-2\lambda^2\frac{\mathcal{B}^{+-}_{K^{*}\pi}}{\mathcal{B}^{+-}_{\rho\pi}}\right)^2} , \qquad \mathcal{A}^{-+}_{\rho\pi} < \sqrt{1-\left(1-2\lambda^2\frac{\mathcal{B}^{-+}_{\rho K}}{\mathcal{B}^{-+}_{\rho\pi}}\right)^2} .$$

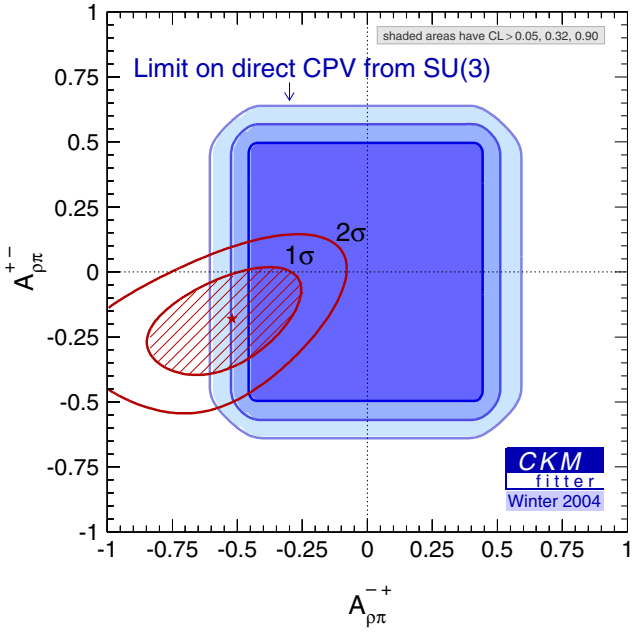

Fig. 47. The direct CP-violating asymmetries $\mathcal{A}_{\rho\pi}^{+-}$ versus $\mathcal{A}_{\rho\pi}^{-+}$ bound using SU(3) flavor symmetry and the measured flavor-specific branching ratios (176) as the only input. Dark, medium and light shaded areas have $CL > 0.90$, 0.32 and 0.05, respectively. Also shown are the experimental values found by *BABAR*

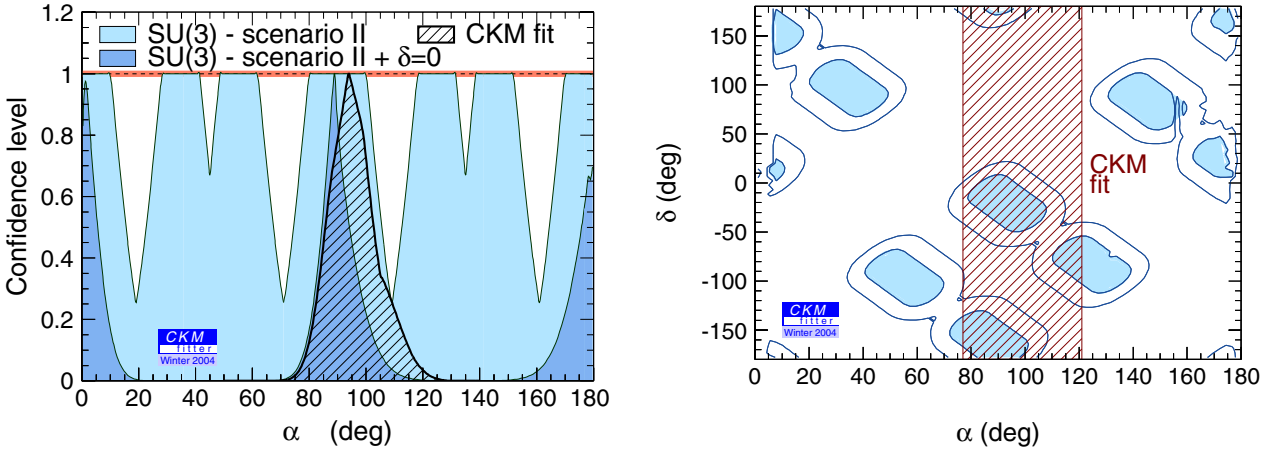

Fig. 48. *Left*: confidence levels obtained for α with the use of SU(3) flavor symmetry within Scenario (II). The light shaded curve gives the nominal constraint, while the dark shaded one corresponds to the solutions one would obtain if the relative strong phase $\hat{\delta}$ were known and equal to zero. The hatched area shows the constraint obtained from the CKM fit using the standard constraints (cf. Part III). *Right*: correlation between α and $\hat{\delta}$. The shaded areas indicate $CL = 0.32$ domains and the solid lines show the $CL = 0.05$ regions. The periodicity is $\Delta\alpha = 45^\circ$ and $\Delta\hat{\delta} = 90^\circ$. The hatched area depicts the $CL \leq 0.05$ allowed region for α obtained from the CKM fit using the standard constraints (cf. Part III)

$$|\mathcal{A}_{\rho\pi}^{+-}| < 0.64\ , \qquad |\mathcal{A}_{\rho\pi}^{-+}| < 0.59\ . \tag{188}$$

Using the results given in Table 11 and the relations (184), we can set CLs for α. We obtain six ambiguous solutions shown by the light shaded region in the left hand plot of Fig. 48. The widths of the plateaus represent the uncertainties $|\alpha - \alpha_{\rm eff}^{+-(-+)}|$ determined by the bounds (185) and (186). The bounds on $|\alpha - \alpha_{\rm eff}^{+-(-+)}|$ are not good enough to resolve all the eight ambiguities, which are partially merged. The $\chi^2_{\rm min} = 0.3$ for the best fit is satisfactory. Fixing arbitrarily the penguin amplitudes to zero results in the significantly worse $\chi^2_{\rm min} = 8.8$. Also shown in the figure is the solution obtained when fixing the relative strong phase $\hat{\delta}$ to zero. Good agreement with the standard CKM fit is observed.

It is interesting to correlate α with the relative strong phase $\hat{\delta}$ between A^{-+} and A^{+-} (cf. (166)). The corresponding CLs are shown in the right hand plot of Fig. 48. We observe a structure of distinctive islands, and, when using the SM constraint (cf. Table 2) on α, we conclude that values of $\hat{\delta} = 0, \pi$ are preferred, one of which ($\hat{\delta} = 0$) is in conformity with expectations from factorization. If $\hat{\delta}$ were given by theory or determined experimentally through a Dalitz plot analysis [253], SU(3) symmetry would result in a useful constraint on α.

4.5.2 Estimating $|P^{+-}|$ and $|P^{-+}|$ from $B^+ \to \rho^+ K^0$ and $B^+ \to K^{*0}\pi^+$

The magnitude of the penguin amplitudes $|P^{+-}|$ and $|P^{-+}|$ can be estimated from the branching fraction of the penguin-dominated decays $B^+ \to \rho^+ K^0$ and $B^+ \to K^{*0}\pi^+$ (Scenario (III)). Neglecting the doubly CKM-suppressed u penguins and annihilation diagrams, the transition amplitudes for these modes are given by

$$\begin{aligned} A_K^{+0} &\equiv A(B^+ \to \rho^+ K^0) = V_{tb}^* V_{ts} P_{\rho K}^{+0} \ , \\ A_K^{0+} &\equiv A(B^+ \to K^{*0}\pi^+) = V_{tb}^* V_{ts} P_{K^*\pi}^{0+} \ . \end{aligned} \tag{189}$$

Correspondingly to the relation (126) and within the same hypotheses, one has

$$\begin{aligned} |P^{+-}| &= \frac{1}{\sqrt{r_\tau}} \frac{f_\rho}{f_{K^*}} \frac{1}{R^{+-}} |P_{K^*\pi}^{0+}|, \\ |P^{-+}| &= \frac{1}{\sqrt{r_\tau}} \frac{f_\pi}{f_K} \frac{1}{R^{-+}} |P_{\rho K}^{+0}|, \end{aligned} \tag{190}$$

where the correction factors R^{+-} and R^{-+} are both fixed to $R = 0.95 \pm 0.23$ (for simplicity we choose the same value as in (126)), but they vary independently in the fit within their theoretical errors. For the $\rho(770)$ and the $K^*(892)$ decay constants we use $f_\rho = (209 \pm 1)$ MeV and $f_{K^*} = (218 \pm 4)$ MeV [135], respectively.

The branching fractions of these modes are given in Table 11. Figure 49 shows the constraints obtained on α for Scenario (III). Since only an upper limit exists for $B^+ \to \rho^+ K^0$, for illustration purpose we assign the value (and error) of $\mathcal{B}(B^0 \to \rho^- K^+)$ to that branching fraction. Note that the number of peaks doubles from eight to sixteen when using $B^+ \to \rho^+ K^0$ since it determines the magnitude of the penguin amplitude rather than an upper limit only (as does Scenario (II)). We draw the following conclusions from this exercise:

- the constraint on α will be improved when the measurement of the branching ratio to $\rho^+ K^0$ is available.
- the uncertainties on the correction factors R^{+-} and R^{-+} do not much degrade the constraints on α, i.e., theoretical uncertainties appear to be subdominant for Scenario (III).
- in all SU(3) scenarios, a precise determination of α would be obtained if the relative strong phase $\hat{\delta}$ were known (for example from a Dalitz plot analysis [253] or from theory [135]), in which case the rôle of the errors on the ratios $R^{\pm}$ may become important. However, without this additional input, the constraints obtained by the different approaches are insignificant.

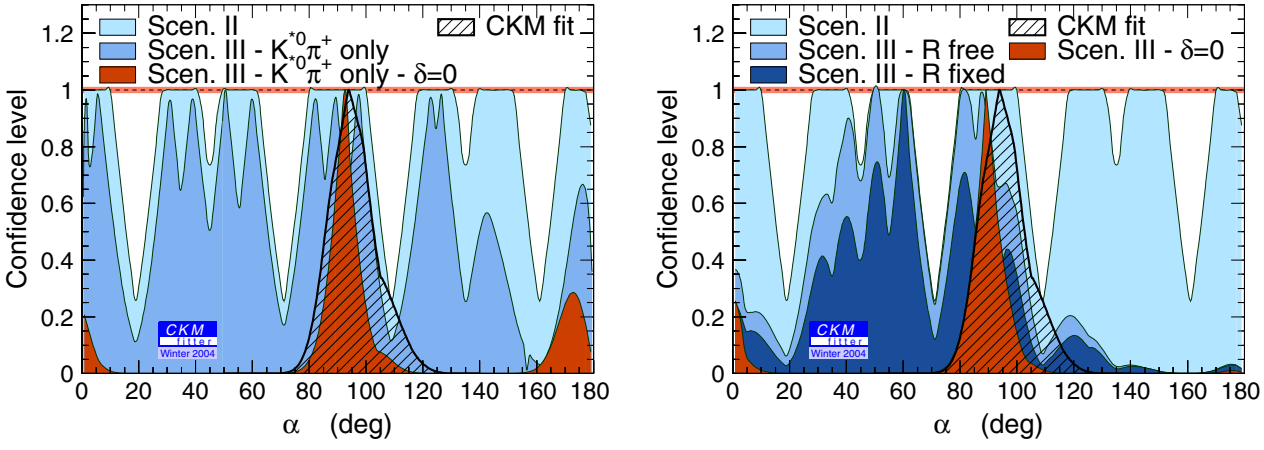

Fig. 49. Confidence levels obtained for α with the use of SU(3) flavor symmetry. *Left*: Scenario (II) (light shaded, same as in left hand plot of Fig. 48), Scenario (III) but only using $B^+ \to K^{*0}\pi^+$ to constrain $|P^{+-}|$ (medium shaded), and Scenario (III) as previous case and assuming in addition that the relative strong phase $\hat{\delta}$ is zero (dark shaded). *Right*: Scenario (II) (light shaded, same as left plot); the medium and medium-dark shaded curves correspond to Scenario (III) with SU(3) constraints on both penguins amplitudes from $B^+ \to K^{*0}\pi^+$ and $B^+ \to \rho^+ K^0$, where we assume for that latter mode (which has not yet been seen) that the branching fraction is equal to the one of $B^0 \to \rho^- K^+$. Medium shaded is for R that varies freely within its uncertainties, while medium-dark shaded is for fixed R. The dark shaded curve gives the result of the previous case when assuming $\hat{\delta} = 0$. In both plots, the hatched area indicates the constraint obtained from the standard CKM fit

5 Analysis of $B \to \rho\rho$ decays

The isospin analysis of $B \to \rho\rho$ decays leads to the extraction of α in a way similar to $B \to \pi\pi$ decays [267]. The specific interest of these channels lies in the potentially small penguin contribution, which is theoretically expected [266] and indirectly confirmed by the smallness of the experimental upper bound on the $B^0 \to \rho^0\rho^0$ branching fraction [147] with respect to the branching fractions of $B^0 \to \rho^+\rho^-$ and $B^+ \to \rho^+\rho^0$ [147,148,145,62]. In addition, and more importantly for a precision measurement, both direct and mixing-induced CP-violating asymmetries of the color-suppressed decay $B^0 \to \rho^0\rho^0$ are experimentally accessible.

The analysis is complicated by the presence of three helicity states for the two vector mesons. One corresponds to longitudinal polarization and is CP-even. Two helicity states are transversely polarized and are admixtures of CP-even and CP-odd amplitudes. In the transversity frame [269], one amplitude accounts for parallel transverse polarization and the other for perpendicular transverse polarization of the vector mesons, with respect to the transversity axis: the first is CP-even and the second CP-odd. Hence the perpendicular polarization (if not identified or zero) dilutes the CP measurement. By virtue of the helicity suppression, the fraction of transversely polarized ρ mesons is expected to be of the order of $(\Lambda_{\rm QCD}/m_B)^2 \sim 2\%$ in the factorization approximation [135,270] supplemented by the symmetry relations between heavy-to-light form factors in the asymptotic limit [271]. This has been confirmed by experiment in $B^+ \to \rho^+\rho^0$ [147,148] and $B^0 \to \rho^+\rho^-$ [145] decays that are both found to be dominantly longitudinally polarized. As a consequence, one is allowed to restrict the SU(2) analysis described in Sect. VI.1.2.1, without significant loss of sensitivity, to the longitudinally polarized states of the $B \to \rho\rho$ system. This also applies to the treatment of electroweak penguins.

The isospin analysis relies on the separation of the tree-level amplitudes ($I = 0$ and $I = 2$) from the penguin-type amplitudes ($I = 0$), since Bose statistics ensures that no odd isospin amplitude is present in two identical meson final states. It has been pointed out in [152] that due to the finite width of the ρ meson, $I = 1$ contributions can occur in $B \to \rho\rho$ decays. Although no prediction is made, one may expect these to be of the order of $(\Gamma_\rho/m_\rho)^2 \sim 4\%$. In the following, we first neglect $I = 1$ contributions, and later present a preliminary study including these effects in Sect. VI.5.4. Also neglected is isospin violation due to the strong interaction as well as effects from the interference with the radial excitations of the ρ, with other $\pi\pi$ resonances and with a non-resonant component; in the future these effects may be studied by the experiments since they depend on the specific analysis requirements.

5.1 Theoretical framework and experimental input

Due to the lack of experimental information, an SU(3) analysis is not feasible at present (the branching fractions of the SU(3) partners $B^0 \to K^{*+}\rho^-$ and the penguin-dominated $B^+ \to K^{*0}\rho^+$ have not been published yet). We hence restrict the numerical analysis to isospin symmetry corresponding to Scenario (I) (cf. Sect. VI.1.2), which is however significantly more fruitful than for the $B \to \pi\pi$ system.

The experimental results used here are collected in Sect. III.2.11. The main ingredient is the measurement of $\sin 2\alpha_{\rm eff}$ from the time-dependent CP and polarization analysis of $B^0 \to \rho^+\rho^-$ decays performed by *BABAR* [149,145].

5.2 Numerical results

We present the CLs obtained from the isospin analysis of $B \to \rho\rho$ decays as a function of α (Fig. 50) and in the $(\overline{\rho}, \overline{\eta})$ plane (left hand plot of Fig. 52). On both figures, the standard CKM fit (excluding the $B \to \rho\rho$ data) is superimposed

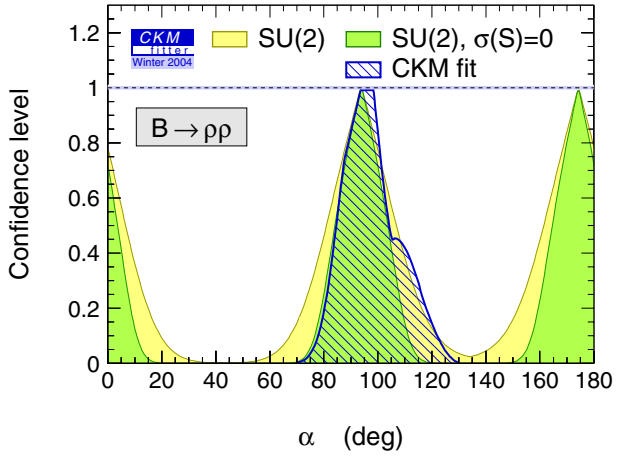

Fig. 50. Confidence levels for α from the SU(2) analysis of the $B \to \rho\rho$ system (light shaded). The dark-shaded function is obtained by setting the error on $S^{+-}_{\rho\rho,L}$ to zero. It hence represents the uncertainty due to the penguin contribution ($\Delta\alpha$). Also shown is the prediction from the standard CKM fit (hatched area), which includes the world average for $\sin 2\beta$ but ignores the $B \to \rho\rho$ data

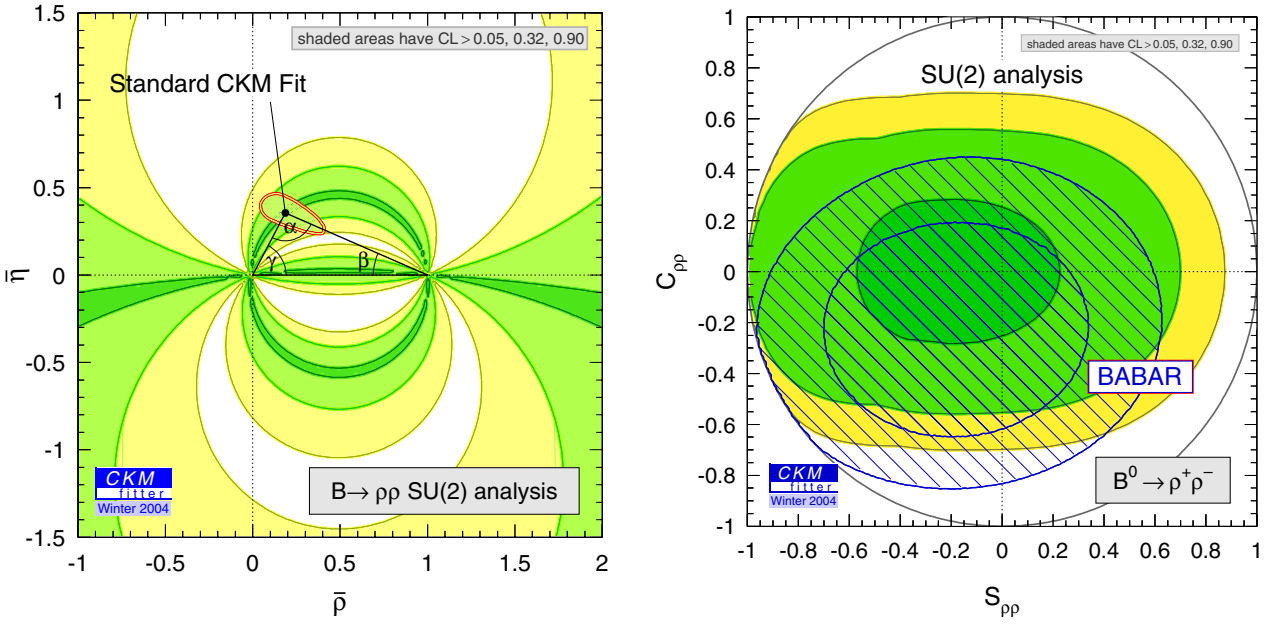

Fig. 51. Confidence levels from the SU(2) analysis of the $B \to \rho\rho$ system. Dark, medium and light shaded areas have $CL > 0.90$, 0.32, 0.05, respectively. *Left*: constraints in the $(\overline{\rho}, \overline{\eta})$ plane. Overlaid is the prediction from the standard CKM fit, which includes the world average for $\sin 2\beta$ but not the $B \to \rho\rho$ data. *Right*: constraints in the $(S^{+-}_{\rho\rho,L}, C^{+-}_{\rho\rho,L})$ plane, with the input values for $\overline{\rho}$ and $\overline{\eta}$ taken from the standard CKM fit. The circle indicates the physical limit ${S^{+-}_{\rho\rho,L}}^2 + {C^{+-}_{\rho\rho,L}}^2 = 1$, and the hatched area represents the CL of the *BABAR* measurement for which the presence of the physical boundary has been properly taken into account (see Sect. II.2.2.3). The contours correspond to 1σ and 2σ, respectively

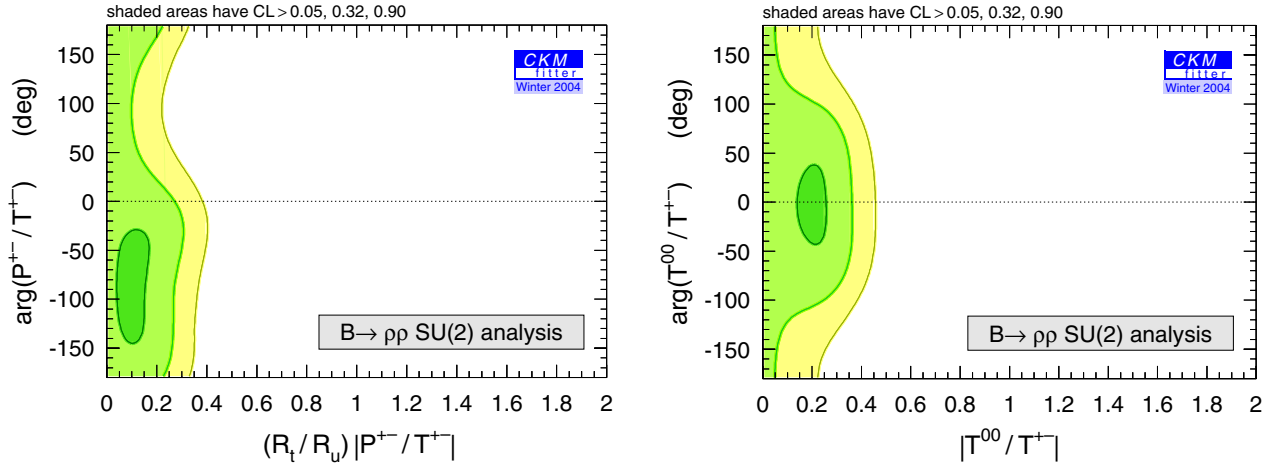

Fig. 52. Constraints on the penguin-to-tree ratio $(R_t/R_u)|P^{+-}/T^{+-}|$ and the relative strong phase $\arg[P^{+-}T^{+-*}]$ (left), and on the color-suppressed to color-allowed ratio $|T_C^{00}/T^{+-}|$ and the relative strong phase $\arg[T_C^{00}T^{+-*}]$ (right), obtained from the SU(2) analysis and using the result from the standard CKM fit as input. Dark, light and very light shaded areas have $CL > 0.90$, 0.32, 0.05, respectively

exhibiting agreement with the $B \to \rho\rho$ constraints and, remarkably, a comparable precision. The p-value of the measurements within the isospin framework (and the result from the standard CKM fit) is found to be 70%. The hatched curve in Fig. 50 is obtained by setting the error on $S^{+-}_{\rho\rho,\,L}$ to zero, thus reflecting the present uncertainty due to the penguin pollution (given the measurement of $C^{+-}_{\rho\rho,\,L}$ and of the branching ratios). From this, the 90% CL bound on $\Delta\alpha$ is found to be

$$-20^\circ \;<\; \Delta\alpha \;<\; 18^\circ \;. \tag{191}$$

Converting this into a result for α and taking the solution that is in agreement with the standard CKM fit, we find

$$\alpha \;=\; \left(94 \,\pm\, 12 \,\left[{}^{+28}_{-25}\right] \,\pm\, 13 \;[19]\right)^\circ \;,$$

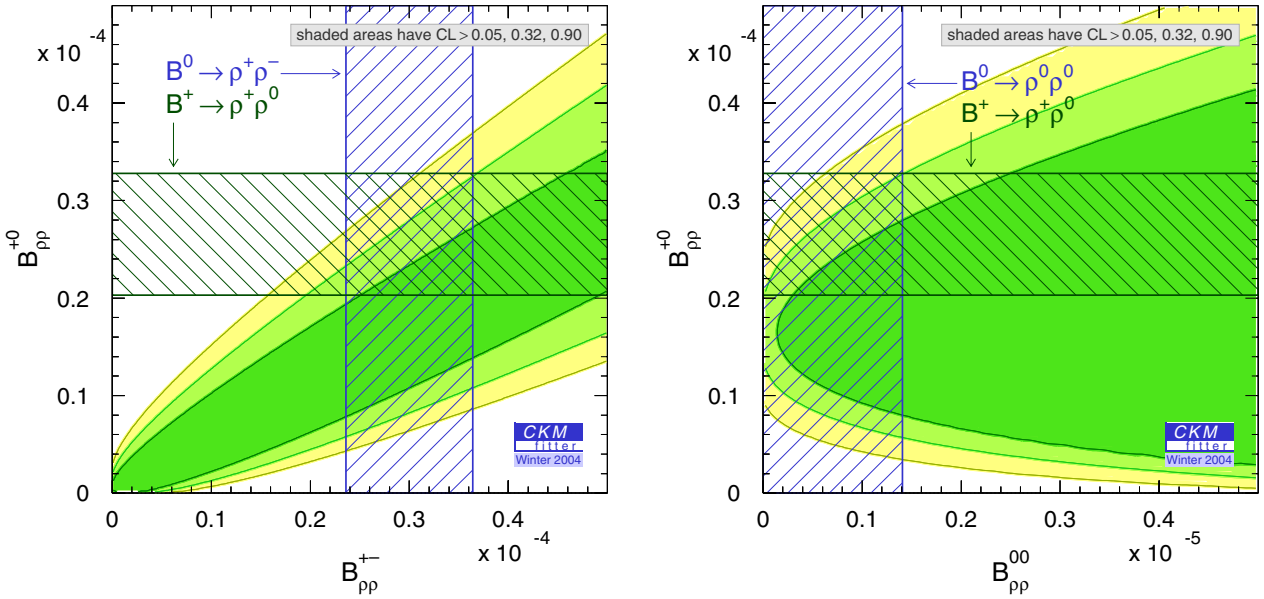

Fig. 53. Confidence levels for $\mathcal{B}(B^+ \to \rho^+\rho^0)$ versus $\mathcal{B}(B^0 \to \rho^+\rho^-)$ (left) and $\mathcal{B}(B^+ \to \rho^+\rho^0)$ versus $\mathcal{B}(B^0 \to \rho^0\rho^0)$ (right), obtained from the isospin analysis ignoring the branching fractions that are determined, and with the use of α from the standard CKM fit. The hatched areas indicate the 1σ bands of the corresponding measurements

where the first errors are experimental and the second due to the penguin uncertainty. For CL $> 10\%$ the overall uncertainty on α amounts to $19°$. Errors in brackets above are given at CL $> 5\%$ (2σ). The penguin error contains a systematic uncertainty of $0.2°$ (interpreted as a theory error by *R*fit) from the treatment of the electroweak penguins (see (121) in Sect. VI.1.2.1). The full shift on α introduced by $P^{\rm EW}$ amounts to $-2.1°$. Taking this into account our result agrees with the *BABAR* result [149]. The slightly larger experimental error here is explained by the difference in the central value of α.

Since the *CP*-violating asymmetries in $B^0 \to \rho^0\rho^0$ have not been measured, the isospin analysis is incomplete and one expects plateaus in the CL as a function of α. The width of these plateaus is driven by the GLSS bound (113). However, peaks are observed in Fig. 50, which is a consequence of the relative values of the three branching fractions: the tight upper limit on $\mathcal{B}(B^0 \to \rho^0\rho^0)$ implies that the sum of the color-suppressed and the penguin amplitudes is small so that $\mathcal{B}(B^+ \to \rho^+\rho^0) \sim 0.5 \times \mathcal{B}(B^0 \to \rho^+\rho^-)$, which is not confirmed by the central values of the measurements ($\mathcal{B}(B^+ \to \rho^+\rho^0)/\mathcal{B}(B^0 \to \rho^+\rho^-) = 0.88^{+0.21}_{-0.15}$). This "incompatibility" (which is well covered by the present experimental errors) lifts the degeneracy in the (infinite) solution space of α. See Fig. 53 for representations of the predictions obtained for $\mathcal{B}(B^+ \to \rho^+\rho^0)$ versus $\mathcal{B}(B^0 \to \rho^+\rho^-)$ and $\mathcal{B}(B^+ \to \rho^+\rho^0)$ versus $\mathcal{B}(B^0 \to \rho^0\rho^0)$ from the isospin analysis combined with the standard CKM fit. The hatched areas give the 1σ bands of the present experimental averages.

Using the standard CKM fit as input (excluding $B \to \rho\rho$ therein) and the $B \to \rho\rho$ branching fraction measurements, one can obtain predictions for $S^{+-}_{\rho\rho,L}$ and $C^{+-}_{\rho\rho,L}$ by means of the isospin analysis. The corresponding CLs are shown in the right hand plot of Fig. 51 together with the measurement from *BABAR*. Due to the favorable bound on $\Delta\alpha$ (191), the SU(2) prediction turns out to be meaningful, in sharp contrast to the corresponding $\pi\pi$ case (cf. Fig. 25).

Constraints on amplitude ratios

By inserting α from the standard CKM fit we derive constraints on the complex amplitude ratios $(R_t/R_u)P^{+-}/T^{+-}$ and $T^{00}_{\rm C}/T^{+-}$. Their CLs in polar coordinates are given in Fig. 52. The smallness of the penguin-to-tree ratio becomes manifest on the left hand plot (although rather large values are still possible). The magnitude of the color-suppressed-to-color-allowed ratio (right hand plot) is found to be of the order of 0.2, in agreement with the naïve expectation. Comparing these plots with Figs. 26 and 27 in the $\pi\pi$ system seems to suggest a non-trivial dynamical mechanism, which drives the behavior of the penguin and color-suppressed amplitudes differently with respect to the leading tree in VV and PP modes. See Sect. VI.6 for further discussion of the amplitude ratios.

5.3 Prospects for the isospin analysis

As for $\pi\pi$ and $\rho\pi$, we attempt extrapolations of the isospin analysis to future integrated luminosities of $500\,\mathrm{fb}^{-1}$ and $1\,\mathrm{ab}^{-1}$. Note that the results strongly depend on the underlying physics, the knowledge of which is insufficient up to now. We understand the scenarios studied here are likely to be optimistic.

In the first scenario considered, with the exception of $\mathcal{B}(B^0 \to \rho^0\rho^0)$, all measurements are extrapolated with the use of the present central values. The branching fraction of $B^0 \to \rho^0\rho^0$ is increased to 1.3×10^{-6} to ensure the compatibility of all observables with the isospin relations (107). It is assumed to be dominated by longitudinal polarization with a longitudinal fraction of $f_L^{00} = 0.976$ (simple arithmetic average of f_L^{+-} and f_L^{+0}). We further assume that both time-dependent CP asymmetries in $B^0 \to \rho^0\rho^0$ are measured, and set them to $S^{00}_{\rho\rho,L} = 0.05$ and $C^{00}_{\rho\rho,L} = 0.70$, the preferred solutions of the standard CKM fit. The statistical and systematic uncertainties are extrapolated according to the luminosity increase. For $\mathcal{B}(B^0 \to \rho^0\rho^0)$, $\mathcal{B}(B^+ \to \rho^+\rho^0)$ and f_L^{+0}, we further reduce the extrapolated errors by a factor of 1.3 reflecting the improvement (at fixed statistics) in the most recent $B^0 \to \rho^+\rho^-$ analysis with respect to the previous one [146]. The errors for $S^{00}_{\rho\rho,L}$, $C^{00}_{\rho\rho,L}$ and f_L^{00} are estimated from $S^{+-}_{\rho\rho,L}$, $C^{+-}_{\rho\rho,L}$ and f_L^{+-}, respectively: they are scaled to the expected number of $B^0 \to \rho^0\rho^0$ events (taking into account the different selection efficiencies), except for the systematic uncertainties on $S^{00}_{\rho\rho,L}$ and $C^{00}_{\rho\rho,L}$, which are roughly estimated from the present values on $S^{+-}_{\rho\rho,\,L}$ and $C^{+-}_{\rho\rho,L}$. We obtain the extrapolations

$$\begin{aligned}
\mathcal{B}^{+-}_{\rho\rho} &= 30.0 \pm 1.6\ [1.1] \pm 2.0\ [1.4]\ , & f_L^{+-} &= 0.990 \pm 0.012\ [0.008] \pm 0.014\ [0.010]\ ,\\
\mathcal{B}^{+0}_{\rho\rho} &= 26.4 \pm 1.6\ [1.1] \pm 1.6\ [1.2]\ , & f_L^{+0} &= 0.962 \pm 0.014\ [0.010] \pm 0.011\ [0.008]\ ,\\
\mathcal{B}^{00}_{\rho\rho} &= 1.30 \pm 0.14\ [0.10] \pm 0.09\ [0.06]\ , & f_L^{00} &= 0.976 \pm 0.030\ [0.021] \pm 0.035\ [0.025]\ ,
\end{aligned}$$

$$\begin{aligned}
S^{+-}_{\rho\rho,L} &= -0.19 \pm 0.16\ [0.11] \pm 0.05\ [0.04]\ , & C^{+-}_{\rho\rho,L} &= -0.23 \pm 0.11\ [0.08] \pm 0.07\ [0.05]\ ,\\
S^{00}_{\rho\rho,L} &= \ \ 0.05 \pm 0.39\ [0.28] \pm 0.08\ [0.06]\ , & C^{00}_{\rho\rho,L} &= \ \ 0.70 \pm 0.28\ [0.20] \pm 0.10\ [0.07]\ ,
\end{aligned}$$

where first errors given are statistical and second systematic. Errors outside [inside] the brackets are extrapolated to $500\,\mathrm{fb}^{-1}$ $[1\,\mathrm{ab}^{-1}]$ integrated luminosity.

The results of the isospin analyses corresponding to these inputs are shown in Fig. 54 (left hand plot). To illustrate the impact of the $S^{00}_{\rho\rho,L}$ measurement, we also give the result at $500\,\mathrm{fb}^{-1}$ ignoring $S^{00}_{\rho\rho,L}$ in the fit (hatched function). If neither $S^{00}_{\rho\rho,L}$ nor $C^{00}_{\rho\rho,L}$ were measured, a very similar constraint would be obtained as in the latter fit: only the tiny double-bumps in the hatched curves reflect the impact of $C^{00}_{\rho\rho,L}$. As for $\pi\pi$, very large statistics would be needed to resolve the discrete ambiguities when relying on $C^{00}_{\rho\rho,L}$ only. The main additional information on α is hence provided by $S^{00}_{\rho\rho,L}$, which is due to its linear dependence on $\sin 2\alpha$ (see the analytical solutions of the isospin analysis derived in Footnote 35 in Sect. VI.1.2.1). With this scenario, the (symmetrized) 1σ (resp. 2σ) uncertainty on α is expected to be of the order of 8° at $500\,\mathrm{fb}^{-1}$ and 6° at $1\,\mathrm{ab}^{-1}$ (resp. 16° and 10°), which is small enough so that the residual SU(2)-breaking effects discussed below have to be taken into account.

In a second scenario, the central value of $\mathcal{B}^{00}_{\rho\rho}$ is fixed to the present one (0.6×10^{-6}) and the branching fraction of the $B^+ \to \rho^+\rho^0$ mode is decreased to 17×10^{-6}, which is the value preferred by the present isospin analysis when using the standard CKM fit as input (see Fig. 53). The new set of extrapolations for the $\rho^+\rho^0$ and $\rho^0\rho^0$ modes are

$$\begin{aligned}
\mathcal{B}^{+0}_{\rho\rho} &= 17.0 \pm 1.3\ [0.9] \pm 1.3\ [1.0]\ , & f_L^{+0} &= 0.962 \pm 0.017\ [0.012] \pm 0.014\ [0.010]\ ,\\
\mathcal{B}^{00}_{\rho\rho} &= 0.60 \pm 0.09\ [0.07] \pm 0.06\ [0.04]\ , & f_L^{00} &= 0.976 \pm 0.044\ [0.031] \pm 0.051\ [0.037]\ ,
\end{aligned}$$

$$S^{00}_{\rho\rho,L} = 0.05 \pm 0.57\ [0.41] \pm 0.12\ [0.09]\ ,\ C^{00}_{\rho\rho,L} = 0.70 \pm 0.41\ [0.29] \pm 0.15\ [0.10]\ ,$$

where again errors outside [inside] the brackets are extrapolated to $500\,\mathrm{fb}^{-1}$ $[1\,\mathrm{ab}^{-1}]$ integrated luminosity. The constraints on α resulting from these extrapolations are shown in Fig. 54 (right hand plot). The (symmetrized) 1σ (resp. 2σ) errors on α obtained with this setup amount to 13° at $500\,\mathrm{fb}^{-1}$ and 7° at $1\,\mathrm{ab}^{-1}$ (resp. 19° and 16°). This is significantly worse than for the previous scenario, in which one benefits from an almost optimal bound on $\Delta\alpha$ since $\mathcal{B}^{00}_{\rho\rho} \approx \mathcal{B}^{00}_{\mathrm{GLSS}^-} = 1.25\times10^{-6}$, while for the second scenario the lower bound $\mathcal{B}^{00}_{\mathrm{GLSS}^-} = 0.20\times10^{-6}$ is rather different[63] from the central value of $\mathcal{B}^{00}_{\rho\rho}$. Furthermore, due to the small $\mathcal{B}^{00}_{\rho\rho}$ the precision on $S^{00}_{\rho\rho,L}$ is insufficient to effectively suppress the ambiguities.

[63] The values for $\mathcal{B}^{00}_{\mathrm{GLSS}^-}$ corresponding to the different scenarios are determined from (115), where we have used as inputs the branching fractions of the longitudinally polarized ρ's. Note that the upper bounds $\mathcal{B}^{00}_{\mathrm{GLSS}^+}$ correspond in both scenarios to very large $\mathcal{B}^{00}_{\rho\rho}$ that are excluded by experiment.

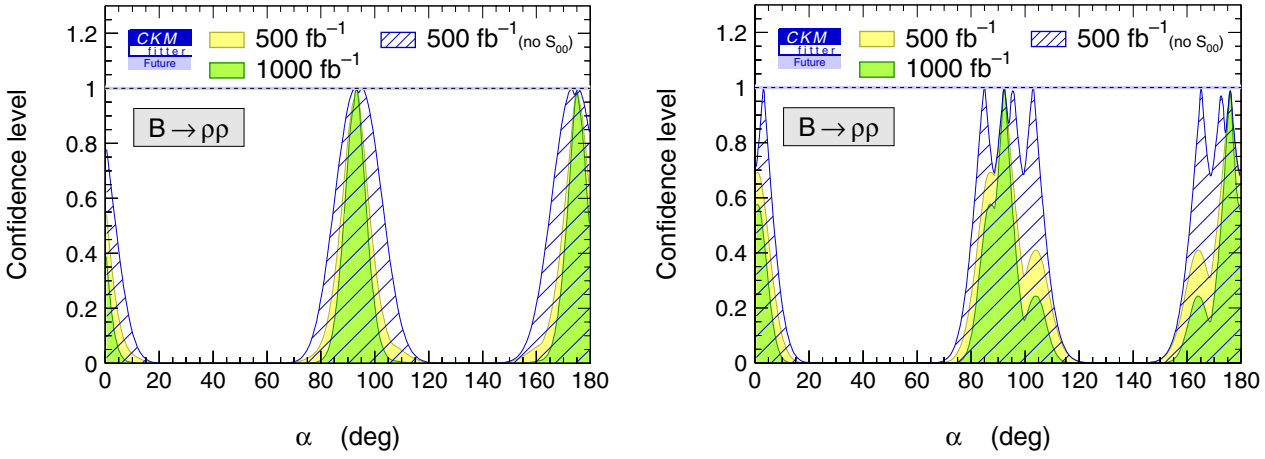

Fig. 54. Confidence level for α from the SU(2) analysis of the $B \to \rho\rho$ system, extrapolated at integrated luminosities of $500\,\mathrm{fb}^{-1}$ (light shaded) and $1\,\mathrm{ab}^{-1}$ (dark shaded). The two scenarios defined in the text are shown: the left (right) hand plot corresponds to a relatively large (small) value for $\mathcal{B}^{00}_{\rho\rho}$, each one compatible with a subset of the current measurements. To illustrate the impact of the $S^{00}_{\pi\pi}$ measurement, we also show the result at $500\,\mathrm{fb}^{-1}$ ignoring the latter input (hatched)

An important source of systematic uncertainty on the time-dependent CP-violating asymmetries is the CP violation exhibited by the B-related background modes [145], that may be hard to measure in the near future. To study its impact, we keep the size of this systematic error unchanged in the extrapolation, while all other systematic errors are appropriately scaled with the increasing luminosity. Applying this procedure to all time-dependent CP asymmetries, no significant deterioration of the accuracy on α is observed.

5.4 Breaking of the triangular relation in $B \to \rho\rho$

Gardner [203] presents a study of isospin-breaking effects in $B \to \pi\pi$ that come from the strong interaction, through the π^0–η–η' mixing. These effects break the triangular relation (107) and entail a systematic error on the angle α. The size of this error depends on the actual values of the non-leptonic matrix elements, and on the relative amount of the $I = 0$ component in the π^0 bound state, which could be of order 1–2%. In $B \to \rho\rho$ decays, besides a similar effect due to the ρ–ω mixing, it is argued in [152] that a $I = 1$ $\rho\rho$ state could be generated by the finite width of the ρ. Although the latter effect does not break isospin symmetry in the sense that it does not vanish in the $m_u = m_d$ limit, it can be parameterized the same way as above, through the introduction of an additional amplitude in the isospin triangle (107).

Hence we model a possible breaking of the closure of the isospin relation by a contribution ΔA^{+0} to the A^{+0} amplitude given by

$$\sqrt{2}\,\Delta A^{+0} \;=\; V_{ud}V^*_{ub}\,\Delta_T T^{+-} + V_{td}V^*_{tb}\,\Delta_P P^{+-}\;. \tag{192}$$

Note that for arbitrary values of the relative coefficients Δ_T and Δ_P, the above equation together with (95) and (106) is the most general parameterization of $B \to \pi\pi$ and $B \to \rho\rho$ decays within and beyond the Standard Model (see Footnote 70 in Sect. VII.3). In this Section however, we assume that Δ_T and Δ_P are unknown within a magnitude of up to $(m_\rho/\Gamma_\rho)^2 \sim 4\%$ [152] and with arbitrary strong phases[64]. The effect on α is given in Fig. 55. The left hand plot shows the present experimental situation (bound on $\mathcal{B}(B^0 \to \rho^0\rho^0)$), where the solid line indicates the isospin analysis where isospin-breaking contributions with the exception of electroweak penguins are neglected (same as Fig. 50), and the dashed line corresponds to the replacement $A^{+0} \to A^{+0} + \Delta A^{+0}$. The right hand plot shows the corresponding constraints for the first scenario, defined in the previous section, at $1\,\mathrm{ab}^{-1}$.

The observed systematic uncertainty on α depends on whether or not the full isospin analysis is applied. It is small for the GLSS bound (equivalent to the isospin analysis with upper limit on $\mathcal{B}(B^0 \to \rho^0\rho^0)$). However, significant effects can occur once the full isospin analysis is performed. We estimate the size of the uncertainty for the setup we have tested to be of the order of 3°. Notwithstanding, one should keep in mind that the resulting effect depends, on the one hand, on the relative size of the additional amplitude (192), and, on the other hand, on the particular solution of the isospin analysis for the contributing amplitudes. It must therefore be (re-)estimated for the set of measurements that is at hand. Furthermore, a careful experimental analysis may partially disentangle these effects [152].

[64] The effect of hadronic isospin-breaking effects is expected to be smaller than the one due to the finite width of the ρ.

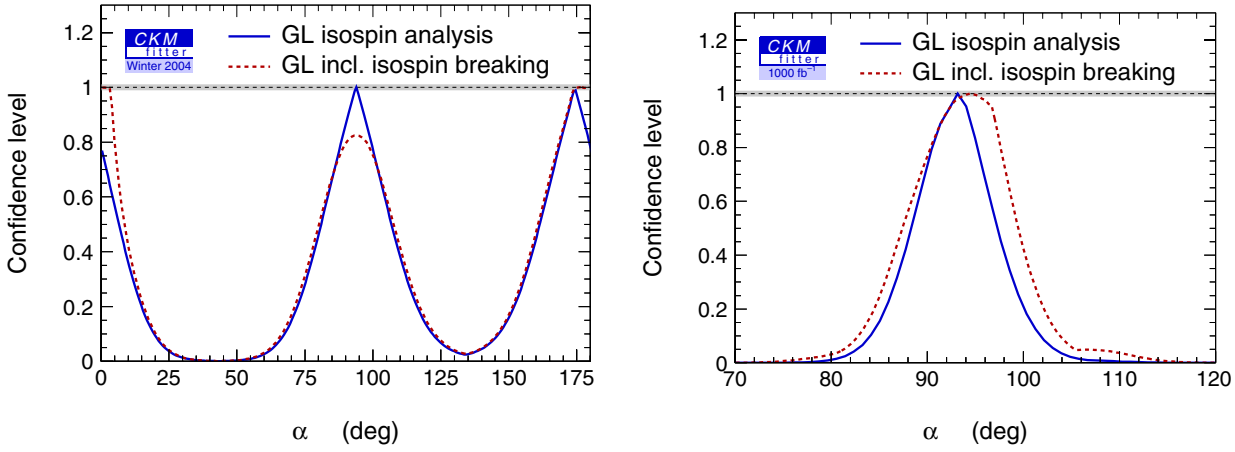

Fig. 55. Confidence levels for α from the $B \to \rho\rho$ isospin analysis where isospin-breaking corrections (with the exception of electroweak penguins) are neglected (solid lines), and when including a relative 4% correction with arbitrary phases on the amplitude level (dashed lines), according to (192). The left hand plot gives the results for the present experimental situation (bound on $\mathcal{B}(B^0 \to \rho^0\rho^0)$), while the right hand plot uses the extrapolation to $1\,\mathrm{ab}^{-1}$, defined in Sect. 5.3. It includes the full isospin analysis with available measurements of $S^{00}_{\rho\rho,L}$ and $C^{00}_{\rho\rho,L}$

6 Comparison of amplitude ratios

Numerical values for the ratios of reduced tree and penguin amplitudes for the $\pi\pi$, $\rho\rho$, $K\pi$ and $\rho\pi$ systems, assuming the standard CKM fit and specific hadronic hypotheses (see table caption) are given in Table 13. Before discussing in more detail the results, two reservations are in order: the overall (mainly experimental) uncertainties on these ratios are still large, and within the 2σ errors no specific conclusions can be drawn from the comparison of the four systems. The amplitude ratios are obtained assuming strict isospin symmetry for $\pi\pi$ and $\rho\rho$, and stronger hadronic hypotheses

Table 13. Magnitudes of penguin-to-tree ($|P^{+-}/T^{+-}|$) and color-suppressed-to-color-allowed ($|T^{00}_C/T^{+-}|$) amplitude ratios obtained for the four charmless decay modes studied in this part. For the purpose of this comparison, the CKM elements are not included in the ratios, but their input is taken from the standard CKM fit. We denote by $B \to \rho\pi[+-]$ ($[-+]$) the branch where the ρ (π) is emitted by the W. For the $\pi\pi$ and $\rho\rho$ modes, only isospin symmetry is assumed. Since SU(2) is insufficient at present, the annihilation and exchange contributions are neglected for the $K\pi$ ratios, and the SU(3) partners $K^{*+}\pi^-$ and $\rho^- K^+$ are used to constrain the corresponding penguin amplitudes for the $\rho\pi$ modes (see text). The last two lines give the results of the combined QCD FA fit to the $\pi\pi$ and $K\pi$ data (Sect. VI.2.2). The strong phases obtained in this framework are: in the $\pi\pi$ system, $\arg(P^{+-}/T^{+-}) = (-29^{+5}_{-2})^\circ$ and $\arg(T^{00}_C/T^{+-}) = (146^{+6}_{-2})^\circ$; and in the $K\pi$ system, $\arg(P^{+-}/T^{+-}) = (-28^{+5}_{-1})^\circ$ and $\arg(T^{00}_C/T^{+-}) = (-25^{+8}_{-5})^\circ$

	Central value ± error at given CL				
	$\lvert P^{+-}/T^{+-}\rvert$		$\lvert T^{00}_C/T^{+-}\rvert$		
Mode	CL = 0.32	CL = 0.05	CL = 0.32	CL = 0.05	Method
$B \to \pi\pi$	$0.23^{+0.41}_{-0.10}$	$^{+0.81}_{-0.16}$	$0.98^{+0.58}_{-0.30}$	$^{+1.54}_{-0.49}$	SU(2)
$B \to \rho\rho$	$0.05^{+0.07}_{-0.05}$	$^{+0.12}_{-0.05}$	$0.21^{+0.11}_{-0.15}$	± 0.21	SU(2)
$B \to K\pi$	$0.04^{+0.03}_{-0.01}$	$^{+0.14}_{-0.04}$	$1.22^{+0.32}_{-0.16}$	$^{+1.20}_{-0.32}$	SU(2)+ no annihil./exch.
$B \to \rho\pi[+-]$	$0.03^{+0.09}_{-0.03}$	$^{+0.11}_{-0.03}$	$0.48^{+0.14}_{-0.16}$	$^{+0.25}_{-0.48}$	SU(3)+ no OZI-peng.
$B \to \rho\pi[-+]$	$0.10^{+0.02}_{-0.03}$	$^{+0.03}_{-0.06}$	$0.57^{+0.17}_{-0.18}$	$^{+0.33}_{-0.57}$	SU(3)+ no OZI peng.
$B \to \pi\pi$	$0.18^{+0.01}_{-0.03}$	$^{+0.03}_{-0.05}$	1.17 ± 0.20	± 0.41	QCD FA combined fit
$B \to K\pi$	$0.17^{+0.01}_{-0.03}$	$^{+0.03}_{-0.05}$	$1.52^{+0.42}_{-0.47}$	$^{+0.69}_{-0.71}$	QCD FA combined fit

for $K\pi$ and $\rho\pi$. The results from the latter two systems should therefore be interpreted with care. The results of the fit of the QCD Factorization on the $\pi\pi$ and $K\pi$ data (see Sect. 2.2) are also reported.

In the $\pi\pi$ system, the measurement of the time-dependent CP asymmetry requires a potentially large penguin-to-tree ratio to be in agreement with the standard CKM fit. This was expected after the first measurement of the surprisingly large branching fraction of $B^0 \to K^+\pi^-$. However a puzzling feature is that the $K\pi$ data alone prefer a small value for the same penguin-to-tree ratio, and that the branching fraction for the $K^+\pi^-$ mode is somewhat smaller than the theoretical expectation (see Table 10). Various sources for this discrepancy have been discussed in Sect. VI.3.

Another feature of the $\pi\pi$, $K\pi$ and, to a lesser extent, $\rho\pi$ modes, is the apparent significant violation of the color-suppression concept. While from the point of view of the $1/N_c \to 0$ limit this suppression is formally of order $1/N_c \sim 0.3$, naïve semi-perturbative counting predicts a further cancellation, leading to the well known $a_2 \lesssim 0.2$ "universal" factor [215]. This property of the so-called "class II" decays, according to the classification of [215], remains partially true in the QCD factorization formalism [207] although the latter admits the possibility of large corrections [135]. There is evidence from Table 13 that the present data suggest that the color-suppression mechanism is ineffective. Different manifestations of violation of the color-suppression concept, and dependence of the a_2 factor with respect to the involved particles, have been observed in simpler B decays[65] without penguin contributions, e.g., $B \to J/\psi\, K^{(*)}$ and $\Delta C = 1$ transitions [272].

The results for the amplitude ratios fitted simultaneously on the $\pi\pi$ and $K\pi$ measurements within the framework of QCD factorization are also given in Table 13. We find that this more predictive approach (compared to the fits based only on flavor symmetry) re-establishes the good agreement between the penguin-to-tree ratios in the $\pi\pi$ and $K\pi$ systems: this can be interpreted as the consequence of the smallness of the annihilation and exchange contributions estimated in this approach. However larger $|T_C^{00}/T^{+-}|$ ratios are found, although with large errors.

Note that our definition of $T_{\rm C}^{00}$ implicitly contains long-distance penguin and exchange contributions. Although the latter are $1/N_c$ suppressed as well, and there is no model-independent distinction between the different topologies that are mixed by rescattering phenomena, it may occur that a number of relatively small corrections constructively interfere in $T_{\rm C}^{00}$ and destructively in T^{+-} to eventually give a globally large effect, which could explain the observed $T_{\rm C}^{00}/T^{+-}$ ratio [135,232].

Finally we stress that although the large penguin and color-suppressed amplitudes in the $\pi\pi$ channels likely come from the same type of non-trivial hadronic dynamics, $B \to \pi^0\pi^0$ cannot be a pure penguin mode. Indeed, were it the case, in the SU(3) limit and neglecting electroweak penguin contributions $\mathcal{B}(B^0 \to \pi^0\pi^0)$ would be equal to $\mathcal{B}(B^0 \to K^0\overline{K}^0)/2$, which is disfavored by the current data (see Table 8). This is somewhat unfortunate because $\mathcal{B}(B^0 \to \pi^0\pi^0) \sim \mathcal{B}(B^0 \to K^0\overline{K}^0)/2$ would imply a stronger constraint on α from the $B \to \pi\pi$ isospin analysis, since it would closer approach the GLSS bound $\mathcal{B}^{00}_{\rm GLSS-}$ (115).

In naïve factorization, there is a clear hierarchy between penguins in PP, PV and VV modes [266]. This is due to the Dirac structure of $(V-A)(V+A)$ penguin operators, which do not contribute when the meson that does not receive the spectator quark (the "upper" meson) is a vector, as in $B^0 \to \rho^+\pi^-$ and $B^0 \to \rho^+\rho^-$. Similarly, these operators contribute constructively (resp. destructively) with $(V-A)(V-A)$ penguin operators when the upper meson is a pseudoscalar and the lower meson is a pseudoscalar (resp. vector), as in $B^0 \to \rho^-\pi^+$ (resp. $B^0 \to \pi^+\pi^-$). This expectation seems to be in agreement with our fits to the present data (see Table 13). However, as a consequence of the fact that $(V-A)(V+A)$ operators are formally power-suppressed in the full QCD factorization approach, the above simple hierarchy may receive large corrections [135]. Hopefully, a more detailed dynamical analysis will be possible when the measurements of the strange PV and VV channels become more complete and precise.

The present pattern of amplitude ratios in the different decays, if confirmed when the experimental errors decrease, might challenge theoretical approaches that are based on the factorization of non-leptonic matrix elements. Naïvely suppressed contributions, such as charming penguins [273] or other type of rescattering effects (see, e.g., [274] for an example of a final state interaction that does not vanish in the $1/m_b \to \infty$ limit), could finally contribute at leading order: the approach of [218], based on the SCET effective theory, might be able to handle these difficult problems in a more systematic way. At present, it seems that it would be difficult to keep all these effects small while maintaining agreement with the central values of the experimental observables, unless one is willing to fine-tune all the observed "anomalies" with New Physics contributions. An interesting question, among others, concerns the behavior of rescattering effects with respect to the isospin or SU(3) quantum numbers of the relevant amplitudes. More data and theoretical work are needed to answer this.

[65] Not to mention the large $1/N_c$ effects in kaon and D-meson decays.

7 Conclusion

Due to the significant CP asymmetries on one hand, and the presence of loop-induced transitions on the other hand, charmless B decays can be used for precision measurements of CP violation within the SM, and they are sensitive probes of physics beyond the SM.

We have studied $B \to \pi\pi, K\pi$ decays using various phenomenological approaches with different dynamical assumptions. These include SU(2) and SU(3) flavor symmetries and QCD Factorization. An extra section has been devoted to the phenomenological analysis of $B \to K\pi$ decays due to the peculiarity of the observed branching fraction pattern. Constraints on $(\overline{\rho}, \overline{\eta})$ from these decays are weak since the sensitivity to the CKM phase through the tree amplitude is CKM-suppressed with respect to $B \to \pi\pi$. However the $K\pi$ modes represent a rich field to test flavor symmetry, QCD Factorization and to search for manifestations of New Physics. For the analysis of $B \to \rho\pi$ decays we have applied SU(2) and SU(3) symmetry, and SU(2) symmetry is used for the $B \to \rho\rho$ system, mostly because the branching fractions of the relevant SU(3) partners are not yet well known. Due to the powerful bound on the penguin pollution in $B^0 \to \rho^+\rho^-$ using the upper limit on $B^0 \to \rho^0\rho^0$, a significant constraint on α can be derived from the measurement of $\sin 2\alpha_{\rm eff}$ in a time-dependent analysis of $B^0 \to \rho^+\rho^-$ performed by the *BABAR* collaboration. The $\pi\pi$ and $\rho\pi$ systems do not (yet) provide useful constraints from the corresponding isospin analyses, because of the poor sensitivity to the penguin contribution ($\pi\pi$) and the lack of a full Dalitz analysis ($\rho\pi$).

More specifically, we find for the $\pi\pi$ system that:

- hints of a large penguin contribution and a large violation of the color-suppression mechanism are found with $|P^{+-}/T^{+-}| = 0.23^{+0.41}_{-0.10}$ and $|T^{00}/T^{+-}| = 0.98^{+0.58}_{-0.30}$ so that the SU(2) upper bound fails to provide a significant constraint on $\Delta\alpha = \alpha - \alpha_{\rm eff}$, for which we find (CL $> 10\%$): $-54^\circ < \Delta\alpha < 52^\circ$.
- a somewhat better bound is obtained from the SU(3) analysis neglecting OZI- and power-suppressed penguin topologies, $-29^\circ < \Delta\alpha < 28^\circ$, with a weak constraint on α.
- at an extrapolation to $1\,{\rm ab}^{-1}$, exclusion areas for α can be obtained with the $B \to \pi\pi$ isospin analysis. However a precise measurement of α from the $\pi\pi$ system alone will likely require larger amounts of data ($\sim 10\,{\rm ab}^{-1}$) that could be reached at a next generation B factory.
- useful information in the $(\overline{\rho}, \overline{\eta})$ plane is obtained with partial input from QCD Factorization: either to gauge the uncertainty on SU(3) breaking, or to obtain an estimate of the tree and penguin matrix elements (magnitudes and phases). The constraints obtained in both cases are in agreement with the standard CKM fit.
- the full calculation of QCD Factorization (taking into account model-dependent power-suppressed terms) is required to accommodate $(\overline{\rho}, \overline{\eta})$ extracted from the CP measurements with the standard CKM fit. A leading order calculation (close to naïve factorization) leads only to the marginal compatibility with a p-value of 5×10^{-5}. By further constraining the full model with all $\pi\pi$ and $K\pi$ branching fractions and CP-violating asymmetries measured so far, one finds the allowed region in the $(\overline{\rho}, \overline{\eta})$ plane in striking agreement with the standard CKM fit (with comparable precision) and an overall p-value of 21%.
- we compute projections on the $\pi\pi$, $K\pi$ observables from the global QCD FA fit, where all observables but the one that is projected upon are included in the fit (as well as the standard CKM fit). The results are unbiased data driven predictions and exhibit high precision. The agreement with the measurements is satisfying, with the notable exceptions of the branching fractions for $B^0 \to K^0\pi^0$ and $B^0 \to K^+\pi^-$. The corresponding predictions from QCD FA alone (without experimental input to constrain the theory parameters) suffer from much larger uncertainties, which is by part due to the conservative *R*fit treatment of the theoretical systematics.
- using SU(3) symmetry we predict the branching fraction and CP-violating asymmetries in $B^0_s \to K^+K^-$ decays from the $B \to \pi\pi$ measurements and the standard CKM fit. We find the 95% CL ranges $0.02 < C^s_{KK} < 0.32$ and $0.12 < S^s_{KK} < 0.27$. Only a weak constraint can be derived for $\mathcal{B}^s_{KK}$, for which however the correlation with C^s_{KK} is strong.

For the $K\pi$ system we note:

- the "historical" proposal by Quinn and Snyder to use $K\pi$ modes and isospin symmetry for the extraction of α in the absence of electroweak penguins leads only to a weak constraint with the present data. The subtle quadrilateral construction would need very precise measurements to become meaningful, while at the same time there are convincing arguments that electroweak penguin contributions cannot be neglected.
- the recent proposal to constrain the apex of the UT assuming isospin symmetry, neglecting all annihilation and long-distance penguin diagrams, and evaluating electroweak penguins in terms of tree amplitudes in the SU(3) limit, is expected to provide meaningful results when the data become more precise. However the dynamical assumptions behind this method should be investigated further, since they are crucial for the result. In particular we observe that the fit systematically prefers a non-zero $V_{us}V^*_{ub}$ contribution to $B^+ \to K^0\pi^+$, although theory predicts a small effect.
- within the same set of dynamical assumptions, we determine the allowed range of amplitude ratios. Color-suppression appears to be significantly violated as in the $\pi\pi$ case, while the penguin-to-tree ratio is, quite paradoxically, smaller than in the $\pi\pi$ system. This is in naïve contradiction with the idea that the large branching ratios

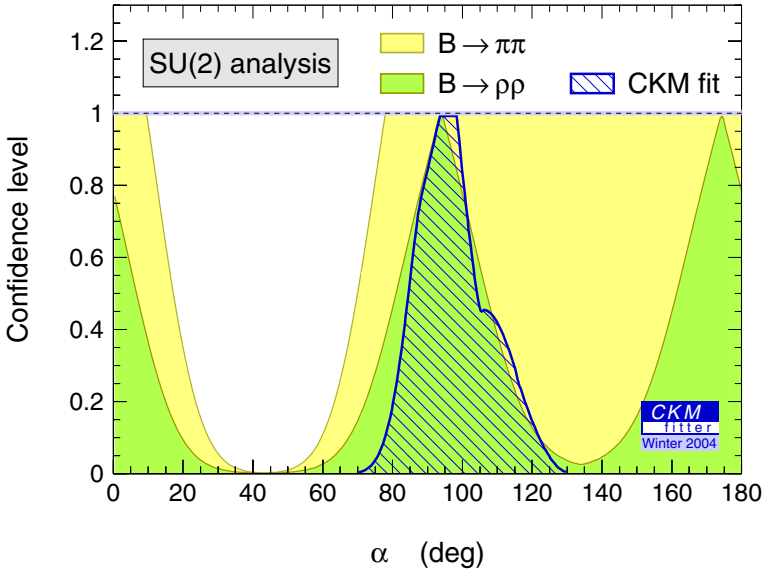

Fig. 56. Confidence level from the SU(2) analysis of $B \to \pi\pi$ (light shaded) and $B \to \rho\rho$ (dark shaded) decays as a function of α. Also shown is the prediction from the standard CKM fit (hatched area), which includes the world average of $\sin 2\beta$ but excludes $B \to \rho\rho$

to $K\pi$ with respect than the ones to $\pi\pi$ are evidence for large penguins in $B \to PP$ transitions. Complicated hadronic mechanisms and/or New Physics effects in either $b \to d$ or $b \to s$ transitions might be at the origin of this intriguing pattern. However present experimental uncertainties still exhibit a decent agreement with SU(3) between $\pi\pi$ and $K\pi$ in the no-rescattering limit.
– the experimental uncertainties hinder us from obtaining significant constraints on electroweak penguin contributions, even in the most restrictive theoretical scenario where annihilation and exchange topologies are entirely ignored. The SM expectation for both color-allowed and color-suppressed (the latter one should not be neglected) electroweak penguins can describe the data; furthermore the feasibility of a more general study including arbitrary NP contributions in either gluonic or electroweak penguins is not clear, again due to the lack of experimental precision.

The following conclusions can be drawn from the analysis of the two-body $\rho\pi$ system:

– scenarios using SU(2) as only input do not constrain α at the first generation B factories if $\mathcal{B}(B^0 \to \rho^0\pi^0)$ is not significantly smaller than expected from color-suppression. The reason for this failure is merely a problem of experimental precision to resolve α in the pentagon. Setting arbitrarily all strong phases to zero and removing the penguins leads to a value for α that is in agreement with the standard CKM fit with a statistical uncertainty of $5.4°$.
– within SU(3) symmetry and neglecting OZI- and power-suppressed penguin contributions, we observe some disagreement between the bound on direct CP-violating asymmetries obtained from $\mathcal{B}(B^0 \to \rho^- K^+)$ for the $B^0 \to \rho^-\pi^+$ branch, and the central value of the measurement. While this is not conflicting within the present experimental errors, it requires a reduction of the observed $\mathcal{A}_{\rho\pi}^{-+}$ with more data, if the SM and SU(3) picture holds.
– within the same SU(3)-based hypotheses, we obtain the bounds $|\alpha - \alpha_{\rm eff}^{+-}| < 17.6°$ and $|\alpha - \alpha_{\rm eff}^{-+}| < 12.6°$ at 95% CL.
– SU(3) flavor symmetry does not help to significantly constrain α when all theory parameters are free to vary since the eightfold ambiguity due to the unknown relative strong phase $\hat{\delta}$ remains. Using the standard CKM fit as input leads to the preferred values $\hat{\delta} \approx 0, \pm\pi$, which is compatible with the no-rescattering expectation.
– all the approaches that we have studied suffer from the lack of knowledge of the interference phase between the two charged ρ's, which generate discrete ambiguities. In particular, a powerful constraint on α, competitive with the standard CKM fit, would be obtained from a Dalitz plot analysis together with the SU(3) constraints from penguin-dominated partners.

We conclude from the SU(2) analysis of the $\rho\rho$ system that

– even without a significant measurement of $\mathcal{B}(B \to \rho^0\rho^0)$ a useful constraint on α is obtained. The smallness of the theoretical uncertainties allows us to include the measurements from the $B \to \rho\rho$ system into the standard CKM fit.
– the success of the $\rho\rho$ system is threefold: (*i*) due to the small mass of the ρ with respect to the B, the ρ mesons have dominant longitudinal polarization (CP-even) with respect to their decay axis; (*ii*) small penguin contributions and color-suppression improve the $\Delta\alpha$ bounds in absence of the full isospin analysis, and (*iii*) the capability to

measure $S^{00}_{\rho\rho,L}$ (not possible for $S^{00}_{\pi\pi}$) significantly enhances the sensitivity of the full isospin analysis to α, once $B \to \rho^0\rho^0$ has been observed.
- the present uncertainty due to the penguin pollution is $-20° < \Delta\alpha < 18°$ for CL $> 10\%$ and the total uncertainty on α is 33° at two standard deviations. Including electroweak penguins induces a shift of $-2.1° \pm 0.2°$ on α.
- two (possibly optimistic) attempts to extrapolate the results from the present central values and errors into the future lead to expected 2σ errors on α of approximately 16°–19° at $500\,\text{fb}^{-1}$ and 10°–16° at $1\,\text{ab}^{-1}$ integrated luminosities, for the solution that is compatible with the standard CKM fit.
- we study the finite width of the ρ and isospin-breaking effects using a simple ansatz. With a breaking of the triangular relation at the 4% level, the corresponding uncertainty on α is found to be of the order of 3° for the full isospin analysis, which however depends on the actual values of the $B \to \rho\rho$ observables. Systematic effects from $\pi\pi$ resonances other than the $\rho(770)$ and/or non-resonant background have been neglected in this study but may become important when the precision on α increases.

Part VII
New Physics in B transitions

1 General remarks

Despite weak inconsistencies in $\sin 2\beta$ from penguin-dominated modes (see Sect. III.2.10) and in $B \to K\pi$ decays (Sect. VI.3), the SM is able to accommodate the data from the B-meson and kaon systems within the present experimental and theoretical uncertainties. Hence there is no need (yet) to introduce contributions from physics beyond the SM. However, this does not necessarily mean that New Physics (NP) contributions are totally absent. It is thus interesting to investigate how far today's experiments can constrain NP parameters.

A large variety of specific NP models exists in the literature, but for the purpose of a global CKM fit, one should adopt a parameterization that is as model-independent as possible. The results obtained under general assumptions may then be used to draw conclusions upon more specific classes of models.

The NP analysis we are performing below proceeds in two steps:

- in the first step, we list the observables that are expected to be dominated by the SM contributions, according to a specific assumption we make on the nature of the potential NP. These observables are used to construct a model-independent Unitarity Triangle [275], followed by a constrained fit on NP contributions in $B^0\overline{B}^0$ mixing.
- in the second step, the result of this fit is used as an input to probe NP in B decays with sizable contributions from $b \to d$ or $b \to s$ gluonic penguins.

Because the present experimental errors are still large, and since several key modes are not yet well known, we do not attempt to perform an exhaustive numerical analysis as we did for the SM fit. In some cases we use a rather "aggressive" interpretation of the experimental results, which is justified in view of the expected improvement of the measurements in the near future. The studies presented hereafter are to be viewed as preliminary proposals, which nevertheless allow us to draw instructive conclusions.

2 New Physics in $\Delta B = 2$ transitions

With the use of dimensional arguments [276], one finds that in a large class of models NP contributes mainly to the $B^0\overline{B}^0$ mixing amplitude ($\Delta B = 2$). We will hence allow for arbitrary NP corrections to the mixing, while however keeping the possibility that also the decays ($\Delta B = 1$) are non-standard.

New Physics effects in $B^0\overline{B}^0$ mixing can be described model-independently by two additional parameters, r_d^2 and $2\theta_d$, with the definition [277,278]

$$r_d^2\, e^{i2\theta_d} \;=\; \frac{\langle B^0|\mathcal{H}_{\text{eff}}^{\text{full}}|\overline{B}^0\rangle}{\langle B^0|\mathcal{H}_{\text{eff}}^{\text{SM}}|\overline{B}^0\rangle}\;, \tag{193}$$

where $\mathcal{H}_{\text{eff}}^{\text{full}}$ comprises NP and SM contributions and where $\mathcal{H}_{\text{eff}}^{\text{SM}}$ contains only the SM contribution. The SM values for these parameters are $r_d^2 = 1$ and $2\theta_d = 0$.

We elaborate an analysis allowing to constrain both CKM ($\overline{\rho}$ and $\overline{\eta}$) and NP (r_d^2 and $2\theta_d$) parameters related to flavor-changing processes. It uses observables from the B-meson system only since they are more sensitive to $\overline{\rho}$ and $\overline{\eta}$ than those obtained from the kaon system. It is inspired by similar previous analyses [278,279,276].

2.1 Basic assumption on New Physics and physical inputs

As in most model-independent NP parameterizations, we assume that NP contributions to tree-mediated decays are negligible. More specifically, we require that *decay transitions with four flavor changes (i.e., $b \to q_1\bar{q}_2q_3$, $q_1 \neq q_2 \neq q_3$) are dominated by the SM (SM4FC).* Hence the CKM parameters related to these decays are extracted within the SM, with the presence of the additional parameters coming from NP in $B^0\overline{B}^0$ mixing. Here we assume that the unitarity of the CKM matrix still holds in the presence of NP, in order to ensure that the SM contribution to the $B^0\overline{B}^0$ mixing keeps its usual expression as a function of $(\overline{\rho},\overline{\eta})$ and other theoretical parameters.

The observables allowing us to constrain the SM and NP parameters within this well-defined assumption are listed below:

- $|V_{ub}|$ and $|V_{cb}|$ from $b \to u$ and $b \to c$ semileptonic decays, which are the same as in the SM (Sect. III.2).
- the constraint on $\tan\gamma$ from the Dalitz plot analysis of $B^+ \to D^0K^+$ decays (the CL on γ obtained in this analysis has to be interpreted with care, as discussed in Sect. V.2).
- the *CP*-asymmetry measurement in $b \to c\bar{u}d$ and $b \to u\bar{c}d$ non-leptonic decays (Sect. V.1), which determines $|\sin(2\beta + 2\theta_d + \gamma)|$. We use the CL determined by the toy simulation described in Sect. V.1, because it gives a stronger constraint than the Gaussian approximation.
- the $\Delta I = 3/2$ amplitude of $b \to u\bar{u}d$ transitions is standard within the *SM4FC* assumption[66]: hence, the isospin analysis of $B \to \pi\pi$ and/or longitudinally polarized $B \to \rho\rho$ decays and the Dalitz plot analysis of $B^0 \to (\rho\pi)^0$ can be used to extract the quantity $\sin(2\beta+2\theta_d+2\gamma)$ (cf. Sect. VI.1.1.3). Since the constraint from the $\pi\pi$ system is rather weak at present and the $\rho\pi$ Dalitz plot analysis is not yet available, we will only use $\rho\rho$ in the following (cf. Sect. VI.5).
- the mixing-induced *CP* asymmetry in $b \to c\bar{c}s$ transitions (e.g., $B^0 \to J/\psi K^0$) determines $(2\beta + 2\theta_d)$, provided that NP contributions to the decay amplitudes of these transitions are negligible (for general arguments see, e.g., [280]). Although this hypothesis does not belong to the *SM4FC* rule, generic non-standard corrections to $b \to c\bar{c}s$ amplitudes are likely to be small, because these modes are dominated by $V_{cb}^*V_{cs}$ SM tree amplitudes: QCD penguins that would receive contributions from new particles in the loop are dynamically suppressed by the weak coupling of, e.g., the J/ψ to gluons, while Z-penguin effects are expected to be at most at the level of the current experimental uncertainty [281].
- the constraint on the sign of $\cos(2\beta + 2\theta_d)$ from the time- and angular-dependent analysis of $B^0 \to J/\psi K^{*0}$ decays (cf. Sect. III.3.5). We use the Gaussian interpretation of the experimental result, which essentially imposes $\cos(2\beta + 2\theta_d) > 0$, since it gives a stronger constraint than the (correct) Monte-Carlo simulation.
- the $B^0\overline{B}^0$ oscillation frequency, as given by $\Delta m_d = r_d^2 \times \Delta m_d^{\rm SM}$.
- the *CP*-violating charge asymmetry in semileptonic B decays $A_{\rm SL}$ defined by

$$A_{\rm SL} \;\equiv\; \frac{\Gamma(\overline{B}^0(t) \to \ell^+X) - \Gamma(B^0(t) \to \ell^-X)}{\Gamma(\overline{B}^0(t) \to \ell^+X) + \Gamma(B^0(t) \to \ell^-X)} \;. \tag{194}$$

In the presence of NP in mixing its theoretical prediction reads [283–286,282]:

$$A_{\rm SL} \;=\; -{\rm Re}\left(\frac{\Gamma_{12}}{M_{12}}\right)^{\rm SM}\frac{\sin 2\theta_d}{r_d^2} + {\rm Im}\left(\frac{\Gamma_{12}}{M_{12}}\right)^{\rm SM}\frac{\cos 2\theta_d}{r_d^2} \;, \tag{195}$$

where Γ_{12} and M_{12} are respectively the absorptive and dispersive parts in the $B^0\overline{B}^0$ mixing amplitude.
The theoretical prediction of $(\Gamma_{12}/M_{12})^{\rm SM}$ at leading order [67] reads [282]:

$$\left(\frac{\Gamma_{12}}{M_{12}}\right)^{\rm SM} = -\frac{4\pi m_b^2}{3m_W^2\overline{\eta}_B S_0\,(m_t^2/m_W^2)}\left[\left(K_1+\frac{K_2}{2}\right)+\left(\frac{K_1}{2}-K_2\right)\frac{m_B^2-m_b^2}{m_b^2 B} + \;(K_2-K_1)\left(\frac{5B_S^{'}}{8B_d}+3z\frac{1-\overline{\rho}-i\overline{\eta}}{(1-\overline{\rho})^2+\overline{\eta}^2}\right)\right] \;, \tag{196}$$

where K_1 and K_2 are Wilson coefficients, $z \equiv m_c^2/m_b^2$ and $\overline{\eta}_B = \eta_B \times [\alpha_s(m_b)]^{-6/23}(1+(\alpha_s/4\pi)(5165/3174))$. The corresponding input values are given in Table 14.

[66] The Gronau-London isospin analysis allows to isolate the $\Delta I = 3/2$ amplitude (see Sect. VI.1.1.3), which is proportional to $V_{ud}V_{ub}^*$ in the *SM4FC* hypothesis (up to a small and computable $V_{td}V_{tb}^*$ electroweak penguin contribution that we take into account). This holds independently of the magnitude and (*CP*-conserving plus *CP*-violating) phase of the $\Delta I = 1/2$ amplitude, which *a priori* receives contributions from both the SM (tree and penguin diagrams) and the NP.

[67] Next-to-leading order calculations of $A_{\rm SL}$ have been performed in [287,288]. We do not use these results in our analysis since experimental errors dominate at present. With increasing precision the NLO results must be included.

Table 14. Inputs used to predict the semileptonic CP-violating asymmetry $A_{\rm SL}$, which are not already defined in Table 1. The errors given are treated as systematic theoretical uncertainties within *R*fit. If no error is given the uncertainty of the corresponding quantity is neglected. The last line quotes the experimental average

Parameter	Value ± error	Reference
$\alpha_S(m_b)$	0.22	[282]
K_1	-0.295	[282]
K_2	1.162	[282]
$m_b^{\rm pole}$	$4.8 \pm 0.1_{\rm theo}$	[282]
z	$0.085 \pm 0.010_{\rm theo}$	[282]
$A_{\rm SL}$	$(-0.7 \pm 1.3) \times 10^{-2}$	see text

Table 15. Inputs to the fit with free New Physics contributions to $B^0\overline{B}^0$ mixing, and their dependence with respect to the SM and NP flavor changing parameters. Discussions on the discrete ambiguities occurring in the measurements of $\tan\gamma$, $|\sin(2\beta+2\theta_d+\gamma)|$ and $\sin(2\beta+2\theta_d+2\gamma)$ are given in the corresponding sections

Constraint	SM & NP dependence	Numerical value
$\lvert V_{cb}\rvert$ and $\lvert V_{ub}\rvert$	$\lvert V_{cb}\rvert$ and $\lvert V_{ub}\rvert$	Sect. III.2
$B^+ \to D^{(*)0}K^+$ Dalitz plot analysis	$\tan\gamma$	Sect. V.2.
$B^0 \to D^{(*)\pm}\pi^\mp$ CP asymmetries	$\lvert\sin(2\beta+2\theta_d+\gamma)\rvert$	Sect. V.1 ("toy")
$B \to \rho\rho$ isospin analysis	$\sin(2\beta+2\theta_d+2\gamma)$	Sect. VI.5
$B^0 \to J/\psi K^0$ CP asymmetry	$\sin(2\beta+2\theta_d)$	Sect. III.2
$B^0 \to J/\psi K^{*0}$ time-dependent angular analysis	$\cos(2\beta+2\theta_d)$	Sect. III.2 ("Gauss.")
Δm_d	$\Delta m_d^{\rm SM} r_d^2$	Sect. III.2
$A_{\rm SL}$	(195), (196)	Table 14

We find the experimental value $A_{\rm SL} = -0.007 \pm 0.013$ as an average of several measurements: the direct determination of $A_{\rm SL}$ [289–292] is dominated by the *BABAR* result $A_{\rm SL} = 0.005 \pm 0.012 \pm 0.014$ [292]. The *BABAR* Collaboration also measured the quantity $|q/p| = 1.029 \pm 0.013 \pm 0.011$ with a fit to fully reconstructed B decays [293]. This translates into $A_{\rm SL} = (1-|q/p|^4)/(1+|q/p|^4) = -0.057 \pm 0.033$.

A summary of the observables used in the NP fit is given in Table 15. The number of independent constraints is sufficient to constrain both $(\overline{\rho},\overline{\eta})$ on the one hand, and $(r_d^2, 2\theta_d)$ on the other hand, up to discrete ambiguities.

We do not include the CP-violation parameter ε_K because it does not improve the constraint on $(\overline{\rho},\overline{\eta})$, unless possible NP contributions to $K^0\overline{K}^0$ mixing are negligible, which is not *a priori* known. We do not consider input from $s \to d$ and $b \to s$ transitions either, which are therefore left free in the fit within and beyond the SM.

2.2 Results

We perform a global fit using the inputs from Table 15 with r_d^2 and $2\theta_d$ left free to vary. The constraint obtained in the $(\overline{\rho},\overline{\eta})$ plane when excluding the sign measurement of $\cos(2\beta+2\theta_d)$ is shown in the left hand plot of Fig. 57. There are eight solutions for the CKM angle γ, numbered from 1 to 8, that lie on a circle determined by $|V_{ub}/V_{cb}|$. Solutions 3, 4 and 7 have CLs below 5 % and are therefore not shown on this plot. The other individual solutions are not well separated yet due to the experimental uncertainties in the determination of γ from $D^{(*)0}K^+$, $D^{(*)\pm}\pi^\mp$ and $\rho\rho$. If we

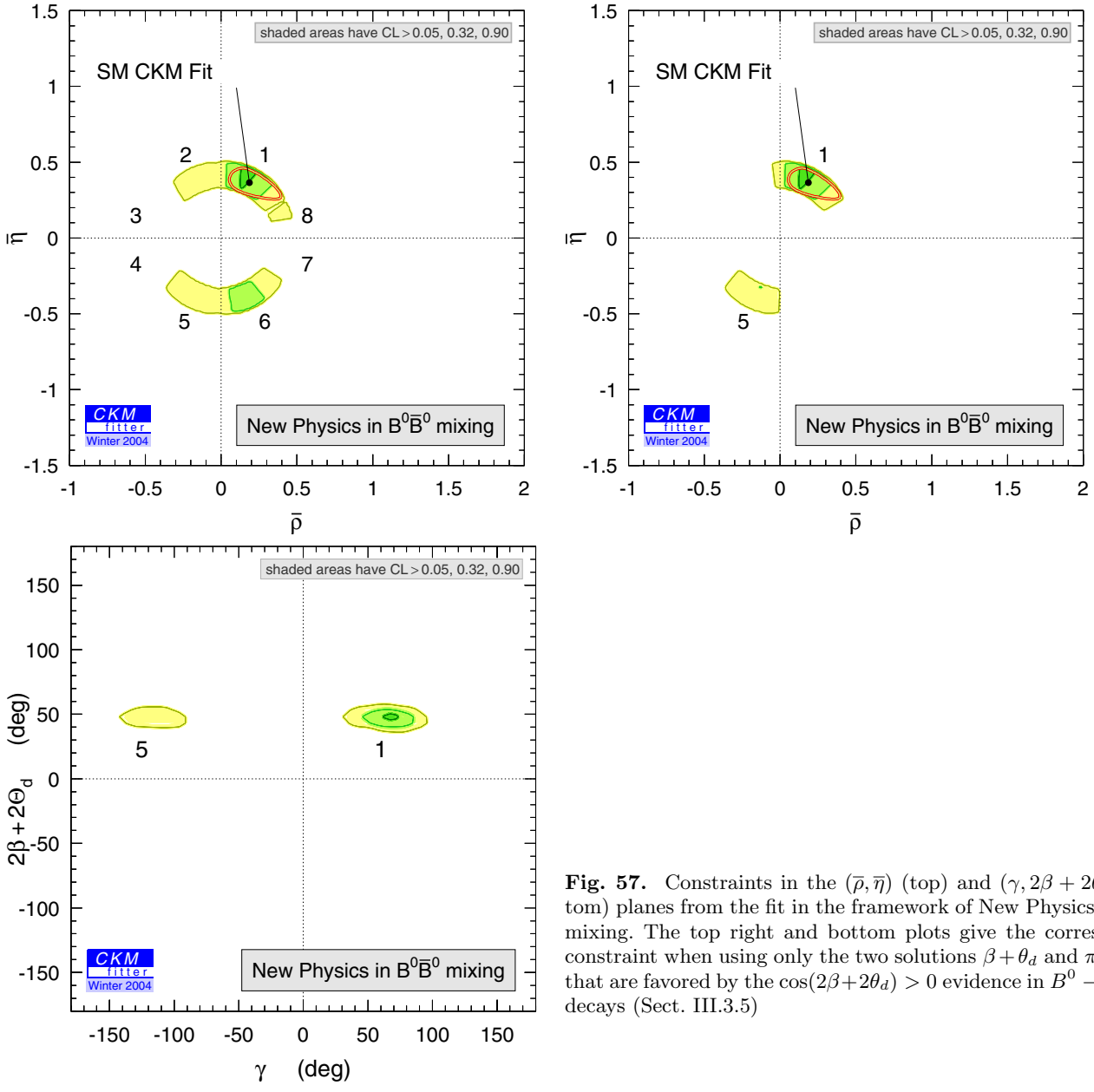

Fig. 57. Constraints in the $(\overline{\rho},\overline{\eta})$ (top) and $(\gamma, 2\beta+2\theta_d)$ (bottom) planes from the fit in the framework of New Physics in $B^0\overline{B}^0$ mixing. The top right and bottom plots give the corresponding constraint when using only the two solutions $\beta+\theta_d$ and $\pi+\beta+\theta_d$ that are favored by the $\cos(2\beta+2\theta_d)>0$ evidence in $B^0\to J/\psi K^*$ decays (Sect. III.3.5)

impose in addition the constraint[68] $\cos(2\beta+2\theta_d)>0$, derived from the analysis of $J/\psi K^*$ decays [138], we obtain the right hand plot of Fig. 57 where four out of eight solutions are further suppressed.

The CL for $\overline{\eta}=0$ in these fits depends crucially on the inputs from Table 15, in particular on the current inputs from the $B^+\to D^{(*)0}K^+$ Dalitz plot analysis ($\tan\gamma$), the $B^0\to D^{(*)\pm}\pi^{\mp}$ CP asymmetries ($|\sin(2\beta+2\theta_d+\gamma)|$), the $B\to\rho\rho$ isospin analysis[69] ($\sin(2\beta+2\theta_d+2\gamma)$) and the $B^0\to J/\psi K^{*0}$ time-dependent transversity analysis ($\cos(2\beta+2\theta_d)$). With these inputs the possibility that CP violation is absent in the SM is quite unlikely. With additional conjectures on the NP's nature, one could obviously improve the constraints: for example, with the assumption that NP is negligible in the decay, any non-zero direct CP-asymmetry measurement implies $\overline{\eta}\neq 0$ (e.g., the measurement of $\varepsilon'/\varepsilon>0$). Generally speaking, the solution $\overline{\eta}=0$ is not a natural value in the SM: the region of very small $\overline{\eta}$ corresponds to

[68] As described in Sect. III.3.5, this is an optimistic assumption, since the $\cos(2\beta)>0$ result found in [138] is not yet statistically significant.

[69] Even if $C^{+-}_{\rho\rho,L}$ significantly departed from zero, the solution $\eta=0$ would still be allowed by the full isospin analysis in $B^0\to\rho\rho$. This is because the isospin analysis only constrains the weak phase of the $\Delta I=3/2$ amplitude, and not the one of the $\Delta I=1/2$ amplitude, which could come from a different source of CP violation. In the SM, these two phases are nevertheless correlated since they are related to common CKM couplings.

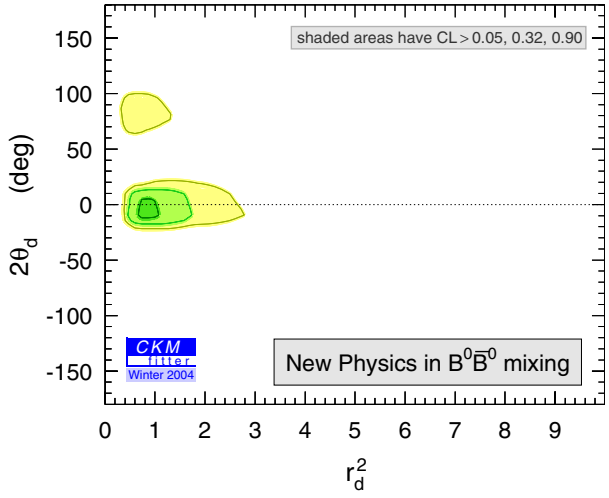

Fig. 58. Confidence level in the $(2\theta_d, r_d^2)$ plane obtained as a result of the global CKM fit that includes New Physics in $B^0\overline{B}^0$ mixing

a fine-tuning scenario, in which the SM generates vanishingly small CP violation, whereas large NP couplings are needed to accommodate the data. See however [294] for an example of multi-Higgs-doublet model that naturally predicts a real-valued CKM matrix. We note that at that time less experimental input was available and consequently a real-valued CKM matrix could not be excluded.

Remarkably, Solution 1 in Fig. 57 is not only consistent with the standard (SM) CKM fit but also has the largest CL: the SM solution is clearly preferred, while however the mirror solution 5 cannot be excluded at the 1σ level. At first sight, this is not surprising since most of the observables used in the fit are expected to be dominated by SM contributions. Nevertheless this leads to an important consequence, namely that NP corrections to $B^0\overline{B}^0$ and $K^0\overline{K}^0$ mixing are likely to be small. In the case of $B^0\overline{B}^0$, this is illustrated in Fig. 58 showing the constraints in the $(r_d^2, 2\theta_d)$ plane: the SM solution $r_d^2 = 1$ and $2\theta_d = 0$ is favored. Values for r_d^2 as large as 2–3 cannot be excluded yet, which means that in principle order one NP contributions to the mixing are allowed. Still, the model-independent constraint on r_d^2 is much better than in the previous similar analyses; the uncertainty will decrease with better precision on Δm_d and $A_{\rm SL}$ and, in particular, on $f_{B_d}\sqrt{B_d}$. This highlights the need for improved determinations of the parameter $f_{B_d}\sqrt{B_d}$ both from theory (e.g., from improved Lattice QCD calculations) and from experiment (e.g., from constraining $|V_{ub}|f_{B_d}$ by a rate measurement of $B \to \ell\nu_\ell$ decays). The constraint on r_d^2 would also be improved with a better knowledge of the angle γ.

With the constraint on $(\overline{\rho}, \overline{\eta})$ shown in the right plot in Fig. 57, we determine the contribution to $|\varepsilon_K|$ coming from the Standard Model. For Solution 1 we find $1.3 \times 10^{-3} < |\varepsilon_K|_{\rm SM} < 5.0 \times 10^{-3}$ for CL $> 5\%$. This can be compared to the experimental value, $|\varepsilon_K| = 2.282 \times 10^{-3}$, and the constraint $1.1 \times 10^{-3} < |\varepsilon_K|_{\rm CKM} < 4.9 \times 10^{-3}$ at CL $> 5\%$ (Table 2, Sect. III.3.2) obtained from the standard CKM fit. That is, neither in the framework of NP in $B^0\overline{B}^0$ mixing nor in the SM, one can exclude NP contributions to $K^0\overline{K}^0$ mixing of order 100% due to the uncertainties on the bag parameter B_K and also, to some extent, on the charm quark mass m_c (cf. Table 1, Sect. III.3.2). Solution 5 leads to negative values for $|\varepsilon_K|_{\rm SM}$ and could only accommodate the measurement in the presence of NP effects in $K^0\overline{K}^0$ mixing that, in addition to being large, would have a sign opposite to the SM contribution.

It is interesting to note that no solution is obtained for $2\theta_d = \pi$. In Minimal Flavor Violation (MFV) NP models (see, e.g., [295]) a single real parameter, F_{tt}, is needed in addition to those of the SM to describe model-independently all the observables. In the SM, the value of this parameter is $F_{tt}|_{\rm SM} = S(m_t^2/m_W^2) = 2.41$, where $S(m_t^2/m_W^2)$ is the Inami-Lim function in the $B^0\overline{B}^0$ mixing amplitude. Our fits exclude a negative sign for F_{tt} corresponding to $2\theta_d = \pi$ leaving $F_{tt} > 0$ as the preferred solution. The parameter F_{tt} is related to our parameterization by $r_d^2 = |F_{tt}|/S(m_t^2/m_W^2)$. With the inputs from Table 15 we obtain the range $1.03 < F_{tt} < 4.41$ for CL $> 10\%$. In MFV models the NP contribution to $B^0\overline{B}^0$ mixing is directly related to the NP contribution to $K^0\overline{K}^0$ mixing. When taking into account the ε_K constraint we obtain $1.03 < F_{tt} < 4.18$ for CL $> 10\%$. In addition, the modification of Δm_s in MFV models is the same as in Δm_d. When also taking into account Δm_s in the fit, the bounds on F_{tt} are further tightened: we find $1.18 < F_{tt} < 4.01$ for CL $> 10\%$.

An interesting question is how the non-standard Solution 5 can be excluded, independently of the argument based on $|\varepsilon_K|$ given above. A reduction of the uncertainties in the $B^+ \to D^{(*)0}K^+$ Dalitz plot analysis, in the $B^0 \to D^{(*)\pm}\pi^\mp$ CP asymmetries and in the $B \to \rho\rho$ isospin analysis will not help in this respect [156], since all these constraints are invariant under the transformation $\gamma \to \gamma + \pi$. However, discriminating the Solutions 1 and 5 would be possible if the measurement of $A_{\rm SL}$ could be significantly improved.

In contrast to the analysis performed in [276], we study NP contributions to $B^0\overline{B}^0$ mixing model-independently, i.e., without the neglect of NP in the decay and without any dynamical assumption. Better constraints can be expected, for instance, when precise measurements of γ from tree-level decays become available.

3 New Physics in $\Delta B = 1$ decays

Flavor-changing neutral currents that occur only at the loop level in the SM receive large corrections in many generic New Physics scenarios [296]. In this section we present constraints on $b \to d$ and $b \to s$ transitions in a model-independent framework.

3.1 $B \to PP$ modes: $B^0 \to \pi^+\pi^-$ versus $B^+ \to K^0\pi^+$

The constraints on the angles γ and $2\beta + 2\theta_d$, obtained in the $\Delta B = 2$ analysis of the previous section, is used to constrain possible NP contributions in $\Delta B = 1$ transitions. For this purpose, we fit the magnitude of the penguin amplitude $|P^{+-}|$ occurring in $B^0 \to \pi^+\pi^-$. More precisely, we define the ratio of $b \to d$ to $b \to s$ transitions by

$$r^P_{\pi\pi} \equiv \sqrt{\frac{\tau_{B^+}}{\tau_{B^0}} \frac{\mathrm{PS}\left|V_{cs}V^*_{cb}P^{+-}_{\pi\pi}\right|^2}{\mathcal{B}(K^0\pi^+)}} , \tag{197}$$

where PS stands for the usual two-body phase space factor and where the penguin amplitude is defined, in contrast to Sect. VI.1.1.1, in the $\mathfrak{T}$ convention

$$A(B^0 \to \pi^+\pi^-) = V_{ud}V^*_{ub}T^{+-}_{\pi\pi} + V_{cd}V^*_{cb}P^{+-}_{\pi\pi} . \tag{198}$$

Although at first sight (198) relies on the SM and CKM unitarity, it remains valid in the presence of arbitrary NP contributions, since any new amplitude with a new CP-violating phase can be decomposed into two independent CKM couplings[70]. In other words, (198) is the most general parameterization of the decay amplitude both within and beyond the SM.

In the SM the ratio $r^P_{\pi\pi}$ is expected to be of order one: it would be equal to one if SU(3) symmetry were exact and in the limit of vanishing annihilation/exchange and electroweak penguin topologies (cf. Sect. VI.1.2.3). Thus, any large ($\gtrsim 30\%$) deviation would be a hint of non-standard particles occurring in the gluonic or electroweak penguin loops. Using (198) for the decay and (193) for the mixing, one can express $r^P_{\pi\pi}$ in terms of the experimental observables and the angles γ and $2\beta + 2\theta_d$

$$r^P_{\pi\pi} = \left[\frac{\tau_{B^+}}{\tau_{B^0}} \frac{\mathcal{B}(\pi^+\pi^-)}{2\lambda^2\mathcal{B}(K^0\pi^+)} \frac{1 - \sqrt{1 - C^{+-2}_{\pi\pi}}\cos(2\beta + 2\theta_d + 2\gamma + 2\alpha_{\mathrm{eff}})}{\sin^2\gamma}\right]^{\frac{1}{2}} . \tag{199}$$

Figure 59 shows the confidence level as a function of γ and $r^P_{\pi\pi}$, using the following input quantities:

- the constraints on γ and $2\beta + 2\theta_d$ obtained from the New Physics fit in $B^0\overline{B}^0$ mixing as shown in the bottom plot of Fig. 57.
- the CP-violating asymmetries in $B \to \pi^+\pi^-$: $C^{+-}_{\pi\pi}$ and $S^{+-}_{\pi\pi} = \sqrt{1 - C^{+-2}_{\pi\pi}}\sin 2\alpha_{\mathrm{eff}}$ (Table 8, Sect. VI.1.3).
- the branching fractions of the three $B \to \pi\pi$ modes (Table 8, Sect. VI.1.3), assuming isospin symmetry.
- the branching fraction of $B^+ \to K^0\pi^+$ (Table 8, Sect. VI.1.3).

The resulting constraints on $r^P_{\pi\pi}$ prefer an order one value. Since we expect deviations up to ± 30 % from one due to the violations of the relation between $\pi^+\pi^-$ and $K^0\pi^+$ penguin amplitudes, non-standard corrections could be as large, in principle, as the SM contribution. More precise measurements of the observables in the $\pi\pi$ system would significantly reduce the allowed domain for $r^P_{\pi\pi}$, while the γ input from the NP fit in $B^0\overline{B}^0$ mixing is found to be less crucial.

[70] This can be seen as follows. Let us denote by $M_{\mathrm{NP}}e^{i\phi_{\mathrm{NP}}}$ an arbitrary NP amplitude with a CP-violating phase ϕ_{NP}. One finds the identity $M_{\mathrm{NP}}e^{i\phi_{\mathrm{NP}}} = V_{ud}V^*_{ub}T_{\mathrm{NP}} + V_{cd}V^*_{cb}P_{\mathrm{NP}}$ with $T_{\mathrm{NP}} = M_{\mathrm{NP}}\mathrm{Im}\left[e^{i\phi_{\mathrm{NP}}}V^*_{cd}V_{cb}\right]/\mathrm{Im}\left[V_{ud}V^*_{ub}V^*_{cd}V_{cb}\right]$ and $P_{\mathrm{NP}} = M_{\mathrm{NP}}\mathrm{Im}\left[V_{ud}V^*_{ub}e^{-i\phi_{\mathrm{NP}}}\right]/\mathrm{Im}\left[V_{ud}V^*_{ub}V^*_{cd}V_{cb}\right]$. The whole effect of NP in the decay amplitude is to modify the "T"-type and "P"-type amplitudes with respect to their SM values.

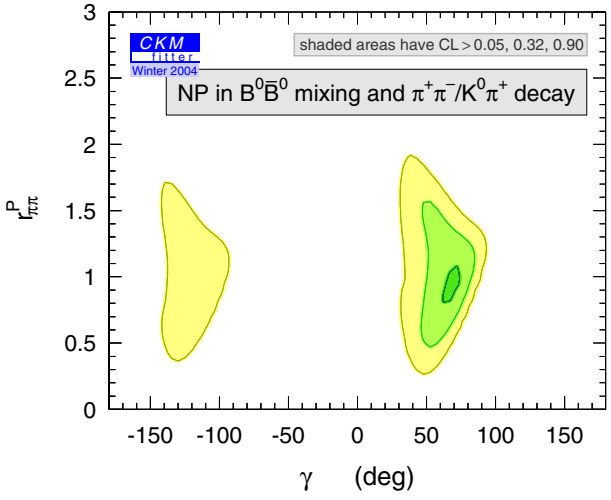

Fig. 59. Confidence level in the $(\gamma, r^P_{\pi\pi})$ plane obtained by the fit including NP in $B^0\overline{B}^0$ mixing and in $b \to d, s$ transitions

3.2 $B \to VP$ modes: $B \to \phi K^0$ versus $B^+ \to K^{*0}\pi^+$

The $b \to d$ to $b \to s$ penguin ratio can be studied in vector-pseudoscalar channels using, for example, the $\rho\pi$ modes compared to the $K^*\pi$ and $K\rho$ partners. However a Dalitz plot analysis of the $\pi^+\pi^-\pi^0$ three-body decay is necessary to extract the penguin amplitudes. Hence we focus on the ratio of two $b \to s$ transitions, represented by the decays $B^0 \to \phi K^0$ and $B^+ \to K^{*0}\pi^+$ (see also [297]). The first is particularly interesting in view of the marginal agreement between *BABAR* and Belle in the measurement of the CP-asymmetry[71] $S_{\phi K}$; general studies of this decay can be found in [298].

We define the $B^0 \to \phi K^0$ amplitude in the $\mathfrak{T}$ convention by

$$A(B^0 \to \phi K^0) \;=\; V_{us}V_{ub}^* P^u_{\phi K} + V_{cs}V_{cb}^* P^c_{\phi K} \;, \tag{200}$$

and the corresponding penguin ratios by

$$r^c_{\phi K} \;\equiv\; \sqrt{\frac{\tau_{B^+}}{\tau_{B^0}} \frac{\mathrm{PS}\left|V_{cs}V_{cb}^* P^c_{\phi K}\right|^2}{\mathcal{B}(K^{*0}\pi^+)}} \;, \qquad r^{u/c}_{\phi K} \;\equiv\; \left|\frac{P^u_{\phi K}}{P^c_{\phi K}}\right| \;. \tag{201}$$

In the SM, $r^c_{\phi K}$ is expected to be close to one, if SU(3) is a good symmetry and if electroweak penguins and annihilation topologies are negligible. Long-distance u- and c- penguins are expected to be suppressed by $1/m_b$ according to QCD FA [207]. Thus a value of $r^c_{\phi K}$ (resp. $r^{u/c}_{\phi K}$) that differs significantly from one would point towards non-standard contributions in electroweak penguins (resp. in either gluonic or electroweak penguins[72]). Note also that $P^u_{\phi K}$ appears in (200) together with a λ^2-suppressed factor. Thus the natural order of magnitude of the ratio $r^{u/c}_{\phi K}$ in the presence of a $b \to s$ NP amplitude that competes with the SM contribution is $1/\lambda^2$.

The explicit expressions for $r^c_{\phi K}$ and $r^{u/c}_{\phi K}$ in terms of the observables are

$$r^c_{\phi K} = \left[\frac{\tau_{B^+}}{\tau_{B^0}} \frac{\mathcal{B}(\phi K^0)}{2\mathcal{B}(K^{*0}\pi^+)} \frac{1 - \sqrt{1 - C^2_{\phi K}}\cos(2\beta + 2\theta_d + 2\gamma - 2\beta_{\mathrm{eff}})}{\sin^2\gamma}\right]^{\frac{1}{2}} , \tag{202}$$

$$r^{u/c}_{\phi K} = \frac{1}{\lambda}\left|\frac{V_{cb}}{V_{ub}}\right| \left[\frac{1 - \sqrt{1 - C^2_{\phi K}}\cos(2\beta + 2\theta_d - 2\beta_{\mathrm{eff}})}{1 - \sqrt{1 - C^2_{\phi K}}\cos(2\beta + 2\theta_d + 2\gamma - 2\beta_{\mathrm{eff}})}\right]^{\frac{1}{2}} . \tag{203}$$

[71] We use here the notation $S_{\phi K}$ and $C_{\phi K}$ for both decays $B^0 \to \phi K^0_S$ and $B^0 \to \phi K^0_L$, where the relative sign in ϕK^0_S with respect to ϕK^0_L is taken into account when the results of both channels for $S_{\phi K}$ are averaged. NP effects that could spoil the relation between the two decays are expected to be highly suppressed [299].

[72] As pointed out in [133], it is not possible from the present data, and from theoretical arguments derived with the use of strict SU(3), to exclude a value of the ratio $r^{u/c}_{\phi K}$ as large as ~ 10 in the SM. Such an extreme value would point to very large non-perturbative rescattering effects. However we stress that the natural expectation in the SM is $r^{u/c}_{\phi K} \sim 1$. More data and a better understanding of rescattering effects in B decays will help to clarify the situation.

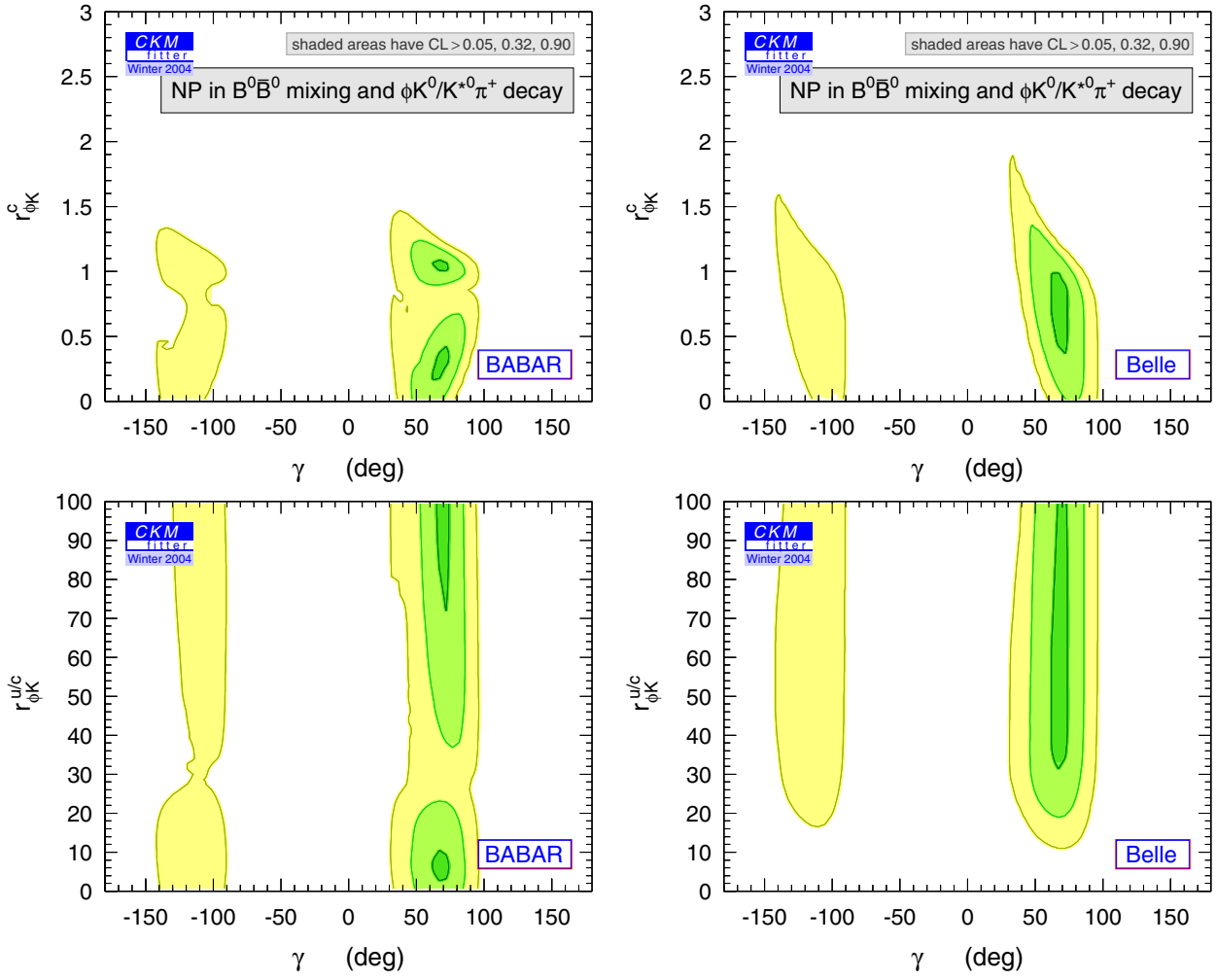

Fig. 60. Confidence levels in the $(\gamma, r^c_{\phi K})$ (upper) and $(\gamma, r^{u/c}_{\phi K})$ (lower) planes for *BABAR* (left) and Belle (right), obtained by the fit including NP in $B^0\overline{B}^0$ mixing and in $b \to s$ transitions. On the *BABAR* plots, small (resp. large) values for $r^c_{\phi K}$ (resp. $r^{u/c}_{\phi K}$) correspond to the solution $\cos 2\beta_{\rm eff} < 0$, and conversely. On the Belle plots, the two solutions are merged

We set CLs on the quantities $r^c_{\phi K}$ and $r^{u/c}_{\phi K}$, where we distinguish between the *BABAR* and Belle results for $C_{\phi K}$ and $S_{\phi K}$ since they lead to different implications. The fit inputs used are:

- the constraints on γ and $2\beta + 2\theta_d$ obtained from the NP fit in $B^0\overline{B}^0$ mixing as shown in the left hand plot of Fig. 57.
- the branching fraction $\mathcal{B}^{00}_{\Phi K} = (8.3^{+1.2}_{-1.0}) \times 10^{-6}$ [62], and the *CP* asymmetries in $B^0 \to \phi K^0$, $C_{\phi K}$ and $S_{\phi K} = \sqrt{1 - C^2_{\phi K}} \sin 2\beta_{\rm eff}$. *BABAR* measures: $S_{\phi K} = 0.47 \pm 0.34^{+0.08}_{-0.06}$, $C_{\phi K} = 0.01 \pm 0.33 \pm 0.10$ [136], and Belle finds: $S_{\phi K} = -0.96 \pm 0.50^{+0.09}_{-0.11}$, $C_{\phi K} = 0.15 \pm 0.29 \pm 0.08$ [137,62], where the first errors given are statistical and the second systematic.
- the branching fraction $\mathcal{B}^{0+}_{K^*\pi}$ (Table 11, Sect. VI.4.2).

The CL on $(\gamma, r^c_{\phi K})$ for $S_{\phi K}$ and $C_{\phi K}$ measured by *BABAR* (upper left hand plot in Fig. 60) shows two solutions for $r^c_{\phi K}$ due to the the twofold ambiguity[73] on $2\beta_{\rm eff}$. One of the solutions ($\cos 2\beta_{\rm eff} > 0$) is in agreement with $r^c_{\phi K}$ being one as expected if non-standard electroweak penguins are absent. In the case of the $S_{\phi K}$ and $C_{\phi K}$ results from Belle (upper right hand plot in Fig. 60) the two mirror solutions cannot be distinguished due to the $S_{\phi K}$ value being close to minus one. Also in this case, the constraint on $r^c_{\phi K}$ is in agreement with one, which recalls the remark in [300] that the measured branching ratio to ϕK is compatible with what is theoretically expected.

[73] In the $\pi^+\pi^-$ case (see the preceding section), the second solution for $\cos 2\alpha_{\rm eff}$ is suppressed by the additional constraints coming from the other $\pi\pi$ branching fractions.

In the case of $r_{\phi K}^{u/c}$, one of the solutions ($\cos 2\beta_{\rm eff} > 0$) for the *BABAR* measurement (lower left hand plot in Fig. 60) is consistent with order one values whereas the other solution ($\cos 2\beta_{\rm eff} < 0$) prefers large values. On the contrary, for the Belle result (lower right hand plot in Fig. 60), rather large values for $r_{\phi K}^{u/c} > 10$ are preferred indicating non-standard gluonic or electroweak penguins. Since $r_{\phi K}^{c}$ is found to be compatible with one, these large $r_{\phi K}^{u/c}$ values suggest that the anomaly, if there, may stem from gluonic penguins rather than from electroweak penguins, in contrast to some proposals in the literature [281,301]. It is worthwhile to note that the constraints $r_{\phi K}^{u/c}$ and $r_{\phi K}^{c}$ can be significantly improved in the future by reducing the experimental uncertainties on $S_{\phi K}$ and $C_{\phi K}$, and that again the γ input is less crucial here.

4 Conclusion

We have studied the constraints from present data on the amplitude parameters in the presence of arbitrary New Physics contributions to $K^0\overline{K}^0$ and $B^0\overline{B}^0$ mixing, and to $b \to d$ and $b \to s$ penguin transitions. The construction of a model-independent Unitarity Triangle is not (yet) precise enough to exclude sizable non-standard corrections to the mixing, in contrast to a prejudice commonly found in the literature.

The above statement should be softened in view of the great success of the standard CKM fit. Although this success could be accidental, the more general description including NP contributions is not particularly satisfying since it does not improve the fit while adding new, unknown parameters. Notably, the preferred region is consistent with the SM values for the NP parameters in $K^0\overline{K}^0$ and $B^0\overline{B}^0$ mixing. It might still be that NP contributions to $K^0\overline{K}^0$ and $B^0\overline{B}^0$ mixing may still be present, but can only be uncovered if the uncertainties on the inputs are significantly reduced. This situation will improve in the future as soon as accurate determinations of the angles α and γ from tree-dominated decays become available, the sign of $\cos(2\beta + 2\theta_d)$ is fully settled and improved determinations of the parameter $f_{B_d}\sqrt{B_d}$ are obtained.

We have proposed a fully model-independent parameterization of $\Delta B = 1$ decays. Present errors are large, thus excluding any definitive statement. A more precise measurement of the observables of the $B \to \pi\pi$ decays, in particular the time-dependent *CP*-asymmetry in $\pi^+\pi^-$, would greatly improve the constraint on the $b \to d$ to $b \to s$ amplitude ratio, while the input on the angle γ from the model-independent UT fit is less crucial. Still it can be said that potential NP contributions cannot exceed 100% of the SM strength of the $b \to d$ transition. More complete data on the $b \to u\bar{u}d$ decays to VP and VV final states would provide valuable independent information. In addition, our fits to the $B^0 \to \phi K^0$ *CP* asymmetries measured by *BABAR* and Belle show that the Belle measurement slightly prefers NP contributions with gluonic, rather than electroweak, penguin quantum numbers. However, the discrepancy with the *BABAR* result prevents us from drawing a firm conclusion.

Part VIII
Conclusion

During five years of successful running of the B factories, the experiments *BABAR* and Belle have produced a wealth of results, which greatly extend the knowledge on B physics acquired at the precursor experiments ARGUS, CLEO, the LEP collaborations as well as CDF. Also using the measurement of indirect *CP* violation in the neutral kaon system, these experiments succeeded to predict *CP* violation in the B system, namely $\sin 2\beta$, with a good precision and far prior to its direct measurement. Today, however, the measurement of $\sin 2\beta$ surpasses in precision the indirect determination. It represents the primary constraint on the Unitarity Triangle, and the only one that is theoretically fully under control. Yet, the determination of $\overline{\rho}$, $\overline{\eta}$ still requires input from measurements for which the theoretical predictions suffer from notable hadronic uncertainties. While these are reasonably well controlled, as far as the corresponding matrix elements can be computed with Lattice QCD, they exhibit large errors. It is the goal of the B factories to reduce this dependence on the strong interaction theory by means of direct and precise measurements of the three Unitarity Triangle angles and the two sides.

Since α and γ are linked to CKM-suppressed $b \to u$ transitions, large statistics samples are required for their measurement. Encouraging results have been presented recently by *BABAR* on the measurement of $\sin 2\alpha_{\rm eff}$ from a time-dependent analysis of $B^0 \to \rho^+\rho^-$. Using its SU(2) partners measured by *BABAR* and Belle, one can determine α with a precision of 19° at 90% CL, limited by the unknown penguin contribution. Due to the weak sensitivity to the penguin contamination of the isospin relations in $B \to \pi\pi$, the results on $\sin 2\alpha_{\rm eff}$ from the measurement of time-dependent *CP* asymmetry are less constraining. The analysis of $B \to \rho\pi$ decays mainly lacks the information from the Dalitz plot on the strong phase between the $\rho^+\pi^-$ and $\rho^-\pi^+$ states of the B^0 decay. The near future will clarify the achievable precision on α with these modes, which strongly depends on the underlying decay dynamics. Large B-related backgrounds, which are unknown to some extend at present, complicate the experimental analysis of $B \to \rho\rho$

and (to a lesser degree) $B \to \rho\pi$ decays, and hence produce sizable systematic uncertainties. The fruitful competition among the leading experiments provides important redundant measurements for these modes. The extraction of γ from the interference of $b \to c$ with $b \to u$ transitions is even more challenging due to the disparateness of the amplitude sizes, which suppresses either the observable *CP*-violating asymmetries or the total rate. A significant measurement of γ in a single mode requires larger data samples than those presently available. One way out of this is to combine measurements from a large number of different modes.

Two-body charmless B decays into pions and kaons are particularly convenient for phenomenological analyses since all modes, apart from those dominated by suppressed annihilation, exchange or $b \to d$ penguin amplitudes, have been measured. Also, the simplicity of the experimental signature reduces the systematic uncertainties. Penguin contributions, even in decays without net strangeness in the final state, make them to potentially sensitive probes of physics beyond the Standard Model.

Similarly, the measurement of mixing-induced or direct *CP* violation in modes that are dominated by $b \to s$ penguin amplitudes enjoy rising interest and are among the most anticipated results of the B factories. We note that a claim for New Physics not only requires that at least one of these modes departs from the Standard Model reference value, but also that they disagree among themselves if one wants to avoid a fine-tuning scenario. Due to the (inspiring) dissonance from the many models introducing New Physics phenomena and predicting specific effects on the observables, it is difficult to investigate New Physics in a systematic way. We have therefore chosen to build a general parameterization of generic New Physics amplitudes that interact in $B^0\overline{B}^0$ mixing and/or penguin B decays. The global CKM fit allows us to derive constraints on these generic New Physics amplitudes. Specific New Physics models have then to be in accordance with the allowed generic variable space.

We summarize in the following the main developments and results described in this work.

- All results are obtained with the use of the software package CKMfitter that employs statistical analysis tools based on the frequentist approach *R*fit. We have extended the analysis to take into account one- and two-dimensional physical boundary conditions as they occur in *CP*-asymmetry measurements.
- Among the main results of this paper are the numerical (Tables 2 and 3) and graphical (Figs. 5, 6, 7 and 8) representations of the global CKM fit. The values of the Wolfenstein parameters λ, A, $\overline{\rho}$, $\overline{\eta}$ are found to be in agreement with the results from our previous analysis (2001), and their 1σ errors have changed by relative $+14\%$, -58%, -45% and -64%, respectively, mainly due to the experimental improvements on $\sin 2\beta$ and $|V_{cb}|$. We find for the apex of the Unitarity Triangle, the coordinate $\overline{\rho} = 0.189^{+0.088}_{-0.070}$ and $\overline{\eta} = 0.358^{+0.046}_{-0.042}$. For the goodness of the global CKM fit within the Standard Model, we find a p-value of 71%.
- We have analyzed observables from rare kaon decays related to $\overline{\rho}$, $\overline{\eta}$ and derived constraints on the hadronic parameters B_6, B_8, related to ε'/ε. We discuss the present and future constraints in the unitarity plane from the rare decays $K^+ \to \pi^+\nu\overline{\nu}$ and $K_L^0 \to \pi^0\nu\overline{\nu}$.
- The constraints on $2\beta + \gamma$ and γ respectively from the *CP* analyses of $B^0 \to D^{(*)\pm}\pi^\mp$ and $B^+ \to D^0K^+$ decays are displayed. The present experimental errors are still too large to be competitive with the other measurements used in the global CKM fit.
- Results on charmless B decays to hh' $(h, h' = \pi, K)$ are studied in four different scenarios based on SU(2) and SU(3) flavor symmetries as well as QCD Factorization. Useful constraints on α are only obtained with significant theoretical input. A global fit of QCD Factorization to all available $\pi\pi, K\pi$ observables leads to an acceptable overall description (p-value of 21%), however with large non-factorizable corrections, and is remarkably predictive (cf. Fig. 35). Two predictions show deviations from the measurements: the branching fractions for $B^0 \to K^+\pi^-$ and $B^0 \to K^0\pi^0$, which come out somewhat large and small, respectively. The discrepancy does however not exceed 2.5 standard deviations in the worse case. The constraint on $\overline{\rho}$, $\overline{\eta}$ obtained from this fit is in agreement with the global CKM fit and competitive in precision. We do not observe significant hints for deviations from the Standard Model in these decays. Using SU(3) symmetry, we predict the branching fraction and *CP*-violating asymmetries in $B_s^0 \to K^+K^-$ decays.
- A specific section has been dedicated to the study of $B \to K\pi$ decays, where we analyze the impact of electroweak penguins in discussing the recent literature. Using a phenomenological parameterization and various dynamical hypotheses, we find that the current data do not significantly constrain electroweak parameters, neither hadronic amplitude ratios. In particular, the determination of the parameters related to electroweak penguins is not possible at present. We do not observe an unambiguous sign of New Physics, whereas central values of the parameters show evidence for potentially large non-perturbative rescattering effects. It is not clear to us whether a unified theoretical approach would be able to explain the whole set of observables in the $\pi\pi$ and $K\pi$ systems, if future measurements confirm the present pattern.
- Results on charmless B decays to $\rho\pi$ and their SU(3) partners are studied with the use of SU(2) and SU(3) flavor symmetry. The discrete ambiguities due to the unknown relative strong phase between the $B^0 \to \rho^+\pi^-$ and $B^0 \to \rho^-\pi^+$ amplitudes obstruct useful constraints on α in these modes. A Dalitz plot analysis is required to measure this phase. Within SU(3) symmetry and neglecting certain suppressed topologies, bounds on direct *CP*-violating asymmetries are derived. It is found that the present amount of direct *CP* violation measured by the

parameter $\mathcal{A}_{\rho\pi}^{-+}$ tends to violate this bound, suggesting that the size of the effect is a statistical fluctuation that is expected to reduce with the availability of more data.
- The isospin analysis of the $B \to \rho\rho$ system provides a useful constraint on α, which is found to be in agreement with the expectation from the global CKM fit. Including isospin-breaking corrections from electroweak penguins, and choosing the solution that is preferred by the CKM fit, we derive from the *BABAR* measurement of time-dependent CP asymmetries in $B^0 \to \rho^+\rho^-$ decays $\alpha = (94 \pm 12\,[^{+28}_{-25}] \pm 13\,[19])^\circ$. Here the first errors given are experimental, the second due to the penguin uncertainty, and the errors in brackets are at 2σ. If color suppression holds and if penguins are small, we expect that the present branching fraction measured for $B^+ \to \rho^+\rho^0$ should reduce with more data in order to close the isospin triangles. The potential to measure mixing-induced CP violation in $B^0 \to \rho^0\rho^0$ promises a brighter future, to reduce the uncertainty $\alpha - \alpha_{\rm eff}$ due to the unknown penguin pollution in $\rho^+\rho^-$, than it can be expected for $\pi\pi$. We have studied a simple extension of the isospin analysis to account for possible isospin-breaking effects. We find that the systematic uncertainties on α for the full isospin analysis can be of the order of 3°, depending on the amplitude structure of the decays.
- We refer to Sect. VI.7 for a more detailed summary of the results on all charmless B decays studied in this paper.
- We have studied the present data constraints on the amplitude parameters in the presence of arbitrary New Physics contributions to $B^0\overline{B}^0$ mixing and to $b \to d$ and $b \to s$ penguin transitions. The construction of a model-independent Unitarity Triangle is not precise enough to exclude sizable non-standard corrections to the mixing, which appears to be somehow in contrast to a prejudice found in the literature. The situation will improve in the future as soon as accurate determinations of the angles α and γ from tree dominated decays become available, and the theoretical errors on the lattice matrix elements relevant for the mixing are reduced. For $\Delta B = 1$ transitions we have shown that a general parameterization may give significant model-independent constraints on potential New Physics contributions, when the CP-violation measurements become more precise.

The outstanding role of B physics in the quest for a better understanding of CP violation in the Standard Model and beyond, as well as for the precise metrology of the off-diagonal CKM matrix elements, is assured by the continuous rise of the peak luminosity at the B factories. New and competitive results from the Tevatron experiments are expected soon, in particular the highly important measurement of $B_s^0\overline{B}_s^0$ oscillation. We have attempted to extrapolate the results leading to the Unitarity Triangle angle α up to luminosities of $1\,{\rm ab}^{-1}$ (and $10\,{\rm ab}^{-1}$ in some cases). It seems reasonable to expect that a determination of α, dominated by $B \to \rho\rho$, to an error of about 6° or better (not including isospin-breaking effects) can be achieved towards the end of the first generation B-factory program, with an expected integrated luminosity of combined roughly $2\,{\rm ab}^{-1}$. Plausible extrapolations for the angle γ are more difficult since all measurements in the beauty-to-charm sector crucially depend on the ratios of the corresponding CKM-suppressed-to-CKM-favored amplitudes, which are only approximately known at present.

In summary, we can hope for a precise metrology of the Unitarity Triangle angles within a few years, but – in view of the present results – we do not expect it to be sufficiently accurate to reveal inconsistencies with the CKM picture. Therefore, besides Δm_s, major attention is directed to the forthcoming measurements of CP-violation parameters in penguin-dominated modes. The near future will show whether the current pattern turns into a significant deviation from the expectation, or if the discrepancies fall behind the theoretical uncertainties that are expected in these modes.

Acknowledgements. We are indebted to Martin Beneke, Achim Denig, Urs Langenegger, Matthias Neubert, Yoshi Sakai and Klaus Schubert for informative discussions. We thank Helen Quinn and Zoltan Ligeti for an animated exchange on the SU(3) relations. The study on rare kaon decays has benefited from valuable correspondence with Shaomin Chen and David Jaffe. Santi Peris pointed out two interesting references. Tom Trippe kindly produced updated input values for the kaon mixing parameters. Fruitful conversations with David London and Tobias Hurth on the isospin study of $B \to K\pi$ decays are gratefully acknowledged. We thank Phil Clark, Malcolm John, David Kirkby and Robert McPherson for the constructive and knowledgeable help in our quest for the right title. JC acknowledges partial support from EC-Contract HPRN-CT-2002-00311 (EURIDICE).

Part IX
Appendices

A: Statistical significance of $B_s^0\overline{B}_s^0$ oscillation

The purpose of this appendix is to evaluate the statistical significance of the world average results on $B_s^0\overline{B}_s^0$ oscillation. At present, the world average likelihood as a function of Δm_s exhibited a roughly parabolic behavior at $\Delta m_s \simeq 17\,{\rm ps}^{-1}$. Following an analytical approach, we address two questions:
- what is the PDF of a likelihood measurement of Δm_s and what is the confidence level (CL) as a function of Δm_s to be associated with an observation obtained with the current level of sensitivity;
- what is the expected likelihood behavior and how reliable it is to use the likelihood to infer CLs.

A.1 Definitions and proper decay time modeling

Using the simplified framework of [123], we denote for a homogeneous event sample:

- $P_{s\pm}$ the (true) time distribution (in unit of the B_s lifetime τ_B) of mixed (P_{s-}) and unmixed (P_{s+}) events, given by
$$P_{s\pm} = \frac{1}{2}e^{-t}(1 \pm \cos(x_s t)) \ , \tag{A.1}$$
with $x_s = \Delta m_s \tau_b$,
- w the mistag rate, and $D = 1 - 2w$ the corresponding dilution factor;
- f_s the fraction of signal events in the sample;
- The background is assumed to:
  - follow the same exponential distribution as the signal,
  - be purely of the unmixed type,
  - be affected by the same mistag rate;
- G_t the detector resolution function for the time measurement $t \to t_{\rm mes}$;
It is assumed to be a Gaussian of zero mean and time dependent width
$$\sigma = \sqrt{a + bt^2} \tag{A.2}$$
$$G_t(t_{\rm mes} - t) = \frac{1}{\sqrt{2\pi}\sigma} \exp\left(-\frac{1}{2}\left(\frac{t_{\rm mes} - t}{\sigma}\right)^2\right) \ , \tag{A.3}$$
with a accounting for the decay length measurement and b accounting for the momentum measurement
$$a = \left(\frac{m}{p}\frac{\sigma_L}{c\tau_B}\right)^2 , \qquad b = \left(\frac{\sigma_p}{p}\right)^2 . \tag{A.4}$$

With these notations the proper time distribution of events, classified as mixed or unmixed, read

$$P_-(t_{\rm mes}) = \left(f_s \frac{1}{2}\left(1 - D\cos(x_s t)\right) + (1 - f_s)w\right) e^{-t} \otimes G_t \ , \tag{A.5}$$
$$P_+(t_{\rm mes}) = \left(f_s \frac{1}{2}\left((1 + D\cos(x_s t)\right) + (1 - f_s)(1 - w)\right) e^{-t} \otimes G_t \ . \tag{A.6}$$

Taken together, these distributions are normalized to unity

$$\int_{-\infty}^{+\infty} (P_- + P_+) dt_{\rm mes} = 1 \ . \tag{A.7}$$

A.2 Measurement

The x_s measurement is assumed to be performed with the use of the log-likelihood

$$\mathcal{L}(x_s) = \sum_- \ln(P_-) + \sum_+ \ln(P_+) \ , \tag{A.8}$$

where the first (second) sum runs over mixed (unmixed) events. The measured value of x_s ($x_s^{\rm mes}$) is defined to be the one maximizing $\mathcal{L}(x_s)$

$$\left.\frac{\partial \mathcal{L}(x_s)}{\partial x_s}\right|_{x_s = x_s^{\rm mes}} = 0 \ . \tag{A.9}$$

The outcome of the experiment $x_s^{\rm mes}$ is a random number, which, for large enough statistics, follows a Gaussian PDF

$$\mathcal{P}(x_s^{\rm mes} \mid x_s) \equiv \Phi_{\rm lo}^{x_s}(x_s^{\rm mes}) = \frac{1}{\sqrt{2\pi}\Sigma(x_s)} \exp\left(-\frac{1}{2}\left(\frac{x_s^{\rm mes} - x_s}{\Sigma(x_s)}\right)^2\right) \ , \tag{A.10}$$

where the standard deviation $\Sigma(x_s)$ is given by the second derivative of $\mathcal{L}$, through the integral A

$$(\sqrt{N}\Sigma(x_s))^{-2} = \int_{-\infty}^{+\infty} \left(\frac{(\dot{P}_-)^2}{P_-} + \frac{(\dot{P}_+)^2}{P_+} \right) dt_{\rm mes} \equiv A(x_s) \ , \tag{A.11}$$

$$\dot{P}_\pm = \frac{\partial P_\pm}{\partial x_s} \tag{A.12}$$

$$= \mp f_s \frac{1}{2} D \ t \sin(x_s t) e^{-t} \otimes G_t \ . \tag{A.13}$$

Here N is the total number of mixed and unmixed events, and the integrals are performed with the use of the *true* value of x_s, not the measured one[74].

It follows from (A.10) that one may set a confidence level $\mathrm{CL}(x_s^{\rm hyp})$ on a given x_s hypothetical value $x_s^{\rm hyp}$ using the χ^2 law

$$\mathrm{CL}(x_s^{\rm hyp}) = \int_< \Phi_{\rm lo}^{x_s}(x_s^{\rm mes\prime}) dx_s^{\rm mes\prime} = \mathrm{Prob}(\chi^2, 1) \ , \tag{A.15}$$

$$\chi_s^x(x_s^{\rm mes}) = \frac{x_s^{\rm mes} - x_s^{\rm hyp}}{\Sigma(x_s^{\rm hyp})} \ , \tag{A.16}$$

where the integral is performed over the $x_s^{\rm mes\prime}$ domain where $\Phi_{\rm lo}^{x_s}(x_s^{\rm mes\prime}) < \Phi_{\rm lo}^{x_s}(x_s^{\rm mes})$, that is to say where $\chi_s^x(x_s^{\rm mes\prime}) > \chi_s^x(x_s^{\rm mes})$.

A.2.1 Parabolic behavior

If the log-likelihood is parabolic nearby its maximum

$$\mathcal{L}(x_s^{\rm hyp}) \simeq \mathcal{L}(x_s^{\rm mes}) + \frac{1}{2} \left. \frac{\partial^2 \mathcal{L}}{\partial x_s^2} \right|_{x_s = x_s^{\rm mes}} \left(x_s^{\rm hyp} - x_s^{\rm mes} \right)^2 \ , \tag{A.17}$$

then, in the vicinity of $x_s^{\rm mes}$, $\Sigma(x_s^{\rm hyp}) \simeq cst = \Sigma(x_s^{\rm mes})$, and one can evaluate Σ as the second derivative of the experimental log-likelihood, taken at the measured value $x_s^{\rm mes}$. In effect

$$- \left. \frac{\partial^2 \mathcal{L}}{\partial x_s^2} \right|_{x_s = x_s^{\rm mes}} = - \left(\sum_- \left(\frac{\ddot{P}_- P_- - (\dot{P}_-)^2}{P_-^2} \right)^2 + \sum_+ \left(\frac{\ddot{P}_+ P_+ - (\dot{P}_+)^2}{P_+^2} \right)^2 \right) \tag{A.18}$$

$$\stackrel{(N\to\infty)}{\longrightarrow} N A(x_s) = \Sigma^{-2} \ , \tag{A.19}$$

where $\ddot{P}_\pm$ denotes the second derivative with respect to x_s

$$\ddot{P}_\pm = \frac{\partial^2 P_\pm}{\partial x_s^2} \tag{A.20}$$

$$= \mp f_s \frac{1}{2} D \ t^2 \cos(x_s t) e^{-t} \otimes G_t \ , \tag{A.21}$$

which however does not appear in the final expression thanks to (A.7), and assuming that $x_s^{\rm mes} = x_s$ (which is true for $N \to \infty$).

[74] If the event sample is not homogeneous but is an admixture of n_s homogeneous subsamples, each with a detector resolution function ${G_t}^i$, a signal fraction f_s^i, a mistag rate w^i, and representing a fraction f_i of the overall sample of N events, the corresponding time distribution are denoted $P_\pm^i$ (the factor f_i being not included). The A integral (as well as other integrals introduced below) is then to be replaced by the weighted sums

$$A(x_s) = \sum_{i=1}^{n_s} f_i A^i(x_s) \ . \tag{A.14}$$

Equivalently, one can evaluate Σ by locating the value of $x_s^{\rm hyp}$ which yields a drop of $-1/2$ of the log-likelihood, for the experiment at hand, or one can compute directly the χ^2 using the approximation

$$\chi^2(x_s^{\rm hyp}) = \left(\frac{x_s^{\rm mes} - x_s^{\rm hyp}}{\Sigma(x_s^{\rm hyp})}\right)^2 \simeq 2(\mathcal{L}(x_s^{\rm mes}) - \mathcal{L}(x_s^{\rm hyp})) \equiv \tilde{\chi}^2(x_s^{\rm hyp}) \ . \tag{A.22}$$

Bayesian point of view
Because of the simplicity of the above relations, one may introduce the concept of the *PDF of the true value of* x_s by remarking that, if $x_s^{\rm mes}$ is viewed as a non-random number (the actual outcome of a finalized single experiment) while the true value of x_s is taken to be a random number, the object

$$\mathcal{P}(x_s \mid x_s^{\rm mes}) \equiv \Phi_{\rm lo}^{x_s^{\rm mes}}(x_s) \ , \tag{A.23}$$

allows to define

$$\mathrm{CL}(x_s^{\rm hyp}) = \mathrm{Prob}(\chi^2, 1) \ , \tag{A.24}$$

$$\chi = \frac{x_s^{\rm hyp} - x_s^{\rm mes}}{\Sigma(x_s^{\rm mes})} \ , \tag{A.25}$$

which is numerically identical to the one of (A.15) – if $\Sigma(x_s^{\rm mes}) = \Sigma(x_s^{\rm hyp})$ – but with a completely different reading: one states that the CL of $x_s^{\rm hyp}$ is given by

$$\mathrm{CL}(x_s^{\rm hyp}) = \int_{<} \mathcal{P}(x_s^{\rm mes} \mid x_s^{\rm hyp\prime}) dx_s^{\rm hyp\prime} \ , \tag{A.26}$$

where the integral is performed over the $x_s^{\rm hyp\prime}$ domain where $\mathcal{P}(x_s^{\rm mes} \mid x_s^{\rm hyp\prime}) < \mathcal{P}(x_s^{\rm mes} \mid x_s^{\rm hyp})$.

A.2.2 Non-parabolic behavior

Obviously, for large enough $x_s^{\rm hyp}$, the approximation $\Sigma(x_s^{\rm hyp}) \simeq \Sigma(x_s^{\rm mes})$ breaks down since the sensitivity of the experiment vanishes due to the finite vertex resolution, i.e., $\Sigma(x_s^{\rm hyp} \to \infty) \to \infty$. It follows that the likelihood is not parabolic for large enough $x_s^{\rm hyp}$. The vanishing sensitivity makes χ^2, as defined by (A.16), a poor test statistics to probe for large x_s values. Furthermore, as discussed in Appendix A.4 to infer from the χ^2 value the correct $\mathrm{CL}(x_s^{\rm hyp})$ is not a straightforward task: (A.15) does not apply (i.e., it is not a real χ^2) because (A.10) is a poor approximation.

The redefinition of the χ^2 using the right hand side of (A.22) provides a more appropriate test statistics to deal with large values of $x_s^{\rm hyp}$. Whereas (A.15) does not apply, $\tilde{\chi}^2$ is capable of ruling out $x_s^{\rm hyp}$ values lying beyond the sensitivity reach[75] (if $\mathcal{L}(x_s^{\rm mes})$ value is large enough) provided one computes the CL using

$$\mathrm{CL}(x_s^{\rm hyp}) \ = \int_{\tilde{\chi}^2(x_s^{\rm hyp})}^{\infty} \Psi^{x_s^{\rm hyp}}(\tilde{\chi}^{2\prime}) \ D\tilde{\chi}^{2\prime} \ , \tag{A.27}$$

where $\Psi^{x_s^{\rm hyp}}$ is the PDF of the $\tilde{\chi}^2$ test statistics, for $x_s = x_s^{\rm hyp}$, to be obtained with the use of toy Monte Carlo. A tempting shortcut is to bypass the toy Monte Carlo simulation and to assume that the approximation

$$\mathrm{CL}(x_s^{\rm hyp}) \approx \mathrm{Prob}(\tilde{\chi}^2(x_s^{\rm hyp}), 1) \ , \tag{A.28}$$

remains valid although the approximation of (A.22) is known to break-down.

Bayesian point of view
The $x_s^{\rm hyp}$ 'PDF' introduced in (A.23) can be redefined as

$$\mathcal{P}(x_s^{\rm hyp} \mid x_s^{\rm mes}) \equiv \varphi_{\mathcal{L}}^{x_s^{\rm mes}}(x_s^{\rm hyp}) = \mathrm{const} \times \exp\left(\mathcal{L}(x_s^{\rm hyp}) - \mathcal{L}(x_s^{\rm mes})\right) \ , \tag{A.29}$$

where the constant should be such that $\varphi_{\mathcal{L}}$ is normalized to unity when integrated over $x_s^{\rm hyp}$. In the present case, such a constant does not exist because

$$\lim_{x_s^{\rm hyp} \to \infty} \mathcal{L}(x_s^{\rm hyp}) \ = \ \text{finite constant} \ , \tag{A.30}$$

[75] The rejection of $x_s^{\rm hyp}$ values beyond the sensitivity reach is not a paradox: it uses the fact that large values are unlikely to yield an indication of a clear signal, especially at low values of x_s.

and hence $\varphi_{\mathcal{L}}$ itself tends asymptotically towards a constant. We will consider below the average value of $\varphi_{\mathcal{L}}$ as computed using the average likelihood which one would obtain. Ignoring statistical fluctuations the average function is denoted

$$\varphi_{\overline{\mathcal{L}}}^{x_s}(x_s^{\rm hyp}) = N \int (P_-^{x_s} \ln(P_-^{x_s^{\rm hyp}}) + P_+^{x_s} \ln(P_+^{x_s^{\rm hyp}}))dt_{\rm mes} \ , \tag{A.31}$$

and its leading order, next-to-leading order and next-to-next-to leading order approximations are denoted $\varphi_{\overline{\mathcal{L}}:lo}$, $\varphi_{\overline{\mathcal{L}}:\rm nlo}$ and $\varphi_{\overline{\mathcal{L}}:\rm nnlo}$. The numerical value of the ratio

$$R_{\rm tail} \equiv \frac{\varphi_{\overline{\mathcal{L}}}(\infty)}{\varphi_{\overline{\mathcal{L}}}(x_s)} \ , \tag{A.32}$$

which vanishes exponentially with N, is a measure of how non-Gaussian the likelihood is.

A.3 Experimental constraint

The question arises as to how to incorporate experimental constraints derived from the B_s mixing analysis into a global CKM fit. A possibility is to add to the (twice)log-likelihood of the global fit the term

$$\chi^2(x_s^{\rm hyp}) = 2(\mathcal{L}(\infty) - \mathcal{L}(x_s^{\rm hyp})) \ , \tag{A.33}$$

or equivalently to multiply the likelihood L by the ratio

$$\Delta L = \frac{\mathcal{P}(x_s^{\rm hyp} \mid x_s^{\rm mes})}{\mathcal{P}(\infty \mid x_s^{\rm mes})} \ , \tag{A.34}$$

where the constant denominator is introduced here for convenience only. Since the $\mathcal{L}$ function is defined up to an irrelevant additive constant, using (A.33) or (A.22) amounts to making the same approximation, which is guaranteed to be correct, for large enough statistics, and in the vicinity of $x_s^{\rm mes}$.

The question remains to determine under which conditions on N and $x_s^{\rm hyp}$ the approximation is

1. **obviously valid:** that is to say to determine the domain of validity of the leading order ($N \to \infty$) key-formula (A.10). To answer this question, one should compute its next-to-leading order (NLO) correction terms: Appendix A.4 is devoted to that.
2. **non-obviously valid:** that is to say to determine whether or not, even though the key-formula does not apply, (A.33) provides nevertheless a means to compute the CL with an acceptable accuracy: Appendix A.5 discusses that.

A.4 Next-to-leading order key-formula

The next-to-leading order key-formula can be written as[76]

$$\Phi_{\rm nlo}^{x_s}(x_s^{\rm mes}) = \Phi_{\rm lo}^{x_s}(x_s^{\rm mes})\ e^{-a_3^{x_s}\chi^3}(1 + a_0^{x_s}\chi) \ , \tag{A.35}$$

$$a_0^{x_s} = \frac{2B - C}{2A}\frac{1}{\sqrt{NA}} = -\dot{\Sigma} \ , \tag{A.36}$$

$$a_3^{x_s} = \frac{3B - C}{6A}\frac{1}{\sqrt{NA}} \ , \tag{A.37}$$

where $A(x_s)$ is the integral defined in (A.11), and $B(x_s)$ and $C(x_s)$ are the two new integrals

$$B(x_s) = \int_{-\infty}^{+\infty} \left(\frac{\dot{P}_- \ddot{P}_-}{P_-} + \frac{\dot{P}_+ \ddot{P}_+}{P_+} \right) dt_{\rm mes} \ , \tag{A.38}$$

$$C(x_s) = \int_{-\infty}^{+\infty} \left(\frac{(\dot{P}_-)^3}{P_-^2} + \frac{(\dot{P}_+)^3}{P_+^2} \right) dt_{\rm mes} \ . \tag{A.39}$$

[76] In the course of the computation, the a_3 correction term appears in the exponential, as indicated. However the formula is correct up to the next-to-leading order only, and the a_3 term can be brought down to the level of the a_0 term without affecting this. Although it would guaranty the proper normalization of $\Phi_{\rm nlo}$ to unity, this simplification is not done below.

The integral C tends to be small because, (i) the two contributions have opposite signs, and (ii) the denominator is of order two: it follows that $a_3 \simeq a_0/2$. The right hand side of (A.36) links the next-to-leading order correction terms a_0 and a_3 to the dependence on x_s of Σ. When Σ depends significantly on x_s the key-formula breaks down: not only is the standard treatment of Appendix A.2.1 invalid (and the Bayesian treatment mathematically unjustified), but the well-known formula (A.15) itself becomes incorrect, even if one uses the correct $\Sigma(x_s)$.

The expression (A.35) is identical to (A.10) for small χ values. Although it extends the range of validity to larger χ values, it cannot be trusted too far away from the origin, where higher order corrections start to play a role. In particular, $\Phi_{\rm nlo}$ becomes negative (hence meaningless) for $\chi > -a_0^{-1}$ (a_0 is negative since it is equal to minus the derivative of Σ with respect to x_s).

Since Φ is sizeable only insofar $\chi \sim \mathcal{O}(1)$ the next-to-leading order terms, when relevant, are of the form $N^{-\frac{1}{2}} \times$ [ratio of integrals]. Hence they are negligible for large enough N and for a small enough ratio of integrals.

The most likely value for $x_s^{\rm mes}$ is no longer x_s, and a non-zero value of B leads to a $\mathcal{O}(1/N)$ bias in the measurement. The expected value of $x_s^{\rm mes}$ reads

$$\langle x_s^{\rm mes} \rangle = x_s - \left(\frac{B(x_s)}{A} \frac{\Sigma}{2} \right) \Sigma \ . \tag{A.40}$$

The bias is negligible (in unit of Σ) if the event sample is large enough, i.e. if $N \gg B^2/(4A^3)$. To next-to-leading order, the double-sided CL reads

$$\mathrm{CL}_{\rm nlo}(x_s^{\rm hyp}) = \int\limits_{<} \Phi_{\rm nlo}^{x_s^{\rm hyp}}(x_s^{\rm mes\prime}) dx_s^{\rm mes\prime} \ , \tag{A.41}$$

where the integral is performed over the $x_s^{\rm mes\prime}$ domain where $\Phi_{\rm nlo}^{x_s^{\rm hyp}}(x_s^{\rm mes\prime}) < \Phi_{\rm nlo}^{x_s^{\rm hyp}}(x_s^{\rm mes})$.

A.5 Using the likelihood function

A.5.1 Average likelihood shape

To next-to-leading order, and in the vicinity of the true x_s value, the average log-likelihood function takes the form (cf. Appendix A.7)

$$\overline{\mathcal{L}}_{\rm nlo}(x_s^{\rm hyp}) \simeq \overline{\mathcal{L}}(x_s) - \overline{\alpha_1}\chi + \overline{\alpha_2}\chi^2 - \overline{\alpha_3}\chi^3 \ , \tag{A.42}$$

with

$$\overline{\alpha_1} = 0 \ , \qquad \overline{\alpha_2} = -\frac{1}{2} \ , \qquad \overline{\alpha_3} = -\frac{3B-2C}{6A}\frac{1}{\sqrt{NA}} \simeq -a_3 \simeq \frac{1}{2}\dot{\Sigma} \ , \tag{A.43}$$

and

$$\chi \equiv \frac{x_s - x_s^{\rm hyp}}{\Sigma(x_s)} \ . \tag{A.44}$$

Although the above expression reaches its maximum at $\chi = 0$, this does not contradict the fact that $x_s^{\rm mes}$ is a biased estimator of x_s: because of the statistical fluctuations, the first term of the expansion is non-zero for a given experiment (cf. Appendix A.7).

A.5.2 Amplitude formalism

It was shown in [123] that the log-likelihood function $\mathcal{L}(x_s)$ can be retrieved from the functions $\mathcal{A}(x_s)$ and $\sigma[\mathcal{A}](x_s)$ defined as the measurement and the uncertainty on the measurement of an *ad hoc* amplitude coefficient $\mathcal{A}$ placed in front of the cosine modulation term

$$P_-(t_{\rm mes})[\mathcal{A}] = \left(f_s \frac{1}{2}\left(1 - D\mathcal{A}\cos(x_s t)\right) + (1-f_s)w \right) e^{-t} \otimes G_t \ , \tag{A.45}$$

$$P_+(t_{\rm mes})[\mathcal{A}] = \left(f_s \frac{1}{2}\left(1 + D\mathcal{A}\cos(x_s t)\right) + (1-f_s)(1-w) \right) e^{-t} \otimes G_t \ . \tag{A.46}$$

Restated in the framework of the present work, the advantage of this indirect probe of the oscillation phenomenon stems from the fact that the dependence on $\mathcal{A}$ is linear and hence the correction terms of the NLO key-formula vanish: the measurement of $\mathcal{A}$ is purely Gaussian, and it follows that merging different experimental measurements is straightforward.

The result established in [123] takes the form

$$\mathcal{L}_s^x(x_s^{\rm hyp}) = \frac{\mathcal{A}(x_s^{\rm hyp}) - \frac{1}{2}}{\sigma^2[\mathcal{A}]} + \mathcal{L}_s^x(\infty) \ . \tag{A.47}$$

It can be shown to be an excellent, though approximate, relationship by introducing the objects

$$\mathcal{E}_- = \left(f_s \frac{1}{2} + (1-f_s)w \right) e^{-t} \otimes G_t \ , \tag{A.48}$$

$$\mathcal{E}_+ = \left(f_s \frac{1}{2} + (1-f_s)(1-w) \right) e^{-t} \otimes G_t \ , \tag{A.49}$$

$$\mathcal{K}_-(x_s) = -\frac{1}{\mathcal{E}_-} \left(f_s \frac{1}{2} D \cos(x_s t) e^{-t} \otimes G_t \right) \ , \tag{A.50}$$

$$\mathcal{K}_+(x_s) = \ \frac{1}{\mathcal{E}_+} \left(f_s \frac{1}{2} D \cos(x_s t) e^{-t} \otimes G_t \right) \ , \tag{A.51}$$

(A.45) takes the form

$$P_\pm(x_s^{\rm hyp}) = \mathcal{E}_\pm(1 + \mathcal{A}\mathcal{K}_\pm(x_s^{\rm hyp})) \ . \tag{A.52}$$

The two $\mathcal{K}_\pm(x_s^{\rm hyp})$ objects bear the properties:

- $\mid \mathcal{K}_\pm \mid \leq 1$, in principle.
- $\mid \mathcal{K}_\pm \mid \ll 1$, in practice. This is because the D coefficient is usually smaller than one, hence higher powers of $\mathcal{K}$ are suppressed, but also because when considering large enough x_s values the convolution with the finite detector response G_t washes out the cosine modulation

$$\lim_{x_s^{\rm hyp} \to \infty} \mathcal{K}_\pm(x_s^{\rm hyp}) = 0 \ . \tag{A.53}$$

Hence the log-likelihood of (A.8) (with or without $\mathcal{A}$) can be expanded to the second order in $\mathcal{K}_\pm$ (omitting here the $\pm$ index distinguishing mixed and unmixed events)

$$\mathcal{L}(x_s^{\rm hyp} : \mathcal{A}) = \sum \ln(P(x_s^{\rm hyp})) \tag{A.54}$$

$$= \sum \ln(\mathcal{E}) + \sum \ln(1 + \mathcal{A}\mathcal{K}(x_s^{\rm hyp})) \tag{A.55}$$

$$\simeq \mathcal{L}_s^x(\infty) + \sum (\mathcal{A}\mathcal{K}(x_s^{\rm hyp}) - \frac{1}{2}\mathcal{A}^2\mathcal{K}^2(x_s^{\rm hyp})) \ . \tag{A.56}$$

The log-likelihood we are interested in is

$$\mathcal{L}(x_s^{\rm hyp}) = \mathcal{L}(x_s^{\rm hyp} : \mathcal{A} \equiv 1) \simeq \mathcal{L}_s^x(\infty) + \sum (\mathcal{K}(x_s^{\rm hyp}) - \frac{1}{2}\mathcal{K}^2(x_s^{\rm hyp})) \ . \tag{A.57}$$

The derivative of the log-likelihood used to compute $\mathcal{A}(x_s^{\rm hyp})$ is

$$\frac{\partial \mathcal{L}(x_s^{\rm hyp} : \mathcal{A})}{\partial \mathcal{A}} = \sum (\mathcal{K}(x_s^{\rm hyp}) - \mathcal{A}\mathcal{K}^2(x_s^{\rm hyp})) \ , \tag{A.58}$$

from which one obtains

$$\mathcal{A}(x_s^{\rm hyp}) = \frac{\sum \mathcal{K}(x_s^{\rm hyp})}{\sum \mathcal{K}^2(x_s^{\rm hyp})} \pm \frac{1}{\sqrt{\sum \mathcal{K}^2(x_s^{\rm hyp})}} \ , \tag{A.59}$$

where the expression for the uncertainty neglects higher order $\mathcal{K}^{n \geq 3}$ terms. Using (A.59) in (A.57) one recovers (A.47). Equation (A.59) yields a slightly biased estimator of $\mathcal{A}$ because the higher order terms do not exactly cancel out, even on the average[77]. This bias is negligible for all values of $x_s^{\rm hyp}$ but for $x_s^{\rm hyp} \simeq x_s$ where, although it remains small, it becomes noticeable.

Table 16. Numerical values entering into the NLO PDF $\Phi_{\rm nlo}$ and NNLO average likelihood, for four values of Δm_s. The definition of the four integrals D, E, F and G are given in Appendix A.7. The value above which $\Phi_{\rm nlo}$ becomes negative is $\Delta m_s[\max] = \Delta {\rm m_s} - {\rm a_0^{-1}}\Sigma \simeq \Delta {\rm m_s} - {\rm A/B} \simeq \Delta {\rm m_s} + 5({\rm\, ps^{-1}})$. The ratio $R_{\rm tail} = \varphi_{\overline{\mathcal{L}}}(\infty)/\varphi_{\overline{\mathcal{L}}}(\Delta m_s)$ provides a measure of how far from its Gaussian limit the likelihood is

Δm_s (ps^{-1})	10	17	20	25
Σ (ps^{-1})	0.33	1.38	2.67	7.36
A	0.77 10^{-2}	0.44 10^{-3}	0.11 10^{-3}	0.15 10^{-4}
B/A	−0.18	−0.19	−0.21	−0.17
C/A	0.03	−0.002	−0.007	0.005
D/A	1.40	0.53	0.65	1.31
E/A	0.08	0.005	0.001	0.00
F/A	0.05	0.007	0.002	-0.001
G/A	−1.27	−0.51	−0.30	-0.38
a_0	−0.06	−0.26	−0.55	-1.26
a_3	−0.03	−0.13	−0.28	−0.62
$\overline{\alpha_3}$	0.03	0.13	0.27	0.63
$\overline{\alpha_4}$	0.004	0.04	−0.22	-5.48
$\Delta m_s[\max]$	15.1	22.2	24.9	30.8
$R_{\rm tail}$	3. 10^{-6}	0.12	0.37	0.75

A.6 Discussion on numerical examples

For illustration, we use here numbers that correspond to the present level of sensitivity of the world average

$$N = 1200\ , \quad f_s = 0.35\ , \quad w \text{ is set to zero}\ , \quad a = 0.0046\ , \quad b = 0.0090\ .$$

The numerical values of the coefficients introduced previously are given in Table 16 for four Δm_s values.

Figure 61 shows the next-to-leading-order $\Phi_{\rm nlo}$ PDF (A.35) of the Δm_s measurement for a true value of $\Delta m_s = 10\,{\rm ps^{-1}}$ and the leading order PDF $\Phi_{\rm lo}$ (A.10). The two PDFs being barely distinguishable, the leading order approximation is excellent.

Figure 62 gives the next-to-leading-order $\Phi^{17}_{\rm nlo}$ PDF of the Δm_s measurement (solid line) and leading order PDF $\Phi^{17}_{\rm lo}$ (dotted line), for a true value $\Delta m_s = 17\,{\rm ps^{-1}}$. The two PDFs differ significantly, but the leading order approximation remains acceptable in the core of the distribution. However it would underestimate by a factor about two the probability to obtain a measurement above $\Delta m_s = 20\,{\rm ps^{-1}}$. The right hand plot in Fig. 62 shows the next-to-leading-order $\Phi^{17}_{\rm nlo}$ PDF (solid line) together with $\Phi^{20}_{\rm nlo}$ PDF (dotted line) and the leading order PDF $\Phi^{20}_{\rm lo}$ for $\Delta m_s = 20\,{\rm ps^{-1}}$ (dashed-dotted line). The integral of $\Phi^{17}_{\rm nlo}$ above $\Delta m_s = 20\,{\rm ps^{-1}}$ is not a good approximation of the CL of a true value $\Delta m_s = 20\,{\rm ps^{-1}}$ leading to a measurement $\Delta m_s = 17\,{\rm ps^{-1}}$, the latter being defined as the integral of Φ^{20}_0 below $\Delta m_s = 17\,{\rm ps^{-1}}$. However, in the present case, one cannot fully rely on the approximation $\Phi^{20}_0 \simeq \Phi^{20}_{\rm nlo}$ owing to the large variation between $\Phi^{20}_{\rm lo}$ and $\Phi^{20}_{\rm nlo}$.

Figure 63 shows the solutions amplitude $\mathcal{A}$ given in (A.59) for different true values of Δm_s.

[77] They would cancel if the background were affecting in the same way P_- and P_+.

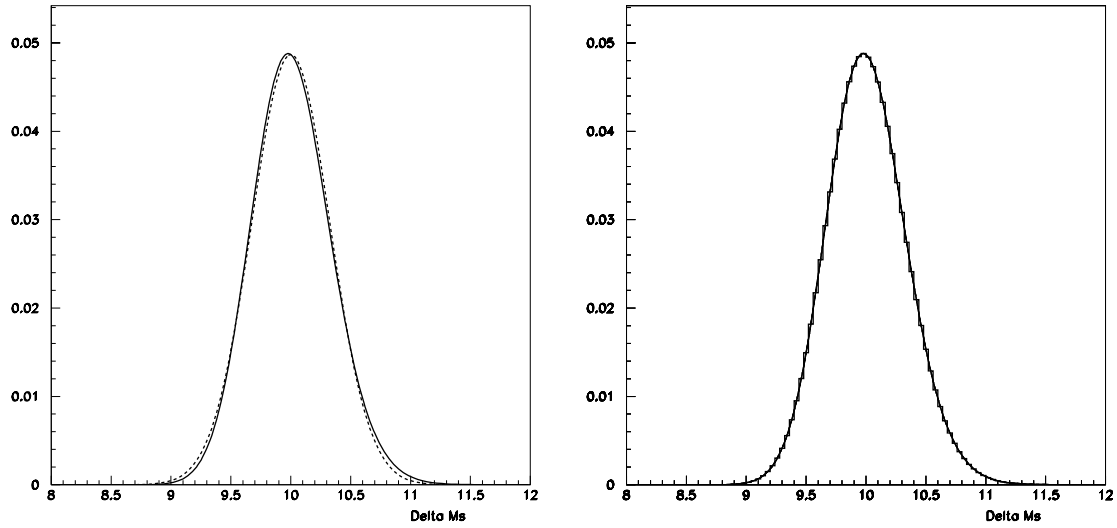

Fig. 61. *Left*: next-to-leading-order $\Phi^{10}_{\rm nlo}$ PDF of the Δm_s measurement (solid line) and leading order PDF $\Phi^{10}_{\rm lo}$ (dotted line), for a true value $\Delta m_s = 10\,\mathrm{ps}^{-1}$. The two PDFs are barely distinguishable. The leading order approximation is excellent. *Right*: next-to-leading-order $\Phi^{10}_{\rm nlo}$ PDF (solid line) and $\Phi^{11}_{\rm nlo}$ PDF, for $\Delta m_s = 11\,\mathrm{ps}^{-1}$ (dotted line). The integral of $\Phi^{10}_{\rm nlo}$ above $\Delta m_s = 11\,\mathrm{ps}^{-1}$ is a good approximation of the CL of a true value $\Delta m_s = 11\,\mathrm{ps}^{-1}$ leading to a measurement $\Delta m_s \leq 10\,\mathrm{ps}^{-1}$, the latter being defined as the integral of Φ^{11}_0 below $\Delta m_s = 10\,\mathrm{ps}^{-1}$

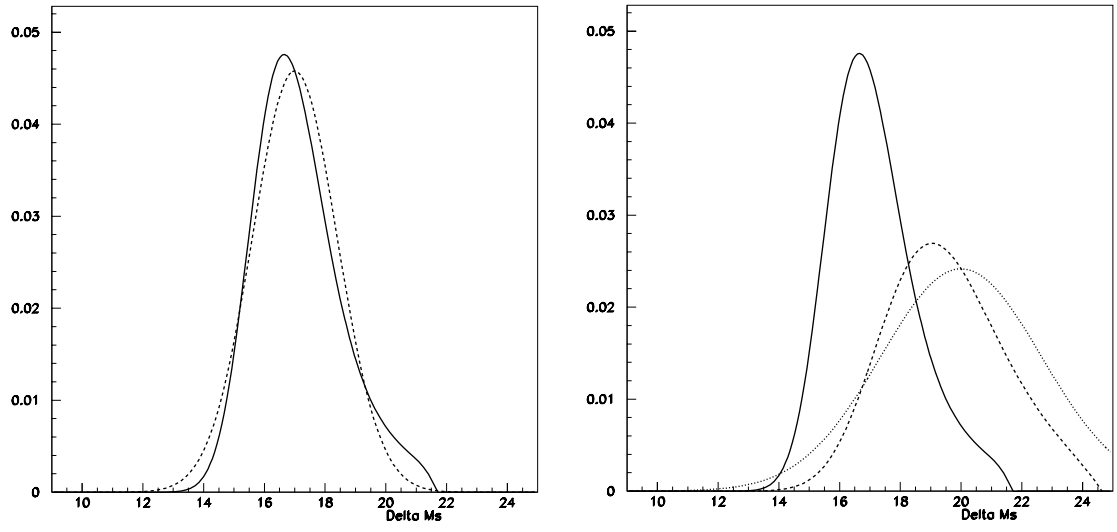

Fig. 62. *Left*: next-to-leading-order $\Phi^{17}_{\rm nlo}$ PDF of the Δm_s measurement (solid line) and leading order PDF $\Phi^{17}_{\rm lo}$ (dotted line), for a true value $\Delta m_s = 17\,\mathrm{ps}^{-1}$. The two PDFs differ significantly, but the leading order approximation remains acceptable in the core of the distribution. However it would underestimate by a factor two about the probability to obtain a measurement above $\Delta m_s = 20\,\mathrm{ps}^{-1}$. *Right*: next-to-leading-order $\Phi^{17}_{\rm nlo}$ PDF (solid line) together with $\Phi^{20}_{\rm nlo}$ PDF (dotted line) and the leading order PDF $\Phi^{20}_{\rm lo}$ for $\Delta m_s = 20\,\mathrm{ps}^{-1}$ (dashed-dotted line). The integral of $\Phi^{17}_{\rm nlo}$ above $\Delta m_s = 20\,\mathrm{ps}^{-1}$ is not a good approximation of the CL of a true value $\Delta m_s = 20\,\mathrm{ps}^{-1}$ leading to a measurement $\Delta m_s = 17\,\mathrm{ps}^{-1}$, the latter being defined as the integral of Φ^{20}_0 below $\Delta m_s = 17\,\mathrm{ps}^{-1}$. However, in the present case, one cannot fully rely on the approximation $\Phi^{20}_0 \simeq \Phi^{20}_{\rm nlo}$ owing to the large variation between $\Phi^{20}_{\rm lo}$ and $\Phi^{20}_{\rm nlo}$

A.7 Next-to-leading order likelihood

We consider a likelihood

$$\mathcal{L} = \sum_{i=1}^{N} \ln P \ , \tag{A.60}$$

where the PDF P depends on the parameter x_s. We denote

– x_s the true value of the parameter,

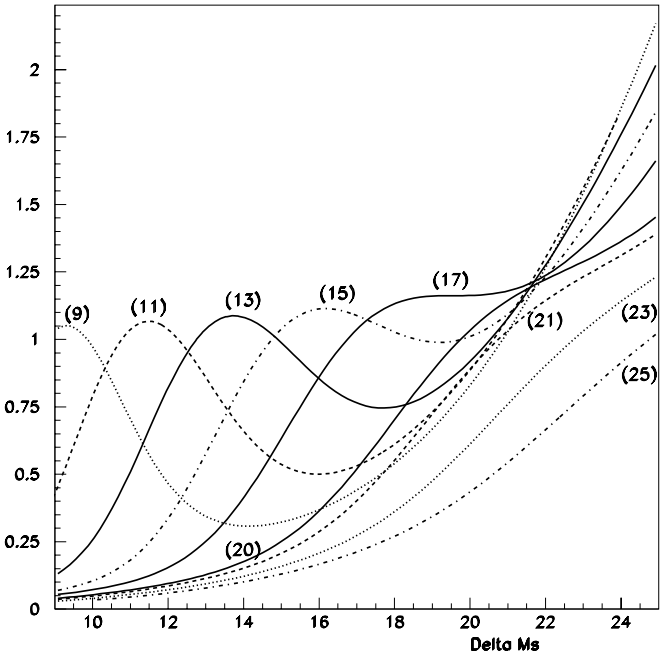

Fig. 63. Amplitude $\mathcal{A}$ solutions given in (A.59) (where orders up to $\mathcal{K}^4(x_s^{\rm hyp})$ are considered in the expansion used here) for different true values of Δm_s

– P_0 the PDF when evaluated with x_s.

In the vicinity of x_s, the Taylor expansion to the fourth order is

$$\mathcal{L}(x_s^{\rm hyp}) = \alpha_0 - \alpha_1\chi + \alpha_2\chi^2 - \alpha_3\chi^3 + \overline{\alpha_4}\chi^4 \ , \tag{A.61}$$

with

$$\alpha_0 = \sum \ln(P_0) \ , \quad \alpha_1 = \sum \left[\frac{\dot{P}_0}{P_0}\right] \Sigma \ , \quad \alpha_2 = \frac{1}{2}\sum \left[\frac{\ddot{P}_0}{P_0} - \frac{\dot{P}_0^2}{P_0^2}\right] \Sigma^2 \ ,$$
$$\alpha_3 = \frac{1}{6}\sum \left[\frac{\dddot{P}_0}{P_0} - 3\frac{\dot{P}_0\ddot{P}_0}{P_0^2} + 2\frac{\dot{P}_0^3}{P_0^3}\right] \Sigma^3 \ , \quad \overline{\alpha_4} = \frac{1}{24}\sum \left[\frac{\ddddot{P}_0}{P_0} - 3\frac{\ddot{P}_0^2}{P_0^2} - 4\frac{\dot{P}_0\dddot{P}_0}{P_0^2} + 12\frac{\dot{P}_0^2\ddot{P}_0}{P_0^3} - 6\frac{\dot{P}_0^4}{P_0^4}\right] \Sigma^4 \ .$$

For a given experiment, the values of the a_i coefficients are correlated random numbers. On the average, their values are obtained by replacing the sum by $N\int P_0$. Using (A.7), one gets

$$\alpha_1 = 0 \ , \quad \overline{\alpha_2} = -\frac{1}{2} \ , \quad \overline{\alpha_3} = \frac{1}{6}\frac{-3B+2C}{\sqrt{N}A^{\frac{3}{2}}} \ , \quad \overline{\alpha_4} = \frac{1}{24}\frac{-3D-6E+12\mathcal{F}-4G}{N^{\frac{3}{2}}A^2} \ ,$$

where the last term involves the new set of integrals

$$D(x_s) = \int_{-\infty}^{+\infty}\left(\frac{\ddot{P}_-^2}{P_-} + \frac{\ddot{P}_+^2}{P_+}\right) dt_{\rm mes} \ , \qquad E(x_s) = \int_{-\infty}^{+\infty}\left(\frac{\dot{P}_-^4}{P_-^3} + \frac{\dot{P}_+^4}{P_+^3}\right) dt_{\rm mes} \ ,$$
$$F(x_s) = \int_{-\infty}^{+\infty}\left(\frac{\dot{P}_-^2\ddot{P}_-}{P_-^2} + \frac{\dot{P}_+^2\ddot{P}_+}{P_+^2}\right) dt_{\rm mes} \ , \qquad G(x_s) = \int_{-\infty}^{+\infty}\left(\frac{\dot{P}_-\dddot{P}_-}{P_-} + \frac{\dot{P}_+\dddot{P}_+}{P_+}\right) dt_{\rm mes} \ .$$

In effect, the maximum of $\mathcal{L}_{\rm nlo}$ is reached for

$$0 = -\alpha_1 + 2\alpha_2\chi - 3\alpha_3\chi^2 \tag{A.62}$$
$$x_s^{\rm mes} \simeq x_s - \left(\frac{\alpha_1}{2\alpha_2} - \frac{3\alpha_1^2\alpha_3}{8\alpha_2^3}\right) \ . \tag{A.63}$$

B: Combining inconsistent measurements

When several measurements $x_{\rm exp}(i) \pm \sigma_{x_{\rm exp}}(i)$, with $i = 1, .., N$, of the same physical observable X are available, the question arises on how to combine them into a single measurement $\langle x_{\rm exp}\rangle$. Combining the measurements can serve two purposes: merely, it can be to provide a summary carrying the overall information within a conveniently easily-quoted global measurement, or, more ambitiously, it can be to provide a means to incorporate the set of measurements into a more involved analysis, like a global CKM fit, where the physical observable X enters as one input among others.

We note that the averaging method introduced below is not yet applied in the present CKM analysis. We reserve its use for forthcoming occasions.

The weighted mean (WM) method defined by

$$\langle x_{\rm exp}\rangle = \sigma^2_{\langle x_{\rm exp}\rangle} \sum_{i=1}^{N} \sigma^{-2}_{x_{\rm exp}}(i)\, x_{\rm exp}(i) \ , \tag{B.1}$$

$$\sigma^{-2}_{\langle x_{\rm exp}\rangle} = \sum_{i=1}^{N} \sigma^{-2}_{x_{\rm exp}}(i) \ , \tag{B.2}$$

is the optimal scheme to merge the individual measurements. However it assumes that the measurements are consistent the ones with the others. It leads to an easily-quoted global measurement $X = \langle x_{\rm exp}\rangle \pm \sigma_{\langle x_{\rm exp}\rangle}$. Furthermore, because the underlying hypothesis is clear (the set of measurements is taken to be consistent) the WM method is statistically well-defined and its result is easy to use: the true value of the physical observable being assumed to be x, the probability for this value to yield for the χ^2

$$\chi^2(x) = \left(\frac{\langle x_{\rm exp}\rangle - x}{\sigma_{\langle x_{\rm exp}\rangle}} \right)^2 , \tag{B.3}$$

a value larger than the observed one, is given by:

$$\mathcal{P}(x) = {\rm Prob}(\chi^2,\, 1) \ . \tag{B.4}$$

A measure of the consistency of the set of measurements is provided by the χ^2

$$\chi^2(\langle x_{\rm exp}\rangle) = \sum_{i=1}^{N} \left(\frac{x_{\rm exp}(i) - \langle x_{\rm exp}\rangle}{\sigma_{x_{\rm exp}}(i)} \right)^2 , \tag{B.5}$$

and, more conveniently, by its associated confidence level

$$\mathcal{P}(\langle x_{\rm exp}\rangle) = {\rm Prob}(\chi^2(\langle x_{\rm exp}\rangle),\, N-1) \ . \tag{B.6}$$

If the value of $\chi^2(\langle x_{\rm exp}\rangle)$ is too large, one may suspect that some of the measurements in the set are flawed. If one insists on a democratic treatment of the $x_{\rm exp}(i)$, i.e., if one refuses to remove the suspected ones, the PDG-recommended scheme [12], termed the rescaled weighted mean below (RWM), consists of rescaling the error $\sigma_{\langle x_{\rm exp}\rangle}$ of (B.2) by the scale factor

$$S = \sqrt{\chi^2(\langle x_{\rm exp}\rangle)/(N-1)} \ , \tag{B.7}$$

if the latter exceeds unity

$$\Sigma_{\langle x_{\rm exp}\rangle} = \sigma_{\langle x_{\rm exp}\rangle}\ S \ . \tag{B.8}$$

The RWM method is simple and convenient, however, it suffers from two important drawbacks:

1. *Psychostatistics*
   On the average, the quoted error is necessarily enlarged with respect to the one of the un-rescaled weighted mean (WM), even for consistent data sets. Tampering with (B.2) implies a departure from well-defined statistics to enter the realm of ill-defined (psycho)statistics, where working hypotheses are no longer fully explicited.
2. *Schizostatistics*
   The average $\langle x_{\rm exp}\rangle$ may lie outside the range of values covered by the measurements. This is because the democratic treatment does not allow to detect measurements which obviously stick out from the set. Such a measurement, termed an outlier in the following, pulls the average toward its value, albeit it may remain inconsistent with the resulting weighted mean, even though the error of the latter is rescaled.

In this paper we advocate the use of a method, termed the *Combiner*, which is an extension to the weighted mean method[78]. Although the Combiner does not provide an escape from the first drawback, it is shown below to be more satisfactory with respect to the second drawback. The discussion of the above drawbacks is further expanded below.

[78] Another approach for the combination of inconsistent measurements has been developed in [302].

B.0.1 Psychostatistics

There is no way out of the first drawback: this is because accepting the *possibility* of having in the set of measurements some that are biased in an unspecified way implies a loss of information, which, furthermore, is ill-defined. When the standard deviation is rescaled following the RWM scheme, the (re)definition of (B.3) is to be taken, at best, as a test statistics. It is no longer a pure χ^2 term and (B.4) does not hold. Moreover, the use of this test statistics is ill-defined. Its distribution cannot be determined, since the underlying hypothesis is now unspecified (the set of measurements is taken to be inconsistent, but this is not a precisely defined hypothesis).

However the aim of the RWM method being to be conservative, the price to pay is to accept the use of ill-defined statistics and to deal with $\chi^2(x)$ as if it were a pure χ^2. Stated differently, applying (B.4) yields over-conservative confidence levels, which, after all, is precisely what one is looking for.

B.0.2 Schizostatistics

The second drawback is worth being spelled out explicitly. If one is dealing with two measurements which are sufficiently apart for the rescaling of (B.8) to be enforced, namely, if

$$\Delta x^2_{\rm exp} \equiv (x_{\rm exp}(2) - x_{\rm exp}(1))^2 > \sigma^2_{x_{\rm exp}}(1) + \sigma^2_{x_{\rm exp}}(2) \ , \tag{B.9}$$

leading to a rescaled uncertainty (cf. (B.8))

$$\Sigma_{\langle x_{\rm exp}\rangle} = \frac{\sigma_{x_{\rm exp}}(1)\sigma_{x_{\rm exp}}(2)|\Delta x_{\rm exp}|}{\sigma^2_{x_{\rm exp}}(1) + \sigma^2_{x_{\rm exp}}(2)} \ , \tag{B.10}$$

then the RWM method is prone to contradict itself.

On the one hand, using $\Sigma_{\langle x_{\rm exp}\rangle}$ in place of $\sigma_{\langle x_{\rm exp}\rangle}$ in (B.3), yields

$$\chi^2(x = x_{\rm exp}(1)) = \left(\frac{\sigma_{x_{\rm exp}}(1)}{\sigma_{x_{\rm exp}}(2)}\right)^2 , \tag{B.11}$$

$$\chi^2(x = x_{\rm exp}(2)) = \left(\frac{\sigma_{x_{\rm exp}}(2)}{\sigma_{x_{\rm exp}}(1)}\right)^2 , \tag{B.12}$$

independently on how far apart the two measurements are, provided (B.9) is fullfilled. Hence, if the two measurements have widely different uncertainties, the measurement with the largest uncertainty (e.g., the second one: $\sigma_{x_{\rm exp}}(2) \gg \sigma_{x_{\rm exp}}(1)$) is viewed as corresponding to a true value of the physical observable $x = x_{\rm exp}(2)$ which is utterly ruled out by the data ($\chi^2(x = x_{\rm exp}(2)) \gg 1$), even though the weighted mean error is rescaled.

On the other hand, the weighted mean is pulled away from both measurements in proportion of $\Delta x_{\rm exp}$. As a result, from the view point of both measurements $i = 1, 2$, the hypothesis that the true value of the physical observable is $x = \langle x_{\rm exp}\rangle$ leads to

$$\chi^2(x = \langle x_{\rm exp}\rangle)(i) = \left(\frac{x_{\rm exp}(i) - \langle x_{\rm exp}\rangle}{\sigma_{x_{\rm exp}}(i)}\right)^2 = \Delta x^2_{\rm exp}\frac{\sigma_{x_{\rm exp}}{}^2(i)}{(\sigma_{x_{\rm exp}}{}^2(1) + \sigma_{x_{\rm exp}}{}^2(2))^2} \ , \tag{B.13}$$

and hence is liable to be ruled out as well, if $\Delta x_{\rm exp}$ is large enough. In particular, if $\sigma_{x_{\rm exp}}(2) \gg \sigma_{x_{\rm exp}}(1)$

$$\chi^2(x = \langle x_{\rm exp}\rangle)(1) \simeq S^2\left(\frac{\sigma_{x_{\rm exp}}(1)}{\sigma_{x_{\rm exp}}(2)}\right)^2 \ll 1 \ , \tag{B.14}$$

$$\chi^2(x = \langle x_{\rm exp}\rangle)(2) \simeq S^2 \ . \tag{B.15}$$

Therefore, if the second measurement has a much larger uncertainty than the first measurement, the conjunction of (B.12–B.14) implies that when the rescaling is significant, the RWM result and the second measurement are mutually incompatible: this contradicts the use of the second measurement to define the weighted mean, especially considering its impact on $\Sigma_{\langle x_{\rm exp}\rangle}$ as displayed by (B.10).

For twin measurements with identical $\sigma_{x_{\rm exp}}$, the RWM method is not self-contradictory: whereas (B.13) indicates that from the view point of both measurements the RWM value may be unacceptable, (B.11–B.12) guarantee that the rescaled uncertainty yields an acceptable χ^2 for both.

If only two measurements enter into play, not much can be done to circumvent this second drawback, since there is no objective way to identify the flawed one. However, if more than two measurements are available, one may rely on the consistency of a subset of them to identify the possible outliers.

B.1 The Combiner

The Combiner method is explicitly build as an extension to the weighted mean: by construction, it tends to reproduce Eqs.(B.1–B.2) in the case of a consistent set of measurements. The (psycho)statistical point of view which is taken here is that some of the measurements to be averaged might be incorrect: if such measurements occur, they should be removed from the set.

B.1.1 Principle

The removal of incorrect measurements relies on the clustering of the other measurements around a common mean. Rather than removing abruptly a measurement if it meets some criteria, the Combiner does not cut but considers all possible hypotheses about the correctness of the measurements. A configuration being defined as a subset of measurements that are assumed to be consistent the ones with others, the Combiner weighs all possible configurations to build an overall likelihood. To reproduce the WM result, the Combiner favors the configurations involving the largest number of measurements, provided they have good probabilities.

B.1.2 Notations

We denote:

- c, an ordered list of N bits. It is referred to as a *configuration*, indicating which measurements are considered. For example, for $N = 3$, the configuration $c \equiv 101$ means that the two measurements $i = 1$ and $i = 3$ are to be merged, while disregarding the measurement $i = 2$. The void configuration being of no interest, the total number of configurations considered amounts to $2^N - 1$.
- n_c, the number of bits set to one. It is referred to as the *multiplicity* of the configuration.
- $c_{\rm all} = 11\ldots1$, the configuration where all measurements are considered ($n_{c_{\rm all}} = N$).
- χ^2_c, the χ^2 obtained from the weighted mean (cf., (B.1–B.5)) of the n_c measurements to be considered in the configuration c.
- $\mathcal{P}_c = {\rm Prob}(\chi^2_c, n_c - 1)$, the corresponding configuration *probability* (cf., (B.5)).
- $\overline{\mathcal{P}}_c = 1 - \mathcal{P}_c$
- $\langle x_{\rm exp}\rangle(c)$ and $\sigma_{\langle x_{\rm exp}\rangle}(c)$, the results of the weighted mean for the configuration c.
- $G_c \equiv G_c(x)$, the Gaussian likelihood (to be interpreted as a PDF when used in a Bayesian approach) with mean value $\langle x_{\rm exp}\rangle(c)$ and standard deviation $\sigma_{\langle x_{\rm exp}\rangle}(c)$.
- w_c, a weight characterizing the configuration c. The sum of these weights over the 2^N-1 configurations is normalized to unity, i.e., $\sum_c w_c = 1$.
- $c' > c$ denotes two configurations such that all the bits set at one in c' are also set at one in c, and there is at least one bit set at one in c' which is not set at one in c (e.g., $1111 > 1101$, but $1101 \not> 1011$). The configuration c', embedding c, is said to be *larger* than c.
- Products of probabilities over void configurations are set to one, e.g., $\prod_{c'}^{c'>c} \mathcal{P}_{c'} \equiv 1$, if no c' exist for which $c' > c$ holds (i.e., c is the largest configuration: $c = 11\ldots1$).

B.1.3 Definition

With these notations, the WM method consists of using only the configuration $c_{\rm all}$. In a likelihood analysis relying on those measurements, this treatment is equivalent to adding to the overall log-likelihood the term

$$\chi^2(x) = -2\ln G(x)\ , \tag{B.16}$$

where the global likelihood G is the fully combined Gaussian $G = G_{c_{\rm all}}$. The RWM method consists of using the same configuration, but, if $S > 1$, it modifies $G_{c_{\rm all}}$ by rescaling its standard deviation. As pointed-out in the Introduction (cf. Appendix B.0.1) even though in that case $-2\ln G_{c_{\rm all}}$ defines a pseudo-χ^2, it should be used as a pure χ^2.

Instead of using a single Gaussian, the Combiner uses for the global likelihood a compound function:

$$G(x) = \sum_c w_c G_c(x)\ , \tag{B.17}$$

which enters into the computation of the pseudo-χ^2 of (B.16) here also to-be-used as a pure χ^2. What remains to be done is to define appropriately the weights w_c. Obviously there is an infinite number of choices. Since the goal is to protect the analysis from biased measurements and over-optimistic $\sigma_{\langle x_{\rm exp}\rangle}$ values, which is admittedly a vague goal, one must rely on educated guesswork to pick-up a particular definition of the weights.

The C-Combiner

For the C-Combiner, the weights are defined as

$$w_c^{(\mathrm{C})} = a\ \mathcal{P}_c \prod_{c'}^{c'>c} \overline{\mathcal{P}}_{c'}\ , \tag{B.18}$$

where the constant a ensures the proper normalization of the weights. The first term is a measure of the validity of the combination, while the second term suppresses it, if any configuration larger than c receives a high probability. If a configuration c is such that all larger configurations are unlikely, it does not get suppressed by the above expression. For example, if an outlier measurement is utterly incompatible with all the others, it is kept by the C-Combiner with a weight equal to a. It is termed the *Cool-Combiner* because of that. However, if the number of consistent measurements grows, the outlier weight, a, decreases accordingly.

The T-Combiner

For the T-Combiner, the weights are defined as

$$w_c = \frac{\mathcal{P}_c}{\sum_{c'}^{n_c=n_{c'}} \mathcal{P}_{c'}} \left(1 - \prod_{c'}^{n_{c'}=n_c} \overline{\mathcal{P}}_{c'}\right) \prod_{c'}^{n_{c'}>n_c} \overline{\mathcal{P}}_{c'}\ . \tag{B.19}$$

The first term is a measure of the relative validity of the configuration c, with respect to configurations of the same multiplicity n_c. The second term weighs the validity of the configurations of multiplicity n_c, taken as a whole. The third term suppresses configurations of multiplicity n_c if any higher multiplicity configuration receives a large probability. Therefore, whether or not a configuration c' is larger than c, if $n_{c'} > n_c$, it is sufficient for c' to receive a large probability to suppress c. For example, if an outlier measurement is utterly incompatible with all the others, it is suppressed by the Combiner, if some of the others are mutually compatible. It is termed the *Tough-Combiner* because of that. For the configuration $c = c_{\mathrm{all}}$, the third term receives no contribution and is defined to be equal to one. The above expression ensures the normalization of the weights to unity.

B.2 Illustrations

B.2.1 Twin measurements

To illustrate how the Combiner works, we first consider the evolution of the likelihood G as a function of the discrepancy between twin measurements $x_{\mathrm{exp}}(1)$ and $x_{\mathrm{exp}}(2)$, with $\sigma_{x_{\mathrm{exp}}}(1) = \sigma_{x_{\mathrm{exp}}}(2) = \sigma_0 = 1$. Figure 64 shows the combined likelihood for the two Combiner approaches and for the RWM method. The measurements, indicated by the vertical lines, develop a mutual disagreement which increases from the upper left figure to the lower right figure. One observes that the Combiner likelihoods become broader with increasing discrepancy and eventually splits up into two Gaussian-like likelihoods, where the T- and C-Combiner behave similarly. In the limit of extreme incompatibility, the two curves become genuine Gaussians with central values $x_{\mathrm{exp}}(1)$ and $x_{\mathrm{exp}}(2)$, respectively, and width σ_0. On the contrary, the RWM Gaussian stays on the central value while the error increases to always keep the two measurements within the (so-called) 68% probability limit. The unsatisfactory behavior of the RWM method becomes obvious at large inconsistencies. One observes on the four lower curves in Fig. 64 that, whereas the Combiner treats the center value $x = 0$ as being unlikely – it is favored by the weighted mean, although there exist no supporting measurement, while the rescaled uncertainty gives rise to unduly broad tails which do not show up when using the Combiner.

This first example already exhibits advantages of using the Combiner. However it does not allow to demonstrate fully the superiority of the method because it uses twin measurements. As discussed previously (cf. Appendix B.0.2), the behavior of the RWM method is even less satisfactory if the two measurements have very different $\sigma_{x_{\mathrm{exp}}}$. In addition, since only two measurements are available, the Combiner cannot use the clustering of correct measurements to suppress the flawed one(s). As shown in the next section, the behavior of the Combiner is markedly different for a set of more than two measurements among which a subset is consistent.

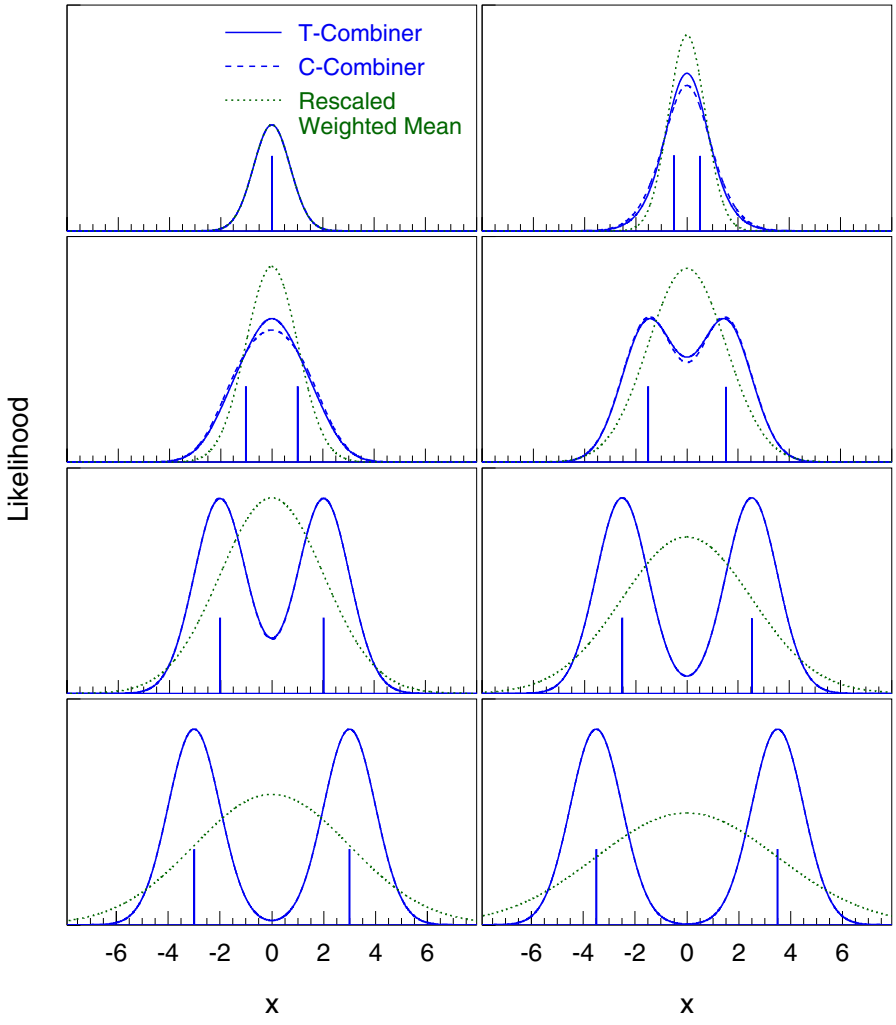

Fig. 64. Likelihoods G for the T-Combiner (solid), the C-Combiner (dashed), and for the RWM method (dotted). The vertical lines indicate the locations of the two individual measurements which develop a mutual disagreement rising from the upper left figure to the lower right figure. The dotted line corresponds to the likelihood of the C-Combiner

B.2.2 Information loss

It was mentioned before that enlarged errors (broader likelihoods) are an unavoidable side-effect when taking into consideration the possibility of biased measurements. This entails a loss of information when the set is consistent. To quantify this loss of information, we perform a toy Monte Carlo simulation of a set of $N = 5$ measurements, each distributed following the same Gaussian, $\langle x_{\rm exp}\rangle(1-5) = \langle x_0\rangle = 5$ and $\sigma_{x_{\rm exp}}(1-5) = \sigma_0 = 1$. We use the RWM method and the T-Combiner to obtain the distributions of the mean value and the distributions of the root mean square (RMS) of the likelihood G.

The results are given in Fig. 65. The left plot shows the distribution of the mean value $\langle x[C]\rangle$ as provided by the T-Combiner. The distribution of $\langle x[C]\rangle$ is very close to be a Gaussian of width $\sigma = 0.47$. This is to be compared with the (optimal) WM Gaussian distribution of width $\sigma_{WM:5} = 5^{-1/2} \simeq 0.45$. This width is also obtained for the rescaled weighted mean, as the center value of the likelihood is not affected by the enlargement of the width. Although statistical outliers are suppressed in the Combiner, giving rise to a narrower effective width, the increase of the width due to the statistical occurrence of seeming inconsistencies superseeds the narrowing suppression effect. The right figure shows the distribution of the RMS, $\sigma[C]$, of the T-Combiner, to be compared to the distribution of the RMS, σ[RWM], of the rescaled weighted mean. The increase of the errors is stronger for the Combiner.

B.2.3 Inconsistent set

The second example uses the following set of $N = 5$ measurements: $x_{\rm exp}(1-5) = 3.7,\ 4.2,\ 5.0,\ 5.5,\ 0.0$, all with identical errors $\sigma_{x_{\rm exp}}(1-5) = 1$. While the first four data points are mutually compatible with a Gaussian distribution ($\chi^2/N_{\rm dof} = 1.9/3$), the last measurement is an outlier leading to a large overall $\chi^2/N_{\rm dof} = 18.9/4$, translated into a scale factor of $S = 2.2$. The C- and the T-Combiner yield for the likelihood G (quoting only the leading terms):

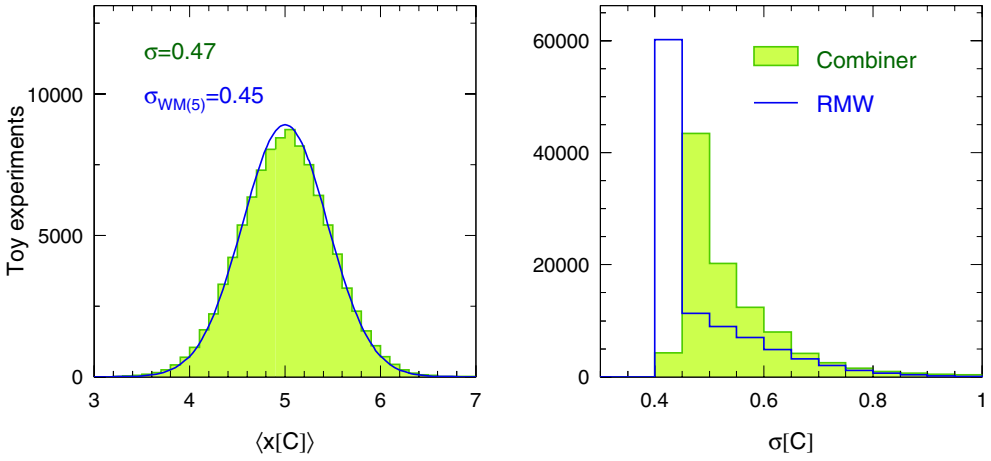

Fig. 65. The left plot shows the toy Monte Carlo distribution of the mean value $\langle x[C]\rangle$ as provided by the T-Combiner (shaded histogram), for a set of five consistent measurements which are Gaussian distributed around $\langle x_{\rm exp}\rangle = 5$, each with a standard deviation $\sigma(i) = 1$. A Gaussian fit to the distribution results in $\sigma = 0.47$. Also shown is the weighted mean distribution (solid line) characterized by the standard deviation $\sigma_{WM:5} = 5^{-1/2} \simeq 0.45$. The right hand plot shows the distribution of the RMS, $\sigma[C]$, of the T-Combiner (shaded histogram) compared to the RMS, σ[RWM], of the rescaled weighted mean

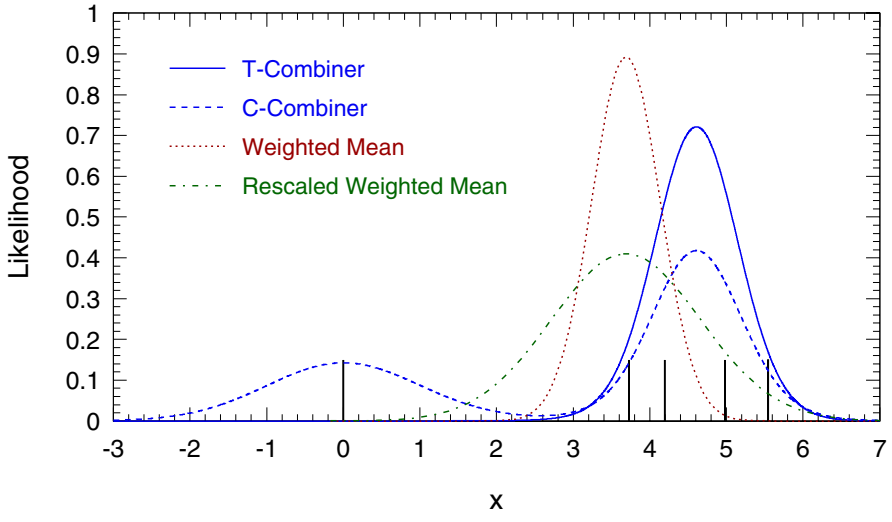

Fig. 66. Likelihoods G obtained by the four approaches: T-Combiner, C-Combiner, weighted mean and the rescaled weighted mean. The vertical lines indicate the five individual measurements of which one is inconsistent

C-Combiner:	c	00001	11110	01110	10110	11010	11100
	$w_c^{(\rm C)}$	0.358	0.213	0.102	0.097	0.064	0.063
T-Combiner:	c	11110	01110	10110	11010	11100	–
	$w_c^{(\rm T)}$	0.580	0.125	0.118	0.079	0.077	–

Quoted are only the configurations with $w_c > 0.05$. One observes that configurations where the incompatible measurements are mixed, i.e., bit five and another one are set to one, have negligible weights for both the C and the T-Combiner. The C-Combiner allows a sizable single weight for outlier (measurements five) which, while it is suppressed by the T-Combiner.

The Combiner likelihoods are shown in Fig. 66 together with the WM and the RWM likelihoods. Whereas one may be satisfied by either the C-Combiner or the T-Combiner, one observes that the WM and the RWM methods contradict themselves: the outlier pulls the mean value significantly but, even in the RWM method, the outlier and the mean value remain incompatible. Furthermore, in the example considered here, the measurement the farthest apart from the outlier, although correct, is also incompatible with the mean value.

To study the recovery capability of the Combiner we plot in Fig. 67 the distribution of the mean value $\langle x[C]\rangle$ as provided by the T-Combiner (on the vertical axis) for the set of inconsistent measurements, four of which are Gaussian distributed around $\langle x_{\rm exp}\rangle = 5$, each with a standard deviation $\sigma(i) = 1$, while the fifth measurement is

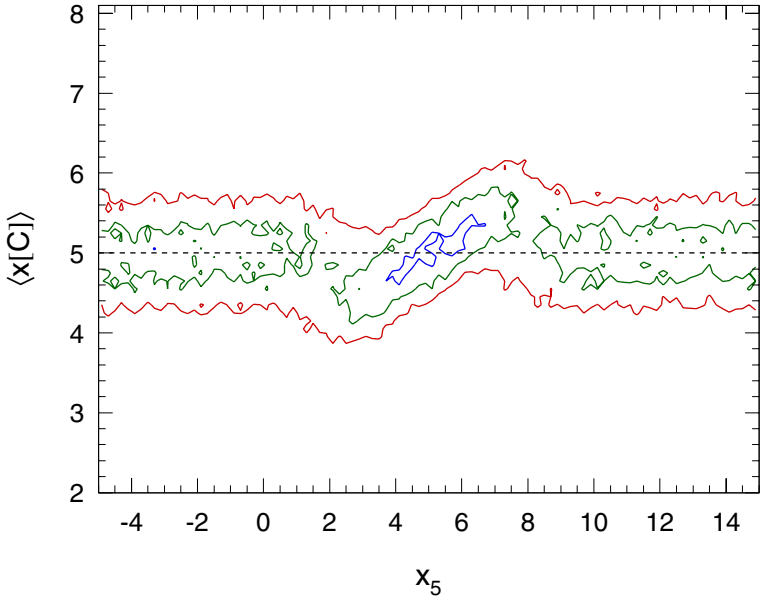

Fig. 67. Distribution of the mean value $\langle x[C]\rangle$ as provided by the T-Combiner (on the vertical axis) for a set of inconsistent measurements, four of which are Gaussian distributed around $\langle x_{\rm exp}\rangle = 5$, each with a standard deviation $\sigma(i) = 1$, while the fifth measurement is uniformly distributed between $x_5 = -5$ and $x_5 = 15$ (on the horizontal axis). The latter is effectively removed from the set by the T-Combinerwhen it departs from $\langle x_{\rm exp}\rangle$ by about $1.5\sigma(i)$

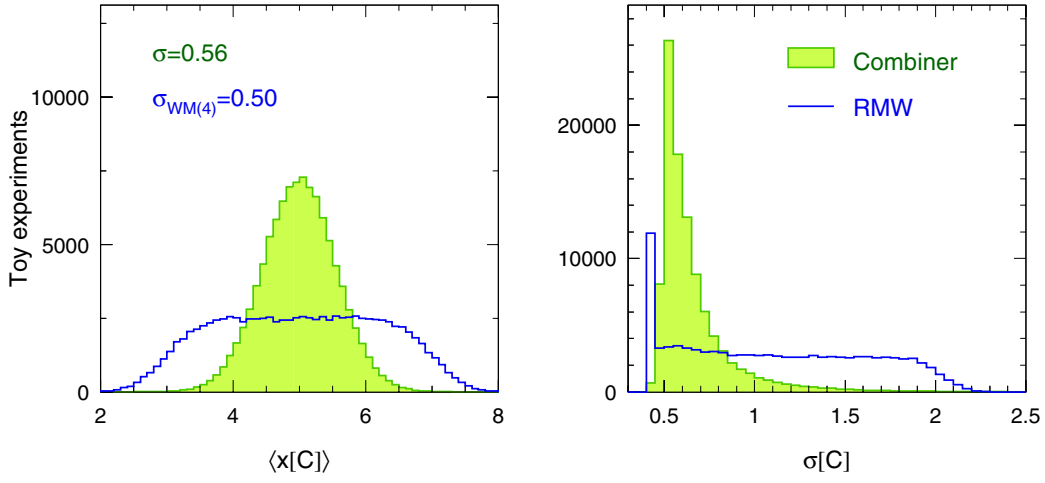

Fig. 68. The left plot shows the toy Monte Carlo distribution of the mean value $\langle x[C]\rangle$ as provided by the T-Combiner (shaded histogram), for a set of inconsistent measurements four of which are Gaussian distributed around $\langle x_{\rm exp}\rangle = 5$, each with a standard deviation $\sigma(i) = 1$, while the fifth measurement is uniformly distributed between $x_5 = -5$ and $x_5 = 15$. A Gaussian fit to the distribution results in $\sigma = 0.56$, which is to be compared with the optimal WM result $\sigma_{WM:4} = 0.5$, obtained when the fifth measurement is removed from the set. Also shown is the weighted mean distribution (solid line). The right hand plot shows the distribution of the RMS, $\sigma[C]$, of the T-Combiner (shaded histogram) compared to the RMS, σ[RWM], of the rescaled weighted mean

uniformly distributed between $x_5 = -5$ and $x_5 = 15$ (on the horizontal axis). The latter is effectively removed from the measurement set by the T-Combiner when it departs from $\langle x_{\rm exp}\rangle$ by about $1.5\sigma(i)$. We show that, for the T-Combiner, the distribution of the mean value and the RMS for the toy experiments in Fig. 68 is very close to be a Gaussian of width $\sigma = 0.47$ (left hand plot). This is to be compared with the optimal WM Gaussian distribution of width $\sigma_{WM:4} = 0.5$ (discarding the inconsistent measurement). The rescaled weighted mean exhibits a significantly larger scattering than the Combiner. The right figure shows the distribution of the RMS, $\sigma[C]$, of the T-Combiner, to be compared to the distribution of the RMS, σ[RWM], of the rescaled weighted mean. The increase of the errors (i.e., the loss of information) is stronger for the rescaled weighted mean.

References

1. N. Cabibbo, Phys. Rev. Lett. **10**, 351 (1963)
2. M. Kobayashi, T. Maskawa, Prog. Theor. Phys. **49**, 652 (1973)
3. L. Wolfenstein, Phys. Rev. Lett. **51**, 1945 (1983)
4. A.J. Buras, M.E. Lautenbacher, G. Ostermaier, Phys. Rev. **D50**, 3433 (1994)
5. I.Y. Bigi, V.A. Khoze, N.G. Uraltsev, A.I. Sanda, in *"CP Violation"*, C. Jarlskog Ed., World Scientific, Singapore (1988)
6. A. Höcker, H. Lacker, S. Laplace, F. Le Diberder, Eur. Phys. J. **C21**, 225 (2001)
7. Partially updated plots and results are available at the CKMfitter web site: http://ckmfitter.in2p3.fr and its mirror http://www.slac.stanford.edu/xorg/ckmfitter
8. M. Ciuchini, G. D'Agostini, E. Franco, V. Lubicz, G. Martinelli, F. Parodi, P. Roudeau, A. Stocchi, J. High Energy Phys. **0107**, 013 (2001)
9. M. Battaglia et al., CERN-2003-002, Cern Yellow Report, Based on the Workshop on CKM Unitarity Triangle (CERN 2002-2003), Geneva, Switzerland, 13–16 Feb 2002, [hep-ph/0304132]
10. A.J. Buras, F. Parodi, A. Stocchi, J. High Energy Phys., **0301**, 029 (2003); A. Ali, Lectures given at the International Meeting on Fundamental Physics, Soto de Cangas, Spain, 23–28 Feb. 2003 [hep-ph/0312303]; G. Eigen, G.P. Dubois-Felsmann, D.G. Hitlin, F.C. Porter, Contributed to International Europhysics Conference on High-Energy Physics (HEP 2003), Aachen, Germany, 17–23 Jul 2003 [hep-ex/0312062] (see also hep-ph/0308262); K. Schubert, Talk given at 2nd Workshop on the CKM Unitarity Triangle, Durham, England, 5-9 Apr 2003, http://www.ippp.dur.ac.uk/čkm/econf/index.html, WG3; see also [6], which cites earlier studies, and [9]
11. L.L. Chau, W.Y. Keung, Phys. Rev. Lett. **53**, 1802 (1984)
12. Particle Data Group (K. Hagiwara et al.), Phys. Rev. **D66**, 010001 (2002 and 2003 update)
13. C. Jarlskog, Phys. Rev. Lett. **55**, 1039 (1985)
14. G.C. Branco, L. Lavoura, J.P. Silva, *CP Violation*, The Intern. Series of Monographs on Physics – 103, Oxford Science Publications, Oxford, UK (1999)
15. E787 Collaboration (S. Adler et al.), Phys. Rev. Lett. **88**, 041803 (2002)
16. E949 Collaboration (A.V. Artamonov et al.) [hep-ex/0403036 (2004)], http://www.phy.bnl.gov/e949
17. I.S. Towner, J.C. Hardy, J. Phys. G: Nucl. Part. Phys. **29**, 197 (2003)
18. K. Saito, A.W. Thomas, Phys. Lett. **B363**, 157 (1995)
19. H. Abele et al., Phys. Rev. Lett. **88**, 211801 (2002)
20. D. Pocanic (for the PIBETA Collaboration), Talk given at 2nd Workshop on the CKM Unitarity Triangle, Durham, England, 5-9 Apr 2003, eConf **C0304052**, WG606
21. J.F. Donoghue, B.R. Holstein, S.W. Klimt, Phys. Rev. **D35**, 934 (1987)
22. R. Flores-Mendieta, A. Garcia, G. Sanchez-Colon, Phys. Rev. **D54**, 6855 (1996)
23. N. Cabibbo, E. C. Swallow, R. Winston, APS-123-QED [hep-ph/0307214] (2003)
24. H. Leutwyler, M. Roos, Z. Phys. **C25**, 91 (1984)
25. E.A. Paschos, U. Türke, Phys. Rep. **178**, 145 (1989)
26. W. Jaus, Phys. Rev. **D44**, 2851 (1991)
27. P. Post, K. Schilcher, Eur. Phys. J. **C25**, 427 (2002)
28. J. Bijnens, P. Talavera, Nucl. Phys. **B 669**, 341 (2003)
29. V. Cirigliano, H. Neufeld, H. Pichl [hep-ph/0401173]
30. D. Becirevic et al. [hep-ph/0403217]
31. W.J. Marciano, A. Sirlin, Phys. Rev. Lett. **56**, 22 (1986)
32. H.H. Williams et al., Phys. Rev. Lett. **33**, 240 (1974); T. Becherrawy et al., Phys. Rev. **D1**, 1452 (1970)
33. V. Cirigliano, Talk given at 38th Rencontres de Moriond on Electroweak Interactions and Unified Theories, Les Arcs, France, 15–22 Mar 2003 [hep-ph/0305154]
34. BNL-E865 Collaboration (A. Sher et al.), AIP Conf. Proc. **698**, 381 (2004), hep-ex/0305042
35. B. Sciascia (for the KLOE Collaboration), Talk given at 2nd Workshop on the CKM Unitarity Triangle, Durham, England, 5-9 Apr 2003, eConf **C0304052**, WG607
36. S. Miscetti (for the KLOE Collaboration), Talk given at 39th Rencontres de Moriond: Electroweak Interactions and Unified Theories La Thuile, Val d'Aoste, Italy, Mar 21-28 2004 [hep-ex/0405040]
37. KTeV Collaboration, (T. Alexopoulos et al.) [hep-ex/0406001]
38. E. Gamiz, M. Jamin, A. Pich, J. Prades, F. Schwab, J. High Energy Phys. **0301**, 060 (2003)
39. CDHS Collaboration (H. Abramowicz et al.), Z. Phys. **C15**, 19 (1982)
40. CCFR Collaboration (A.O. Bazarko et al.), Z. Phys. **C65**, 189 (1995)
41. CHARM II Collaboration (P. Vilain et al.), Eur. Phys. J. **C11**, 19 (1999)
42. T. Bolton, KSU-HEP-97-04 [hep-ex/9708014] (1997)
43. FNAL-E531 Collaboration (N. Ushida et al.), Phys. Lett. **B206**, 375 (1988)
44. CLEO Collaboration (Y. Kubota et al.), Phys. Rev. **D54**, 2994 (1996)
45. M. Bargiotti et al., Riv. Nuovo Cim. **23** N3, 1 (2000)
46. L. Montanet et al., Phys. Rev. **D50**, 1173 (1994)
47. ALEPH Collaboration (R. Barate et al.), Phys. Lett. **B453**, 107 (1999); ALEPH Collaboration (R. Barate et al.), ALEPH 99-064 CONF-99-038; ALEPH Collaboration (R. Barate et al.), Phys. Lett. **B465**, 349 (1999)

48. DELPHI Collaboration (P. Abreu et al.), Phys. Lett. **B439**, 209 (1998)
49. OPAL Collaboration (G. Abbiendi et al.), Phys. Lett. **B490**, 71 (2000)
50. LEP Electroweak Working Group, CERN-EP-2001-098 [hep-ex/0112021] (2001)
51. K. Benslama (for the CLEO-c Collaboration), Talk given at 37th Rencontres de Moriond on Electroweak Interactions and Unified Theories, Les Arcs, France, 9-16 Mar 2002, hep-ex/0205003
52. N. Isgur, M. Wise, Phys. Lett. **B232**, 113 (1989); Phys. Lett. **237**, 527 (1990)
53. H. Georgi, Phys. Lett. **B238**, 395 (1990)
54. M. Luke, Phys. Lett. **B252**, 447 (1990)
55. N. Uraltsev, Talk given at Flavor Physics and CP Violation (FPCP 2003), Paris, France, 3–6 Jun 2003 [hep-ph/0309081]
56. M. Shifman, N. Uraltsev, A. Vainshtein, Phys. Rev. **D51**, 2217 (1995); Erratum-ibid. **D52**, 3149 (1995)
57. M. Neubert, Phys. Lett. **B338**, 84 (1994)
58. A. Falk, M. Neubert, Phys. Rev. **D47**, 2965 (1993)
59. A. Kronfeld, Phys. Rev. **D62**, 014505 (2000)
60. J. Harada et al., Phys. Rev. **D65**, 094514 (2002)
61. S. Hashimoto et al., Phys. Rev. **D66**, 014503 (2002)
62. The Heavy Flavor Averaging Group, http://www.slac.stanford.edu/xorg/hfag/ (Summer 2003 and Winter 2004 averages)
63. I.I. Bigi, M. Shifman, N.G. Uraltsev, Annu. Rev. Nucl. Part. Sci. **47**, 591 (1997)
64. I.I. Bigi, M. Shifman, N. Uraltsev, A. Vainshtein, Phys. Rev. **D56**, 4017 (1997); Phys. Rev. **D52**, 196 (1995)
65. CLEO Collaboration (S. Chen et al.), Phys. Rev. Lett. **87**, 251807 (2001)
66. C.W. Bauer, Z. Ligeti, M. Luke, A.V. Manohar, M. Trott, Phys. Rev. **D70**, 094017 (2004)
67. K. Schubert, Talk given at 21st International Symposium on Lepton and Photon Interactions at High Energies (LP 03), Batavia, Illinois, 11-16 Aug 2003
68. *BABAR* Collaboration (B. Aubert et al.), *BABAR*-PUB-03-045 [hep-ex/0403030]
69. *BABAR* Collaboration (B. Aubert et al.), *BABAR*-CONF-03-034 [hep-ex/0403031]
70. *BABAR* Collaboration (B. Aubert et al.), *BABAR*-PUB-04-007 [hep-ex/0404017]
71. *BABAR* Collaboration (B. Aubert et al.), Phys. Rev. Lett. **90**, 181801 (2003)
72. CLEO Collaboration (S.B. Athar et al.), Phys. Rev. **D68**, 072003 (2003)
73. ARGUS Collaboration (H. Albrecht et al.), Phys. Lett. **B255**, 297 (1991)
74. CLEO Collaboration (R. Fulton et al.), Phys. Rev. Lett. **64**, 16 (1990)
75. CLEO Collaboration (J. Bartelt et al.), Phys. Rev. Lett. **71**, 4111 (1993)
76. G. Altarelli, N. Cabibbo, G. Corbò, L. Maiani, G. Martinelli, Nucl. Phys. **B208**, 365 (1982)
77. N. Isgur, D. Scora, B. Grinstein, M.B. Wise, Phys. Rev. **D39**, 799 (1989)
78. J.G. Körner, G.A. Schuler, Z. Phys. **C38**, 511 (1988); Erratum-ibid. **C41**, 690 (1989)
79. M. Wirbel, B. Stech, M. Bauer, Z. Phys. **C29**, 637 (1985)
80. CLEO Collaboration (A. Bornheim et al.), Phys. Rev. Lett. **88**, 231803 (2002)
81. *BABAR* Collaboration (B. Aubert et al.), BABAR-CONF-02-012, Contributed to 31st International Conference on High Energy Physics (ICHEP 2002), Amsterdam, The Netherlands, 24–31 Jul 2002 [hep-ex/0207081]
82. Belle Collaboration (K. Abe et al.), BELLE-CONF-0325 (2003), Contributed to International Europhysics Conference on High-Energy Physics (HEP 2001), Budapest, Hungary, 12–18 Jul 2001
83. A.K. Leibovich, Z. Ligeti, M.B. Wise, Phys. Lett. **B539**, 242 (2002)
84. C.W. Bauer, M. Luke, T. Mannel, Phys. Lett. **B543**, 261 (2002)
85. M. Neubert, Phys. Lett. **B543**, 269 (2002)
86. C.N. Burrell, M.E. Luke, A.R. Williamson, Phys.Rev. **D69**, 074015 (2004)
87. I.I.Y. Bigi, N. Uraltsev, Int. J. Mod. Phys. **A16**, 5201 (2001)
88. M.B. Voloshin, Phys. Lett. **B515**, 74 (2001)
89. DELPHI Collaboration (P. Abreu et al.), Phys. Lett. **B478**, 14 (2000)
90. *BABAR* Collaboration (B. Aubert et al.), Phys. Rev. Lett. **92**, 071802 (2004)
91. CLEO Collaboration (A. Bornheim et al.), CLEO-CONF-02-08, Contributed to 31st International Conference on High Energy Physics (ICHEP 2002), Amsterdam, The Netherlands, 24–31 Jul 2002 [hep-ex/0207064]
92. A. Sugiyama (for the Belle Collaboration), Talk given at 38th Rencontres de Moriond on Electroweak Interactions and Unified Theories, Les Arcs, France, 15–22 Mar 2003 [hep-ex/0306020]
93. ALEPH collaboration (R. Barate et al.), Eur. Phys. J. **C6**, 555 (1999)
94. OPAL collaboration, (G. Abbiendi et al.), Eur. Phys. J. **C21**, 399 (2001)
95. L. Gibbons (for the CLEO Collaboration), To appear in the proceedings of 9th International Conference on B Physics at Hadron Machines (Beauty 2003), Pittsburgh, Pennsylvania, 14–18 Oct 2003 [hep-ex/0402009]
96. O. Catà, S. Peris [hep-ph/0406094]
97. T. Trippe, private communication (2004)
98. KTeV Collaboration, (T. Alexopoulos et al.) [hep-ex/0406002]
99. L. Lellouch, Nucl. Phys. Proc. Suppl. **94**, 142 (2001)
100. J. Bijnens, J. Prades, Nucl. Phys. **B444**, 523 (1995); J. High Energy Physics **01**, 002 (2000); S. Peris, E. de Rafael, Phys. Rev. Lett. **490**, 213 (2000).
101. G. Buchalla, A.J. Buras, M.E. Lautenbacher, Rev. Mod. Phys. **68**, 1125 (1996)
102. T. Inami, C.S. Lim, Prog. Theor. Phys. **65**, 297 (1981); Erratum-ibid. **65**, 1772 (1981)

103. L. Cerrito (for the CDF and D0 Collaboration), To appear in the proceedings of 39th Rencontres de Moriond on QCD and High-Energy Hadronic Interactions, La Thuile, Italy, 28 Mar – 4 Apr 2004 [hep-ex/0405046]
104. K. Melnikov, T. van Ritbergen, Phys. Lett. **B482**, 99 (2000)
105. N. Gray, D.J. Broadhurst, W. Grafe, K. Schilcher, Z. Phys. **C48**, 673 (1990)
106. D.J. Broadhurst, N. Gray, K. Schilcher, Z. Phys. **C52**, 111 (1991)
107. S. Herrlich, U. Nierste, Nucl. Phys. **B419**, 292 (1994)
108. U. Nierste, [9] and private communication (2003)
109. D. Becirevic, Talk given at 2nd Workshop on the CKM Unitarity Triangle, Durham, England, 5–9 Apr 2003 [hep-ph/0310072]
110. M.J. Booth, Phys. Rev. **D51**, 2338 (1995)
111. S.R. Sharpe, Y. Zhang, Phys. Rev. **D53**, 5125 (1996)
112. C. Bernard, T. Blum, A. Soni, Phys. Rev. **D58** 014501 (1998)
113. JLQCD Collaboration (N. Yamada et al.), Nucl. Phys. B Proc. Suppl. **106**, 397 (2002) [hep-lat/0110087]
114. S. Kronfeld, S.M. Ryan, Phys. Lett. **B543**, 59 (2002)
115. D. Becirevic et al., Phys. Lett. **B563**, 150 (2003)
116. C. Davies, Talk given at Flavor Physics and CP Violation (FPCP 2003), Paris, France, 3–6 Jun 2003 [hep-ph/0311040]
117. J.L. Rosner, Nucl. Instrum. Meth. **A462**, 304 (2001)
118. ALEPH Collaboration (A. Heister et al.), Eur. Phys. J. **C29**, 143 (2003)
119. DELPHI Collaboration (P. Abreu et al.), Eur. Phys. J. **C16**, 555 (2000); DELPHI Collaboration (P. Abreu et al.), Eur. Phys. J. **C18**, 229 (2000); DELPHI Collaboration (J. Adballah et al.), Eur. Phys. J. **C28**, 155 (2003); DELPHI Collaboration (J. Adballah et al.), Contribution 607 to 30th International Conference on High-Energy Physics (ICHEP 2002), Amsterdam, The Netherlands, Jul 24–31 2002
120. OPAL Collaboration (G. Abbiendi et al.), Eur. Phys. J. **C11** 587, (1999); OPAL Collaboration (G. Abbiendi et al.), Eur. Phys. J. **C19**, 241 (2001)
121. SLD Collaboration (K. Abe et al.), Phys. Rev. **D66**, 032009 (2002); SLD Collaboration (K. Abe et al.), Phys. Rev. **D67**, 012006 (2003); SLD Collaboration (K. Abe et al.), SLAC-PUB-8568, Contributed to 30th International Conference on High-Energy Physics (ICHEP 2000), Osaka, Japan, 27 Jul – 2 Aug 2000 [hep-ex/0012043]
122. CDF Collaboration (F. Abe et al.), Phys. Rev. Lett. **82**, 3576 (1999)
123. H.G. Moser, A. Roussarie, Nucl. Inst. Meth. **A384**, 491 (1997)
124. D. Abbaneo, G. Boix, J. High Energy Phys. **08**, 4 (1999)
125. P. Checchia, E. Piotto, F. Simonetto, Contributed to International Europhysics Conference on High-Energy Physics (EPS-HEP 99), Tampere, Finland, 15–21 Jul 1999 [hep-ph/9907300]
126. A. Ali, M. Misiak, Chapter 6.2 in [9]
127. M. Iwasaki (for the Belle Collaboration), Talk given at 39th Rencontres de Moriond: Electroweak Interactions and Unified Theories La Thuile, Val d'Aoste, Italy, 21-28 Mar 2004
128. A. Ali, E. Lunghi, A.Y. Parkhomenko, DESY-04-065 [hep-ph/0405075] (2004)
129. *BABAR* Collaboration (B. Aubert et al.), Phys. Rev. Lett. **89**, 201802 (2002)
130. Belle Collaboration (K. Abe et al.), BELLE-CONF-0344, Contributed to 21st International Symposium on Lepton and Photon Interactions at High Energies (LP 03), Batavia, Illinois, 11–16 Aug 2003 [hep-ex/0308036]
131. R. Fleischer, Phys. Lett. **B365**, 399 (1996)
132. D. London, A. Soni, Phys. Lett. **B407**, 61(1997); see also [201]
133. Y. Grossman, Z. Ligeti, Y. Nir, H. Quinn Phys. Rev. **D68**, 015004 (2003)
134. M. Gronau, Y. Grossman, J.L. Rosner, Phys. Lett. **B579**, 331 (2004)
135. M. Beneke, M. Neubert, Nucl. Phys. **B675** 333 (2003)
136. *BABAR* Collaboration (B. Aubert et al.), *BABAR*-PUB-04/004 [hep-ex/0403026] (2004)
137. Belle Collaboration (K. Abe et al.), Phys. Rev. Lett. **91**, 261602 (2003)
138. M. Verderi (for the *BABAR* Collaboration), Talk given at 39th Rencontres de Moriond: Electroweak Interactions and Unified Theories La Thuile, Val d'Aoste, Italy, 21-28 Mar 2004
139. *BABAR* Collaboration (B. Aubert et al.), *BABAR*-PUB-04-017 [hep-ex/0406040] (2004)
140. *BABAR* Collaboration (B. Aubert et al.), Phys. Rev. Lett. **91**, 161801 (2003)
141. M. Gronau, D. London, Phys. Rev. Lett. **65**, 3381 (1990)
142. Y. Grossman, H.R. Quinn, Phys. Rev. **D58**, 017504 (1998)
143. J. Charles, Thèse de l'Université Paris-Sud, April 1999, LPT-Orsay 99-31; available (in French) at http://www.tel.ccsd.cnrs.fr (ID 00002502)
144. M. Gronau, D. London, N. Sinha, R. Sinha, Phys. Lett. **B514**, 315 (2001)
145. *BABAR* Collaboration (B. Aubert et al.), *BABAR*-PUB-04-09 [hep-ex/0404029] (2004)
146. *BABAR* Collaboration (B. Aubert et al.), Phys. Rev. **D69**, 031102 (2004)
147. *BABAR* Collaboration (B. Aubert et al.), Phys. Rev. Lett. **91**, 171802 (2003)
148. Belle Collaboration (J. Zhang et al.), Phys. Rev. Lett. **91**, 221801 (2003)
149. L. Roos (for the *BABAR* Collaboration), Talk given at 39th Rencontres de Moriond: Electroweak Interactions and Unified Theories La Thuile, Val d'Aoste, Italy, 21-28 Mar 2004
150. CMD-2 Collaboration (R. Akhmetshin et al.) Phys. Lett. **B578**, 285 (2004)
151. ALEPH Collaboration (R. Barate et al.), Z. Phys. **C76**, 15 (1997)

152. A. Falk, Z. Ligeti, Y. Nir, H. R. Quinn, Phys. Rev. **D69**, 011502 (2004)
153. *BABAR* Collaboration (B. Aubert et al.), *BABAR*-CONF-03-004, Contributed to 38th Rencontres de Moriond on Electroweak Interactions and Unified Theories, Les Arcs, France, 15–22 Mar 2003 [hep-ex/0304030]
154. Belle Collaboration, (K. Abe et al.), BELLE-CONF-0247, Contributed to 31st International Conference on High Energy Physics (ICHEP 2002), Amsterdam, The Netherlands, 24–31 Jul 2002
155. Y. Nir, Nucl. Phys. Proc. Suppl. **117**, 111 (2003) [hep-ph/0208080]
156. Y. Grossman, H. R. Quinn, Phys. Rev. **D56**, 7259 (1997)
157. LASS Collaboration (D. Aston et al.), Nucl. Phys. **B296**, 493 (1988)
158. J. Charles et al., Phys. Lett. **B425**, 375 (1998); Erratum-ibid. **B433**, 441 (1998)
159. C.W. Chiang, L. Wolfenstein, Phys. Rev. **D61**, 074031 (2000)
160. A.S. Dighe, I. Dunietz, R. Fleischer, Eur. Phys. J. **C6**, 647 (1999)
161. B. Kayser, in Proceedings of the 32nd Rencontres de Moriond on Electroweak Interactions and Unified Theories, Les Arcs, France, edited by J. Trân Thanh Vân, Ed. Frontières (1997), p.389; Y.I. Azimov, JETP Lett. **50**, 447 (1989); Phys. Rev. **D42**, 3705 (1990)
162. H.R. Quinn, T. Schietinger, J.P. Silva, A.E. Snyder, Phys. Rev. Lett. **85**, 5284 (2000)
163. Y. Grossman, D. Pirjol, J. High Energy Phys. **006**, 029 (2000)
164. A.J. Buras, M. Jamin, J. High Energy Phys. **0401**, 048 (2004)
165. A. J. Buras, F. Schwab, S. Uhlig, TUM-HEP-547, MPP-2004-47 [hep-ph/0405132] (2004)
166. NA31 Collaboration (G.D. Barr et al.), Phys. Lett. **B317**, 233 (1993)
167. E731 Collaboration (L.K. Gibbons et al.), Phys. Rev. **D55**, 6625 (1997)
168. NA48 Collaboration (J.R. Batley et al.), Phys. Lett. **B544**, 97 (2002)
169. KTeV Collaboration (A. Alavi-Harati et al.), Phys. Rev. **D67**, 012005 (2003)
170. A. Buras, M. Jamin, M.E. Lautenbacher, Nucl. Phys. **B408**, 209 (1993)
171. M. Ciuchini, E. Franco, G. Martinelli, L. Reina, Phys. Lett. **B301**, 263 (1993)
172. E. Pallante, A. Pich, I. Scimemi, Nucl. Phys. **B617**, 441 (2001)
173. D. Becirevic (for the SPQCDR Collaboration), Nucl. Phys. Proc. Suppl. **119**, 359 (2003) [hep-lat/0209136]
174. CP-PACS Collaboration (S. Aoki et al.), Nucl. Phys. Proc. Suppl. **106**, 332 (2002)
175. RBC Collaboration (T. Blum et al.), Phys. Rev. **D68**, 114506 (2003)
176. M. Golterman, S. Peris, Phys. Rev. **D68**, 094506 (2003)
177. T. Hambye, S. Peris, E. de Rafael, J. High Energy Phys. **0305**, 027 (2003)
178. J. Bijnens, E. Gamiz, J. Prades, J. High Energy Phys. **0110**, 009 (2001)
179. E. Gamiz, J. Prades, I. Scimemi, J. High Energy Phys. 0310, 042 (2003)
180. G. Buchalla, A. Buras, Nucl. Phys. **B548**, 309 (1999)
181. W.J. Marciano, Z. Parsa, Phys. Rev. **D53**, 1 (1996)
182. The CKM Collaboration, Proposal to the FNAL PAC, http://www.fnal.gov/projects/ckm/documentation/public/proposal/proposal.html
183. T. Inagaki (for the E391 Collaboration), KEK-PREPRINT-96-181, Talk given at 3rd International Workshop on Particle Physics Phenomenology, Taipei, Taiwan, 14-17 Nov 1996
184. The KOPIO Collaboration, RSVP MRE Proposal, http://pubweb.bnl.gov/people/rsvp/proposal.ps
185. *BABAR* Collaboration (B. Aubert et al.), *BABAR*-PUB-03-031 [hep-ex/0309017] (2003)
186. Belle Collaboration (P. Krokovny et al.), Phys. Rev. Lett. **89**, 231804 (2002); *BABAR* Collaboration (B. Aubert et al.), BABAR-CONF-02-034 Contributed to 31st International Conference on High Energy Physics (ICHEP 2002), Amsterdam, The Netherlands, 24–31 Jul 2002 [hep-ex/0207053]
187. *BABAR* Collaboration (B. Aubert et al.), *BABAR*-PUB-03-033 [hep-ex/0310037] (2003)
188. Belle Collaboration (K. Abe et al.), BELLE-CONF-0341, Contributed to 21st International Symposium on Lepton and Photon Interactions at High Energies (LP 03), Batavia, Illinois, 11–16 Aug 2003 [hep-ex/0308048]
189. M. Gronau, D. London, Phys. Lett. **B253**, 483 (1991)
190. M. Gronau, D. Wyler, Phys. Lett. **B265**, 172 (1991)
191. I. Dunietz, Phys. Lett. **B270**, 75 (1991)
192. I. Dunietz, Z. Phys. **C56**, 129 (1992)
193. D. Atwood, I. Dunietz, A. Soni, Phys. Rev. Lett. **78**, 3257 (1997); Phys. Rev. **D63**, 036005 (2001)
194. *BABAR* Collaboration (B. Aubert et al.), *BABAR*-PUB-04-002 [hep-ex/0402024] (2004)
195. A. Giri, Y. Grossman, A. Soffer, J. Zupan, Phys. Rev. **D68**, 054018 (2003)
196. Belle Collaboration (K. Abe et al.), BELLE-CONF-0343 [hep-ex/0308043] (2003); updated analysis presented by A. Poluektof (for the Belle Collaboration) at 39th Rencontres de Moriond: Electroweak Interactions and Unified Theories La Thuile, Val d'Aoste, Italy, Mar 21-28, 2004.
197. Belle Collaboration (K. Abe et al.), BELLE-CONF-0343 [hep-ex/0406067] (2004)
198. CLEO Collaboration (H. Muramatsu et al.), Phys. Rev. Lett. **89**, 251802 (2002); Erratum-ibid. **90**, 059901 (2003); CLEO Collaboration (S. Kopp et al.), Phys. Rev. **D63**, 092001 (2001)
199. J. Haïssinski, 21st Ecole de Gif (1989), in English, and references therein
200. M. Pivk, Thèse de l'Université Paris VII, May 2003, *BABAR*-THESIS-03/012, available (in French) at http://tel.ccsd.cnrs.fr (ID 00002991)
201. *BABAR* Collaboration (P.F Harrison, H. Quinn eds.), "The *BABAR* Physics Book: Physics at an Asymmetric B Factory", SLAC-R-0504 (1998)

202. J. Charles, Phys. Rev. **D59** 054007, (1999)
203. S. Gardner, Phys. Rev. **D59**, 077502 (1999)
204. A. Höcker, H. Lacker, M. Pivk, L. Roos, LAL 02-103 (2002), LPNHE 2002-15; writeup available at http://www.slac.stanford.edu/xorg/ckmfitter/ckm_talks.html
205. M. Gronau, J.L. Rosner, Phys. Rev. **D65**, 013004 (2002); Erratum-ibid. **D65**, 079901 (2002)
206. R. Fleischer, T. Mannel, Phys. Lett. **B397**, 269 (1997)
207. M. Beneke, G. Buchalla, M. Neubert, C.T. Sachrajda, Phys. Rev. Lett. **83**, 1914 (1999)
208. M. Beneke, G. Buchalla, M. Neubert, C.T. Sachrajda, Nucl. Phys. **B606**, 245 (2001)
209. M. Pivk, F.R. Le Diberder, LAL 04-10 [hep-ph/0406263,] Eur. Phys. J. **C39**, 397 (2005)
210. A.J. Buras, R. Fleischer, Eur. Phys. J. **C11**, 93 (1999)
211. M. Neubert, J.L. Rosner, Phys. Lett. **B441**, 403 (1998); Phys. Rev. Lett. **81**, 5076 (1998)
212. J.P. Silva, L. Wolfenstein, Phys. Rev. **D49**, 1151 (1994)
213. R. Fleischer, Phys. Lett. **B459**, 306 (1999)
214. J.D. Bjorken in *"New Developments in High Energy Physics"*, eds. E.G Floratos, A. Verganelakis, Nucl. Phys. **B11** (Proc. Suppl.), 325 (1989)
215. M. Neubert, B. Stech, Adv. Ser. Direct. High Energy Phys. **15** 294 (1998)
216. Y.Y. Keum, H. Li, A.I. Sanda Phys. Lett. **B504**, 6 (2001)
217. M. Ciuchini et al., Phys. Lett. **B515**, 33 (2001)
218. C.W. Bauer, D. Pirjol, I.Z. Rothstein, I.W. Stewart, MIT-CTP-3469 [hep-ph/0401188] (2004)
219. H. Jawahery, Talk given at 21st International Symposium on Lepton and Photon Interactions at High Energies (LP 03), Batavia, Illinois, 11-16 Aug 2003
220. Belle Collaboration (K. Abe et al.), BELLE-PREPRINT-2004-1 [hep-ex/0401029] (2004)
221. T. Browder, Talk given at 21st International Symposium on Lepton and Photon Interactions at High Energies (LP 03), Batavia, Illinois, 11-16 Aug 2003
222. *BABAR* Collaboration (B. Aubert et al.), Phys. Rev. Lett. **91**, 021801 (2003)
223. T. Tomura (for the Belle Collaboration), Proceedings of 38th Rencontres de Moriond on Electroweak Interactions and Unified Theories, Les Arcs, France, 15–22 Mar 2003 [hep-ex/0305036]
224. J. Fry, Talk given at 21st International Symposium on Lepton and Photon Interactions at High Energies (LP 03), Batavia, Illinois, 11-16 Aug 2003
225. CLEO Collaboration (S. Chen et al.), Phys. Rev. Lett.85, 525 (2000)
226. M. Bona (for the *BABAR* Collaboration), Talk given at Flavor Physics and *CP* Violation (FPCP 2003), Paris, France, 3-6 Jun 2003
227. *BABAR* Collaboration (B. Aubert et al.), Phys. Rev. Lett. **89**, 281802 (2001).
228. Belle Collaboration (Y. Chao et al.), BELLE-PREPRINT-2003-26 [hep-ex/0311061] (2003)
229. CLEO Collaboration (A. Bornheim et al.), Phys. Rev. **D68**, 052002 (2003)
230. *BABAR* Collaboration (B. Aubert et al.), Phys. Rev. Lett. **91**, 241801 (2003)
231. CDF Collaboration (C. Paus et al.), Results prepared for Summer conferences (2003), http://www-cdf.fnal.gov/physics/new/bottom/030529.blessed-bhh/
232. A.J. Buras, R. Fleischer, S. Recksiegel, F. Schwab, Phys. Rev. Lett. **92**, 101804 (2004); A.J. Buras, R. Fleischer, S. Recksiegel, F. Schwab, CERN-PH-TH-2004-020 [hep-ph/0402112] (2004)
233. S. Barshay, L.M. Sehgal, J. van Leusen, Phys. Lett. **B591**, 97 (2004); A. Ali, E. Lunghi, A.Ya. Parkhomenko, DESY-04-036 [hep-ph/0403275] (2004); M. Gronau, J.L. Rosner, TECHNION-PH-2004-21 [hep-ph/0405173] (2004); G. Buchalla, A. Salim Safir, LMU-24-03 [hep-ph/0406016] (2004)
234. L. Roos, Talk given at 2nd Workshop on the CKM Unitarity Triangle, Durham, England, 5-9 Apr 2003, eConf **C0304052**, WG418
235. C.-W. Chiang, M. Gronau, J.L. Rosner, D.A. Suprun, MADPH-04-1372 [hep-ph/0404073] (2004);
236. D. Pirjol, Phys. Rev. **D60**, 054020 (1999)
237. M. Gronau, J.L. Rosner, Phys. Rev. **D59**, 113002 (1999); H.J. Lipkin, Phys. Lett. **B445**, 403 (1999); J. Matias, Phys. Lett. **B520**, 131 (2001)
238. M. Gronau, J.L. Rosner, Phys. Lett. **B572**, 43 (2003)
239. A.J. Buras, R. Fleischer, S. Recksiegel, F. Schwab, Eur. Phys. J. **C32**, 45 (2003)
240. V. Barger, C.-W. Chiang, P. Langacker, H.S. Lee, MADPH-04-1381 [hep-ph/0406126] (2004)
241. Y. Nir, H.R. Quinn, Phys. Rev. Lett. **67**, 541 (1991)
242. L. Lavoura, Mod. Phys. Lett. **A7**, 1553 (1992)
243. M. Imbeault, A. St-Laurent Lemerle, V. Page, D. London, Phys. Rev. Lett. **92**, 081801 (2004)
244. M. Gronau, O.F. Hernandez, D. London, J.L. Rosner, Phys. Rev. **D52**, 6374 (1995)
245. M. Gronau, J.L. Rosner, CLNS 03/1852, TECHNION-PH-2003-41, To appear in the proceedings of Workshop on the Discovery Potential of an Asymmetric B Factory at 10^{36} Luminosity, Menlo Park, California, 8–10 May 2003 [hep-ph/0311280] (2003)
246. M. Gronau, D. Pirjol, T.M. Yan, Phys. Rev. **D60**, 034021 (1999); Erratum-ibid. **D69**, 119901 (2004)
247. *BABAR* Collaboration (B. Aubert et al.), Phys. Rev. Lett. **91**, 201802 (2003); updated results *BABAR*-PLOT-0055 (2003)
248. D. Du, J. Sun, G. Zhu, D. Du, Phys. Rev. **D68**, 054003 (2003) D. Du, J. Sun, D. Yang, G. Zhu, Phys. Rev. **D67**, 014023 (2003); D. Du, H. Gong, J. Sun, D. Yang, G. Zhu Phys. Rev. **D65**, 094025 (2002); Erratum-ibid. **D66**, 079904 (2002);

249. R. Aleksan, P.-F. Giraud, V. Morénas, O. Pène, A. S. Safir, Phys. Rev. **D67**, 094019 (2003)
250. N. de Groot, W.N. Cottingham, I.B. Whittingham, Contributed to 38th Rencontres de Moriond on QCD and Hadronic Interactions, Les Arcs, France, 22–29 Mar 2003 [hep-ph/0305263] eConf **C0304052**, WG405
251. C.-W. Chiang, M. Gronau, Z. Luo, J.L. Rosner, D.A. Suprun, Phys. Rev. **D69**, 034001 (2004)
252. A. Höcker, M. Laget, S. Laplace, J. von Wimmersperg-Toeller, LAL 03-17 (2003), writeup available at http://www.slac.stanford.edu/xorg/ckmfitter/ckm_talks.html
253. H.R. Quinn, A.E. Snyder, Phys. Rev. **D48**, 2139 (1993)
254. S. Versillé, Thèse de l'Université Paris-Sud, April 1999; available (in French) at http://www-lpnhep.in2p3.fr/babar/public/versille/Thesis/
255. Belle Collaboration, (K. Abe et al.), BELLE-CONF-0318, Contributed to International Europhysics Conference on High-Energy Physics (HEP 2001), Budapest, Hungary, 12-18 Jul 2001
256. CLEO Collaboration (C.P. Jessop et al.), Phys. Rev. Lett. **85**, 2881 (2000)
257. *BABAR* Collaboration, (B. Aubert et al.), *BABAR*-PUB-03-037 [hep-ex/0311049] (2003)
258. *BABAR* Collaboration, (B. Aubert et al.), *BABAR*-CONF-03-14, Contributed to International Europhysics Conference on High-Energy Physics (HEP 2003), Aachen, Germany, 17–23 Jul 2003 [hep-ex/0307087]
259. Belle Collaboration (J. Zhang et al.), Belle-PREPRINT-2004-15 [hep-ex/0406006] (2004)
260. Belle Collaboration (J. Dragic et al.), BELLE-PREPRINT-2004-14 [hep-ex/0405068] (2004)
261. Belle Collaboration (K. Abe et al.), BELLE-CONF-0317, Contributed to International Europhysics Conference on High-Energy Physics (HEP 2003), Aachen, Germany, 17-23 Jul 2003
262. CLEO Collaboration (E. Eckhart et al.), Phys. Rev. Lett. **89**, 251801 (2002)
263. CLEO Collaboration (D.M. Asner et al.), Phys. Rev. **D53**, 1039 (1996)
264. *BABAR* Collaboration (B. Aubert et al.), *BABAR*-PUB-03-027 [hep-ex/0308065] (2003)
265. Belle Collaboration (K. Abe et al.), BELLE-CONF-0338, Contributed to 21st International Symposium on Lepton and Photon Interactions at High Energies (LP 03), Batavia, Illinois, 11-16 Aug 2003
266. R. Aleksan, F. Buccella, A. Le Yaouanc, L. Oliver, O. Pène, J.-C. Raynal Phys. Lett. **B356**, 96 (1995)
267. H.J. Lipkin, Y. Nir, H.R. Quinn, A. Snyder, Phys. Rev. **D44**, 1454 (1991)
268. H.R. Quinn, J. Silva, Phys. Rev. **D62**, 054002 (2000)
269. I. Dunietz, H.R. Quinn, A. Snyder, W. Toki, H.J. Lipkin, Phys. Rev. **D43**, 2193 (1991); A.S. Dighe, I. Dunietz, HJ. Lipkin, J.L. Rosner, Phys. Lett. **B369**, 144 (1996)
270. A.L. Kagan, UCTP-102-04 [hep-ph/0405134] (2004)
271. J. Charles, A. Le Yaouanc, L. Oliver, O. Pène , J.C. Raynal, Phys. Rev. **D60**, 014001 (1999)
272. M. Zito, Phys. Lett. **B586**, 314 (2004)
273. M. Ciuchini, E. Franco, G. Martinelli, L. Silvestrini, Nucl. Phys. **B501**, 271 (1997); M. Ciuchini, R Contino, E. Franco, G. Martinelli , L. Silvestrini, Nucl. Phys. **B512**, 3 (1998); Erratum-ibid. **B531**, 656 (1998); M. Ciuchini, E. Franco, G. Martinelli, M. Pierini , L. Silvestrini, Phys. Lett. **B515**, 33 (2001); A. Khodjamirian, Th. Mannel and B. Melic, Phys. Lett. **B571**, 75 (2003)
274. J.F. Donoghue, E. Golowich, A.A. Petrov, J.M. Soares, Phys. Rev. Lett. **77**, 2178 (1996)
275. See, e.g., [278] and references therein
276. R. Fleischer, G. Isidori, J. Matias, J. High Energy Phys. **0305**, 053 (2003)
277. J.M. Soares, L. Wolfenstein, Phys. Rev. **D47**, 1021 (1993)
278. Y. Grossman, Y. Nir, M.P. Worah, Phys. Lett. **B407**, 307 (1997)
279. A.L. Kagan, M. Neubert, Phys. Lett. **B492**, 115 (2000)
280. R. Fleischer, T. Mannel, Phys. Lett. **B506**, 311 (2001)
281. D. Atwood, G. Hiller, LMU-09-03 [hep-ph/0307251] (2003)
282. S. Laplace, Z. Ligeti, Y. Nir, G. Perez, Phys. Rev. **D65**, 094040 (2002)
283. A.I. Sanda, Z-z. Xing, Phys. Rev. **D56**, 6866 (1997)
284. L. Randall, S. Su, Nucl. Phys. **B540**, 37 (1999)
285. R.N. Cahn, M.P. Worah, Phys. Rev. **D60**, 076006 (1999)
286. G. Barenboim, G. Eyal, Y. Nir, Phys. Rev. Lett. **83**, 4486 (1999)
287. M. Beneke, G. Buchalla, A. Lenz, U. Nierste, Phys. Lett. B **576** 173 (2003)
288. M. Ciuchini, E. Franco, V. Lubicz, F. Mescia, C. Tarantino, JHEP **0308** 031 (2003)
289. OPAL Collaboration (G. Abbiendi et al.), Eur. Phys. J. **C12**, 609 (2000)
290. CLEO Collaboration (D.E. Jaffe et al.), Phys. Rev. Lett. **86**, 5000 (2001)
291. ALEPH Collaboration (R. Barate et al.), Eur. Phys. J. **C20**, 431 (2001)
292. *BABAR* Collaboration (B. Aubert et al.), Phys. Rev. Lett. **88**, 231801 (2002)
293. *BABAR* Collaboration (B. Aubert et al.), Phys. Rev. Lett. **92**, 181801 (2004)
294. G.C. Branco, F. Cagarrinho, F. Krüger, Phys. Lett. **B459** 224, (1999)
295. M. Ciuchini, G. Degrassi, P. Gambino, G.F. Giudice, Nucl. Phys. **B534**, 3 (1998); A. Ali, D. London, Eur. Phys. J. **C9**, 687 (1999); A. Ali, D. London Phys. Rept. **320**, 79 (1999; A.J. Buras, P. Gambino, M. Gorbahn, S. Jager, L. Silvestrini, Phys. Lett. **B500**, 161 (2001); A. J. Buras, P. Gambino, M. Gorbahn, S. Jager, L. Silvestrini, Nucl. Phys. **B592**, 55 (2001); A. J. Buras, R. Buras, Phys. Lett. **B501**, 223 (2001); A. J. Buras, R. Fleischer, Phys. Rev. **D64**, 115010 (2001); S. Bergmann, G. Perez, Phys. Rev. **D64**, 115009 (2001)

296. For recent references see, e.g., Y. Grossman, Int. J. Mod. Phys. **A19**, 907 (2004); M. Neubert, CLNS-04-1878 [hep-ph/0405105] (2004)
297. C.W. Chiang, J. Rosner, Phys. Rev. **D68**, 014007 (2003)
298. Y. Grossman, G. Isidori, M.P. Worah, Phys. Rev. **D58**, 057504 (1998); R. Fleischer, T. Mannel, Phys. Lett. **B511**, 240 (2001); M. Ciuchini, L. Silvestrini, Phys. Rev. Lett. **89**, 231802 (2002); see also [300]
299. Y. Grossman, A.L. Kagan, Z. Ligeti Phys. Lett. **B538**, 327 (2002)
300. G. Hiller, Phys. Rev. **D66**, 071502 (2002)
301. V. Barger, C.-W. Chiang, P. Langacker, H.-S. Lee, Phys. Lett. **B580**, 186 (2004); N.G. Deshpande, D. K. Ghosh, OITS-742 [hep-ph/0311332] (2003)
302. G. D'Agostini, CERN-EP-99-139 [hep-ex/9910036] (1999)